Instability and Radiative Effects in Pair Production of W-Bosons

A.P. Chapovsky

Instability and radiative effects in pair production of W-bosons

Instability and radiative effects
in pair production of W-bosons

P R O E F S C H R I F T

TER VERKRIJGING VAN
DE GRAAD VAN DOCTOR AAN DE UNIVERSITEIT LEIDEN,
OP GEZAG VAN DE RECTOR MAGNIFICUS DR. W.A. WAGENAAR,
HOOGLERAAR IN DE FACULTEIT DER SOCIALE WETENSCHAPPEN,
VOLGENS BESLUIT VAN HET COLLEGE VOOR PROMOTIES
TE VERDEDIGEN OP DONDERDAG 23 SEPTEMBER 1999
TE KLOKKE 16.15 UUR

DOOR

Alexander Pavlovich Chapovsky

GEBOREN TE NOVOSIBIRSK IN 1974

Promotiecommissie:

Promotor:	Prof. dr. F.A. Berends
Co-promotor:	Dr. W.J.P. Beenakker (University of Durham, UK)
Referent:	Prof. dr. R.H.P. Kleiss
Overige leden:	Prof. dr. P. van Baal
	Dr. A. Denner (Paul Scherrer Institut, CH)
	Prof. dr. L.J.F. Hermans
	Dr. W.L.G.A.M. van Neerven

Contents

Contents

1   Introduction

The Standard Model of interactions between elementary particles is believed to describe accurately all present-day collider experiments. The elementary particles in the model are fermions, specifically quarks and leptons, which carry spin 1/2, and bosons. The bosons have spin 0, the Higgs boson, or have spin 1, the gauge bosons: gluons, photon, $W^{\pm}$ and Z bosons. The Standard Model consists of the strong interactions described by $SU(3)$ gauge theory, and the unified Glashow-Salam-Weinberg Model of electroweak interactions [1] described by an $SU(2) \times U(1)$ gauge theory. In terms of particles, the strong interactions are mediated by massless gluons, whereas the electroweak interactions are carried by the massless photon and the massive $W^{\pm}$ and Z gauge bosons. The theory predicts detailed properties of the particles and the interactions, which should be verified by experiment. The massive gauge bosons are a crucial part of the theory.

So far all experimental results agree within the experimental accuracy with the predictions of the Standard Model. Although it looks like a success story, the check is not complete. There are effects predicted by the Standard Model (for example the Higgs boson), which have not yet been observed. Besides that, theoretical arguments exist, which point out that the Standard Model cannot be a consistent theory at higher energies. All this serves as a motivation for further studies and tests of the Standard Model. Therefore, at future accelerator experiments the limits will be pushed to even higher energies and accuracies. The results of these experiments have to be confronted with the predictions of the Standard Model, which should match the quality and accuracy of the experimental data.

The predictions of the theory can be written as a series in terms of a small parameter α, the fine structure constant. In first instance, the experimental results will be confronted with the lowest order prediction of the theory. With increasing experimental accuracy the next term of the perturbative expansion in α, and possibly even higher order terms, should be taken into account. The lowest order prediction is improved by these $\mathcal{O}(\alpha)$, $\mathcal{O}(\alpha^2)$,... corrections. They are usually called radiative corrections. The complexity of high precision calculations within the Standard Model poses a clear challenge to the theory. In this thesis the focus will be on precision calculations for pair production of unstable particles. In particular the case of W-pair production will be studied in detail.

1.1   W-pair production at LEP2

In order to test the Standard Model (SM) of electroweak interactions, millions of Z bosons have been produced and studied at LEP1 [2]. High-precision measurements
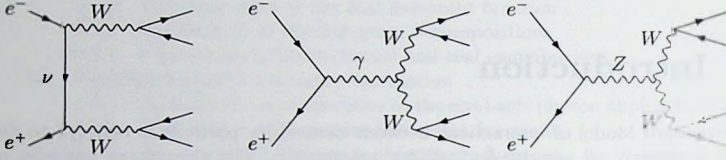
Figure 1-1. The diagrams corresponding to the process (1.1.3).

of the Z-boson parameters have been performed by measuring

$$e^+e^- \to Z \to \bar{f}f \qquad (1.1.1)$$

and comparing the results with the theoretical predictions. This requires theoretical precision calculations for the reaction

$$e^+e^- \to \bar{f}f, \qquad (1.1.2)$$

involving *all* lowest-order diagrams and the radiative corrections (RC) to them [3].

The logical next step is the study of the W boson, which can be produced in pairs in electron-positron collisions at higher energies. For this purpose the energy of the LEP machine has been roughly doubled: the LEP2 collider. Measuring the parameters of the W boson provides further tests of the SM. In particular, the accuracy of the measurement of the W-boson mass (M_W) has to be improved, since it can give indirect information on the Higgs sector and on physics beyond the SM. By this we mean that with an accurate M_W and with other already precisely known SM parameters the range of possible mass values, M_H, for the Higgs boson can be limited and therefore M_H can be roughly predicted. It is however conceivable that M_W and other accurately known parameters might lead to inconsistencies, i.e. no M_H value would give the correct SM quantities. In that case it would become apparent that the SM is incomplete and has to be enlarged beyond the present theory.

At LEP2, W bosons can be studied in the W-pair production reaction

$$e^+e^- \to W^+W^- \to 4 \text{ fermions.} \qquad (1.1.3)$$

The lowest order (Born) prediction for the cross-section of reaction (1.1.3) is based on the three diagrams of Fig. 1-1, representing respectively neutrino, photon and Z-boson exchange. In the latter two diagrams the interaction between gauge bosons, characteristic for Yang-Mills gauge theories, manifests itself in the vertices with γW^+W^- and ZW^+W^- couplings. Reaction (1.1.3) therefore offers the possibility of performing direct tests of the Yang-Mills form of the triple gauge-boson couplings (TGC). Deviations from the SM couplings can be searched for most effectively by a detailed investigation of angular distributions [4].
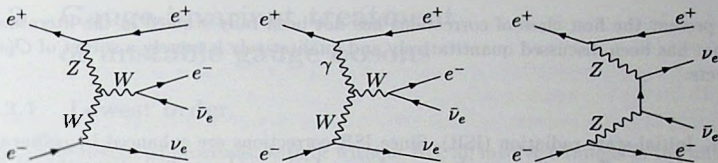
Figure 1-2. Examples of background diagrams contributing to the process (1.1.4).

Just like in the case of the Z boson, the precise determination of the W-boson parameters requires both accurate experiments and accurate theoretical predictions. Since the statistics at LEP2 is much smaller than at LEP1, the theoretical calculations do not have to be as precise as those for LEP1. However, just the Born prediction for process (1.1.3), involving only three diagrams, is not sufficient [5]. Therefore, one would like to have an idea how the cross-sections for the four-fermion process

$$e^+e^- \rightarrow 4 \text{ fermions} \tag{1.1.4}$$

are affected by the inclusion of the remaining lowest-order diagrams (so-called background diagrams) and the RC to the *complete* set of lowest-order diagrams. As an exampe we give a few of the many diagrams contributing to the $e^+\nu_e e^-\bar{\nu}_e$ final state in Fig. 1-2. The first and second diagram contain a single resonant W boson and the third none at all. Note that the second diagram contains a photon, which can become almost real.

The question of the complete lowest-order calculation of process (1.1.4) has been studied in the literature [5, 6]. Roughly speaking, those diagrams that contain a single W boson are a factor of $\mathcal{O}(\Gamma_W/M_W)$ smaller than those for the W-pair production process (1.1.3). Diagrams that do not contain a W boson at all are down by $\mathcal{O}(\Gamma_W^2/M_W^2)$. Note, however, that some diagrams that do not contain two W bosons can nevertheless be large, e.g. as a result of the exchange of almost real photons. Besides such special cases, the lowest-order background diagrams in (1.1.4), i.e. the non-W-pair diagrams, will give at most a correction of $\mathcal{O}(\Gamma_W/M_W)$ to the Born cross-section of process (1.1.3).

The RC to process (1.1.3) are *a priori* of $\mathcal{O}(\alpha)$, i.e. they are generically of the same order as the lowest-order background diagrams, which are of $\mathcal{O}(\Gamma_W/M_W)$. In analogy to the lowest-order case, the RC to the background diagrams are at most of $\mathcal{O}(\alpha\Gamma_W/M_W)$.

In view of the above estimates, the most relevant corrections to the Born cross-section of process (1.1.3) are divided into two classes:

1. $\mathcal{O}(\alpha)$ RC to the W-pair process (1.1.3).

2. $\mathcal{O}(\Gamma_W/M_W)$ lowest-order background contributions from the full four-fermion process (1.1.4).

At present the first class of corrections has not been fully studied in the literature. What has been discussed quantitatively and qualitatively is merely a subset of $\mathcal{O}(\alpha)$ effects:

1.1. Initial-state radiation (ISR). Since ISR corrections are enhanced by collinear-photon effects, they are large and even higher-order contributions should be taken into account [5]–[7].

1.2. In the vicinity of the W-pair threshold the Coulomb interaction between the unstable W bosons has been studied in great detail [8]. The corrections are relatively large.

1.3. The effects 1.1 and 1.2 are all of QED origin. Complete electroweak RC to process (1.1.3) have not been applied yet, but some attempts have been made to take into account the dominant effects. An overall effect of electroweak corrections has been considered by using the Fermi constant G_μ as coupling constant instead of α. From other calculations it is known that a G_μ parametrization of the lowest-order term reduces the size of the one-loop non-photonic RC considerably. In addition to this overall effect, the full electroweak RC to *stable* W-pair production [9]–[11] and *on-shell* W decay [12] are already known for quite some time.

The purpose of this thesis is twofold. In the first place we will present a complete quantitative evaluation of $\mathcal{O}(\alpha)$ electroweak RC to W-pair-mediated four-fermion production. To this end we calculate all $\mathcal{O}(\alpha)$ factorizable corrections in Chapter 2 and add them to our results on non-factorizable corrections of Chapter 4. The distinction between factorizable and non-factorizable corrections is based on the distinction between diagrams that explicitly have two overall resonating W-boson propagators and diagrams that at first sight do not seem to have this. In Chapter 2 we discuss the separation between the factorizable and non-factorizable corrections in more detail. In this way the gap in the above list of corrections 1.1–1.3 will be filled, and the exact size of all $\mathcal{O}(\alpha)$ corrections to reaction (1.1.3) will be known. In the light of the physics motivation given above, this practical result is clearly wanted.

Secondly, this thesis discusses in detail the so-called pole scheme. This scheme offers a way to avoid theoretical problems associated with the gauge-invariant treatment of reactions that involve the production and subsequent decay of unstable particles. The study of the W-pair case serves as a relevant example of this method and can be used as a guideline for other cases. Since there are more unstable-particle production processes to be studied at future accelerators, the relevance of the presented study goes beyond the W-pair case.

1.2   Gauge-invariant treatment
of unstable gauge bosons

1.2.1   Lowest order

The above-described processes, with or without RC, all involve fermions in the initial and final state and unstable gauge bosons as intermediate particles. Sometimes a photon is also present in the final state. If complete sets of graphs contributing to a given process are taken into account, the associated matrix elements are in principle gauge-invariant, i.e. they are independent of gauge fixing and respect Ward identities. This is, however, not guaranteed for incomplete sets of graphs like the ones corresponding to the off-shell W-pair production process (1.1.3). Indeed this process was found to violate the $SU(2)$ Ward identities [7].

In addition, the unstable gauge bosons that appear as intermediate particles can give rise to poles $1/(p^2 - M^2)$ in physical observables if they are treated as stable particles. This can be cured by introducing the finite decay widths (Γ) for these gauge bosons. In field theory, such widths arise naturally from the imaginary parts of higher-order diagrams describing the gauge-boson self-energies, resummed to all orders. However, in doing a Dyson summation of self-energy graphs, we are singling out only a very limited subset of all possible higher-order diagrams. It is therefore not surprising that one often ends up with a result that violates Ward identities and/or retains some gauge dependence resulting from incomplete higher-order contributions.

Since the latter gauge breaking is caused by the finite decay width and is, as such, in principle suppressed by powers of Γ/M, one might think that it is of academic nature. For LEP1 observables we indeed know that gauge breaking can be negligible for all practical purposes. However, the presence of small scales can amplify the gauge-breaking terms. This is for instance the case for almost real space-like photons [13, 14] or longitudinal gauge bosons (V_L) at high energies [15], involving scales of $\mathcal{O}(p_B^2/E_B^2)$ for $B = \gamma, V_L$. The former plays an important role in TGC studies in the reaction $e^+e^- \to e^-\bar{\nu}_e u\bar{d}$, where the electron may emit a virtual photon with an invariant mass p_γ^2 as small as m_e^2. The latter determines the high-energy behaviour of the generic reaction $e^+e^- \to 4$ fermions. In these situations the external current coupled to the photon or to the longitudinal gauge boson becomes approximately proportional to p_B. Sensible theoretical predictions, with a proper dependence on p_γ^2 and a proper high-energy behaviour, are only possible if the amplitudes with external currents replaced by the corresponding gauge-boson momenta fulfil appropriate Ward identities.

So, how should one go about including the finite decay widths? The simplest approach is the so-called "fixed-width scheme", involving the systematic replacement $1/(p_V^2 - M_V^2) \to 1/(p_V^2 - M_V^2 + iM_V\Gamma_V)$, where Γ_V denotes the physical width of the gauge boson V with mass M_V and momentum p_V. Since in perturbation theory the propagator for space-like momenta does not develop an imaginary part, the introduction of a finite width also for $p_V^2 < 0$ has no physical motivation and in fact violates unitarity, i.e. the cutting equations. This can be cured by using a running

width $iM_V\Gamma_V(p_V^2)$ instead of the constant one $iM_V\Gamma_V$ ("running-width scheme"). However, as in general the resonant diagrams [like the ones corresponding to (1.1.3)] are not gauge-invariant by themselves, the introduction of a constant or running width destroys gauge invariance.

A truly gauge-invariant scheme evidently has to be a bit more sophisticated than this. It should be stressed, however, that any such scheme is arbitrary to a greater or lesser extent: since the Dyson summation must necessarily be taken at all orders of perturbation theory, and we are not able to compute the complete set of Feynman diagrams to *all* orders, the various schemes differ even if they lead to formally gauge-invariant results. Bearing this in mind, we need besides gauge invariance some physical motivation for choosing a particular scheme. In this context two options can be mentioned. The first option is the so-called "pole scheme" [16]. In this scheme one decomposes the complete amplitude by expanding around the poles. As the physically observable residues of the poles are gauge-invariant, gauge invariance is not broken if the finite width is taken into account in the pole terms $\propto 1/(p_V^2 - M_V^2)$. Note that the leading terms in such an expansion play a special role in view of their close relation to on-shell production and decay of the unstable particles. This point will be explained in more detail in Sect. 2.1 of Chapter 2.

The second option is based on the philosophy of trying to determine and include the minimal set of Feynman diagrams that is necessary for compensating the gauge violation caused by the self-energy graphs. This is obviously the theoretically most satisfying solution, but it may cause an increase in the complexity of the matrix elements and consequently a slowing down of the numerical calculations. For the gauge bosons we are guided by the observation that the lowest-order decay widths are exclusively given by the imaginary parts of the fermion loops in the one-loop self-energies. It is therefore natural to perform a Dyson summation of these fermionic one-loop self-energies and to include the other possible one-particle-irreducible fermionic one-loop corrections ("fermion-loop scheme") [14, 15]. For the LEP2 process $e^+e^- \to$ 4 fermions this amounts to adding the fermionic corrections to the triple gauge-boson vertex. The complete set of fermionic contributions forms a gauge-independent subset and obeys all Ward identities exactly, even with resummed propagators [15].

The above arguments, although general, apply in particular to tree diagrams. Therefore an additional discussion for RC is required.

1.2.2   Radiative corrections

The next question that should be addressed involves the interplay between RC and gauge invariance. After all, the RC are indispensable for coming up with reliable theoretical predictions for the LEP2 process $e^+e^- \to$ 4 fermions.

As far as real-photon corrections are concerned, not much changes as compared to the lowest-order case. Still both the pole scheme and fermion-loop scheme yield gauge-invariant results. However, in the fermion-loop-scheme treatment of the process $e^+e^- \to 4f\gamma$ the full set of fermionic corrections to the quartic gauge-boson vertex

emerges. This evidently is too much complexity for a tree-level calculation. The pole-scheme, with its close relation to on-shell subprocesses, remains relatively simple. As we shall see later on, some subtleties arise when photons are radiated from a virtual W boson, because this W boson may give rise to two poles.

The implementation of the one-loop RC adds an additional level of complexity by the sheer number of contributions ($10^3 - 10^4$) that have to be evaluated. By employing a gauge-invariant lowest-order finite-width scheme it is possible to cover the most important electroweak effects, like running couplings and leading QED corrections (see previous section), which are controlled by factorization theorems. However, there is still the question about the remaining corrections, which can be large, especially at high energies [5, 7, 17].

In order to include these corrections one might attempt to extend the fermion-loop scheme. At present this solution is not yet workable in view of the fact that a gauge-invariant inclusion of the one-loop corrections to the decay width in turn requires the inclusion of (the imaginary parts of) some two-loop corrections. Moreover, the number of one-loop contributions that have to be evaluated remains large.

As a more appealing and economic strategy we discuss in Sect. 2.2 of Chapter 2 how the RC can be calculated in the framework of the pole-scheme expansion.

1.3 This thesis

Let us summarize the above and give an outline of the various issues to be discussed in this thesis. The purpose of the thesis is twofold. On one hand, we discuss the one-loop $\mathcal{O}(\alpha)$ radiative corrections to the four-fermion production process (1.1.4) in the context of the pole-scheme expansion around the W-boson poles. It should be realized that the error of the method is roughly $\mathcal{O}(\alpha^2, \alpha\Gamma_W/M_W)$. The main contribution comes from four-fermion production mediated by pair production of W bosons, which is of phenomenological interest for the current LEP2 experiments. On the other hand, we believe that the pole-scheme is a proper and rather efficient method for dealing with processes involving unstable particles in general. This makes our study relevant for many other forthcoming experiments, where unstable particles will be produced.

In Chapter 2 we discuss the method of pole expansions and the split-up of the radiative corrections into a sum of factorizable and non-factorizable corrections, which is essential for the method. The problems of gauge invariance associated with this procedure are dealt with in detail. We calculate the factorizable corrections and combine them with the non-factorizable ones, calculated in detail in Chapter 4. At the end of Chapter 2 extensive numerical results are presented. These results cover for the first time the complete $\mathcal{O}(\alpha)$ radiatively corrected cross-sections for pair production of off-shell W bosons.

In Chapter 3 the issue of the final state radiation is discussed, which is prompted by a remarkable numerical result of Chapter 2. This result is that final state radiation can give a large contribution to the invariant mass distribution of the unstable particle, which is *a priori* quite unexpected and even surprising. In order to convince

the reader that this effect is not an artefact of our treatment in Chapter 2 we consider a toy model in which the calculation can be performed exactly, without the pole expansion. The same effect in the context of the pole expansion is also discussed there.

In Chapter 4 we present a calculation of the non-factorizable corrections. We develop two calculational techniques. One of them is applicable to more complicated processes with more unstable particles participating.

As another application of the methods developed in Chapter 4 we calculate in Chapter 5 one-loop QCD interconnection effects in pair production of

References

[1] S.L. Glashow, *Nucl. Phys.* **B22** (1961) 579;
    S. Weinberg, *Phys. Rev. Lett.* **19** (1967) 19;
    A. Salam, in: "Elementary Particle Theory", p. 367, ed. N. Svartholm (Stockholm 1968).

[2] The LEP Collaborations ALEPH, DELPHI, L3, OPAL and the LEP Electroweak Working Group, and the SLD Heavy Flavour Working Group, *"A Combination of Preliminary LEP Electroweak Measurements and Constraints on the Standard Model"* CERN-EP/99-15 (1999);
    The LEP Collaborations ALEPH, DELPHI, L3, OPAL and the LEP Electroweak Working Group, and the SLD Heavy Flavour Working Group, *"A Combination of Preliminary LEP Electroweak Measurements and Constraints on the Standard Model"* CERN-PPE/97-154 (1997).

[3] D. Bardin *et al.*, in *Reports of the working group on precision calculations for the Z resonance*, eds. D. Bardin, W. Hollik and G. Passarino, (CERN-95-03, Genève, 1995) p. 7, *hep–ph*/9709229.

[4] G. Gounaris *et al.*, in *Physics at LEP2*, eds. G. Altarelli, T. Sjöstrand and F. Zwirner, (CERN 96-01, Genève, 1996) Vol. 1, p. 525, *hep–ph*/9601233;
    R.L. Sekulin, *Journal of Physics* **G24** (1998) 297;
    F.A. Berends *et al.*, *ibid.* 405.

[5] W. Beenakker *et al.*, in *Physics at LEP2*, eds. G. Altarelli, T. Sjöstrand and F. Zwirner, (CERN 96-01, Genève, 1996) Vol. 1, p. 79, *hep–ph*/9602351.

[6] D. Bardin, *et al.*, in *Physics at LEP2*, eds. G. Altarelli, T. Sjöstrand and F. Zwirner, (CERN 96-01, Genève, 1996) Vol. 2, p. 3, *hep–ph*/9709270.

[7] W. Beenakker and A. Denner, *Int. J. Mod. Phys.* **A9** (1994) 4837.

[8] V.S. Fadin and V.A. Khoze, *Yad. Fiz.* **48** (1988) 487; *Sov. J. Nucl. Phys.* **48** (1988) 309;
    V.S. Fadin and V.A. Khoze, *Sov. J. Nucl. Phys.* **48** (1988) 309;
    V.S. Fadin, V.A. Khoze and A.D. Martin, *Phys. Lett.* **B311** (1993) 311;
    D. Bardin, W. Beenakker and A. Denner, *Phys. Lett.* **B317** (1993) 213;
    V.S. Fadin et al., *Phys. Rev.* **D52** (1995) 1377.

[9] M. Böhm *et al.*, *Nucl. Phys.* **B304** (1988) 463;
    W. Beenakker, K. Kolodziej and T. Sack, *Phys. Lett.* **B258** (1991) 469.

[10] J. Fleischer, F. Jegerlehner and M. Zrałek, Z. Phys. **C42** (1989) 409;
     K. Kołodziej and M. Zrałek, Phys. Rev. **D43** (1991) 3619;
     J. Fleischer, F. Jegerlehner and K. Kołodziej, Phys. Rev. **D47** (1993) 830.

[11] W. Beenakker, F.A. Berends and T. Sack, Nucl. Phys. **B367** (1991) 287.

[12] A. Denner and T. Sack, Z. Phys. **C46** (1990) 653 and papers quoted therein.

[13] F.A. Berends and G.B. West, Phys. Rev. **D1** (1970) 122.

[14] E.N. Argyres et al., Phys. Lett. **B358** (1995) 339.

[15] W. Beenakker et al., Nucl. Phys. **B500** (1997) 255.

[16] R.G. Stuart, Phys. Lett. **B262** (1991) 113;
     A. Aeppli, G.J. van Oldenborgh and D. Wyler, Nucl. Phys. **B428** (1994) 126.

[17] M. Böhm, A. Denner and S. Dittmaier, Nucl. Phys. **B376** (1992) 29;
     W. Beenakker et al., Nucl. Phys. **B410** (1993) 245 and Phys. Lett. **B317** (1993)
     622;
     M. Kuroda and D. Schildknecht, Nucl. Phys. **B531** (1998) 24.

2 Factorizable corrections

In this chapter we discuss the method of the pole expansion, which offers a convenient framework for gauge invariant calculations for processes involving unstable particles. We apply this method to pair production of W bosons. In particular we discuss in detail the split-up between the so-called factorizable and non-factorizable corrections, and calculate the former. At the end of the chapter extensive numerical results for the complete $\mathcal{O}(\alpha)$ corrected cross-sections are given. The material of this chapter has been published in the literature, [1].

2.1 The pole scheme in double-pole approximation

As mentioned in Sect. 1.2.1, the pole scheme consists in decomposing the complete amplitude by expanding around the poles of the unstable particles. The residues in this expansion are physically observable and therefore gauge-invariant. The pole-scheme expansion can be viewed as a gauge-invariant prescription for performing an expansion in powers of Γ_V/M_V. The calculation of the residues involves a mapping of off-shell matrix elements with off-shell kinematics on on-resonance matrix elements with restricted kinematics. This mapping, however, is not unambiguously fixed. After all, it involves more than just the invariant masses of the unstable particles and one thus has to specify the variables that have to be kept fixed in the mapping. The resulting implementation dependence manifests itself in differences of subleading nature, e.g. $\mathcal{O}(\Gamma_V/M_V)$ suppressed deviations in the leading pole-scheme residue. In special regions of phase space, where the matrix elements vary rapidly, the implementation dependence can take noticeable proportions. This happens in particular near phase-space boundaries, like thresholds.

In order to make these statements a bit more transparent, we sketch the pole-scheme method for a single unstable particle. In this case the Dyson resummed lowest-order matrix element is given by

$$
\mathcal{M}^{\infty} = \frac{W(p_V^2, \omega)}{p_V^2 - \bar{M}_V^2} \sum_{n=0}^{\infty} \left(\frac{-\bar{\Sigma}_V(p_V^2)}{p_V^2 - \bar{M}_V^2} \right)^n = \frac{W(p_V^2, \omega)}{p_V^2 - \bar{M}_V^2 + \bar{\Sigma}_V(p_V^2)}
$$
$$
= \frac{W(M^2, \omega)}{p_V^2 - M^2} \frac{1}{Z(M^2)} + \left[\frac{W(p_V^2, \omega)}{p_V^2 - \bar{M}_V^2 + \bar{\Sigma}_V(p_V^2)} - \frac{W(M^2, \omega)}{p_V^2 - M^2} \frac{1}{Z(M^2)} \right], \quad (2.1.1)
$$

where $\bar{\Sigma}_V(p_V^2)$ is the unrenormalized self-energy of the unstable particle V with momentum p_V and unrenormalized mass $\bar{M}_V$. The renormalized quantity M^2 is the pole in the complex p_V^2 plane, whereas $Z(M^2)$ denotes the wave-function factor:

$$
M^2 - \bar{M}_V^2 + \bar{\Sigma}_V(M^2) = 0, \qquad Z(M^2) = 1 + \bar{\Sigma}_V'(M^2). \quad (2.1.2)
$$

The first term in the last expression of Eq. (2.1.1) represents the single-pole residue, which is closely related to on-shell production and decay of the unstable particle. The second term between the square brackets has no pole and can be expanded in powers of $p_V^2 - M^2$. The argument ω denotes the dependence on the other variables. After all, the unstable particle is always accompanied by other particles in the production and decay stages. For instance, consider the LEP1 reaction $e^+e^- \to \bar{f}f$. In the mapping $p_Z^2 \to M^2$ one can either keep $t = (p_{e^-} - p_f)^2 = -p_Z^2(1 - \cos\theta)/2$ fixed or $\cos\theta$. In the former mapping $\cos\theta_{\text{pole}}$ is obtained from the on-shell relation $\cos\theta_{\text{pole}} = 1 + 2t/M^2$, whereas in the latter mapping $t_{\text{pole}} = -M^2(1 - \cos\theta)/2$. It may be that a particular mapping leads to an unphysical point in the 'on-shell' phase space. In the present example t_{pole} will always be physical when $\cos\theta$ is kept fixed in the mapping. However, since $|\cos\theta_{\text{pole}}| > 1$ for $t < -\operatorname{Re} M^2$, it is clear that mapping fixed Mandelstam variables harbour the potential risk of producing such unphysical phase-space points.[1] This can have repercussions on the convergence of the pole-scheme expansion. Therefore we choose in our calculations only implementations that are free of unphysical on-shell phase-space points.

It should be noted that the mass and width of the W and Z bosons are usually defined in the so-called on-shell scheme:

$$M_V^2 - \bar{M}_V^2 + \operatorname{Re}\bar{\Sigma}_V(M_V^2) = 0,$$

$$Z_{\text{OS}}(M_V^2) = 1 + \operatorname{Re}\bar{\Sigma}'_V(M_V^2), \qquad M_V\Gamma_V = \frac{\operatorname{Im}\bar{\Sigma}_V(M_V^2)}{Z_{\text{OS}}(M_V^2)}. \tag{2.1.3}$$

Both schemes can be related according to (see e.g. Ref. [2]):

$$M^2 = (M_V^2 - iM_V\Gamma_V)\left[1 - \frac{\Gamma_V^2}{M_V^2} + \mathcal{O}\!\left(\frac{\Gamma_V^3}{M_V^3}\right)\right],$$

$$(p_V^2 - M^2)\,Z(M^2) = \left(p_V^2 - M_V^2 + ip_V^2\,\frac{\Gamma_V}{M_V}\right)\left[Z_{\text{OS}}(M_V^2) + \mathcal{O}(\alpha^2)\right]. \tag{2.1.4}$$

As we are aiming for $\mathcal{O}(\alpha)$ precision in our study, the differences between both schemes can be ignored. For the same reason $ip_V^2\Gamma_V/M_V$ can be replaced by $iM_V\Gamma_V$, since the difference only induces $\mathcal{O}(\alpha^2)$ corrections to the cross-sections.

The at present only workable approach for evaluating the RC to resonance-pair-production processes, like W-pair production, involves the so-called double-pole approximation (DPA). This approximation restricts the complete pole-scheme expansion to the term with the highest degree of resonance. In the case of W-pair production only the double-pole residues are hence considered. The intrinsic error associated with this procedure is $\alpha\Gamma_W/(\pi M_W) \lesssim 0.1\%$, except far off resonance, where the pole-scheme expansion cannot be viewed as an effective expansion in powers of Γ_V/M_V, and close to phase-space boundaries, where the DPA cannot be trusted to produce

---

[1] In the resonance region, $|p_Z^2 - M^2| \ll |M^2|$, the unphysical 'on-shell' phase-space points occur near the edge of the off-shell phase space, since $t < -\operatorname{Re} M^2$ requires $\cos\theta \approx -1$.
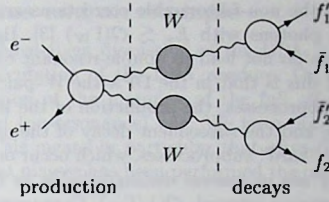
Figure 2-1. The generic structure of the factorizable W-pair contributions. The shaded circles indicate the Breit–Wigner resonances, whereas the open circles denote the Green functions for the production and decay subprocesses up to $\mathcal{O}(\alpha)$ precision.
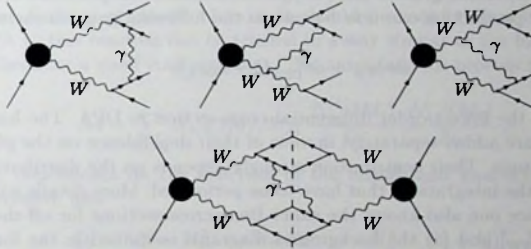
Figure 2-2. Examples for virtual (top) and real (bottom) non-factorizable corrections to W-pair production. The black circles denote the lowest-order Green functions for the production of the virtual W-boson pair.

the dominant contributions. In the latter situations the implementation dependence of the double-pole residues can lead to enhanced errors. Close to the nominal (on-shell) W-pair threshold, for instance, the intrinsic error is effectively enhanced by a factor $M_W/(\sqrt{s} - 2M_W)$. In view of this it is wise to apply the DPA only if the energy is several Γ_W above the threshold.

In the DPA one can identify two types of contributions. One type comprises all diagrams that are strictly reducible at both unstable W-boson lines (see Fig. 2-1). These corrections are therefore called factorizable and can be attributed unambiguously either to the production of the W-boson pair or to one of the subsequent decays. The second type consists of all diagrams in which the production and/or decay subprocesses are not independent and which therefore do not seem to have two overall W propagators as factors (see Fig. 2-2). We refer to these effects as non-factorizable

corrections.[2] In the DPA the non-factorizable corrections arise exclusively from the exchange or emission of photons with $E_\gamma \lesssim \mathcal{O}(\Gamma_W)$ [3]. Hard photons as well as massive-particle exchanges do not lead to double-resonant contributions. The physical picture behind all of this is that in the DPA the W-pair process can be viewed as consisting of several subprocesses: the production of the W-boson pair, the propagation of the W bosons, and the subsequent decay of the unstable W bosons. The production and decay are "hard" subprocesses, which occur on a relatively short time interval, $\mathcal{O}(1/M_W)$. They are in general distinguishable as they are separated by a relatively big propagation interval, $\mathcal{O}(1/\Gamma_W)$. Consequently, the corresponding amplitudes have certain factorization properties. The same holds for the hard subprocesses. The only way the various stages can be interconnected is via the radiation of soft photons with energy of $\mathcal{O}(\Gamma_W)$. These photons induce long-range interactions and thereby allow the various subprocesses to communicate with each other.

Within the DPA the generic form of the virtual and soft-photonic $\mathcal{O}(\alpha)$ RC to off-shell W-pair production can now be cast in the following gauge-invariant form:

$$do_{\mathrm{DPA}} = d\sigma^0_{\mathrm{DPA}}(1 + \delta_{\mathrm{DPA}}), \qquad (2.1.5)$$

where $d\sigma^0_{\mathrm{DPA}}$ is the lowest-order differential cross-section in DPA. The hard-photon effects in DPA are added separately, in view of their dependence on the phase-space of the hard photons. Their contribution strongly depends on the distribution that is studied, i.e. on the integrations that have to be performed. More details will be given in Sect. 2.2. Since one also knows the exact Born cross-sections for off-shell W-pair production $[d\sigma^0_{\mathrm{WW}}]$ and for the background diagrams contained in the four-fermion process (1.1.4) $[d\sigma^0_{\mathrm{bkg}}]$, one can also add those to the above expression. The final gauge-invariant result up to $\mathcal{O}(\alpha)$ or, equivalently, $\mathcal{O}(\Gamma_W/M_W)$ precision reads

$$d\sigma = d\sigma^0_{\mathrm{DPA}}(1 + \delta_{\mathrm{DPA}}) + (d\sigma^0_{\mathrm{WW}} - d\sigma^0_{\mathrm{DPA}}) + d\sigma^0_{\mathrm{bkg}}. \qquad (2.1.6)$$

The purpose of this chapter is to give a detailed discussion of δ_{DPA}, i.e. the $\mathcal{O}(\alpha)$ corrections to $d\sigma^0_{\mathrm{DPA}}$. In order to make contact with experimental cross-sections the other terms, $d\sigma^0_{\mathrm{WW}} - d\sigma^0_{\mathrm{DPA}}$ and $d\sigma^0_{\mathrm{bkg}}$, are also relevant. The full gauge-invariant Born term, including all diagrams, has been discussed in the literature [4]. It has also been compared with the non-gauge-invariant cross-section $d\sigma^0_{\mathrm{WW}}$, calculated in the unitary gauge. In many cases $d\sigma^0_{\mathrm{WW}}$ gives numerically a good approximation to the complete Born cross-section, at least for energies below 1 TeV. Moreover, in practice it is often extracted from the data in the experimental analyses. Therefore it is useful to present a numerical comparison between $d\sigma^0_{\mathrm{WW}}$ and $d\sigma^0_{\mathrm{DPA}}$. This will be done in Sect. 2.1.2.

---

[2]It should be noted that the exact split-up between factorizable and non-factorizable radiative corrections requires a precise (gauge-invariant) definition. We will come back to this point in Sect. 2.2.

2.1.1 Conventions and an example

As is clear from the above-given discussion of the DPA, a specific prescription has to be given for the calculation of the DPA residues. Or, in other words, we have to fix the implementation of the mapping of the full off-shell phase space on the kinematically restricted (on-resonance) one. We have opted to always extract *pure double-pole residues*. This means in particular that after the integration over decay kinematics and invariant masses has been performed the on-shell cross-section should be recovered.

In the rest of this subsection we will explain our method in more detail by applying it to the lowest-order reaction

$$e^+(q_1)\, e^-(q_2) \to W^+(p_1)\, W^-(p_2) \to \bar{f}_1(k_1) f_1'(k_1')\, f_2(k_2) \bar{f}_2'(k_2'), \qquad (2.1.7)$$

involving only those diagrams that contain as factors the Breit–Wigner propagators for the W^+ and W^- bosons. Here $\bar{f}_1$ and f_1' are the decay products of the W^+ boson, and f_2 and $\bar{f}_2'$ those of the W^- boson. It should be noted that a large part of the RC in DPA to this reaction can be treated in a way similar to the lowest-order case, which is therefore a good starting point. The amplitude for process (2.1.7) takes the form

$$\mathcal{M} = \sum_{\lambda_1,\lambda_2} \Pi_{\lambda_1\lambda_2}(M_1, M_2)\, \frac{\Delta_{\lambda_1}^{(+)}(M_1)}{D_1}\, \frac{\Delta_{\lambda_2}^{(-)}(M_2)}{D_2}\,, \qquad (2.1.8)$$

where any dependence on the helicities of the initial- and final-state fermions has been suppressed, and

$$D_i = M_i^2 - M_W^2 + iM_W\Gamma_W, \qquad M_i^2 = (k_i + k_i')^2. \qquad (2.1.9)$$

The quantities $\Delta_{\lambda_1}^{(+)}(M_1)$ and $\Delta_{\lambda_2}^{(-)}(M_2)$ are the off-shell W-decay amplitudes for specific spin-polarization states λ_1 (for the W^+) and λ_2 (for the W^-), with $\lambda_i = (-1, 0, +1)$. The off-shell W-pair production amplitude $\Pi_{\lambda_1\lambda_2}(M_1, M_2)$ depends on the invariant fermion-pair masses M_i and on the polarizations λ_i of the virtual W bosons. In the limit $M_i \to M_W$ the amplitudes Π and $\Delta^{(\pm)}$ go over into the on-shell production and decay amplitudes.

The choice of the polarization states labelled by λ_i is in principle free. The amplitude $\mathcal{M}$ is obtained by summing over the polarizations and is therefore independent of such a specific choice. As it turns out, it will be convenient to use different choices in different parts of the RC calculation (see Apps. A and B).

In the cross-section the above factorization leads to

$$\sum_{\text{fermion helicities}} |\mathcal{M}|^2 = \sum_{\lambda_1,\lambda_2,\lambda_1',\lambda_2'} \mathcal{P}_{[\lambda_1\lambda_2][\lambda_1'\lambda_2']}(M_1, M_2)\, \frac{\mathcal{D}_{\lambda_1\lambda_1'}(M_1)}{|D_1|^2}\, \frac{\mathcal{D}_{\lambda_2\lambda_2'}(M_2)}{|D_2|^2}. \qquad (2.1.10)$$

In Eq. (2.1.10) the production part is given by a 9×9 density matrix

$$\mathcal{P}_{[\lambda_1\lambda_2][\lambda_1'\lambda_2']}(M_1, M_2) = \sum_{e^\pm \text{ helicities}} \Pi_{\lambda_1\lambda_2}(M_1, M_2)\, \Pi_{\lambda_1'\lambda_2'}^*(M_1, M_2). \qquad (2.1.11)$$

Similarly the decay part is governed by 3×3 density matrices

$$\mathcal{D}_{\lambda_i \lambda_i'}(M_i) \;=\; \sum_{\text{fermion helicities}} \Delta_{\lambda_i}(M_i)\, \Delta_{\lambda_i'}^*(M_i), \qquad (2.1.12)$$

where the summation is performed over the helicities of the final-state fermions.

It is clear that Eq. (2.1.11) is closely related to the absolute square of the matrix element for stable unpolarized W-pair production. In that case the cross-section contains the trace of the above density matrix

$$\mathbf{Tr}\; \mathcal{P}(M_W, M_W) = \sum_{\lambda_1, \lambda_2} \mathcal{P}_{[\lambda_1 \lambda_2][\lambda_1 \lambda_2]}(M_W, M_W) \;=\; \sum_{\text{all polarizations}} |\Pi_{\lambda_1 \lambda_2} (\cdots)|^2.$$

$$(2.1.13)$$

The decay of an unpolarized on-shell W boson is determined by

$$\mathbf{Tr}\; \mathcal{D}(M_W) = \sum_{\lambda_i} \mathcal{D}_{\lambda_i \lambda_i}(M_W) \;=\; \sum_{\text{all polarizations}} |\Delta_{\lambda_i}(M_W)|^2. \qquad (2.1.14)$$

Note, however, that also the off-diagonal elements of $\mathcal{P}(M_W, M_W)$ and $\mathcal{D}(M_W)$ are required for determining Eq. (2.1.10) in the limit $M_i \to M_W$.

As a next step it is useful to describe the kinematics of process (2.1.7) in a factorized way, i.e. using the invariant masses M_1 and M_2 of the fermion pairs. The differential cross-section takes the form

$$d\sigma = \frac{1}{2s} \sum |\mathcal{M}|^2 \, d\Gamma_{4f} = \frac{1}{2s} \sum |\mathcal{M}|^2 \, d\Gamma_{\text{pr}} \cdot d\Gamma_{\text{dec}}^+ \cdot d\Gamma_{\text{dec}}^- \cdot \frac{dM_1^2}{2\pi} \cdot \frac{dM_2^2}{2\pi}, \qquad (2.1.15)$$

where $d\Gamma_{4f}$ indicates the complete four-fermion phase-space factor and $s = (q_1 + q_2)^2$ the centre-of-mass energy squared. The phase-space factors for the production and decay subprocesses, $d\Gamma_{\text{pr}}$ and $d\Gamma_{\text{dec}}^\pm$, read

$$d\Gamma_{\text{pr}} = \frac{1}{(2\pi)^2}\, \delta(q_1 + q_2 - p_1 - p_2)\, \frac{d\vec{p}_1}{2p_{10}}\, \frac{d\vec{p}_2}{2p_{20}},$$

$$d\Gamma_{\text{dec}}^+ = \frac{1}{(2\pi)^2}\, \delta(p_1 - k_1 - k_1')\, \frac{d\vec{k}_1}{2k_{10}}\, \frac{d\vec{k}_1'}{2k_{10}'},$$

$$d\Gamma_{\text{dec}}^- = \frac{1}{(2\pi)^2}\, \delta(p_2 - k_2 - k_2')\, \frac{d\vec{k}_2}{2k_{20}}\, \frac{d\vec{k}_2'}{2k_{20}'}. \qquad (2.1.16)$$

When the factorized form for $\sum |\mathcal{M}|^2$ is inserted one obtains

$$d\sigma = \frac{1}{2s} \sum_{\lambda_1, \lambda_2, \lambda_1', \lambda_2'} \mathcal{P}_{[\lambda_1 \lambda_2][\lambda_1' \lambda_2']}(M_1, M_2)\, d\Gamma_{\text{pr}} \times \mathcal{D}_{\lambda_1 \lambda_1'}(M_1)\, d\Gamma_{\text{dec}}^+ \times \mathcal{D}_{\lambda_2 \lambda_2'}(M_2)\, d\Gamma_{\text{dec}}^- \times$$

$$\times \frac{1}{2\pi} \frac{dM_1^2}{|D_1|^2} \times \frac{1}{2\pi} \frac{dM_2^2}{|D_2|^2}. \qquad (2.1.17)$$

As mentioned before, the definition of the DPA residues is not unique. To define them we first organize the four-fermion kinematics in a special way. In the laboratory

(LAB) frame we write the four-fermion phase space in terms of a solid production angle for the W^+ boson and solid decay angles for two of the final-state fermions, one originating from the W^+ boson and one from the W^- boson. These angles will be kept fixed at any time during the process of defining the DPA residues. For later use we explicitly write down our conventions for the momenta, invariants, and phase-space factors. The momenta read

$$q_1 = E(1, \sin\theta, 0, \cos\theta), \qquad q_2 = E(1, -\sin\theta, 0, -\cos\theta),$$

$$p_1 = E_1(1, 0, 0, \frac{p}{E_1}), \qquad p_2 = E_2(1, 0, 0, -\frac{p}{E_2}),$$

$$k_1 = E_3(1, \sin\theta_3\cos\phi_3, \sin\theta_3\sin\phi_3, \cos\theta_3),$$

$$k_2 = E_4(1, \sin\theta_4\cos\phi_4, \sin\theta_4\sin\phi_4, -\cos\theta_4), \qquad (2.1.18)$$

with

$$E = \frac{1}{2}\sqrt{s}, \qquad p = \frac{1}{2\sqrt{s}}\lambda^{1/2}(\sqrt{s}, M_1, M_2),$$

$$E_{1,2} = \frac{1}{2\sqrt{s}}(s + M_{1,2}^2 - M_{2,1}^2), \qquad E_{3,4} = \frac{1}{2}\frac{M_{1,2}^2}{E_{1,2} - p\cos\theta_{3,4}},$$

$$\lambda(\sqrt{s}, M_1, M_2) = [s - (M_1 + M_2)^2][s - (M_1 - M_2)^2]. \qquad (2.1.19)$$

The momenta of the other final-state particles follow from $k_i' = p_i - k_i$. The masses of the fermions are neglected whenever possible. This, hence, excludes situations in which the fermion masses are needed to regularize singularities from the radiation of collinear photons. The Mandelstam invariants are defined as

$$s = (q_1 + q_2)^2, \qquad t = (p_1 - q_1)^2, \qquad u = (p_2 - q_1)^2 = M_1^2 + M_2^2 - s - t. \quad (2.1.20)$$

From all this it should be clear that the invariant masses M_i only appear explicitly in the energies and velocities of the W bosons and their decay products.

In this notation the production phase-space factor reads

$$d\Gamma_{\mathrm{pr}} = \frac{1}{8\pi}\frac{p}{E}\frac{d\Omega}{4\pi}, \qquad (2.1.21)$$

with $d\Omega$ denoting the solid angle between the W^+ boson and the positron. The decay phase-space factors are given by

$$d\Gamma_{\mathrm{dec}}^+ = \frac{1}{8\pi}\frac{M_1^2}{(E_1 - p\cos\theta_3)^2}\frac{d\Omega_3}{4\pi} \qquad (2.1.22)$$

and a similar expression for $d\Gamma_{\mathrm{dec}}^-$. Here $d\Omega_3$ denotes the solid decay angle between the W^+ boson and $\bar{f}_1$.

Our choice of the DPA residues amounts to a two-step procedure for fixing the invariant masses M_1 and M_2, appearing in the four-fermion kinematics and the amplitudes $\Pi(M_1, M_2)$, $\Delta^{(+)}(M_1)$, and $\Delta^{(-)}(M_2)$. The first step is the replacement

$$M_i^2 \to M_W^2 - iM_W\Gamma_W, \qquad (2.1.23)$$

i.e. the residue is taken at the Breit–Wigner poles [see discussion below Eq. (2.1.4)].
Note that this replacement, of course, does not apply to the Breit–Wigner resonances
themselves. The phase-space conventions displayed above fix our choice for the im-
plementation. The solid angles are kept fixed, whereas the energies and velocities
become complex [as can be seen from Eq. (2.1.19)]. Note that the so-obtained set of
momenta preserves momentum conservation. This protects the DPA residues against
effectively crossing the four-fermion phase-space boundaries, which might lead to a
reduced quality of the DPA.

For practical purposes, however, it is messy to evaluate the $\mathcal{O}(\alpha)$ RC the
amplitudes $\Pi(M_1, M_2)$, $\Delta^{(+)}(M_1)$, and $\Delta^{(-)}(M_2)$ at the complex Breit values.
This would require the analytic continuation of the one-loop expression to the second
Riemann sheet. As such we approximate the DPA residues by using

$$M_i = M_W. \tag{2.1.24}$$

The error introduced by the *on-shell* approximation (2.1.24) is of order $\mathcal{O}(\Gamma_W/M_W)$.
When this error comes on top of the $\mathcal{O}(\alpha)$ RC it can be neglected, since terms
of $\mathcal{O}(\alpha\Gamma_W/M_W)$ are neglected anyhow in the DPA approach. By having fixed the
solid angles in the mapping, the on-shell phase-space points defined with Eq. (2.1.24)
remain physical. From this point of view it is a sound implementation procedure.
A procedure that fixes Mandelstam variables in the mapping involves phase-space
regions where it may be regarded as being unsound, as has been indicated in the
example below Eq. (2.1.2). In such cases it is preferable to set the cross-section to
zero rather than evaluating it for unphysical values.

The thus-obtained amplitudes become (gauge-invariant) on-shell ones, whereas
the four-fermion phase space is reduced to the phase space of two fermion pairs with
invariant masses M_W. Since the DPA forces us to only consider collider energies that
are several Γ_W above the on-shell W-pair threshold, the W-boson velocities stay well
defined in our approximation. The only place where the invariant masses M_i still
show up is in the Breit–Wigner resonances D_i, which can be pulled out as overall
factors. The integration over the Breit–Wigner resonances need not be restricted to
the physical region $M_i > 0$, $M_1 + M_2 < \sqrt{s}$. Since the DPA is anyhow not valid far
off resonance, we can just as well integrate over the full range of the distributions,
$(-\infty, +\infty)$, which guarantees that the on-shell results are recovered when the decay
kinematics and invariant masses are integrated out. This means that the following
integral will be used:

$$\frac{1}{2\pi} \int_{-\infty}^{\infty} dM_i^2 \frac{1}{|D_i|^2} = \frac{1}{2M_W \Gamma_W}. \tag{2.1.25}$$

So far we have explained how to calculate the canonical multidifferential cross-
section $d\sigma/(d\Omega d\Omega_3 d\Omega_4 dM_1^2 dM_2^2)$ in the DPA. In case one needs a multidifferential
cross-section in other variables one should relate that cross-section to the canonical
one by means of a Jacobian. In order to obtain this Jacobian the off-shell kinematical
relations (2.1.18) and (2.1.19) should be used.

2.1.2   Numerical comparision of Born cross-sections

In order to have an idea of the differences between the exact Born cross-section $d\sigma^0_{\mathrm{WW}}$, corresponding to process (1.1.3), and its DPA limit $d\sigma^0_{\mathrm{DPA}}$, we now present a brief numerical comparison.

First we discuss the set of parameters used to produce the plots throughout this chapter. To facilitate cross-checks with the results presented in the literature, we adopt the LEP2 input-parameter scheme advocated in Ref. [5]. In this scheme the Fermi constant G_μ, the fine-structure constant α, and the masses of the light fermions[3] and W, Z bosons are the independent input parameters. The mass of the top quark, m_t, follows from the Standard Model prediction for muon decay

$$G_\mu = \frac{\alpha\pi}{\sqrt{2}M_W^2(1 - M_W^2/M_Z^2)}\frac{1}{1 - \Delta r}. \qquad (2.1.26)$$

The quantity Δr denotes the loop corrections to muon decay. It is zero at tree level, but when loop corrections are included it depends on the input parameters as well as on m_t, the Higgs-boson mass M_H, and the strong coupling α_{S}.[4]

In analogy to Ref. [5] we use in our numerical evaluations the following set of (slightly outdated) input parameters:

$$\alpha = 1/137.0359895, \qquad G_\mu = 1.16639 \times 10^{-5}\,\mathrm{GeV}^{-2},$$
$$M_Z = 91.1884\,\mathrm{GeV}, \qquad M_W = 80.26\,\mathrm{GeV},$$

$$m_e = 0.51099906\,\mathrm{MeV}, \qquad m_\mu = 105.658389\,\mathrm{MeV}, \qquad m_\tau = 1.7771\,\mathrm{GeV},$$

$$m_u = 47\,\mathrm{MeV}, \qquad m_d = 47\,\mathrm{MeV},$$
$$m_s = 150\,\mathrm{MeV}, \qquad m_c = 1.55\,\mathrm{GeV},$$
$$m_b = 4.7\,\mathrm{GeV}, \qquad\qquad\qquad\qquad (2.1.27)$$

and choose

$$M_H = 300\,\mathrm{GeV}, \qquad \alpha_{\mathrm{S}}(M_Z^2) = 0.123. \qquad (2.1.28)$$

The solution of Eq. (2.1.26), using a calculation of Δr that contains all the known higher-order effects, gives the value for the top-quark mass [5]

$$m_t = 165.26\,\mathrm{GeV}. \qquad (2.1.29)$$

As was already mentioned in Sect. 1.1, the use of G_μ instead of α in the lowest-order cross-sections very often reduces the size of the one-loop non-photonic RC considerably. This so-called G_μ-parametrization consists in the replacement

$$d\sigma = d\sigma^0(1 + \delta^{\text{1-loop}}) \quad \rightarrow \quad d\sigma^0\frac{(1 + \delta^{\text{1-loop}} - n\Delta r^{\text{1-loop}})}{(1 - \Delta r)^n} \equiv d\bar\sigma^0(1 + \bar\delta^{\text{1-loop}}), \quad (2.1.30)$$

---

[3]The masses of the light quarks are adjusted in such a way that the experimentally measured hadronic vacuum polarization is reproduced.

[4]The so-obtained top-quark mass will become α_{S}- and M_H-dependent. It can be confronted with the direct measurements at Fermilab and the indirect ones from LEP in order to obtain indirect information on M_H.

where $d\sigma^0 \propto \alpha^n$ and according to Eq. (2.1.26) $d\bar{\sigma}^0 \propto G_\mu^n$. The results presented in this chapter are all calculated in this parametrization.

Another important parameter featuring in our calculations is the width of the W boson. As explained below Eq. (2.1.4), we will use the calculated on-shell width. Since we want the Breit–Wigner resonances to be as close to reality as possible, we will always use the $\mathcal{O}(\alpha)$- and $\mathcal{O}(\alpha_S)$-corrected width Γ_W, regardless of the fact that we sometimes consider lowest-order distributions. Using the above set of input parameters we find in the G_μ-parametrization

$$\Gamma_W = 2.08174\,\text{GeV}. \qquad (2.1.31)$$

For future use we note that the lowest-order W-boson width in this parametrization reads $\Gamma_W^0 = 2.03540\,\text{GeV}$. It is also relevant to stress that the $\mathcal{O}(\alpha)$ corrections to the leptonic partial widths $\Gamma_{W \to \ell \nu_\ell}$ are small and negative ($\sim -0.3\%$). The $\mathcal{O}(\alpha_S)$ corrections to the hadronic partial widths are positive, leading to the positive overall correction to the total W-boson width.

Having fixed the input, we now compare $d\sigma_{WW}^0$ and $d\sigma_{DPA}^0$ for the total cross-section σ_{tot} (in Fig. 2-3) and the differential cross-section $d\sigma/d\cos\theta$ (in Fig. 2-4), where θ is the polar angle between the W^+ boson and the positron in the LAB frame [see Eq. (2.1.18)]. The latter distribution is given for $2E = 184\,\text{GeV}$, whereas σ_{tot} is presented for a range of LEP2 energies. We select one particular purely leptonic final state, $\mu^+ \nu_\mu \tau^- \bar{\nu}_\tau$. In view of the massless treatment of the final-state fermions and the universal lowest-order interaction between the fermions and the W bosons, the results for the various final states can be obtained by multiplying the purely leptonic result by a factor $N_C^{f_1} |V_{f_1' f_1}|^2 N_C^{f_2} |V_{f_2' f_2}|^2$. Here $V_{f_i' f_i}$ is the mixing matrix and $N_C^{f_i}$ the colour factor. For leptons only $V_{\nu_\ell \ell} = 1$ is non-vanishing and $N_C^\ell = 1$.

We consider the following four cases:

i) The calculation for stable W bosons, multiplied by the branching ratio $(\Gamma_{W \to \ell \nu_\ell}^0 / \Gamma_W^0)^2$.

ii) The DPA calculation, where in Eq. (2.1.17) the on-shell approximation is applied to both the matrix elements and the four-fermion phase space. The M_i^2 integrations over the Breit–Wigner resonances are extended to the full range $(-\infty, +\infty)$, i.e. Eq. (2.1.25) is used.

iii) The calculation where the matrix element (2.1.8) is on-shell, but the four-fermion phase space in Eq. (2.1.17) is not. The M_i^2 integrations are performed in the physical region.

iv) The off-shell calculation according to Eq. (2.1.17), with the M_i^2 integrations performed in the physical region. This corresponds to $d\sigma_{WW}^0$.

In cases ii), iii), and iv) the W-boson propagators contain the width Γ_W, as given in Eq. (2.1.31). The matrix element in case iv) is not gauge-invariant, it is calculated in the unitary gauge.
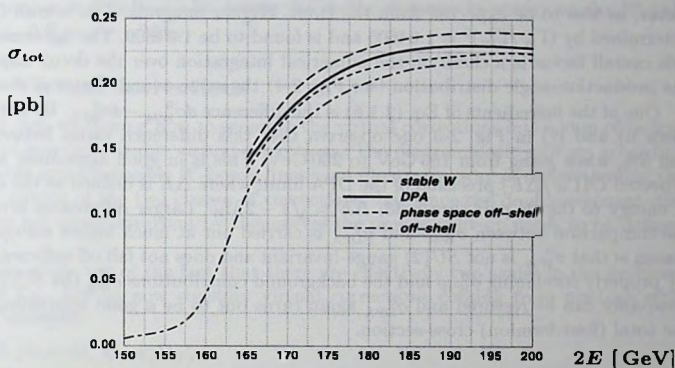
Figure 2-3. Comparison of different Born approximations for the total cross-section σ_{tot} as a function of the accelerator energy. The four curves correspond to the cases i) – iv) introduced in the text.
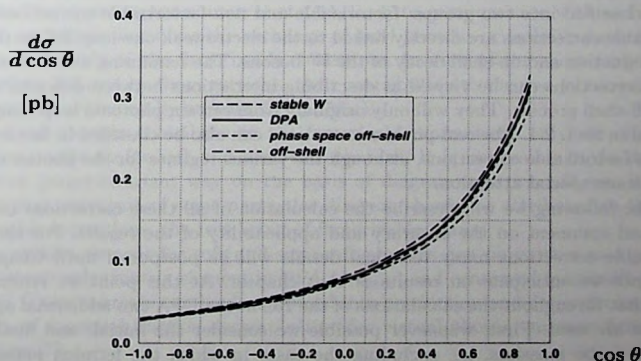

Figure 2-4. The same curves as in the previous plot, this time for the lowest-order production-angle distribution $d\sigma/d\cos\theta$ at $2E = 184\,\text{GeV}$.

For the total cross-section (see Fig. 2-3) cases i) and ii) differ by a fixed overall factor, as was to be expected from the Breit–Wigner integrals. The overall factor is determined by $(\Gamma_W/\Gamma_W^0)^2 = 1.04605$ and is found to be 1.04609. The agreement with this overall factor is a check on the numerical integration over the decay angles. For the production-angle distribution (see Fig. 2-4) the same overall factor is observed.

One of the ingredients of Eq. (2.1.6) is the difference $d\sigma_{WW}^0 - d\sigma_{\mathrm{DPA}}^0$. By comparing cases ii) and iv) in Fig. 2-3 one observes that this difference varies between 18% and 5%, when going from 165 GeV to 200 GeV. This is in good agreement with the expected $\mathcal{O}(\Gamma_W/\Delta E)$ precision of the DPA limit, where ΔE is defined as the distance in energy to the W-pair threshold, $\Delta E = \sqrt{s} - 2M_W$. Larger differences arise when the comparison between σ_{WW}^0 and σ_{DPA}^0 is carried out at much higher energies. The reason is that σ_{WW}^0 is not $SU(2)$ gauge-invariant and does not fall off so fast. By properly combining σ_{WW}^0 and the background contributions σ_{bkg}^0 the full gauge invariance can be restored and σ_{DPA}^0 again turns out to be a good approximation to the total (four-fermion) cross-section.

2.2   Radiative corrections in the DPA approximation

In this section we discuss the complete $\mathcal{O}(\alpha)$ RC to process (2.1.7) in the context of the DPA. As mentioned in Sect. 2.1, the most economic way of calculating the RC up to $\mathcal{O}(\alpha)$ precision involves the DPA. In this approximation all virtual corrections can be classified into two groups: factorizable and non-factorizable corrections. The factorizable corrections are directly linked to the electroweak one-loop RC to the on-shell production and on-shell decay of the W bosons. The remaining non-factorizable virtual corrections can be viewed as describing interactions between different stages of the off-shell process. They will only originate from certain photonic loop diagrams, as stated in Sect. 2.1. The real-photon corrections can also be classified in factorizable and non-factorizable corrections, although the various regimes for the photon energy require some special attention.

In the following we will describe the calculation of all these corrections in more detail and comment on the accuracy and applicability of the results. For the non-factorizable corrections many technical details will be postponed until Chapter 4. Sometimes we anticipate on results of that chapter. At this point we remind the reader that throughout the calculations of the RC in the DPA two additional approximations are used. First, whenever possible we consider the initial- and final-state fermions to be massless, i.e. excluding the cases in which the fermion masses are needed to regularize singularities from the radiation of collinear photons. The error of this approximation is at most $\mathcal{O}(\alpha\, m_\tau/M_W)$ or $\mathcal{O}(\alpha\, |V_{cb}|\, m_b/M_W)$, which is beyond the accuracy of our calculation. Second, we assume that the accelerator energy is sufficiently far (read: several Γ_W) above the threshold for on-shell W-pair production. Close to threshold the DPA cannot be trusted to produce the dominant contributions

and therefore our approach breaks down. The accuracy of this "far-from-threshold" approximation is $\mathcal{O}(\alpha \Gamma_W / \Delta E)$, where ΔE is the distance in energy to the W-pair threshold, $\Delta E = \sqrt{s} - 2M_W$

2.2.1 Virtual corrections

As a first step we discuss how to separate the virtual corrections into a sum of factorizable and non-factorizable virtual corrections. The diagrammatic split-up according to reducible and irreducible W-boson lines is an illustrative way of understanding the different nature of the two classes of corrections, but since the double-resonant diagrams are not gauge-invariant by themselves the precise split-up needs to be defined properly.

We can make use of the fact that there are effectively two scales in the problem: M_W and Γ_W. Let us now consider virtual corrections coming from photons with different energies:

- soft photons, $E_\gamma \ll \Gamma_W$,

- semi-soft photons, $E_\gamma = \mathcal{O}(\Gamma_W)$,

- hard photons, $\Gamma_W \ll E_\gamma = \mathcal{O}(M_W)$.

Only soft and semi-soft photons contribute to both factorizable and non-factorizable corrections. The latter being defined to describe interactions between different stages of the off-shell process. The reason for this is that only these photons can induce relatively long-range interactions and thereby allow the various subprocesses, which are separated by a propagation interval of $\mathcal{O}(1/\Gamma_W)$, to communicate with each other. Virtual corrections involving the exchange of hard photons or massive particles contribute exclusively to the factorizable corrections. In view of the short range of the interactions induced by these particles, their contribution to the non-factorizable corrections are suppressed by at least $\mathcal{O}(\Gamma_W/M_W)$.

As hard photons contribute to the factorizable corrections only, we only need to define a split-up for soft and semi-soft photons. It is impossible to do this in a consistent gauge-invariant way on the basis of diagrams. As we will see, it might happen that only part of some particular diagram should be attributed to the non-factorizable corrections, the rest being of factorizable nature.

The matrix element for soft and semi-soft photons can be written as a product of the lowest-order matrix element in DPA ($\mathcal{M}_{DPA}^0$) and conserved (semi)soft-photon currents. These currents can be decomposed into production and decay currents with the help of a partial-fraction decomposition for virtual-photon emission from a W-boson line [7]:

$$\frac{1}{[p^2 - M^2][p^2 + 2pk - M^2 + io]} = \frac{1}{2pk + io}\left(\frac{1}{p^2 - M^2} - \frac{1}{p^2 + 2pk - M^2 + io}\right)$$

$$= \frac{1}{2pk + io}\left(\frac{1}{D} - \frac{1}{D + 2pk + io}\right). \tag{2.2.1}$$
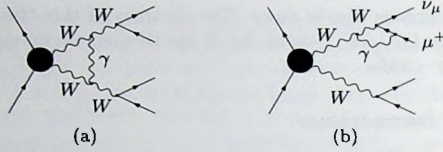
Figure 2-5. Examples of one-loop diagrams that contribute to both factorizable and non-factorizable corrections.

Here $M^2 = M_W^2 - iM_W\Gamma_W$, k is the loop momentum of the exchanged photon, $p + k$ is the momentum of the W boson inside the integral, and p is the momentum of the W boson outside the integral. The infinitesimal imaginary part io is needed to ensure a proper incorporation of causality. In this way one obtains a sum of two resonant W-boson propagators multiplied by an ordinary on-shell current factor. This decomposition allows a gauge-invariant split-up of the matrix element in terms of one contribution where the photon is effectively emitted from the production part, and two others where the photon is effectively emitted from one of the two decay parts. The squares of the three contributions can be identified as factorizable corrections, whereas the interference terms are of non-factorizable nature.

In order to illustrate our method, we explicitly apply it to two special one-loop contributions (see Fig. 2-5). The first one [diagram (a)] is the so-called Coulomb graph, involving photon exchange between the two W bosons. The corresponding semi-soft matrix element reads

$$
\begin{aligned}
\mathcal{M}_a &= ie^2 \mathcal{M}_{\text{DPA}}^0 \int \frac{d^4k}{(2\pi)^4[k^2 + io]} \frac{4p_1 p_2}{[D_1 + 2kp_1 + io][D_2 - 2kp_2 + io]} \\
&= ie^2 \mathcal{M}_{\text{DPA}}^0 \int \frac{d^4k}{(2\pi)^4[k^2 + io]} \frac{4p_1 p_2}{[2kp_1 + io][-2kp_2 + io]} \left\{ 1 - \frac{D_1}{D_1 + 2kp_1 + io} \right. \\
&\left. - \frac{D_2}{D_2 - 2kp_2 + io} + \frac{D_1 D_2}{[D_1 + 2kp_1 + io][D_2 - 2kp_2 + io]} \right\}.
\end{aligned}
\tag{2.2.2}
$$

The first term in the last expression gives rise to a factorizable (on-shell) contribution to the production stage, whereas the other three terms are counted as non-factorizable contributions. These three terms are classified as (prod × dec$^+$), (prod × dec$^-$), and (dec$^+$ × dec$^-$), respectively. In other words, the Coulomb graph contributes both to the usual Coulomb effect in on-shell W-pair production and to a non-factorizable part. For the photonic interaction between the W^+ boson and its μ^+ decay product [diagram (b)] we obtain

$$
\begin{aligned}
\mathcal{M}_b &= -ie^2 \mathcal{M}_{\text{DPA}}^0 \int \frac{d^4k}{(2\pi)^4[k^2 + io]} \frac{4p_1 k_1}{[2kk_1 + io][D_1 + 2kp_1 + io]} \\
&= -ie^2 \mathcal{M}_{\text{DPA}}^0 \int \frac{d^4k}{(2\pi)^4[k^2 + io]} \frac{4p_1 k_1}{[2kp_1 + io][2kk_1 + io]} \left\{ 1 - \frac{D_1}{D_1 + 2kp_1 + io} \right\}.
\end{aligned}
\tag{2.2.3}
$$

Again the first term is a factorizable contribution, belonging to the W^+ decay stage, whereas the second term is a non-factorizable contribution of the type (prod × dec$^+$). Some other examples of the split-up can be found in Ref. [8]. As is clear from these examples, the non-factorizable contributions always involve the Breit–Wigner ratios $D_i/(D_i \pm 2kp_i)$, which effectively remove the overall W propagator $1/D_i$. The more energetic the exchanged photon is, the more suppressed such a ratio will be in the vicinity of the M_i^2 resonance. In fact, for $k_0 > \Lambda$ the non-factorizable contributions are suppressed by $\mathcal{O}(M_W \Gamma_W/[E\Lambda])$ (see App. C).

Every one-loop diagram with a semi-soft photon can be treated in this way. By collecting all terms that contain the ratios $D_i/[D_i \pm 2kp_i]$ the formula for non-factorizable corrections is obtained. As one can see explicitly below, this expression is gauge-invariant. Since the expression contains those diagrams where irreducible W-boson lines are present, it can be viewed as a gauge-invariant extension of the set of W-irreducible diagrams.

The so-defined non-factorizable corrections read

$$\mathcal{M}_{\mathrm{nf}}^{\mathrm{virt}} = i\mathcal{M}_{\mathrm{DPA}}^0 \int \frac{d^4k}{(2\pi)^4[k^2+io]}\Big[(\mathcal{J}_0^\mu+\mathcal{J}_\oplus^\mu)\mathcal{J}_{+,\mu}+(\mathcal{J}_0^\mu+\mathcal{J}_\ominus^\mu)\mathcal{J}_{-,\mu}+\mathcal{J}_+^\mu\mathcal{J}_{-,\mu}\Big]. \quad (2.2.4)$$

The currents are given by

$$\mathcal{J}_0^\mu = e\left[\frac{p_1^\mu}{kp_1+io} + \frac{p_2^\mu}{-kp_2+io}\right],$$

$$\mathcal{J}_\oplus^\mu = -e\left[\frac{q_1^\mu}{kq_1+io} - \frac{q_2^\mu}{kq_2+io}\right], \quad \mathcal{J}_\ominus^\mu = +e\left[\frac{q_1^\mu}{-kq_1+io} - \frac{q_2^\mu}{-kq_2+io}\right] \quad (2.2.5)$$

for photon emission from the production stage of the process, and

$$\mathcal{J}_+^\mu = -e\left[\frac{p_1^\mu}{kp_1+io} + Q_{f_1}\frac{k_1^\mu}{kk_1+io} - Q_{f_1'}\frac{k_1'^\mu}{kk_1'+io}\right]\frac{D_1}{D_1+2kp_1},$$

$$\mathcal{J}_-^\mu = -e\left[\frac{p_2^\mu}{-kp_2+io} + Q_{f_2}\frac{k_2^\mu}{-kk_2+io} - Q_{f_2'}\frac{k_2'^\mu}{-kk_2'+io}\right]\frac{D_2}{D_2-2kp_2} \quad (2.2.6)$$

for photon emission from the decay stages of the process. Here Q_f stands for the charge of fermion f in units of e. After having defined the gauge-invariant currents, the $+io$ terms can be dropped from D_1+2kp_1 and D_2-2kp_2, since $\mathrm{Im}\, D_i > 0$. Note the difference in the sign of the io parts appearing in the currents $\mathcal{J}_\ominus$ and $\mathcal{J}_\oplus$. These signs actually determine which interference terms give rise to a non-vanishing non-factorizable contribution after virtual and real-photon corrections have been added. As can be seen from Eq. (2.2.3), in the upper hemisphere of the complex k_0 plane there is only one pole: the so-called 'photon pole', originating from the photon propagator $1/[k^2+io]$. When virtual and real-photon corrections are combined, such a non-factorizable contribution will vanish [3]. For the Coulomb graph, Eq. (2.2.2), this is not the case, as also poles from the other propagators are present in both hemispheres. As

a result of such considerations only a very limited subset of 'final-state' interferences survives [6, 8]: the virtual corrections corresponding to Figs. 2-2 and 2-5(a) as well as the associated real-photon corrections. In Chapter 4 more details on the non-factorizable corrections can be found.

The virtual factorizable corrections consist of all hard contributions and the above-indicated part of the semi-soft ones. The so-defined factorizable corrections have the nice feature that they can be expressed in terms of corrections to on-shell subprocesses, i.e. the production of two on-shell W bosons and their subsequent on-shell decays. The corresponding matrix element can be expressed in the same way as described in Sect. 2.1:

$$\mathcal{M}_{\text{fact}}^{\text{virt}} = \sum_{\lambda_1, \lambda_2} \Pi_{\lambda_1 \lambda_2}(M_1, M_2) \, \frac{\Delta_{\lambda_1}^{(+)}(M_1)}{D_1} \, \frac{\Delta_{\lambda_2}^{(-)}(M_2)}{D_2}. \tag{2.2.7}$$

Here two of the amplitudes are taken at lowest order, whereas the remaining one contains all possible one-loop contributions, including the W wave-function factors that appear in Eq. (2.1.1). In this way the well-known on-shell RC to the production and decay of pairs of W bosons [9]–[12] appear as basic building blocks of the factorizable corrections.[5] In the semi-soft limit the virtual factorizable corrections to the production stage, contained in Π, will cancel against the corresponding real-photon corrections. Non-vanishing contributions from Π occur as soon as the k^2 terms in the propagators cannot be neglected anymore. An example of this is the factorizable correction from the Coulomb graph, given in Eq. (2.2.2). For the on-shell (factorizable) part of the Coulomb effect photons with momenta $k_0 = \mathcal{O}(\Delta E)$ and $|\vec{k}| = \mathcal{O}(\sqrt{M_W \Delta E})$ are important [13], i.e. k^2 cannot be neglected in the propagators of the unstable particles. Since we stay well away from the W-pair threshold ($\Delta E \gg \Gamma_W$), this situation occurs outside the realm of the semi-soft photons. This fits nicely into the picture of the production stage being a "hard" subprocess, governed by relatively short time scales as compared with the much longer time scales required for the non-factorizable corrections, which interconnect the different subprocesses.

2.2.2   Real-photon radiation

In this subsection we discuss the aspects of real-photon radiation in the DPA. To this end we consider the process

$$e^+(q_1) \, e^-(q_2) \to W^+(p_1) \, W^-(p_2) \, [\gamma(k)] \to \bar{f}_1(k_1) f_1'(k_1') \, f_2(k_2) \bar{f}_2'(k_2') \, \gamma(k), \tag{2.2.8}$$

where in the intermediate state there may or may not be a photon. We will show how to extract the gauge-invariant double-pole residues in different situations. The exact cross-section for process (2.2.8) can be written in the following form

$$d\sigma = \frac{1}{2s} |\mathcal{M}_\gamma|^2 d\Gamma_{4f\gamma} = \tag{2.2.9}$$

---

[5] Note that the complete density matrix is required in this case, in contrast to the pure on-shell calculation which involves the trace of the density matrix only.

$$= \frac{1}{2s}\left[2\mathrm{Re}\left(\mathcal{M}_0\mathcal{M}_+^* + \mathcal{M}_0\mathcal{M}_-^* + \mathcal{M}_+\mathcal{M}_-^*\right) + |\mathcal{M}_0|^2 + |\mathcal{M}_+|^2 + |\mathcal{M}_-|^2\right]d\Gamma_{4f\gamma},$$

where $d\Gamma_{4f\gamma}$ indicates the complete five-particle phase-space factor, and the matrix elements $\mathcal{M}_0$ and $\mathcal{M}_\pm$ correspond to the diagrams where the photon is attached to the production or decay stage of the three W-pair diagrams, respectively. This split-up can be achieved with the help of the real-photon version of the partial-fraction decomposition (2.2.1). Each contribution to the cross-section can be written in terms of polarization density matrices, which originate from the amplitudes

$$\mathcal{M}_0 = \Pi_\gamma(M_1, M_2) \, \frac{\Delta^{(+)}(M_1)}{D_1} \, \frac{\Delta^{(-)}(M_2)}{D_2} \, , \tag{2.2.10}$$

$$\mathcal{M}_+ = \Pi(M_{1\gamma}, M_2) \, \frac{\Delta^{(+)}(M_{1\gamma})}{D_{1\gamma}} \, \frac{\Delta^{(-)}(M_2)}{D_2} \, , \tag{2.2.11}$$

$$\mathcal{M}_- = \Pi(M_1, M_{2\gamma}) \, \frac{\Delta^{(+)}(M_1)}{D_1} \, \frac{\Delta_\gamma^{(-)}(M_{2\gamma})}{D_{2\gamma}} \, , \tag{2.2.12}$$

where all polarization indices for the W bosons and the photon have been suppressed, and

$$D_{i\gamma} = D_i + 2kk_i + 2kk_i', \quad M_{i\gamma}^2 = M_i^2 + 2kk_i + 2kk_i', \quad M_i^2 = (k_i + k_i')^2. \tag{2.2.13}$$

The matrix elements Π_γ and $\Delta_\gamma^{(\pm)}$ describe the production and decay of the W bosons accompanied by the radiation of a photon. The matrix elements without subscript γ have been introduced in Eq. (2.1.8).

In the calculation of the Born matrix element and virtual corrections only two poles could be identified in the amplitudes, originating from the Breit–Wigner propagators $1/D_i$. The pole-scheme expansion was performed around these two poles. In contrast, the bremsstrahlung matrix element has four in general different poles, originating from the four Breit–Wigner propagators $1/D_i$ and $1/D_{i\gamma}$. As mentioned above, the matrix element can be rewritten as a sum of three matrix elements $(\mathcal{M}_0, \mathcal{M}_+, \mathcal{M}_-)$, each of which only contain two Breit–Wigner propagators. For these three individual matrix elements the pole-scheme expansion is fixed, as before, to an expansion around the corresponding two poles. However, when calculating cross-sections [see Eq. (2.2.9)] the mapping of the five-particle phase space introduces a new type of ambiguity. The interference terms in Eq. (2.2.9) involve two different double-pole expansions simultaneously. As such there is no natural choice for the phase-space mapping in those cases. The resulting ambiguity (implementation dependence) might have important repercussions on the quality of the DPA calculation and therefore deserves some special attention. In this context the three earlier-defined regimes for the photon energy play a role:

- for hard photons $[E_\gamma \gg \Gamma_W]$ the Breit–Wigner poles of the W-boson resonances before and after photon radiation are well separated in phase space (see $M_{i\gamma}^2$

and M_i^2 defined above). As a result, the interference terms in Eq. (2.2.9) can be neglected. This leads to three *distinct* regions of on-shell contributions, where the photon can be assigned unambiguously to the W-pair-production subprocess or to one of the two decays. This assignment is determined by the pair of invariant masses (out of M_i^2 and $M_{i\gamma}^2$) that is in the M_W^2 region. Therefore, the double-pole residue can be expressed as the sum of the three on-shell contributions without increasing the intrinsic error of the DPA. Note that in the same way it is also possible to experimentally assign the photon to one of the subprocesses, since misassignment errors are suppressed, assuming for convenience that all final-state momenta can ideally be measured.

- for semi-soft photons $[E_\gamma = \mathcal{O}(\Gamma_W)]$ the Breit–Wigner poles are relatively close together in phase space, resulting in a substantial overlap of the line shapes. The assignment of the photon is now subject to larger errors. Moreover, since the interference terms in Eq. (2.2.9) cannot be neglected, the issue of the phase-space mapping has to be addressed. In the following we give a proper prescription for calculating the DPA residues and discuss their quality.

- for soft photons $[E_\gamma \ll \Gamma_W]$ the Breit–Wigner poles are on top of each other, resulting in a pole-scheme expansion that is identical to the one without the photon.

Hard photons

Let us first consider the hard-photon regime in more detail. Due to the fact that the poles are well separated in the hard-photon regime, it is clear that the interference terms are suppressed and can be neglected:

$$d\sigma = \frac{1}{2s}\Big[|\mathcal{M}_0|^2 + |\mathcal{M}_+|^2 + |\mathcal{M}_-|^2\Big]d\Gamma_{4f\gamma}. \tag{2.2.14}$$

Note that each of the three terms has two poles, originating from two resonant propagators. However, these poles are different for different terms. The phase-space factor can be rewritten in three equivalent ways. The first is

$$d\Gamma_{4f\gamma} = d\Gamma_0^\gamma = d\Gamma_{pr}^\gamma \cdot d\Gamma_{dec}^+ \cdot d\Gamma_{dec}^- \cdot \frac{dM_1^2}{2\pi} \cdot \frac{dM_2^2}{2\pi}, \tag{2.2.15}$$

with

$$d\Gamma_{pr}^\gamma = \frac{1}{(2\pi)^2}\,\delta(q_1 + q_2 - p_1 - p_2 - k)\,\frac{d\vec{p}_1}{2p_{10}}\,\frac{d\vec{p}_2}{2p_{20}}\,\frac{d\vec{k}}{(2\pi)^3 2k_0}. \tag{2.2.16}$$

The two others are

$$d\Gamma_{4f\gamma} = d\Gamma_+^\gamma = d\Gamma_{pr} \cdot d\Gamma_{dec}^{+\gamma} \cdot d\Gamma_{dec}^- \cdot \frac{dM_{1\gamma}^2}{2\pi} \cdot \frac{dM_2^2}{2\pi}, \tag{2.2.17}$$

with

$$d\Gamma_{\text{dec}}^{+\gamma} = \frac{1}{(2\pi)^2} \, \delta(p_1 - k_1 - k_1' - k) \frac{d\vec{k}_1}{2k_{10}} \frac{d\vec{k}_1'}{2k_{10}'} \frac{d\vec{k}}{(2\pi)^3 2k_0}, \qquad (2.2.18)$$

and a similar expression for $d\Gamma_-^\gamma$. The phase-space factors $d\Gamma_{\text{pr}}$ and $d\Gamma_{\text{dec}}^\pm$ are just the lowest-order ones. The cross-section can then be written in the following equivalent form

$$d\sigma = \frac{1}{2s} \Big[|\mathcal{M}_0|^2 \, d\Gamma_0^\gamma + |\mathcal{M}_+|^2 \, d\Gamma_+^\gamma + |\mathcal{M}_-|^2 \, d\Gamma_-^\gamma \Big]. \qquad (2.2.19)$$

In order to extract gauge-invariant quantities, the DPA limit should be taken. This amounts to taking the limit $p_{1,2}^2 \to M_W^2$, using a prescription that resembles the one presented in Sect. 2.1. Note however that $p_{1,2}$ can be different according to the δ-functions in the decay parts of the different phase-space factors. To be specific, the production term $|\mathcal{M}_0|^2$ has poles at $p_i^2 = M_i^2 = M_W^2$, $|\mathcal{M}_+|^2$ has poles at $p_1^2 = M_{1\gamma}^2 = M_W^2$ and $p_2^2 = M_2^2 = M_W^2$, and $|\mathcal{M}_-|^2$ has poles at $p_1^2 = M_1^2 = M_W^2$ and $p_2^2 = M_{2\gamma}^2 = M_W^2$. Again we fix solid angles in the mapping, including the solid angle of the photon. Since the energy range of the photon in the on-shell kinematics of the W bosons is different from the off-shell case, it may happen that the energy of the photon in an off-shell four-fermion – one-photon event with certain solid angles lies outside the on-shell phase space with the same solid angles. A possible procedure is to assign a zero cross-section to those events. Since the events are anyhow rare, being close to the edge of the off-shell phase space, this procedure constitutes an acceptable and simple solution. An alternative way to avoid unphysical on-shell phase-space points would be to write the photon energy as a fraction of the maximum attainable photon energy for given invariant masses $\sqrt{p_i^2}$ of the resonant W bosons and given solid angles:

$$E_\gamma = x_\gamma E_\gamma^{\text{max}}(\sqrt{p_1^2}, \sqrt{p_2^2}, \text{angles}). \qquad (2.2.20)$$

In this way the photon energy is projected on the interval $[0, 1]$. The maximum photon energy E_γ^{max} depends on the specific term in Eq. (2.2.19). Subsequently the fraction x_γ and the afore-mentioned solid angles are kept fixed during the mapping from off- to on-shell events. Then E_γ for the on-shell case is found from Eq. (2.2.20), where p_i^2 are replaced by M_W^2.

It should be stressed that in the on-shell phase space there is no ambiguity concerning the treatment of the photon. One obtains in the DPA limit three gauge-invariant on-shell contributions to Eq. (2.2.19). The calculation of the corresponding matrix elements is presented in App. B.

Semi-soft and soft photons

We complete our survey of the different photon-energy regimes by considering semi-soft and soft photons. The split-up of factorizable and non-factorizable real-photon corrections proceeds in the same way as described in the previous subsection for

virtual corrections. The result reads in semi-soft approximation

$$
\begin{aligned}
d\sigma &= \frac{1}{2s}|\mathcal{M}_\gamma|^2 d\Gamma_{4f\gamma} \qquad\qquad\qquad\qquad\qquad\qquad\qquad (2.2.21)\\
&\approx -d\sigma^0_{\text{DPA}} \frac{d\vec{k}}{(2\pi)^3 2k_0}\left[2\mathrm{Re}\left(\mathcal{I}_0^\mu \mathcal{I}^*_{+,\mu} + \mathcal{I}_0^\mu \mathcal{I}^*_{-,\mu} + \mathcal{I}_+^\mu \mathcal{I}^*_{-,\mu}\right) + |\mathcal{I}_0^2| + |\mathcal{I}_+^2| + |\mathcal{I}_-^2|\right].
\end{aligned}
$$

The gauge-invariant currents $\mathcal{I}_0$ and $\mathcal{I}_\pm$ are given by

$$
\begin{aligned}
\mathcal{I}_0^\mu &= e\left[\frac{p_1^\mu}{kp_1} - \frac{p_2^\mu}{kp_2} - \frac{q_1^\mu}{kq_1} + \frac{q_2^\mu}{kq_2}\right],\\
\mathcal{I}_+^\mu &= -e\left[\frac{p_1^\mu}{kp_1} + Q_{f_1}\frac{k_1^\mu}{kk_1} - Q_{f_1'}\frac{k_1'^{\,\mu}}{kk_1'}\right]\frac{D_1}{D_1 + 2kp_1},\\
\mathcal{I}_-^\mu &= +e\left[\frac{p_2^\mu}{kp_2} + Q_{f_2}\frac{k_2^\mu}{kk_2} - Q_{f_2'}\frac{k_2'^{\,\mu}}{kk_2'}\right]\frac{D_2}{D_2 + 2kp_2}.
\end{aligned} \qquad (2.2.22)
$$

The first three interference terms in Eq. (2.2.21) correspond to the real non-factorizable corrections. The last three squared terms in Eq. (2.2.21) belong to the factorizable real-photon corrections. They constitute the semi-soft limit of Eq. (2.2.19). Note also that the currents are the same for both possible expressions for p_i, i.e. it does not matter whether $p_i = k_i + k_i'$ or $p_i = k_i + k_i' + k$.

As mentioned before, the DPA residues have to be defined properly in the presence of overlapping Breit–Wigner resonances in the semi-soft regime. The above equation (2.2.21) specifies such a procedure: the Born cross-section for a four-particle phase space is factored out and does not depend on the photon momentum. The factor between the square brackets is the usual soft-photon factor, except that the rapid variation of the Breit–Wigner resonances has been kept, leading to the ratios $D_i/D_{i\gamma}$ which take into account the shift in the Breit–Wigner distributions due to the photon. In the vicinity of the M_i^2 resonance these ratios are negligible for hard photons, unity for soft photons, and of $\mathcal{O}(1)$ for semi-soft photons.

This prescription is by no means unique. In principle one could have chosen any of the two Breit–Wigner resonances, $1/D_i$ or $1/D_{i\gamma}$, to define the phase-space mapping for the interference terms. Or in other words, both on-shell phase-space limits, $M_i^2 = M_W^2$ or $M_{i\gamma}^2 = M_W^2$, constitute equally plausible DPA mappings. The differences between both phase-space mappings are of $\mathcal{O}(k)$. Since the interference terms are only non-negligible in the semi-soft regime, it is conceivable that the implementation dependence associated with these different on-shell limits remains of $\mathcal{O}(\Gamma_W/M_W)$. Let us, for instance, consider the M_i^2 distribution in the vicinity of the resonance. Any $\mathcal{O}(k)$ shift in the factor multiplying $1/D_i$ would result in additional terms of $\mathcal{O}(k/M_W)$, i.e. at worst $\mathcal{O}(\Gamma_W/M_W)$ in the semi-soft limit. A similar shift in the factor belonging to $1/D_{i\gamma}$ results in additional contributions to the DPA residues that are suppressed by $\mathcal{O}(\Gamma_W/E)$ for *all* values of the photon energy, as is explained in App. C. Therefore one can conclude that overlapping Breit–Wigner resonances do not necessarily imply a reduced quality of the DPA.

Based on this observation, we have the freedom to choose a suitable procedure for semi-soft photons. The fact whether hard-photon contributions are suppressed or not will serve as our guideline for fixing the choice. Whenever the hard-photon effects yield vanishing contributions to certain observables, we will use the semi-soft currents of Eqs. (2.2.21) and (2.2.22). As a consequence, the non-factorizable corrections are always calculated with the help of the semi-soft interference terms. In order to specify our approach, we indicate in the following how the above-defined matrix elements and currents are used in the various distributions of experimental interest.

Real-photon contributions to various distributions

As in all RC, the role of the bremsstrahlung process is twofold. In the first place the off-shell W-pair process (1.1.3) has at lowest-order level all kinds of distributions to which one would like to calculate $\mathcal{O}(\alpha)$ RC. These RC consist of virtual and real-photon contributions. An integration over all allowed photon energies should be carried out, i.e. the radiated photon should be treated inclusively.

The second application of the bremsstrahlung process involves the evaluation of exclusive photon distributions. Since the photon has to be detected it should be sufficiently hard. How hard depends on the experimental resolution. An example of such an exclusive photon distribution is the photon-energy spectrum $d\sigma/dE_\gamma$. This distribution receives contributions from the three hard-photon terms in Eq. (2.2.19) as well as from the semi-soft interference terms of Eq. (2.2.21). The latter terms of course only contribute for photon energies that are not too hard.

In the next section results will be given for various distributions. For exclusive photons we present the photon-energy spectrum $d\sigma/dE_\gamma$. For the inclusive photon distributions we discuss in the following how the bremsstrahlung part is treated. Depending on the distribution, different approximations can be made.

As indicated above, the calculation of RC to distributions of the off-shell W-pair process (1.1.3) involves an integration over the photon phase space that is left available when fixing other kinematic variables. This means that the photon phase space for hard, semi-soft, and soft photons will in general be integrated over. The soft-photon part is standard and should be combined with the virtual corrections. How the non-soft part should be treated depends on the distribution one likes to study. In general one considers distributions of the form $d\sigma_{\text{DPA}}/dX$, where dX stands for $dM_1^2 dM_2^2$ and a product of solid angles for W-boson production and decay. For the following discussion it does not matter whether these solid angles are kept or integrated out. However, it does matter whether one wants a double distribution in M_1^2 and M_2^2, a single distribution in M_i^2, or no distribution in M_i^2 at all. In other words, the treatment differs depending on whether one integrates over M_i^2 or not.

Let us first discuss the procedure for the real-photon corrections to the double Breit–Wigner distribution $d\sigma/dM_1^2 dM_2^2$ in the vicinity of the peak, i.e. one is not interested in the tails of this peaked distribution. In Table 2-1 we specify which expressions are used in the different regimes for the photon energy. For this specification we use the positions of the Breit–Wigner poles as listed below Eq. (2.2.19).

E_γ	contributions to $d\sigma/dM_1^2 dM_2^2$			
	prod. $+ \gamma$	W^+ decay $+ \gamma$	W^- decay $+ \gamma$	non-factorizable
hard	$|\mathcal{M}_0|^2$ (2.2.19)	$\to 0$	$\to 0$	$\to 0$
semi-soft	$|\mathcal{M}_0|^2$ (2.2.19)	$|\mathcal{I}_+^2|$ (2.2.21)	$|\mathcal{I}_-^2|$ (2.2.21)	interf. (2.2.21)
soft	$|\mathcal{I}_0^2|$ (2.2.21)	$|\mathcal{I}_+^2|_{\text{soft}}$ (2.2.21)	$|\mathcal{I}_-^2|_{\text{soft}}$ (2.2.21)	soft interf. (2.2.21)

Table 2-1. Formulae for the bremsstrahlung matrix elements for the distribution $d\sigma/dM_1^2 dM_2^2$.

The entries of Table 2-1 can be explained as follows. The real-photon corrections to the distribution $d\sigma/dM_1^2 dM_2^2$ come in the first place from the production part, where the hard-photon matrix element squared $|\mathcal{M}_0|^2$ contains the overall Breit–Wigner line shapes in M_1^2 and M_2^2. This term should be taken from Eq. (2.2.19) and should be integrated over the photon phase space. In the soft-photon limit the usual soft-photon factorization in terms of $|\mathcal{I}_0^2|$ is obtained. This explains the second column in Table. 2-1, where the usual RC to stable W-pair production appear, except that one now calculates the full density matrices rather than merely the trace.

The second type of contribution involves the W-boson decays with additional photon. When the photon is hard these contributions tend to zero as Γ_W^2/k_0^2 (see App. C), since they do not contain a double Breit–Wigner distribution in both M_1^2 and M_2^2 according to the list below Eq. (2.2.19). For (semi)soft photons, however, one gets overlapping Breit–Wigner resonances and the $|\mathcal{I}_\pm^2|$ terms of Eq. (2.2.21) can be used. These (semi)soft-photon factors have to be integrated while keeping D_i fixed, i.e. we keep the variables M_i^2 fixed. The corresponding integrals can be found in App. C. The integration over the semi-soft photon momenta leads to contributions from M_i^2 values that are higher then M_i^2, resulting in a distortion of the original M_i^2 Breit–Wigner distribution. This final-state-radiation effect turns out to be quite sizeable, as will be discussed in Chapter 3 (see also [14]). The reason why the distortion is so large lies in the fact that the final-state collinear singularities $[\propto \frac{\alpha}{\pi} Q_f^2 \ln(m_f^2/M_W^2)]$ do not vanish, even not for fully inclusive photons. After all, a fixed value of M_i^2 makes it impossible to sum over all degenerate final states by a mere integration over the photon momentum.[6] On top of that the infrared (IR) poles $\propto 1/k$ induce a further enhancement of the collinear logarithms by a factor $\ln(D_i/M_W^2)$.

So far we have included all factorizable corrections. To this one should add the non-factorizable corrections. Again effectively only the (semi)soft region is relevant. For more information on these non-factorizable corrections we refer to the detailed discussion in Chapter 4 and in the literature [6, 8, 15].

As the next relevant distribution we discuss the real-photon corrections to the single Breit–Wigner distribution $d\sigma/dM_1^2$, obtained from the previous case by inte-

---

[6]The usual cancellation of final-state collinear singularities is achieved only if also M_i^2 is integrated over.

E_γ	contributions to $d\sigma/dM_1^2$			
	prod. $+ \gamma$	W^+ decay $+ \gamma$	W^- decay $+ \gamma$	non-factorizable
hard	$|\mathcal{M}_0|^2$ (2.2.19)	$\to 0$	$|\mathcal{M}_-|^2$ (2.2.19)	$\to 0$
semi-soft	$|\mathcal{M}_0|^2$ (2.2.19)	$|\mathcal{I}_+^2|$ (2.2.21)	$|\mathcal{M}_-|^2$ (2.2.19)	interf. (2.2.21)
soft	$|\mathcal{I}_0^2|$ (2.2.21)	$|\mathcal{I}_+^2|_{\text{soft}}$ (2.2.21)	$|\mathcal{I}_-^2|_{\text{soft}}$ (2.2.21)	soft interf. (2.2.21)

Table 2-2. Formulae for the bremsstrahlung matrix elements for the distribution $d\sigma/dM_1^2$.

grating over M_2^2. To this end we make a similar table (Table 2-2) and discuss the necessary changes. Based on the discussion below Eq. (2.2.19), it is clear that a Breit–Wigner distribution in M_1^2 is present explicitly in $|\mathcal{M}_0|^2$ and $|\mathcal{M}_-|^2$, both for hard and semi-soft photons. These two terms should be taken from Eq. (2.2.19) and should be integrated over the photon phase space and M_2^2. The $|\mathcal{M}_+|^2$ term does not have a Breit–Wigner distribution in M_1^2 as long as the photon is hard. Therefore it effectively only contributes in the (semi)soft regime, like in the previous case. Therefore the $|\mathcal{I}_+^2|$ term in Eq. (2.2.21) is used and the photon integration is performed while keeping M_1^2 fixed. The non-factorizable corrections contribute in the same way as described for the previous case.

We conclude by considering pure angular distributions. In this case the picture is simple. All contributions should be taken from Eq. (2.2.19) and should be integrated over the photon phase space and the invariant masses M_i^2. The non-factorizable corrections vanish in this situation, which is typical for these interference effects [3], as will be discussed in Chapter 4.

2.3   Numerical results

All the corrections discussed in the previous sections were combined into a Fortran program. In this section we present some numerical results. In particular we study the implications of the RC on various distributions. For the numerical evaluations we use the G_μ-parametrization (see Sect. 2.1.2) and the input parameters listed in Eqs. (2.1.27)–(2.1.31).

2.3.1   One-dimensional distributions

We start off by considering various one-dimensional distributions. Where applicable both the lowest-order distribution ($d\sigma_{\text{DPA}}^0$) and the corrected one ($d\sigma_{\text{DPA}}$) will be presented, followed by a separate plot for the relative correction factor δ_{DPA} [see Eq. (2.1.5)].
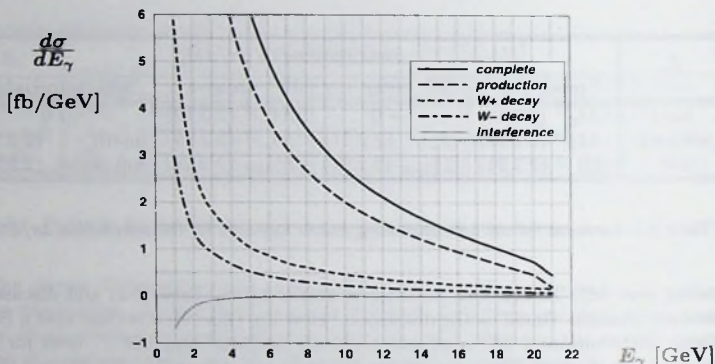
Figure 2-6. The photon-energy distribution $d\sigma/dE_\gamma$ for the $\mu^+\nu_\mu\tau^-\bar{\nu}_\tau\gamma$ final state at $2E = 184\,\text{GeV}$. In addition the separate production and decay contributions are given.

The photon-energy spectrum

Since real-photon bremsstrahlung contributes to the RC to various distributions, it is useful to evaluate the photon-energy spectrum $d\sigma/dE_\gamma$ separately as well. In DPA it gets contributions from the three terms in Eq. (2.2.19) and the semi-soft interference terms of Eq. (2.2.21). The photon spectrum originating from the production stage is the same for all final states, but the spectra from the decay stages depend on the specific final state. In Fig. 2-6 the DPA photon-energy distribution $d\sigma/dE_\gamma$ is shown for the $\mu^+\nu_\mu\tau^-\bar{\nu}_\tau\gamma$ final state at $2E = 184\,\text{GeV}$, together with the production and decay parts of the spectrum. In Fig. 2-7 we separately list the three possible leptonic radiative-decay contributions, originating from $W \rightarrow \ell\nu_\ell\gamma$ ($\ell = e, \mu, \tau$). The substantial differences are caused by the explicit fermion-mass dependence for collinear photon radiation (see App. B.4).

The total cross-section as a function of energy

In Fig. 2-8 we compare the total cross-section with and without RC for the $\mu^+\nu_\mu\tau^-\bar{\nu}_\tau$ final state. The corresponding relative correction factor δ is given in Fig. 2-9. As a check of our calculation we have verified that the corrected cross-section coincides within the integration errors with the corrected cross-section for stable W bosons multiplied by the corrected branching ratio $(\Gamma_{W\rightarrow\ell\nu_\ell}/\Gamma_W)^2$.

The observed RC are large and negative, especially close to the W-pair threshold. This is mainly caused by real-photon ISR, which effectively lowers the available W-pair energy, combined with the fact that near the W-pair threshold the cross-section is rapidly decreasing with decreasing energy.

$$\frac{d\sigma}{dE_\gamma}$$

[fb/GeV]
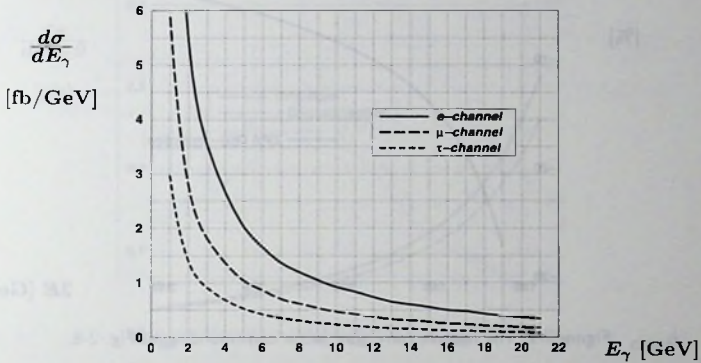
Figure 2-7. Decay contributions to the photon spectrum from different leptonic W decays.
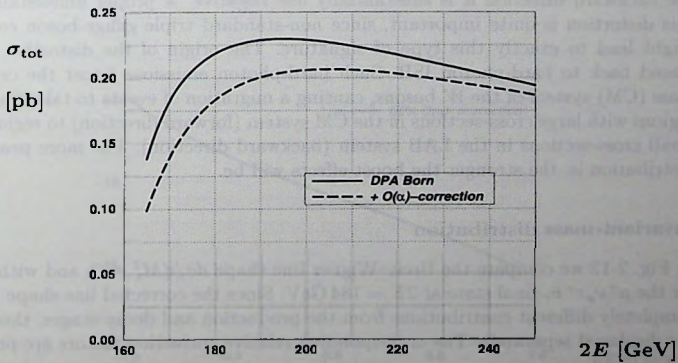
σ_{tot}

[pb]

Figure 2-8. The energy dependence of the total cross-section σ_{tot} for the $\mu^+\nu_\mu\tau^-\bar{\nu}_\tau$ final state.
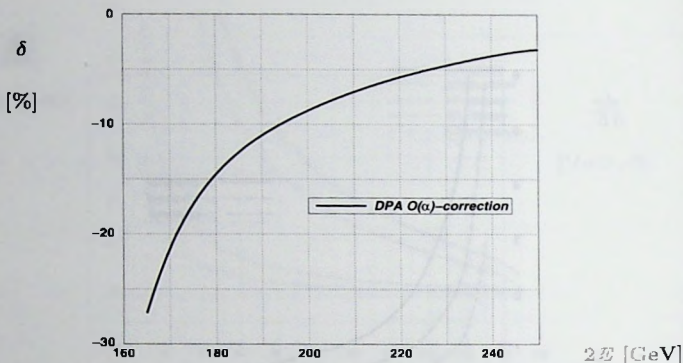
Figure 2-9. The relative correction factor corresponding to Fig. 2-8.

Production-angle distribution

In Fig. 2-10 we plot the production-angle distribution $d\sigma/d\cos\theta$ for the $\mu^+\nu_\mu\tau^-\bar{\nu}_\tau$ final state at $2E = 184\,\text{GeV}$. The relative correction factor displayed in Fig. 2-11 differs substantially from the -12.8% normalization effect that was observed for the total cross-section. In the forward direction it is slightly more negative, whereas in the backward direction it is substantially less negative. A proper understanding of this distortion is quite important, since non-standard triple gauge-boson couplings might lead to exactly this type of signature. The origin of the distortion can be traced back to hard-photon ISR. Such hard-photon emissions boost the centre-of-mass (CM) system of the W bosons, causing a migration of events to take place from regions with large cross-sections in the CM system (forward direction) to regions with small cross-sections in the LAB system (backward direction). The more peaked the distribution is, the stronger the boost effects will be.

Invariant-mass distribution

In Fig. 2-12 we compare the Breit–Wigner line shape $d\sigma/dM_1^2$ with and without RC for the $\mu^+\nu_\mu\tau^-\bar{\nu}_\tau$ final state at $2E = 184\,\text{GeV}$. Since the corrected line shape receives completely different contributions from the production and decay stages, these parts are displayed separately. The corresponding relative correction factors are presented in Fig. 2-13.

The correction to the production stage leads to a constant reduction of the Breit–Wigner line shape. The corrections to the decay stages comprise the factorizable decay corrections (columns 3 and 4 in Table 2-2) and the non-factorizable corrections (column 5 in Table 2-2). The latter are very small [6, 8]. We see that also the decay

$$\frac{d\sigma}{d\cos\theta}$$

[pb]

Figure 2-10. The production-angle distribution $d\sigma/d\cos\theta$ for the $\mu^+\nu_\mu\tau^-\bar{\nu}_\tau$ final state at $2E = 184\,\text{GeV}$.

δ

[%]
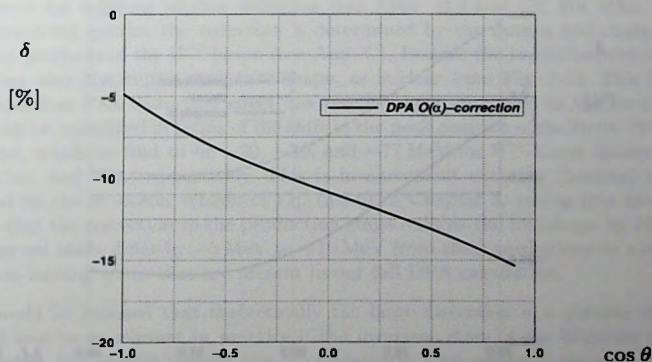
Figure 2-11. The relative correction factor corresponding to Fig. 2-10.
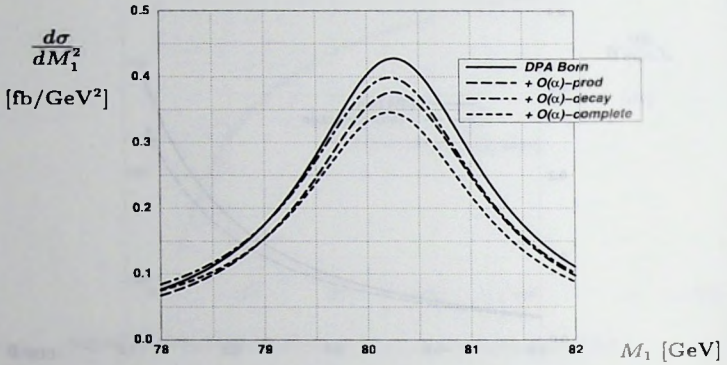
Figure 2-12. The invariant-mass distribution $d\sigma/dM_1^2$ for the $\mu^+\nu_\mu\tau^-\bar{\nu}_\tau$ final state at $2E = 184\,\mathrm{GeV}$.
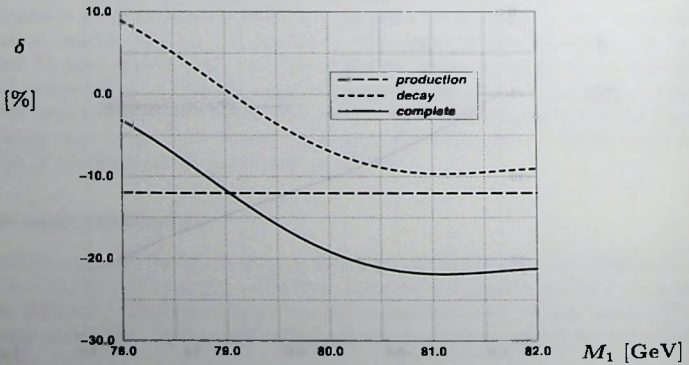
Figure 2-13. The relative correction factors δ corresponding to Fig. 2-12.

$$\frac{d\sigma}{dM_1^2}$$

$[\text{fb}/\text{GeV}^2]$
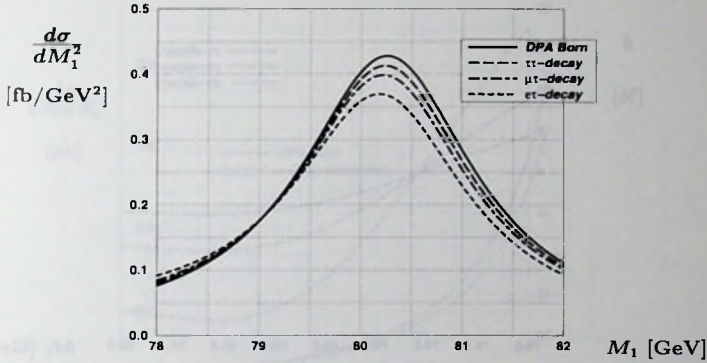
Figure 2-14. Distortion of the invariant-mass distribution $d\sigma/dM_1^2$ at $2E = 184\,\text{GeV}$ due to the decay corrections. Three leptonic final states are considered: $\tau^+\nu_\tau\tau^-\bar{\nu}_\tau$ ($\tau\tau$-decay), $\mu^+\nu_\mu\tau^-\bar{\nu}_\tau$ ($\mu\tau$-decay), and $e^+\nu_e\tau^-\bar{\nu}_\tau$ ($e\tau$-decay).

corrections reduce the Breit–Wigner line shape. The amount of reduction depends on the particular final state, as can be seen from Figs. 2-14 and 2-15, where we consider different leptonic final states. The differences are caused by the explicit fermion-mass dependence for collinear photon radiation (see Apps. B.4 and C). For other final states, involving quarks, the reduction is determined by the masses and charges of the decay products of the W^+ boson (see App. C). Besides the reduction, the decay corrections also distort the resonance shape, as is clear from Fig. 2-13. This final-state-dependent FSR distortion effect has recently been discussed in the literature [14]. It can be quantified in terms of the shift in the peak position of the Breit–Wigner line shape, which we find to be -20, -39, and $-77\,\text{MeV}$ for W^+-boson decays into $\tau^+\nu_\tau$, $\mu^+\nu_\mu$, and $e^+\nu_e$, respectively. This is in agreement with the (leading) shifts predicted by the W-boson version of Eq. (3.3.6) in Chapter 3, taking into account the fact that the correction to the production stage reduces the line shape by 12.0%. The observed shifts differ by $-5\,\text{MeV}$ to $-10\,\text{MeV}$ from these predictions as a result of the non-leading terms that are present in our full DPA calculation.

It should be stressed that theoretically the large distortion is a genuine effect. It would also be as relevant in practice if the invariant mass of the fermions could be measured. For various reasons this is problematic. One reason is the almost unavoidable inclusion of a collinear photon in the measured invariant mass. Such an inclusion would effectively decrease the leading logarithm $[\ln(M_W^2/m_f^2)]$ that dominates the effect. What remains of the distortion in practice should be studied with an event generator, which simulates the actual measurement.
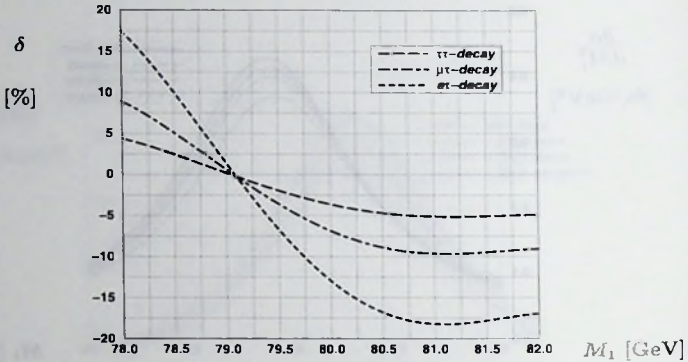
Figure 2-15. The relative correction factors δ corresponding to Fig. 2-14
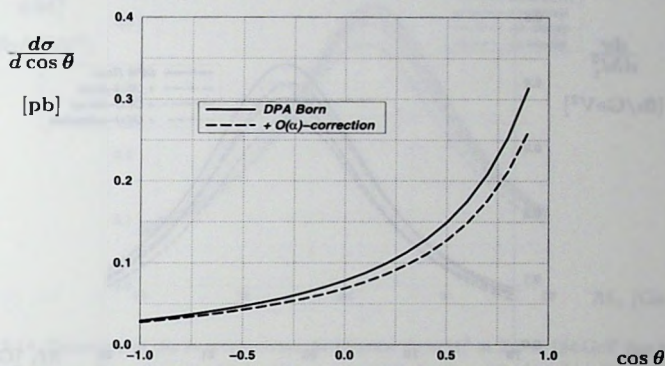
Decay-angle distribution

In Figs. 2-16 and 2-17 the results are shown for the decay-angle distribution $d\sigma/d\cos\theta_3$ for the $\mu^+\nu_\mu\tau^-\bar{\nu}_\tau$ final state at $2E = 184\,\text{GeV}$. Here θ_3 is the angle between the μ^+ and the W^+ boson in the LAB frame [see Eq. (2.1.18)]. The correction is negative and becomes more negative for forward angles. The shape of the relative correction factor is again the result of hard-photon boost effects.

2.3.2   Double invariant-mass distribution

Finally we consider the two-dimensional distribution $d\sigma/dM_1^2 dM_2^2$ at $2E = 184\,\text{GeV}$, evaluated using the contributions specified in Table 2-1. Instead of plotting the absolute distributions, only the relative correction factors δ are presented. We do this for two specific leptonic final states. In Fig. 2-18 the $e^+\nu_e e^-\bar{\nu}_e$ final state is considered. This final state has the largest correction. Keeping one M_i^2 fixed, the correction to the other distribution is qualitatively the same as the correction to the one-dimensional distribution in Fig. 2-15. For the $e^+\nu_e\tau^-\bar{\nu}_\tau$ final state (Fig. 2-19) the correction is clearly not symmetric in the M_i^2. This was to be expected, since the decay corrections for $e^+\nu_e$ and $\tau^-\bar{\nu}_\tau$ differ appreciably.

In Tables 2-3 and 2-4 we present some explicit values for the relative correction factor, split up into the separate contributions according to

$$\delta_{DPA}(M_1, M_2) = \delta_{\text{pr}} + \delta_{\text{dec}}^+(M_1) + \delta_{\text{dec}}^-(M_2) + \delta_{\text{nf}}(M_1, M_2).$$

The correction from the production stage is constant as a function of the invariant masses, $\delta_{\text{pr}} = -12.0\%$. The non-factorizable contribution $\delta_{\text{nf}}(M_1, M_2)$ is given in Table 2-3 for three near-resonant values for the invariant masses M_i. We indicate these

$$\frac{d\sigma}{d\cos\theta_3}$$

[pb]
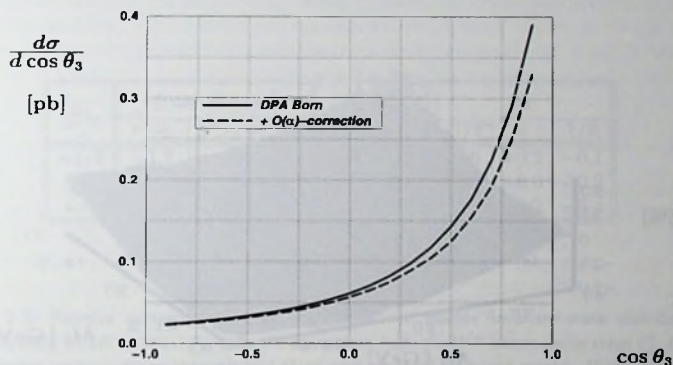
Figure 2-16. The decay-angle distribution $d\sigma/d\cos\theta_3$ for the $\mu^+\nu_\mu\tau^-\bar{\nu}_\tau$ final state at $2E = 184\,\text{GeV}$. Here $\theta_3 = \angle(\mu^+, W^+)$ in the LAB frame.

δ

[%]
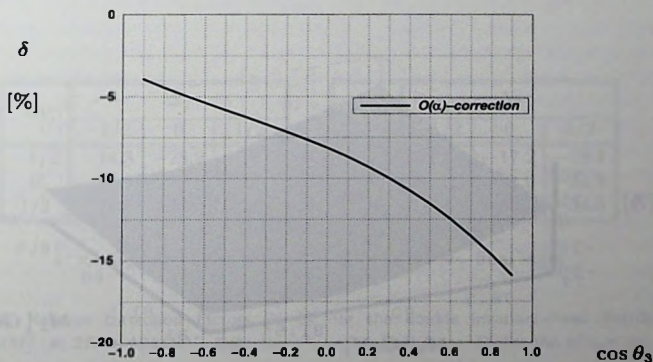
Figure 2-17. The relative correction factor δ corresponding to Fig. 2-16.
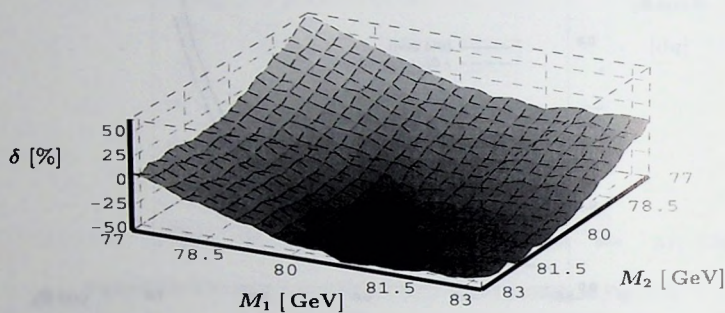
Figure 2-18. Correction to the double invariant-mass distribution $d\sigma/dM_1^2 dM_2^2$ for the $e^+\nu_e e^-\bar{\nu}_e$ final state at $2E = 184\,\mathrm{GeV}$.
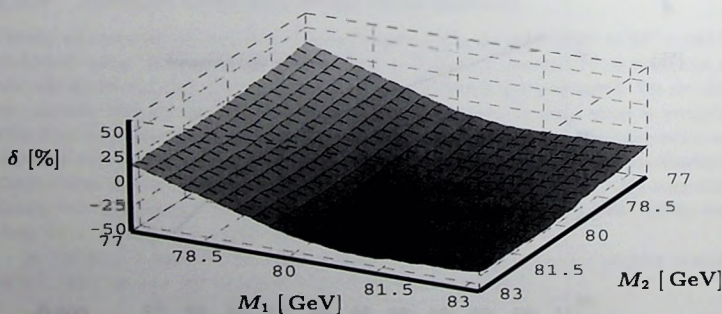
Figure 2-19. Correction to the double invariant-mass distribution $d\sigma/dM_1^2 dM_2^2$ for the $e^+\nu_e \tau^-\bar{\nu}_\tau$ final state at $2E = 184\,\mathrm{GeV}$.

Δ_1	decay channel		
	$e^+\nu_e$	$\mu^+\nu_\mu$	$\tau^+\nu_\tau$
$-1/2$	-1.4	-0.8	-0.5
0	-15.0	-7.8	-4.0
$1/2$	-17.3	-9.0	-4.6

$$\delta_{dec}^+(M_1)$$

Δ_1	Δ_2		
	$-1/2$	0	$1/2$
$-1/2$	$+0.5$	$+0.2$	-0.1
0	$+0.2$	$+0.0$	-0.2
$1/2$	-0.1	-0.2	-0.4

$$\delta_{nf}(M_1, M_2)$$

Table 2-3. Relative correction factors [in %] for the double invariant-mass distribution $d\sigma/dM_1^2 dM_2^2$ at $2E = 184$ GeV. Left: the corrections from the W^+-boson decay stage $\delta_{dec}^+(M_1)$ for different leptonic decay channels and three near-resonant invariant masses. Right: the non-factorizable corrections $\delta_{nf}(M_1, M_2)$.

Δ_1	Δ_2		
	$-1/2$	0	$1/2$
$-1/2$	-14.3	-28.2	-30.8
0	-28.2	-42.0	-44.5
$1/2$	-30.8	-44.5	-47.0

$e^+\nu_e e^-\bar{\nu}_e$ final state

Δ_1	Δ_2		
	$-1/2$	0	$1/2$
$-1/2$	-13.4	-17.2	-18.1
0	-27.3	-31.0	-31.8
$1/2$	-29.9	-33.5	-34.3

$e^+\nu_e \tau^-\bar{\nu}_\tau$ final state

Table 2-4. Relative correction factors [in %] for the double invariant-mass distribution $d\sigma/dM_1^2 dM_2^2$ at $2E = 184$ GeV. Left: the $e^+\nu_e e^-\bar{\nu}_e$ final state. Right: the $e^+\nu_e \tau^-\bar{\nu}_\tau$ final state.

three values by $\Delta_i = (M_i - M_W)/\Gamma_W = -1/2,\ 0,\ 1/2$. The non-factorizable corrections do not depend on the particular leptonic final state. The corrections $\delta^{\pm}_{\text{dec}}(M_i)$ from the decay stages do depend on the particular leptonic final state as explained before. In Table 2-3 we present these corrections for the three leptonic decay modes and the three near-resonant values for the invariant mass.

2.4   Discussion and conclusions

In this chapter $\mathcal{O}(\alpha)$ radiative corrections (RC) to four-fermion production in e^+e^- collisions have been studied. The energy region chosen is that of LEP2, where the four-fermion final state is predominantly formed through intermediate W-pair production.

Since a complete $\mathcal{O}(\alpha)$ RC calculation for a two-particle to four-particle process is beyond present possibilities, a sensible approximation scheme has to be used. The smallness of Γ_W/M_W offers the possibility to use the double-pole approximation (DPA). In practice it means that we calculate $\mathcal{O}(\alpha)$ and $\mathcal{O}(\Gamma_W/M_W)$ corrections but neglect $\mathcal{O}(\alpha\Gamma_W/M_W)$ corrections.

We have applied the method to W-pair-mediated four-fermion production for a number of reasons. There is the methodological aspect of dealing with unstable particles in DPA, involving issues like gauge invariance, interactions between different stages of the reaction, RC to density matrices, and the phase-space mappings. All of these issues play a role in the W-pair-mediated four-fermion production process. There is also the practical aspect of assessing how large $\mathcal{O}(\alpha)$ corrections can be for certain distributions. This is of importance for W-pair studies at LEP2.

On the methodological side, we have succeeded in finding a consistent prescription for applying the idea of the DPA. The kinematics for calculating the poles of the matrix elements is necessarily on-shell kinematics. Also the phase-space factor in the cross-section is treated in on-shell kinematics. The off-shell invariant masses occur only in the Breit–Wigner factors. All of this is well defined both for the radiative and non-radiative parts of the cross-section and therefore our calculation itself is unambiguous.

An unavoidable problem is the relation between off-shell four-fermion events and the on-shell calculated events. This question arises when one likes to connect experimental cross-sections to the calculated DPA cross-sections. Also here recipes are chosen both for the radiative and non-radiative phase-space points. For the latter the mapping is natural if one chooses the invariant masses $M_{1,2}$ and angles as variables. All off-shell points can be mapped onto on-shell points. For the radiative events in an off-shell phase space, the photon variables have to be added. A natural choice is the photon energy and angles. If the mapping is chosen such that the photon variables remain the same, one sometimes maps outside the on-shell phase space. Different remedies for this problem are possible. One can choose a procedure that assigns zero cross-sections to those points. On the other hand, the photon energy in the off-shell four-fermion–one-photon phase space may be rescaled in order to obtain a physical point in the on-shell phase space. In general, there will be a dependence on the chosen

mapping between off-shell and on-shell phase spaces. However, the induced numerical differences remain within the accuracy of the calculation, i.e. $\mathcal{O}(\alpha\Gamma_W/M_W)$. At high energies, say above 2 TeV, when peaks in the cross-section become much more pronounced, a more sizeable implementation dependence may occur. The present calculation is primarily meant for LEP2 energies and slightly above, say up to 500 GeV.

On the practical side, the results give an insight in the size of RC for off-shell W-pair production. Within the claimed accuracy it is a complete calculation. It should be stated that imaginary parts of loop diagrams have been neglected in the expectation that they only induce small effects. Moreover, such terms are characterized by an explicit $\sin\phi_3$ and/or $\sin\phi_4$ dependence in the cross-section, since they select the antisymmetric parts of the $\mathcal{D}$-matrices. Integration over these azimuthal angles removes the imaginary parts of loop diagrams from the cross-section. So they do not contribute to the distributions of Sect. 2.3. It should also be stated that some large corrections (ISR, FSR), which usually require the inclusion of higher-order terms, are considered purely in first order here. The corresponding higher-order terms can be determined in a straightforward way within our approach, using the usual exponentiation/factorization techniques.

We have presented the results for leptonic final states. The reason is that those states are theoretically well defined. In exactly the same way also quark final states can be treated as long as one assumes certain masses for the quarks. It is this mass assignment which gives some arbitrariness in the actual numbers. The RC presented are corrections to ideal theoretical situations, which cannot be realized experimentally in the same way. For that purpose the calculation should be implemented in an event generator. In principle this is possible. Events can be generated in the on-shell phase space with a radiatively corrected weight. The outside Breit–Wigner distributions can then generate the invariant masses and consequently off-shell events could be constructed from the on-shell ones (with certain angles kept fixed). Event generators offer the possibility to include realistic experimental cuts and therefore to study effects like the line-shape deformation in practical cases. The actual numbers presented here should give the reader an indication of the size of RC in ideal cases, of which remnants survive in practical situations.

For some questions the present study could already be useful in its present form. An example of this would be the comparison of a DPA Born cross-section with CP-conserving anomalous triple gauge-boson couplings and a normal DPA cross-section with RC.

In conclusion, the DPA method for unstable-particle production has been shown to give reasonable results. It could also be applied to other unstable-particle production processes that undergo electroweak or QCD radiative corrections. An example is pair production of top-quarks, for which the non-factorizable corrections will be presented in Chapter 5.

Appendix A:
Helicity amplitudes for virtual corrections

In this appendix we give the basic ingredients for the calculation of the virtual factor-izable corrections. The one-loop RC to on-shell W-pair production have been carried out in the literature in terms of helicity amplitudes with a particular choice for the decomposition into basic matrix elements and invariant functions [9]. This calcu-lation serves as our basis for obtaining the RC to the production density matrix $\mathcal{P}_{[\lambda_1\lambda_2][\lambda'_1\lambda'_2]}(M_W, M_W)$, defined in Eq. (2.1.11). Therefore we will set up our conven-tions in close analogy to what has been used in the numerical routines of Ref. [9]. Once we have fixed the choice of polarization basis in the production stage, the same choice should be applied to the decay stages as well, i.e to $\mathcal{D}_{\lambda,\lambda'}(M_W)$ in Eq. (2.1.12).

A.1   Virtual corrections to the production stage

The amplitude $\Pi_{\lambda_1\lambda_2}(M_W, M_W)$ for on-shell W-pair production depends on the spinors of the initial-state $e^{\pm}$ and on the polarization vectors $\varepsilon_i^{\mu}(p_i, \lambda_i)$ of the W bosons. In order to define the latter we first introduce

$$
\begin{aligned}
\varepsilon_{1,2}^{\mu}(p_{1,2}, ||) &= \frac{q_{1,2}^{\mu}(M_W^2 + u) - q_{2,1}^{\mu}(M_W^2 + t) + p_{1,2}^{\mu}(t - u)}{\sqrt{ut - M_W^4}\sqrt{s - 4M_W^2}}, \\
\varepsilon_i^{\mu}(p_i, \perp) &= -2\frac{\epsilon^{\mu\nu\rho\tau}q_{2\nu}q_{1\rho}p_{i\tau}}{\sqrt{s(ut - M_W^4)}}, \\
\varepsilon_i^{\mu}(p_i, L) &= \frac{sp_i^{\mu} - 2M_W^2(q_1 + q_2)^{\mu}}{M_W\sqrt{s(s - 4M_W^2)}},
\end{aligned}
\tag{A.1}
$$

using the conventions defined in Sect. 2.1 and $\epsilon^{0123} = -1$. The helicity states, defined in the LAB frame, can be expressed in terms of the energy E and velocity $\beta = p/E = \sqrt{1 - M_W^2/E^2}$ of the W bosons in the following way:

$$
\begin{aligned}
\varepsilon_1^{\mu}(p_1, \pm 1) &= \frac{1}{\sqrt{2}}\left[\varepsilon_1^{\mu}(p_1, ||) \pm i\varepsilon_1^{\mu}(p_1, \perp)\right] = \frac{1}{\sqrt{2}}(0, -1, \pm i, 0), \\
\varepsilon_1^{\mu}(p_1, 0) &= \varepsilon_1^{\mu}(p_1, L) = \frac{E}{M_W}(\beta, 0, 0, 1), \\
\varepsilon_2^{\mu}(p_2, \pm 1) &= \frac{1}{\sqrt{2}}\left[\varepsilon_2^{\mu}(p_2, ||) \mp i\varepsilon_2^{\mu}(p_2, \perp)\right] = \frac{1}{\sqrt{2}}(0, 1, \pm i, 0), \\
\varepsilon_2^{\mu}(p_2, 0) &= \varepsilon_2^{\mu}(p_2, L) = \frac{E}{M_W}(\beta, 0, 0, -1).
\end{aligned}
\tag{A.2}
$$

This polarization basis satisfies the usual identities

$$
p_i^{\mu}\varepsilon_{i,\mu}(p_i, \lambda_i) = 0, \qquad \varepsilon_i^{\mu}(p_i, \lambda_i)\,\varepsilon_{i,\mu}^*(p_i, \lambda'_i) = -\delta_{\lambda_i\lambda'_i}.
\tag{A.3}
$$

In its most general form, the amplitude $\Pi_{\lambda_1\lambda_2}(M_W, M_W)$ can be written as a sum of invariant functions $\mathcal{C}_j(\sigma)$ multiplied by Lorentz-invariant basic matrix elements $\mathcal{M}_j^\sigma(\lambda_1, \lambda_2)$. The basic matrix elements are simple, purely kinematical objects and contain the complete dependence on the W-boson polarizations. The invariant functions contain the dynamical information, i.e. details of the model, but are independent of the W-boson polarizations. Both parts depend on the helicity of the electron, $\lambda_{e^-} \equiv \sigma/2$ ($\sigma = \pm 1$). In view of our massless treatment of the $e^\pm$, the helicity of the positron is fixed to $\lambda_{e^+} = -\lambda_{e^-}$ in the virtual corrections. For a specific helicity of the electron the decomposition of the helicity amplitudes reads

$$\Pi_{\sigma;\lambda_1\lambda_2}(M_W, M_W) = \sum_{j=1}^{9} \mathcal{C}_j(\sigma)\mathcal{M}_j^\sigma(\lambda_1, \lambda_2), \tag{A.4}$$

with

$$\begin{aligned}
\mathcal{M}_1^\sigma(\lambda_1, \lambda_2) &= \left[\bar{v}(q_1)\not{p}_1\omega_\sigma u(q_2)\right](\varepsilon_1\varepsilon_2), \\
\mathcal{M}_2^\sigma(\lambda_1, \lambda_2) &= \left[\bar{v}(q_1)\not{p}_1\omega_\sigma u(q_2)\right](p_1\varepsilon_2)(p_2\varepsilon_1), \\
\mathcal{M}_3^\sigma(\lambda_1, \lambda_2) &= \bar{v}(q_1)\left[\not{\varepsilon}_1(p_1\varepsilon_2) - \not{\varepsilon}_2(p_2\varepsilon_1)\right]\omega_\sigma u(q_2), \\
\mathcal{M}_4^\sigma(\lambda_1, \lambda_2) &= \bar{v}(q_1)\not{\varepsilon}_1(\not{p}_1 - \not{q}_1)\not{\varepsilon}_2\omega_\sigma u(q_2), \\
\mathcal{M}_5^\sigma(\lambda_1, \lambda_2) &= \bar{v}(q_1)\left[\not{\varepsilon}_1(q_1\varepsilon_2) - \not{\varepsilon}_2(q_2\varepsilon_1)\right]\omega_\sigma u(q_2), \\
\mathcal{M}_6^\sigma(\lambda_1, \lambda_2) &= \left[\bar{v}(q_1)\not{p}_1\omega_\sigma u(q_2)\right](q_1\varepsilon_2)(q_2\varepsilon_1), \\
\mathcal{M}_7^\sigma(\lambda_1, \lambda_2) &= \left[\bar{v}(q_1)\not{p}_1\omega_\sigma u(q_2)\right]\left[(p_1\varepsilon_2)(q_2\varepsilon_1) + (p_2\varepsilon_1)(q_1\varepsilon_2)\right], \\
\mathcal{M}_8^\sigma(\lambda_1, \lambda_2) &= i\left[\bar{v}(q_1)\gamma^\mu\omega_\sigma u(q_2)\right]\epsilon_{\mu\nu\rho\tau}\varepsilon_2^\nu\varepsilon_1^\rho(p_1 - p_2)^\tau, \\
\mathcal{M}_9^\sigma(\lambda_1, \lambda_2) &= i\left[\bar{v}(q_1)\gamma^\mu\omega_\sigma u(q_2)\right]\epsilon_{\mu\nu\rho\tau}p_2^\nu p_1^\rho[\varepsilon_1^\tau(p_1\varepsilon_2) - \varepsilon_2^\tau(p_2\varepsilon_1)]. \tag{A.5}
\end{aligned}$$

The helicity projectors

$$\omega_\sigma = \frac{1 + \sigma\gamma_5}{2}, \tag{A.6}$$

with $\gamma_5 = i\gamma^0\gamma^1\gamma^2\gamma^3$, project on right- and left-handed massless fermions. Note that our set of 18 basic matrix elements $\mathcal{M}_j^\sigma$ is overcomplete. Because of the massless treatment of the fermions, CP invariance implies the relation[7]

$$\mathcal{M}_j^\sigma(\lambda_1, \lambda_2) = \mathcal{M}_j^\sigma(-\lambda_2, -\lambda_1), \tag{A.7}$$

resulting in only 12 independent matrix elements. The last three pairs, $\mathcal{M}_{7,8,9}^\sigma$, have been kept for convenience and can be expressed in terms of the others according to

$$\mathcal{M}_7^\sigma = \frac{s}{4}\sigma\mathcal{M}_8^\sigma + \mathcal{M}_2^\sigma + \frac{t-u}{4}\mathcal{M}_3^\sigma, \qquad \mathcal{M}_9^\sigma = -\frac{s}{2}\mathcal{M}_8^\sigma,$$

[7] We have fixed the overall phase of the matrix elements such that this relation holds. The density matrix will of course not be affected by this choice.

$$\sigma \mathcal{M}_8^\sigma = 2\left(\mathcal{M}_1^\sigma + \mathcal{M}_4^\sigma + \mathcal{M}_5^\sigma\right) - 3\mathcal{M}_3^\sigma. \tag{A.8}$$

For the lowest-order matrix element only a few of these basic matrix elements are relevant:

$$\Pi^0_{\sigma;\lambda_1\lambda_2}(M_W, M_W) = \delta_{(\sigma,-1)}\, G_1(t)\, \mathcal{M}_4^\sigma(\lambda_1, \lambda_2) + 2\, G_2(s,\sigma)\Big[\mathcal{M}_3^\sigma(\lambda_1, \lambda_2) - \mathcal{M}_1^\sigma(\lambda_1, \lambda_2)\Big], \tag{A.9}$$

where the coefficients $G_{1,2}$ are defined as

$$G_1(t) = -\frac{ie^2}{2s_W^2}\frac{1}{t}, \qquad G_2(s,\sigma) = ie^2\left(\frac{Q_e}{s} + \frac{c_W}{s_W}\frac{g_e(\sigma)}{s - M_Z^2}\right). \tag{A.10}$$

Here s_W and c_W are the sine and cosine of the weak mixing angle θ_W:

$$c_W = \cos\theta_W = \frac{M_W}{M_Z}, \qquad s_W = \sin\theta_W = \sqrt{1 - c_W^2}, \tag{A.11}$$

and $g_e(\sigma)$ denotes the coupling between the Z boson and electrons:

$$g_e(+1) = -\frac{s_W}{c_W}\, Q_e, \qquad g_e(-1) = -\frac{1 + 2Q_e s_W^2}{2s_W c_W}, \tag{A.12}$$

where $Q_e = -1$ is the charge of the electron.

For the virtual corrections to on-shell W-pair production we need the complete list of basic matrix elements $\mathcal{M}_j^\sigma$. For the W-boson helicity states (A.2) the non-vanishing matrix elements read:

$$\begin{aligned}
\mathcal{M}_4^\sigma(\pm1,\mp1) &= 2E^2(\cos\theta \mp \sigma)\sin\theta \\
\mathcal{M}_5^\sigma(\pm1,\mp1) &= -2E^2(\cos\theta \mp \sigma)\sin\theta \\
\mathcal{M}_6^\sigma(\pm1,\mp1) &= E^4\beta\sin^3\theta
\end{aligned} \tag{A.13}$$

$$\begin{aligned}
\mathcal{M}_1^\sigma(\pm1,\pm1) &= 2E^2\beta\sin\theta \\
\mathcal{M}_4^\sigma(\pm1,\pm1) &= 2E^2(\cos\theta - \beta)\sin\theta \\
\mathcal{M}_5^\sigma(\pm1,\pm1) &= -2E^2\cos\theta\sin\theta \\
\mathcal{M}_6^\sigma(\pm1,\pm1) &= E^4\beta\sin^3\theta
\end{aligned} \tag{A.14}$$

$$\begin{aligned}
\mathcal{M}_3^\sigma(\pm1,0) &= \mathcal{M}_3^\sigma(0,\mp1) = \frac{\sqrt{2}E}{M_W}\, 2E^2\beta\,(\cos\theta \mp \sigma) \\
\mathcal{M}_4^\sigma(\pm1,0) &= \mathcal{M}_4^\sigma(0,\mp1) = \frac{\sqrt{2}E}{M_W}\, E^2\left[2\beta - 2\cos\theta \mp \sigma(1 - \beta^2)\right](\cos\theta \mp \sigma) \\
\mathcal{M}_5^\sigma(\pm1,0) &= \mathcal{M}_5^\sigma(0,\mp1) = \frac{\sqrt{2}E}{M_W}\, E^2(\beta + 2\cos\theta \pm \sigma)(\cos\theta \mp \sigma) \\
\mathcal{M}_6^\sigma(\pm1,0) &= \mathcal{M}_6^\sigma(0,\mp1) = -\frac{\sqrt{2}E}{M_W}\, E^4\beta\,(\beta + \cos\theta)\sin^2\theta
\end{aligned}$$

$$\mathcal{M}_7^\sigma(\pm 1, 0) = \mathcal{M}_7^\sigma(0, \mp 1) = -\frac{\sqrt{2}E}{M_W} 2E^4\beta^2 \sin^2\theta$$

$$\mathcal{M}_8^\sigma(\pm 1, 0) = \mathcal{M}_8^\sigma(0, \mp 1) = \pm\frac{\sqrt{2}E}{M_W} 2E^2\beta^2(\cos\theta \mp \sigma)$$

$$\mathcal{M}_9^\sigma(\pm 1, 0) = \mathcal{M}_9^\sigma(0, \mp 1) = \mp\frac{\sqrt{2}E}{M_W} 4E^4\beta^2(\cos\theta \mp \sigma) \qquad \text{(A.15)}$$

$$\mathcal{M}_1^\sigma(0, 0) = \frac{E^2}{M_W^2} 2E^2\beta(1 + \beta^2)\sin\theta$$

$$\mathcal{M}_2^\sigma(0, 0) = \frac{E^2}{M_W^2} 8E^4\beta^3\sin\theta$$

$$\mathcal{M}_3^\sigma(0, 0) = \frac{E^2}{M_W^2} 8E^2\beta\sin\theta$$

$$\mathcal{M}_4^\sigma(0, 0) = \frac{E^2}{M_W^2} 2E^2[3\beta - \beta^3 - 2\cos\theta]\sin\theta$$

$$\mathcal{M}_5^\sigma(0, 0) = \frac{E^2}{M_W^2} 4E^2(\beta + \cos\theta)\sin\theta$$

$$\mathcal{M}_6^\sigma(0, 0) = \frac{E^2}{M_W^2} 2E^4\beta(\beta + \cos\theta)^2\sin\theta$$

$$\mathcal{M}_7^\sigma(0, 0) = \frac{E^2}{M_W^2} 8E^4\beta^2(\beta + \cos\theta)\sin\theta. \qquad \text{(A.16)}$$

From this list and the invariant functions of Ref. [9] one can obtain the density matrix $\mathcal{P}_{[\lambda_1\lambda_2][\lambda_1'\lambda_2']}(M_W, M_W)$ in a straightforward way.

A.2   Virtual corrections to the decay stages

Since we have chosen a specific polarization basis for the calculation of the production stage, both at lowest order and at virtual one-loop order, the same basis has to be used for describing the on-shell W-boson decays. All results presented in this subsection are therefore given in the LAB frame, rather than the often used rest frame of the decaying W boson.

Like in the on-shell W-pair-production case, we again write the decay matrix element as a sum of invariant functions $\mathcal{E}_j^{(\pm)}$ multiplied by Lorentz-invariant basic matrix elements $\mathcal{M}_j^{(\pm)}(\lambda_i)$:

$$\Delta_{\lambda_1}^{(+)}(M_W) = \sum_j \mathcal{E}_j^{(+)}\mathcal{M}_j^{(+)}(\lambda_1), \qquad \Delta_{\lambda_2}^{(-)}(M_W) = \sum_j \mathcal{E}_j^{(-)}\mathcal{M}_j^{(-)}(\lambda_2). \qquad \text{(A.17)}$$

In the most general case of the decay of a W boson into massive quarks, there are four basic matrix elements [12]. For the decay of the W^- boson, $W^-(p_2) \to f_2(k_2)\bar{f}_2'(k_2')$, they are given by

$$\mathcal{M}_0^{(-)}(\lambda_2) = \bar{u}(k_2)\not{\epsilon}_2^*\omega_- v(k_2'),$$

$$
\begin{aligned}
\mathcal{M}_1^{(-)}(\lambda_2) &= \bar{u}(k_2)\,\slashed{\epsilon}_2^*\,\omega_+\,v(k_2'), \\
\mathcal{M}_2^{(-)}(\lambda_2) &= [\bar{u}(k_2)\,\omega_-\,v(k_2')](\varepsilon_2^* k_2), \\
\mathcal{M}_3^{(-)}(\lambda_2) &= [\bar{u}(k_2)\,\omega_+\,v(k_2')](\varepsilon_2^* k_2),
\end{aligned}
\tag{A.18}
$$

with similar expressions for the decay of the W^+ boson. For massless particles in the final state only $\mathcal{M}_0^{(\pm)}$ occurs. At lowest-order we then obtain

$$
\Delta_{\lambda_i}^0(M_W) = \frac{ieV_{f_i' f_i}}{\sqrt{2}s_W}\,\mathcal{M}_0^{(\pm)}(\lambda_i),
\tag{A.19}
$$

with $V_{f'f}$ the quark mixing matrix.

For the decay density matrix $\mathcal{D}_{\lambda_i \lambda_i'}(M_W)$ it is useful to have the expressions for

$$
\mathcal{M}_{00}^{(\pm)}(\lambda_i, \lambda_i') = \sum_{\text{fermion helicities}} \mathcal{M}_0^{(\pm)}(\lambda_i)\,\mathcal{M}_0^{(\pm)\,*}(\lambda_i').
\tag{A.20}
$$

For the decay of the W^- boson one finds

$$
\begin{aligned}
\mathcal{M}_{00}^{(-)}(0, 0) &= \frac{M_W^4}{E^2}\,\frac{\sin^2\theta_4}{(1 - \beta\cos\theta_4)^2}, \\
\mathcal{M}_{00}^{(-)}(\pm1, \pm1) &= \frac{M_W^2}{2}\,(1 \pm \beta)^2\,\frac{(1 \mp \cos\theta_4)^2}{(1 - \beta\cos\theta_4)^2}, \\
\mathcal{M}_{00}^{(-)}(\pm1, 0) &= \pm\frac{M_W^3}{\sqrt{2}E}\,(1 \pm \beta)\,e^{\mp i\phi_4}\,\frac{(1 \mp \cos\theta_4)\sin\theta_4}{(1 - \beta\cos\theta_4)^2}, \\
\mathcal{M}_{00}^{(-)}(0, \pm1) &= \pm\frac{M_W^3}{\sqrt{2}E}\,(1 \pm \beta)\,e^{\pm i\phi_4}\,\frac{(1 \mp \cos\theta_4)\sin\theta_4}{(1 - \beta\cos\theta_4)^2}, \\
\mathcal{M}_{00}^{(-)}(\pm1, \mp1) &= -\frac{M_W^4}{2E^2}\,e^{\mp 2i\phi_4}\,\frac{\sin^2\theta_4}{(1 - \beta\cos\theta_4)^2}.
\end{aligned}
\tag{A.21}
$$

The expressions for the charge-conjugate process, describing the decay of the W^+ boson, can be obtained through the simple relation

$$
\mathcal{M}_{00}^{(+)}(\lambda_1, \lambda_1') = \mathcal{M}_{00}^{(-)}(-\lambda_1, -\lambda_1'),
$$

$$
\text{with} \quad \phi_4 \to \phi_3, \ \cos\theta_4 \to \cos\theta_3, \ \sin\theta_4 \to -\sin\theta_3.
\tag{A.22}
$$

These expressions can be combined with the invariant functions from Ref. [12] to obtain the decay density matrices including virtual RC. It can be seen from Eq. (A.21) that the matrices $\mathcal{M}_{00}^{(\pm)}(\lambda_i, \lambda_i')$ contain asymmetric imaginary parts proportional to $\sin\phi_{3,4}$. These terms will be responsible for picking up imaginary loop effects present in the invariant functions, which do not depend on $\phi_{3,4}$. The symmetric parts of $\mathcal{M}_{00}^{(\pm)}(\lambda_i, \lambda_i')$ are real and depend on $\cos\phi_{3,4}$. Upon integration over the azimuthal angles $\phi_{3,4}$ the matrices $\mathcal{M}_{00}^{(\pm)}(\lambda_i, \lambda_i')$ become real and diagonal, and the same holds for the corresponding decay density matrices.

Appendix B:
Bremsstrahlung in Weyl–v.d. Waerden formalism

Like in the case of the virtual factorizable corrections, also for the real-photon factor-
izable corrections our choice for the polarization basis and the calculational scheme
is guided by existing calculations in the literature. As mentioned in Sect. 2.1, there
is no objection against having different choices for the polarization basis in differ-
ent contributions to the RC, provided that the contribution to the density matrix
is calculated consistently within the chosen approach. We adopt the conventions of
Ref. [11] and calculate the real-photon RC in the Weyl–van der Waerden formalism.

B.1   The Weyl–v.d. Waerden formalism
for massive gauge bosons

Before giving the results for the various matrix elements, we first give a few essential
details of the Weyl–van der Waerden formalism for massive gauge bosons. We follow
the conventions of Ref. [11] and define the two-dimensional Weyl spinor for a massless
particle with light-like momentum q as

$$q_A = \begin{pmatrix} \sqrt{q_0 - q_3} \\ -(q_1 + iq_2)/\sqrt{q_0 - q_3} \end{pmatrix}, \qquad q_{\dot{A}} = (q_A)^\bullet. \tag{B.1}$$

The indices can be raised and lowered by the spinor metric

$$\epsilon^{AB} = \begin{pmatrix} 0 & 1 \\ -1 & 0 \end{pmatrix} = \epsilon_{AB} = \epsilon^{\dot{A}\dot{B}} = \epsilon_{\dot{A}\dot{B}} \tag{B.2}$$

according to

$$q^A = q_B \, \epsilon^{BA}, \qquad q_A = \epsilon_{AB} \, q^B. \tag{B.3}$$

The spinor products

$$\langle qk \rangle = q_A k^A = -q^A k_A, \qquad \langle qk \rangle^\bullet = q_{\dot{A}} k^{\dot{A}} = -q^{\dot{A}} k_{\dot{A}} \tag{B.4}$$

are hence antisymmetric. In the Weyl representation for the γ-matrices we obtain the
following set of translation rules into two-dimensional spinor language:

$$u(q,+) = v(q,-) = \begin{pmatrix} q_A \\ 0 \end{pmatrix},$$

$$u(q,-) = v(q,+) = \begin{pmatrix} 0 \\ q^{\dot{A}} \end{pmatrix},$$

$$\gamma^\mu = \begin{pmatrix} 0 & \sigma^\mu_{\dot{B}A} \\ \sigma^{\mu\,\dot{A}B} & 0 \end{pmatrix},$$

$$Q_\mu \sigma^\mu_{\dot{A}B} = Q_{\dot{A}B} \quad \Rightarrow \quad 2QK = Q^{\dot{A}B} K_{\dot{A}B},$$

$$q_\mu \sigma^\mu_{\dot{A}B} = q_{\dot{A}B} = q_{\dot{A}} q_B \quad \Rightarrow \quad 2qk = |\langle qk \rangle|^2, \tag{B.5}$$

with Q, K arbitrary Lorentz vectors and q, k light-like ones. The Dirac spinors $u(q, \pm)$ denote right-handed $(+)$ and left-handed $(-)$ states. The matrices $\sigma^{\mu \, \dot A B} = (\sigma^0, \vec{\sigma})$ consist of the 2×2 unit matrix σ^0 and the standard Pauli matrices σ^i $(i = 1, 2, 3)$

$$\sigma^0 = \begin{pmatrix} 1 & 0 \\ 0 & 1 \end{pmatrix}, \quad \sigma^1 = \begin{pmatrix} 0 & 1 \\ 1 & 0 \end{pmatrix}, \quad \sigma^2 = \begin{pmatrix} 0 & -i \\ i & 0 \end{pmatrix}, \quad \sigma^3 = \begin{pmatrix} 1 & 0 \\ 0 & -1 \end{pmatrix}. \quad (B.6)$$

For a photon with momentum k we use the polarization vectors describing the two helicity eigenstates

$$\varepsilon_\gamma^{\dot A B}(+1) = \sqrt{2} \, \frac{k^{\dot A} b^B}{\langle kb \rangle}, \qquad \varepsilon_\gamma^{\dot A B}(-1) = \sqrt{2} \, \frac{b^{\dot A} k^B}{\langle kb \rangle^*} = \varepsilon_\gamma^{\dagger \, \dot A B}(+1). \quad (B.7)$$

To handle the massive $W^\pm$ bosons we first decompose their massive momenta $p_{1,2}$ into a sum of two light-like momenta:

$$p_{1,2}^\mu = p_{3,4}^\mu + c_{1,2} \, m_{3,4}^\mu, \qquad c_1 \, (2p_3 m_3) = c_2 \, (2p_4 m_4) = M_W^2. \quad (B.8)$$

Note that the so-defined light-like vectors $m_{3,4}$ can be chosen freely. An orthogonal basis for the three physical polarizations of the massive $W^\pm$ bosons is now given by

$$\varepsilon_1^{\dot A B}(+1) = \sqrt{2} \, \frac{p_3^{\dot A} m_3^B}{\langle p_3 m_3 \rangle}, \qquad \varepsilon_1^{\dot A B}(-1) = \sqrt{2} \, \frac{m_3^{\dot A} p_3^B}{\langle p_3 m_3 \rangle^*},$$

$$\varepsilon_1^{\dot A B}(0) = \frac{1}{M_W} \, (p_3 - c_1 m_3)^{\dot A B},$$

$$\varepsilon_2^{\dot A B}(+1) = \sqrt{2} \, \frac{p_4^{\dot A} m_4^B}{\langle p_4 m_4 \rangle}, \qquad \varepsilon_2^{\dot A B}(-1) = \sqrt{2} \, \frac{m_4^{\dot A} p_4^B}{\langle p_4 m_4 \rangle^*},$$

$$\varepsilon_2^{\dot A B}(0) = \frac{1}{M_W} \, (p_4 - c_2 m_4)^{\dot A B}, \quad (B.9)$$

with $\varepsilon_i^{\dot A B}(-1) = \varepsilon_i^{\dagger \, \dot A B}(+1)$. It should be stressed that the so-obtained polarization basis does not correspond to the helicity eigenstates. However, the corresponding states transform like helicity eigenstates under a parity transformation, which is very useful for practical calculations.

An example: lowest-order on-shell W-pair production

As an example we apply the above method to the lowest-order on-shell production stage. To this end we choose $m_{3,4} = p_{4,3}$ in Eqs. (B.8) and (B.9), and write $c_1 = c_2 = M_W^2/(2p_3 p_4) \equiv c$.

The complete Born amplitude of the process is of the form

$$\Pi_{\sigma; \lambda_1 \lambda_2}^0(M_W, M_W) = G_1(t) \, \mathcal{M}_t(\sigma, \lambda_1, \lambda_2) + G_2(s, \sigma) \mathcal{M}_s(\sigma, \lambda_1, \lambda_2), \quad (B.10)$$

where the coefficients $G_{1,2}$ are defined in Eq. (A.10), and

$$\mathcal{M}_t(\sigma, \lambda_1, \lambda_2) = \bar{v}(q_1)\,\slashed{\varepsilon}_1(\slashed{q}_2 - \slashed{p}_2)\slashed{\varepsilon}_2\,\omega_- u(q_2),$$
$$\mathcal{M}_s(\sigma, \lambda_1, \lambda_2) = \bar{v}(q_1)\slashed{V}(p_1, \varepsilon_1, p_2, \varepsilon_2)\,\omega_\sigma u(q_2), \tag{B.11}$$

where

$$V^\mu(p_1, \varepsilon_1, p_2, \varepsilon_2) = 2\varepsilon_1^\mu(\varepsilon_2 p_1) - 2\varepsilon_2^\mu(\varepsilon_1 p_2) + (p_2^\mu - p_1^\mu)(\varepsilon_1 \varepsilon_2). \tag{B.12}$$

These matrix elements can be translated into two-dimensional representation, e.g. for $\sigma = -1$ one obtains

$$\mathcal{M}_t(\sigma = -1, \lambda_1, \lambda_2) = q_1^A \varepsilon_{1\,BA}(q_2 - p_2)^{BC}\varepsilon_{2\,\dot{D}C}\,q_2^{\dot{D}},$$
$$\mathcal{M}_s(\sigma = -1, \lambda_1, \lambda_2) = q_1^A V_{\dot{B}A}(p_1, \varepsilon_1, p_2, \varepsilon_2)\,q_2^{\dot{B}}. \tag{B.13}$$

For $\sigma = +1$ we can make use of the relations

$$\mathcal{M}_t(\sigma = +1, \lambda_1, \lambda_2) = 0, \qquad \mathcal{M}_s(\sigma = +1, \lambda_1, \lambda_2) = \mathcal{M}_s^*(\sigma = -1, -\lambda_1, -\lambda_2), \tag{B.14}$$

where the last identity is the result of parity conservation of the s-channel matrix element $\mathcal{M}_s$, since all parity violation is contained in the coefficient $G_2(s, \sigma)$. From CP invariance one obtains two more relations:

$$\mathcal{M}_{s,t}(q_1, -\sigma, q_2, \sigma, p_1, \lambda_1, p_2, \lambda_2) = -\mathcal{M}_{s,t}^*(q_2, -\sigma, q_1, \sigma, p_2, -\lambda_2, p_1, -\lambda_1), \tag{B.15}$$

so only 6 independent polarization states remain. The independent matrix elements read:

$$\mathcal{M}_t(-1, +1, +1) = \frac{2}{\langle p_3 p_1\rangle^2}\langle q_1 p_4\rangle\langle q_2 p_4\rangle^*\big[2q_1 p_3 - M_W^2\big],$$

$$\mathcal{M}_t(-1, +1, -1) = -\frac{\langle q_1 p_4\rangle\langle q_2 p_4\rangle\langle q_2 p_3\rangle^{*\,2}}{p_3 p_4},$$

$$\mathcal{M}_t(-1, -1, +1) = \frac{\langle q_1 p_3\rangle^2\langle q_1 p_4\rangle^*\langle q_2 p_4\rangle^*}{p_3 p_4},$$

$$\mathcal{M}_t(-1, +1, 0) = \frac{\sqrt{2}\langle q_1 p_4\rangle\langle q_2 p_3\rangle^*}{M_W\langle p_3 p_4\rangle}\big[2q_2 p_4 - 2c\,q_2 p_3 + M_W^2\big],$$

$$\mathcal{M}_t(-1, -1, 0) = \frac{\sqrt{2}\langle q_1 p_3\rangle\langle q_2 p_4\rangle^*}{M_W\langle p_3 p_4\rangle^*}\big[2q_2 p_4 - 2c\,q_2 p_3 - M_W^2\big],$$

$$\mathcal{M}_t(-1, 0, 0) = \langle q_1 p_3\rangle\langle q_2 p_3\rangle^*\Big\{1 - c + \frac{2}{M_W^2}(1 + c)\big[q_2 p_4 - c\,q_2 p_3\big]\Big\} \tag{B.16}$$

for the t-channel matrix elements, and

$$\mathcal{M}_s(-1, +1, +1) = -2\langle q_1 p_3\rangle\langle q_2 p_3\rangle^*\frac{\langle p_3 p_4\rangle^*}{\langle p_3 p_4\rangle}(1 - c),$$

$$\mathcal{M}_s(-1, +1, -1) = \mathcal{M}_s(-1, -1, +1) = 0,$$

$$
\begin{aligned}
\mathcal{M}_s(-1,+1,0) &= \frac{\sqrt{2}}{\bar{M}_W}\,\langle q_1 p_4\rangle\langle q_2 p_3\rangle^*\langle p_3 p_4\rangle^*(1-c^2),\\
\mathcal{M}_s(-1,-1,0) &= \frac{\sqrt{2}}{\bar{M}_W}\,\langle q_1 p_3\rangle\langle p_3 p_4\rangle\langle q_2 p_1\rangle^*(1-c^2),\\
\mathcal{M}_s(-1,0,0) &= \langle q_1 p_3\rangle\langle q_2 p_3\rangle^*\left(\frac{1}{c}+3-3c-c^2\right)
\end{aligned}
\tag{B.17}
$$

for the s-channel matrix elements.

B.2   Non-collinear photon radiation from the production stage

Using the above example as guideline, we now address the process of non-collinear real-photon radiation from the production stage:

$$
e^+(q_1,\sigma_1)e^-(q_2,\sigma_2)\to W^+(p_1,\lambda_1)W^-(p_2,\lambda_2)\gamma(k,\lambda).
\tag{B.18}
$$

Since we are dealing with non-collinear radiation and massless initial-state electrons and positrons, we can ignore the possibility of helicity flip in the initial state. Therefore again the condition $\sigma_1=-\sigma_2=-\sigma$ applies. As a first step we extend the list of kinematical invariants of Sect. 2.1:

$$
\begin{aligned}
s &= (q_1+q_2)^2, & t &= (q_1-p_1)^2, & u &= (q_1-p_2)^2,\\
s' &= (p_1+p_2)^2, & t' &= (q_2-p_2)^2, & u' &= (q_2-p_1)^2.
\end{aligned}
\tag{B.19}
$$

The complete matrix element can now be written in the form

$$
\Pi_\gamma(M_W,M_W)=-e\Big[G_1(t')\mathcal{M}_1^\gamma+G_1(t)\mathcal{M}_2^\gamma+G_2(s',\sigma)\mathcal{M}_3^\gamma+G_2(s,\sigma)\mathcal{M}_4^\gamma\Big],
\tag{B.20}
$$

where the functions $G_{1,2}$ are the same as the ones defined in Eq. (A.10). The basic matrix elements $\mathcal{M}_j^\gamma$ are invariant under gauge transformations of the radiated photon. This is due to the fact that the photon is attached to a combination of lines through which the charge flows. For instance, $\mathcal{M}_1^\gamma$ is obtained by photon emission from the e^+ and W^+ lines of the t-channel Born diagram. The matrix elements are given by

$$
\begin{aligned}
\mathcal{M}_1^\gamma &= \bar{v}(q_1)\Bigg\{\slashed{\epsilon}_\gamma\frac{\slashed{q}_1-\slashed{k}}{2q_1 k}\slashed{\epsilon}_1(\slashed{q}_2-\slashed{p}_2)\slashed{\epsilon}_2+\\
&\quad +\Big[-2\slashed{\epsilon}_1(\epsilon_\gamma p_1)+2\slashed{\epsilon}_\gamma(\epsilon_1 k)-2\slashed{k}(\epsilon_\gamma\epsilon_1)\Big]\frac{\slashed{q}_2-\slashed{p}_2}{2p_1 k}\slashed{\epsilon}_2\Bigg\}\omega_-u(q_2),\\[4pt]
\mathcal{M}_2^\gamma &= \bar{v}(q_1)\Bigg\{\slashed{\epsilon}_1(\slashed{q}_1-\slashed{p}_1)\slashed{\epsilon}_2\frac{\slashed{q}_2-\slashed{k}}{2q_2 k}\slashed{\epsilon}_\gamma+\\
&\quad +\slashed{\epsilon}_1\frac{\slashed{p}_1-\slashed{q}_1}{2p_2 k}\Big[2\slashed{\epsilon}_2(\epsilon_\gamma p_2)-2\slashed{\epsilon}_\gamma(\epsilon_2 k)+2\slashed{k}(\epsilon_\gamma\epsilon_2)\Big]\Bigg\}\omega_-u(q_2),\\[4pt]
\mathcal{M}_3^\gamma &= \bar{v}(q_1)\Bigg\{\slashed{\epsilon}_\gamma\frac{\slashed{q}_1-\slashed{k}}{2q_1 k}\slashed{V}(p_1,\epsilon_1,p_2,\epsilon_2)-\slashed{V}(p_1,\epsilon_1,p_2,\epsilon_2)\frac{\slashed{q}_2-\slashed{k}}{2q_2 k}\slashed{\epsilon}_\gamma\Bigg\}\omega_\sigma u(q_2),\\[4pt]
\mathcal{M}_4^\gamma &= \bar{v}(q_1)\Bigg\{-2\slashed{\epsilon}_\gamma(\epsilon_1\epsilon_2)+\slashed{V}_b(p_1,\epsilon_1,p_2,\epsilon_2)+\slashed{V}_b(p_2,\epsilon_2,p_1,\epsilon_1)\Bigg\}\omega_\sigma u(q_2),
\end{aligned}
\tag{B.21}
$$

where we introduced the shorthand notation

$$\frac{p_1 k}{2} V_b^\mu(p_1, \varepsilon_1, p_2, \varepsilon_2) =$$

$$= -\frac{\varepsilon_\gamma p_1}{2} V^\mu(p_1 + k, \varepsilon_1, p_2, \varepsilon_2) + \left[p_1^\mu(\varepsilon_1 \varepsilon_\gamma) + \varepsilon_\gamma^\mu(\varepsilon_1 k) \right] (\varepsilon_2 p_1 + \varepsilon_2 k)$$

$$+ \varepsilon_2^\mu \left[(\varepsilon_1 \varepsilon_\gamma)(k p_1 + k p_2) - (\varepsilon_1 k)(\varepsilon_\gamma p_2) \right] + p_2^\mu \left[(\varepsilon_2 \varepsilon_\gamma)(\varepsilon_1 k) + (\varepsilon_1 \varepsilon_\gamma)(\varepsilon_2 p_1) \right]. \quad (B.22)$$

The vertex function V can be taken from Eq. (B.12). Note that the term $-2\not{k}(\varepsilon_\gamma \varepsilon_1)$ between the square brackets of $\mathcal{M}_1^\gamma$ originally had the form $(\not{p}_1 - \not{k})(\varepsilon_\gamma \varepsilon_1)$. The difference $(\not{p}_1 + \not{k})(\varepsilon_\gamma \varepsilon_1)$ cancels against similar terms in $\mathcal{M}_1^\gamma$. This cancellation is a consequence of the lowest-order Ward identity of the W^+ boson. In the same way also the Ward identity of the W^- boson has been used to simplify $\mathcal{M}_2^\gamma$.

For the calculation in the Weyl – van der Waerden formalism we choose $m_{3,4} = k$ in Eqs. (B.8) and (B.9). Furthermore we choose the free gauge parameter b in Eq. (B.7) to be equal to q_1. Like in the case without photon radiation, we can exploit some symmetry relations. First of all CP invariance implies the relations

$$\mathcal{M}_1^\gamma(q_1, -\sigma, q_2, \sigma, p_1, \lambda_1, p_2, \lambda_2, k, \lambda) = \mathcal{M}_2^{\gamma *}(q_2, -\sigma, q_1, \sigma, p_2, -\lambda_2, p_1, -\lambda_1, k, -\lambda),$$

$$\mathcal{M}_{3,4}^\gamma(q_1, -\sigma, q_2, \sigma, p_1, \lambda_1, p_2, \lambda_2, k, \lambda) = \mathcal{M}_{3,4}^{\gamma *}(q_2, -\sigma, q_1, \sigma, p_2, -\lambda_2, p_1, -\lambda_1, k, -\lambda).$$

$$(B.23)$$

The matrix elements for right-handed electrons are again completely determined:

$$\mathcal{M}_1^\gamma(\sigma = +1) = \mathcal{M}_2^\gamma(\sigma = +1) = 0,$$

$$\mathcal{M}_{3,4}^\gamma(\sigma = +1, \lambda_1, \lambda_2, \lambda) = \mathcal{M}_{3,4}^{\gamma *}(\sigma = -1, -\lambda_1, -\lambda_2, -\lambda), \quad (B.24)$$

where the last identity is the result of parity conservation of the s-channel matrix elements $\mathcal{M}_{3,4}^\gamma$. Due to the symmetry (antisymmetry) property of the quartic (triple) gauge boson vertex under the exchange of the W^+ and W^- bosons, one can derive two more relations:

$$\mathcal{M}_3^\gamma(p_1, \lambda_1, p_2, \lambda_2, k, \lambda) = -\mathcal{M}_3^\gamma(p_2, \lambda_2, p_1, \lambda_1, k, \lambda),$$

$$\mathcal{M}_4^\gamma(p_1, \lambda_1, p_2, \lambda_2, k, \lambda) = +\mathcal{M}_4^\gamma(p_2, \lambda_2, p_1, \lambda_1, k, \lambda). \quad (B.25)$$

After all these preparations we now list the independent matrix elements for $\sigma = -1$. In order to keep the results as compact as possible we use the shorthand notations $\langle r_i r_j \rangle = \langle ij \rangle$ and $(r_i r_j) = (ij)$, with $r_i = (q_1, q_2, p_3, p_4, k)$ for $i = (1, 2, 3, 4, 5)$. For the amplitude $\mathcal{M}_1^\gamma(\lambda_1, \lambda_2, \lambda)$ we find:

$$\mathcal{M}_1^\gamma(+1, +1, +1) = -4\sqrt{2} \frac{\langle 15 \rangle \langle 24 \rangle^\bullet}{\langle 35 \rangle^2 \langle 45 \rangle} \left[(35) - (13) - (15) \right],$$

$$\mathcal{M}_1^\gamma(+1, -1, +1) = -\frac{2\sqrt{2} \langle 25 \rangle^\bullet}{\langle 35 \rangle^2 \langle 45 \rangle^\bullet} \left[\langle 24 \rangle \left(\langle 13 \rangle \langle 23 \rangle^\bullet + \langle 15 \rangle \langle 25 \rangle^\bullet \right) - c_2 \langle 13 \rangle \langle 45 \rangle \langle 35 \rangle^\bullet \right],$$

$$\mathcal{M}_1^\gamma(-1,+1,+1) = -2\sqrt{2}\,\frac{\langle 13\rangle^2\langle 24\rangle^\bullet}{\langle 15\rangle\langle 45\rangle}\left[1-\frac{\langle 15\rangle}{\langle 35\rangle}\right],$$

$$\mathcal{M}_1^\gamma(-1,-1,+1) = -\sqrt{2}\,\frac{\langle 13\rangle^2\langle 24\rangle\langle 25\rangle^{\bullet 2}}{\langle 15\rangle\langle 45\rangle^\bullet\langle 35\rangle},$$

$$\mathcal{M}_1^\gamma(+1,0,+1) = -\frac{2}{\langle 35\rangle^2 M_W}\Big\{\big[\langle 13\rangle\langle 23\rangle^\bullet+\langle 15\rangle\langle 25\rangle^\bullet\big]\big[t'+4(24)\big]$$
$$-2c_2\langle 13\rangle\langle 45\rangle\langle 24\rangle^\bullet\langle 35\rangle^\bullet\Big\},$$

$$\mathcal{M}_1^\gamma(-1,0,+1) = -\frac{\langle 13\rangle^2\langle 25\rangle^\bullet}{\langle 15\rangle\langle 35\rangle M_W}\big[t'+4(24)\big],$$

$$\mathcal{M}_1^\gamma(0,+1,+1) = -4\,\frac{\langle 13\rangle\langle 24\rangle^\bullet}{\langle 35\rangle\langle 45\rangle M_W}\Big\{-(13)+(1-c_1)\big[(35)-(15)\big]\Big\},$$

$$\mathcal{M}_1^\gamma(0,-1,+1) = -2\,\frac{\langle 13\rangle\langle 25\rangle^\bullet}{\langle 35\rangle\langle 45\rangle^\bullet M_W}\bigg[\frac{\langle 13\rangle}{\langle 15\rangle}\big(\langle 24\rangle\langle 23\rangle^\bullet-c_2\langle 45\rangle\langle 35\rangle^\bullet\big)+$$
$$+(1-c_1)\langle 24\rangle\langle 25\rangle^\bullet\bigg],$$

$$\mathcal{M}_1^\gamma(0,0,+1) = -\frac{\sqrt{2}\langle 13\rangle}{\langle 35\rangle M_W^2}1\bigg[-2c_2\frac{\langle 13\rangle}{\langle 15\rangle}\langle 45\rangle\langle 24\rangle^\bullet\langle 35\rangle^\bullet$$
$$+\big[t'+4(24)\big]\left(\frac{\langle 13\rangle}{\langle 15\rangle}\langle 23\rangle^\bullet+(1-c_1)\langle 25\rangle^\bullet\right)\bigg],$$

$$\mathcal{M}_1^\gamma(+1,+1,-1) = \sqrt{2}\,\frac{\langle 15\rangle^2\langle 13\rangle^{\bullet 2}\langle 24\rangle^\bullet}{\langle 45\rangle\langle 15\rangle^\bullet\langle 35\rangle},$$

$$\mathcal{M}_1^\gamma(+1,-1,-1) = -\sqrt{2}\,\frac{\langle 15\rangle\langle 13\rangle^\bullet\langle 25\rangle^\bullet}{\langle 15\rangle^\bullet\langle 45\rangle\langle 35\rangle}\big[\langle 24\rangle\langle 23\rangle^\bullet-c_2\langle 45\rangle\langle 35\rangle^\bullet\big],$$

$$\mathcal{M}_1^\gamma(-1,+1,-1) = -\frac{8\sqrt{2}\langle 24\rangle^\bullet}{\langle 45\rangle\langle 15\rangle^\bullet\langle 35\rangle^{\bullet 2}}\big[(15)-(35)\big]\big[(35)-(13)-(15)\big],$$

$$\mathcal{M}_1^\gamma(-1,-1,-1) = \frac{4\sqrt{2}\langle 24\rangle\langle 25\rangle^{\bullet 2}}{\langle 35\rangle^{\bullet 2}\langle 45\rangle^\bullet\langle 15\rangle^\bullet}\big[(35)-(13)-(15)\big],$$

$$\mathcal{M}_1^\gamma(+1,0,-1) = -\frac{\langle 15\rangle\langle 13\rangle^\bullet}{\langle 15\rangle^\bullet\langle 35\rangle M_W}\Big\{-2c_2\langle 45\rangle\langle 24\rangle^\bullet\langle 35\rangle^\bullet+\langle 23\rangle^\bullet\big[t'+4(24)\big]\Big\},$$

$$\mathcal{M}_1^\gamma(-1,0,-1) = \frac{4\langle 25\rangle^\bullet}{\langle 15\rangle^\bullet\langle 35\rangle^{\bullet 2}M_W}\big[t'+4(24)\big]\big[(35)-(13)-(15)\big],$$

$$\mathcal{M}_1^\gamma(0,+1,-1) = -\frac{4\langle 15\rangle\langle 13\rangle^\bullet\langle 24\rangle^\bullet}{\langle 45\rangle\langle 15\rangle^\bullet\langle 35\rangle^\bullet M_W}\Big\{c_1\big[(15)-(35)\big]-(13)-(15)+(35)\Big\},$$

$$\mathcal{M}_1^\gamma(0,-1,-1) = \frac{2\langle 25\rangle^\bullet}{\langle 15\rangle^\bullet\langle 35\rangle^\bullet\langle 45\rangle^\bullet M_W}\Big\{c_1\langle 15\rangle\langle 24\rangle\langle 13\rangle^\bullet\langle 25\rangle^\bullet$$
$$+2\big(\langle 24\rangle\langle 23\rangle^\bullet-c_2\langle 45\rangle\langle 35\rangle^\bullet\big)\big[(35)-(13)-(15)\big]\Big\},$$

$$\mathcal{M}_1^\gamma(0,0,-1) = \frac{\sqrt{2}}{\langle 15\rangle^\bullet \langle 35\rangle^\bullet M_W^2}\left\{ -4c_2\langle 24\rangle^\bullet\langle 35\rangle^\bullet\langle 45\rangle\big[(35)-(13)-(15)\big]\right.$$
$$\left. + \big[t'+4(24)\big]\Big(c_1\langle 15\rangle\langle 13\rangle^\bullet\langle 25\rangle^\bullet + 2\langle 23\rangle^\bullet\big[(35)-(13)-(15)\big]\Big)\right\}.$$
$$(B.26)$$

The independent matrix elements $\mathcal{M}_3^\gamma(\lambda_1,\lambda_2,\lambda)$ read:

$$\mathcal{M}_3^\gamma(+1,+1,+1) = -\frac{4\sqrt{2}\langle 15\rangle\langle 34\rangle^\bullet}{\langle 25\rangle\langle 35\rangle\langle 45\rangle}\big[-(12)+(35)+(45)\big],$$

$$\mathcal{M}_3^\gamma(+1,-1,+1) = \frac{2\sqrt{2}}{\langle 25\rangle\langle 35\rangle\langle 45\rangle^\bullet}\left\{ 2\frac{\langle 12\rangle}{\langle 15\rangle}(45)\langle 14\rangle\langle 23\rangle^\bullet + c_2\langle 12\rangle\langle 45\rangle\langle 25\rangle^\bullet\langle 35\rangle^\bullet\right.$$
$$\left. - \langle 35\rangle^\bullet\Big[\langle 34\rangle\big(\langle 12\rangle\langle 23\rangle^\bullet + \langle 15\rangle\langle 35\rangle^\bullet\big) - 2(45)\langle 14\rangle\Big]\right\},$$

$$\mathcal{M}_3^\gamma(-1,-1,+1) = -\frac{2\sqrt{2}(12)^2\langle 34\rangle\langle 25\rangle^{\bullet 2}}{\langle 15\rangle\langle 25\rangle\langle 35\rangle^\bullet\langle 45\rangle^\bullet},$$

$$\mathcal{M}_3^\gamma(+1,0,+1) = \frac{-4}{\langle 25\rangle\langle 35\rangle M_W}\left\{ -c_2\langle 12\rangle\langle 45\rangle\langle 25\rangle^\bullet\langle 34\rangle^\bullet\right.$$
$$\left. + \big[\langle 12\rangle\langle 23\rangle^\bullet + \langle 15\rangle\langle 35\rangle^\bullet\big]\big[(34)+c_1(45)-c_2(35)\big]\right\},$$

$$\mathcal{M}_3^\gamma(-1,0,+1) = -\frac{4\langle 12\rangle\langle 25\rangle^\bullet}{\langle 15\rangle\langle 25\rangle\langle 35\rangle^\bullet M_W}\left\{ -c_2\langle 15\rangle\langle 34\rangle\langle 45\rangle^\bullet +\right.$$
$$\left. + \langle 13\rangle\big[(34)+c_1(45)-c_2(35)\big]\right\},$$

$$\mathcal{M}_3^\gamma(0,0,+1) = -\frac{\sqrt{2}}{\langle 25\rangle M_W^2}\left\{ -2\frac{\langle 13\rangle}{\langle 15\rangle}\langle 14\rangle\langle 34\rangle^\bullet\big[(34)+c_2(35)+c_1(45)\big]\right.$$

$$+ \langle 13\rangle\langle 35\rangle^\bullet\big[2c_2^2(35)-4c_1^2(45)+(2c_2-4c_1)(34)-(3c_1-2c_2)M_W^2\big]$$
$$- \langle 14\rangle\langle 45\rangle^\bullet\big[2c_1^2(45)-4c_2^2(35)+(2c_1-4c_2)(34)-(3c_2-2c_1)M_W^2\big]\bigg\}.\,(B.27)$$

For $\mathcal{M}_4^\gamma(\lambda_1,\lambda_2,\lambda)$ we obtain:

$$\mathcal{M}_4^\gamma(+1,+1,+1) = -4\sqrt{2}\frac{\langle 15\rangle^2\langle 12\rangle^\bullet}{\langle 35\rangle^2\langle 45\rangle^2}\big[(34)+(35)+(45)\big],$$

$$\mathcal{M}_4^\gamma(+1,-1,+1) = \frac{2\sqrt{2}}{\langle 35\rangle^2\langle 45\rangle^\bullet}\left\{ c_1\langle 15\rangle\langle 34\rangle\langle 25\rangle^\bullet\langle 35\rangle^\bullet + 2\frac{\langle 14\rangle}{\langle 45\rangle}\langle 34\rangle\langle 23\rangle^\bullet(35)\right.$$
$$\left. + 2\langle 14\rangle\langle 25\rangle^\bullet\big[(34)+(45)\big]\right\},$$

$$\mathcal{M}_4^\gamma(-1,-1,+1) = \frac{\sqrt{2}}{2}\frac{\langle 12\rangle\langle 34\rangle^2\langle 25\rangle^{\bullet 2}}{(35)(45)},$$

$$\mathcal{M}_4^\gamma(+1,0,+1) = \frac{4}{M_W\langle 35\rangle^2}\left\{\frac{\langle 15\rangle}{\langle 45\rangle}\langle 34\rangle\langle 23\rangle^*\left[(34)+(35)(1-c_2)+(45)(1+c_1)\right]\right.$$
$$\left. - \langle 15\rangle\langle 25\rangle^*\left[(34)(1+2c_2)+(35)(1+c_2)+(45)(1+c_1)+M_W^2\right]\right\},$$

$$\mathcal{M}_4^\gamma(-1,0,+1) = \frac{2\langle 25\rangle^*}{M_W\langle 45\rangle\langle 35\rangle}\left\{-c_2\langle 14\rangle\langle 35\rangle\langle 34\rangle\langle 45\rangle^*\right.$$
$$\left. + \langle 13\rangle\langle 34\rangle\left[(34)+(35)(1-c_2)+(45)(1+c_1+2c_2)\right]\right\},$$

$$\mathcal{M}_4^\gamma(0,0,+1) = \frac{2\sqrt{2}\langle 34\rangle\langle 15\rangle\langle 25\rangle^*}{M_W^2\langle 35\rangle\langle 45\rangle}\left[-2c_1(1+c_1)(45)+c_2(1+c_2)(35)\right.$$
$$\left. + (c_2-2c_1)(34)+\left(c_2-\frac{3}{2}c_1-\frac{1}{2}\right)M_W^2\right]$$

$$-\frac{2\sqrt{2}\langle 14\rangle}{M_W^2\langle 45\rangle}\left[\langle 25\rangle^*+\langle 24\rangle^*\frac{\langle 34\rangle}{\langle 35\rangle}\right]\left[(34)+(35)(1+c_2)+(45)(1+c_1)\right]. \tag{B.28}$$

Lowest-order decay of the W bosons

Having fixed the polarization choice for the real-photon factorizable corrections to the production stage, we now calculate the lowest-order decay parts accordingly, since they are needed for obtaining the DPA limit of the full matrix element $\mathcal{M}_0$ in Eq. (2.2.10). The matrix elements for the W-boson decays are given by

$$\Delta_{\lambda_i}^0(M_W) = \frac{ieV_{f_i'f_i}}{\sqrt{2}s_W}\mathcal{M}_0^{(\pm)}(\lambda_i). \tag{B.29}$$

Using again $m_{3,4}=k$ in Eqs. (B.8) and (B.9), one ends up with

$$\mathcal{M}_0^{(+)}(+1) = \sqrt{2}\frac{\langle k_1'p_3\rangle\langle k_1k\rangle^*}{\langle p_3k\rangle^*}, \qquad \mathcal{M}_0^{(+)}(-1) = \sqrt{2}\frac{\langle k_1'k\rangle\langle k_1p_3\rangle^*}{\langle p_3k\rangle},$$

$$\mathcal{M}_0^{(+)}(0) = \frac{1}{M_W}\left(\langle k_1'p_3\rangle\langle k_1p_3\rangle^*-c_1\langle k_1'k\rangle\langle k_1k\rangle^*\right) \tag{B.30}$$

for the W^+ boson, and

$$\mathcal{M}_0^{(-)}(+1) = \sqrt{2}\frac{\langle k_2p_4\rangle\langle k_2'k\rangle^*}{\langle p_4k\rangle^*}, \qquad \mathcal{M}_0^{(-)}(-1) = \sqrt{2}\frac{\langle k_2k\rangle\langle k_2'p_4\rangle^*}{\langle p_4k\rangle},$$

$$\mathcal{M}_0^{(-)}(0) = \frac{1}{M_W}\left(\langle k_2p_4\rangle\langle k_2'p_4\rangle^*-c_2\langle k_2k\rangle\langle k_2'k\rangle^*\right) \tag{B.31}$$

for the W^- boson.

B.3   Non-collinear photon radiation from the decay stages

Next we address the process of non-collinear real-photon radiation from the decay stages. We start off with the decay of the W^+ boson:

$$W^+(p_1, \lambda_1) \to \bar{f}_1(k_1) f_1'(k_1') \gamma(k, \lambda). \tag{B.32}$$

We do not explicitly write the helicities of the final-state fermions. The final-state fermions are treated as being massless, hence for non-collinear radiation their helicities are fixed by the left-handed interaction with the W bosons: $\lambda_{f_1} = -\lambda_{f_1'} = +1$. The matrix element for process (B.32) can be written as

$$\Delta_\gamma^{(+)}(M_W) = \frac{ie^2 V_{f_1' f_1}}{\sqrt{2} s_W} \Big[-Q_{f_1} \mathcal{M}_1^{\gamma(+)} + Q_{f_1'} \mathcal{M}_2^{\gamma(+)} + \mathcal{M}_3^{\gamma(+)} \Big], \tag{B.33}$$

with

$$
\begin{aligned}
\mathcal{M}_1^{\gamma(+)} &= \bar{u}(k_1') \not{\epsilon}_1^* \omega_- \frac{\not{k}_1 + \not{k}}{2k_1 k} \not{\epsilon}_\gamma v(k_1) = k_1'^A \epsilon_{1\,\dot{B}A}^\dagger \frac{(k_1+k)^{\dot{B}C}}{2k_1 k} \epsilon_{\gamma\,\dot{D}C} k_1^{\dot{D}}, \\
\mathcal{M}_2^{\gamma(+)} &= \bar{u}(k_1') \not{\epsilon}_\gamma \frac{\not{k}_1' + \not{k}}{2k_1' k} \not{\epsilon}_1^* \omega_- v(k_1) = k_1'^A \epsilon_{\gamma\,\dot{B}A} \frac{(k_1'+k)^{\dot{B}C}}{2k_1' k} \epsilon_{1\,\dot{D}C}^\dagger k_1^{\dot{D}}, \\
\mathcal{M}_3^{\gamma(+)} &= \bar{u}(k_1') \frac{\not{V}(-p_1, \epsilon_1^*, k, \epsilon_\gamma)}{2 p_1 k} \omega_- v(k_1) = k_1'^A \frac{V(-p_1, \epsilon_1^*, k, \epsilon_\gamma)_{\dot{B}A}}{2 p_1 k} k_1^{\dot{B}}. \tag{B.34}
\end{aligned}
$$

Here the vertex function V can be taken from Eq. (B.12), but $(\not{k}+\not{p}_1)$ can be replaced by $2\not{k}$ as a result of the lowest-order Ward identity of the W^+ boson.

For the calculation in the Weyl – van der Waerden formalism we choose the same polarization basis as adopted for the on-shell W-pair example in Sect. B.1, i.e. $m_{3,4} = p_{4,3}$. For the definition of the photon polarizations we choose the free gauge parameter b in Eq. (B.7) to be equal to k_1. A straightforward calculation gives the following results for the amplitudes $\mathcal{M}_1^{\gamma(+)}(\lambda_1, \lambda)$:

$$
\begin{aligned}
\mathcal{M}_1^{\gamma(+)}(+1, +1) &= -2 \frac{\langle k_1' p_3 \rangle \langle p_4 k \rangle^*}{\langle k_1 k \rangle \langle p_3 p_4 \rangle^*}, \\
\mathcal{M}_1^{\gamma(+)}(+1, -1) &= \mathcal{M}_1^{\gamma(+)}(-1, -1) = \mathcal{M}_1^{\gamma(+)}(0, -1) = 0, \\
\mathcal{M}_1^{\gamma(+)}(-1, +1) &= -2 \frac{\langle k_1' p_4 \rangle \langle p_3 k \rangle^*}{\langle k_1 k \rangle \langle p_3 p_4 \rangle}, \\
\mathcal{M}_1^{\gamma(+)}(0, +1) &= \frac{\sqrt{2}}{\langle k_1 k \rangle M_W} \Big[c \langle k_1' p_4 \rangle \langle p_4 k \rangle^* - \langle k_1' p_3 \rangle \langle p_3 k \rangle^* \Big]. \tag{B.35}
\end{aligned}
$$

The corresponding expressions for $\mathcal{M}_{2,3}^{\gamma(+)}(\lambda_1, \lambda)$ read:

$$\mathcal{M}_2^{\gamma(+)}(+1, +1) = 2 \frac{\langle k_1 k_1' \rangle \langle k_1' p_3 \rangle \langle k_1 p_4 \rangle^*}{\langle k_1 k \rangle \langle k_1' k \rangle \langle p_3 p_4 \rangle^*},$$

$$
\begin{aligned}
\mathcal{M}_2^{\gamma(+)}(+1,-1) &= -2\,\frac{c\langle p_3 p_4\rangle\langle k_1 p_4\rangle^{\bullet\,2}}{\langle k_1 k\rangle^{\bullet}\langle k_1' k\rangle^{\bullet}\langle p_3 p_4\rangle^{\bullet}}, \\
\mathcal{M}_2^{\gamma(+)}(-1,+1) &= 2\,\frac{\langle k_1 k_1'\rangle\langle k_1' p_4\rangle\langle k_1 p_3\rangle^{\bullet}}{\langle k_1 k\rangle\langle k_1' k\rangle\langle p_3 p_4\rangle}, \\
\mathcal{M}_2^{\gamma(+)}(-1,-1) &= 2\,\frac{\langle k_1 p_3\rangle^{\bullet\,2}}{\langle k_1 k\rangle^{\bullet}\langle k_1' k\rangle^{\bullet}}, \\
\mathcal{M}_2^{\gamma(+)}(0,+1) &= \frac{\sqrt{2}\langle k_1 k_1'\rangle}{M_W\langle k_1 k\rangle\langle k_1' k\rangle}\Big[\langle k_1' p_3\rangle\langle k_1 p_3\rangle^{\bullet} - c\,\langle k_1' p_4\rangle\langle k_1 p_4\rangle^{\bullet}\Big], \\
\mathcal{M}_2^{\gamma(+)}(0,-1) &= -2\sqrt{2}c\,\frac{\langle p_3 p_4\rangle\langle k_1 p_3\rangle^{\bullet}\langle k_1 p_4\rangle^{\bullet}}{M_W\langle k_1 k\rangle^{\bullet}\langle k_1' k\rangle^{\bullet}},
\end{aligned} \tag{B.36}
$$

and

$$
\begin{aligned}
2p_1 k\,\mathcal{M}_3^{\gamma(+)}(+1,+1) &= -\frac{2\langle k_1' p_3\rangle}{\langle k_1 k\rangle\langle p_3 p_4\rangle^{\bullet}}\Big[\langle k_1 k_1'\rangle\langle k_1 p_4\rangle^{\bullet}\langle k_1' k\rangle^{\bullet} - 2k_1 k\langle p_4 k\rangle^{\bullet}\Big], \\
2p_1 k\,\mathcal{M}_3^{\gamma(+)}(+1,-1) &= 2c\,\frac{\langle k_1' k\rangle\langle p_3 p_4\rangle\langle k_1 p_4\rangle^{\bullet\,2}}{\langle k_1 k\rangle^{\bullet}\langle p_3 p_4\rangle^{\bullet}}, \\
2p_1 k\,\mathcal{M}_3^{\gamma(+)}(-1,+1) &= -\frac{2\langle k_1' p_4\rangle}{\langle k_1 k\rangle\langle p_3 p_4\rangle}\Big[\langle k_1 k_1'\rangle\langle k_1 p_3\rangle^{\bullet}\langle k_1' k\rangle^{\bullet} - 2k_1 k\langle p_3 k\rangle^{\bullet}\Big], \\
2p_1 k\,\mathcal{M}_3^{\gamma(+)}(-1,-1) &= -2\,\frac{\langle k_1' k\rangle\langle k_1 p_3\rangle^{\bullet\,2}}{\langle k_1 k\rangle^{\bullet}}, \\
2p_1 k\,\mathcal{M}_3^{\gamma(+)}(0,+1) &= -\frac{\sqrt{2}}{\langle k_1 k\rangle M_W}\Big[\langle k_1 k_1'\rangle\langle k_1' k\rangle^{\bullet}\big(\langle k_1' p_3\rangle\langle k_1 p_3\rangle^{\bullet} - c\,\langle k_1' p_4\rangle\langle k_1 p_4\rangle^{\bullet}\big) \\
&\quad - 2k_1 k\big(\langle k_1' p_3\rangle\langle p_3 k\rangle^{\bullet} - c\,\langle k_1' p_4\rangle\langle p_4 k\rangle^{\bullet}\big)\Big], \\
2p_1 k\,\mathcal{M}_3^{\gamma(+)}(0,-1) &= 2\sqrt{2}c\,\frac{\langle k_1' k\rangle\langle p_3 p_4\rangle\langle k_1 p_3\rangle^{\bullet}\langle k_1 p_4\rangle^{\bullet}}{M_W\langle k_1 k\rangle^{\bullet}}.
\end{aligned} \tag{B.37}
$$

The expressions for the charge-conjugate process, describing the decay of the W^- boson, can be obtained as follows:

$$
\Delta_\gamma^{(-)}(M_W) = -\frac{ie^2 V_{f_1' f_2}}{\sqrt{2}s_W}\Big[-Q_{f_2}\mathcal{M}_1^{\gamma(-)} + Q_{f_2'}\mathcal{M}_2^{\gamma(-)} + \mathcal{M}_3^{\gamma(-)}\Big], \tag{B.38}
$$

where

$$
\mathcal{M}_j^{\gamma(-)}(\lambda_2,\lambda) = \Big[\mathcal{M}_j^{\gamma(+)}(-\lambda_2,-\lambda)\Big]^{\bullet}, \qquad \text{with} \quad (k_1, k_1', p_3, p_4) \rightarrow (k_2, k_2', p_4, p_3). \tag{B.39}
$$

When the above matrix elements for real-photon radiation from the decay stages are combined with the lowest-order matrix element for the production stage, presented in App. B.1, one obtains the DPA limit of the full matrix elements $\mathcal{M}_\pm$ in Eqs. (2.2.11) and (2.2.12).

B.4   Radiation of collinear photons

Up to now we have only discussed the case of non-collinear photon radiation, which allowed us to neglect the fermion masses and the possibility of spin-flip in the initial state. The picture changes, however, if the radiated photons are sufficiently collinear with one of the external fermions. In such cases factorization takes place, i.e. the matrix element squared including collinear radiation can be approximately written in terms of the lowest-order matrix element squared and collinear factors.

Let us first consider collinear photon radiation in the direction of one of the light fermions in the production stage of the process, e.g. the positron. In that case the matrix element squared can be written in the following form [16]:

$$\sum_{\lambda} |\mathcal{M}_{\text{coll},e^+}(q_1, \sigma_1, q_2, \sigma_2, k, \lambda)|^2 \approx e^2 f_{\text{coll}}^{(\sigma_2)}(q_1, \sigma_1, k) |\mathcal{M}_{\text{DPA}}^0(x_1 q_1, -\sigma_2, q_2, \sigma_2)|^2,$$

(B.40)

where $x_1 = (E - k_0)/E$ is the ratio of the positron energy after and before photon radiation, $\sigma_{1,2}$ are the helicities of the $e^\pm$, and

$$
\begin{aligned}
f_{\text{coll}}^{(\sigma_2)}(q_1, \sigma_1, k) &= \delta_{(\sigma_1, -\sigma_2)} \left[\frac{1 + x_1^2}{x_1(1 - x_1)} \frac{1}{q_1 k} - \frac{1 + x_1^2}{2x_1} \frac{m_e^2}{(q_1 k)^2} \right] \\
&\quad + \delta_{(\sigma_1, \sigma_2)} \frac{(1 - x_1)^2}{2x_1} \frac{m_e^2}{(q_1 k)^2}.
\end{aligned}
$$

(B.41)

The last term in this collinear factor gives rise to the so-called spin-flip, which allows the positron to have the same helicity as the electron. Note that we have only indicated the momenta and helicities of the relevant particles ($e^\pm, \gamma$) and that the photon helicities are summed over, as the photon cannot be detected anyway. Collinear radiation in the direction of the initial-state electron can be obtained in the same way, with the role of the e^+ and e^- interchanged. If the initial-state particles are not polarized, as is the case at LEP2, the collinear factor takes on the well known form

$$\sum_{\sigma_1} f_{\text{coll}}^{(\sigma_2)}(q_1, \sigma_1, k) = \frac{1 + x_1^2}{x_1(1 - x_1)} \frac{1}{q_1 k} - \frac{m_e^2}{(q_1 k)^2}.$$

(B.42)

When the photon angles are integrated out, the terms $\propto 1/q_1 k$ yield contributions of the large-logarithmic type $[\propto \ln(s/m_e^2)]$, whereas the term $\propto m_e^2/(q_1 k)^2$ gives rise to additional $\mathcal{O}(1)$ contributions, which would have been neglected in a massless treatment of the initial state.

In the case of collinear photon radiation in the direction of one of the final-state fermions, say the fermion f_2 from the W^- decay, the factorization reads

$$\sum |\mathcal{M}_{\text{coll},f_2}(k_1, k_1', k_2, k_2', k)|^2 \approx e^2 Q_{f_2}^2 \left[\frac{1 + y_2^2}{1 - y_2} \frac{1}{k_2 k} - \frac{m_{f_2}^2}{(k_2 k)^2} \right] |\mathcal{M}_{\text{DPA}}^0(k_1, k_1', k_2/y_2, k_2')|^2,$$

(B.43)

where the summation is performed over all final-state helicities and $y_2 = E_4/(E_4 + k_0)$ is the ratio of the f_2 energy after and before photon radiation. The other final-state collinear factors can be obtained in the same way.

Appendix C:
Special integrals for semi-soft photon radiation

In this appendix we have a closer look at the inclusive treatment of the photon in
shifted Breit–Wigner resonances $1/[D_i + 2kp_i]$ in the vicinity of the M_i^2 resonance (see
Sect. 2.2). We start off with factorizable real-photon radiation, involving the ratios

$$\frac{|D_i|^2}{|D_i + 2kp_i|^2} = \left[\frac{1}{D_i^* + 2kp_i} - \frac{1}{D_i + 2kp_i}\right]\frac{|D_i|^2}{2iM_W\Gamma_W} = \frac{|D_i|^2}{M_W\Gamma_W}\,\mathrm{Re}\,\frac{i}{D_i + 2kp_i}. \quad (C.1)$$

In order to study the phenomenon of hard-photon suppression we consider the generic
integrals

$$I_n = \frac{|D_i|^2}{M_W\Gamma_W}\,\mathrm{Re}\left\{\int_{\lambda_s < k_0 < \Lambda} \frac{d\vec{k}}{(2\pi)^3 2k_0}\,\frac{M_W^{n-2}}{k_0^n}\,\frac{i}{D_i + 2kp_i}\right\} \quad (C.2)$$

for $n = 1$ or 2. The integration is performed over the photon angles and the photon-
energy range $\lambda_s < k_0 < \Lambda$, where λ_s is a soft-photon cut-off ($\lambda_s \ll \Gamma_W$). For $n = 2$
this integral quantifies the influence of the shifted resonance on the M_i^2 distribution
in the vicinity of the pole $M_i^2 = M_W^2$. For $n = 1$ it quantifies the effect of $\mathcal{O}(k)$ shifts
in the definition of the DPA residues. In the latter case we find

$$I_1 = -\frac{|D_i|^2}{16\pi^2 E\beta M_W^2 \Gamma_W}\,\mathrm{Im}\left\{\mathrm{Li}_2\left(\frac{-1+\beta}{z}\right) - \mathrm{Li}_2\left(\frac{-1-\beta}{z}\right)\right\}, \quad (C.3)$$

with $z = D_i/(2E\Lambda)$ and Li_2 the usual dilogarithm

$$\mathrm{Li}_2(z) = -\int_0^1 dt\,\frac{\ln(1-tz)}{t},\quad z \in \mathbf{C}\setminus\{x \in \mathbf{R}, x > 1\}. \quad (C.4)$$

One can immediately read off that I_1 is suppressed by $\mathcal{O}(\Gamma_W/E)$, irrespective of the
precise value for Λ. For $n = 2$ the integral reads

$$I_2 = -\frac{1}{4\pi^2}\,\mathrm{Im}\left\{\frac{D_i^*}{M_W\Gamma_W}\left[1 + \ln\left(\frac{D_i}{2E\lambda_s}\right) + \frac{z+1-\beta}{2\beta}\,\ln(z+1-\beta)\right.\right.$$
$$\left.\left. - \frac{z+1+\beta}{2\beta}\,\ln(z+1+\beta)\right]\right\}. \quad (C.5)$$

This type of integral will lead to an $\mathcal{O}(1)$ contribution. The dependence on the cut-off
Λ, however, is suppressed by $\mathcal{O}(\Gamma_W^2/\Lambda^2)$. So, the more energetic the photon is the
more suppressed its contribution will be. Hence, as soon as Λ is taken to be much
larger than Γ_W it can safely be replaced by infinity.

Based on the latter observation, we can now list the relevant integrals needed for
the inclusive treatment of final-state radiation effects involving shifted Breit–Wigner

resonances (see columns 3,4 of Table 2-1 and column 3 of Table 2-2). For the radiation from the W^+-boson decay stage the following four integrals are required:

$$\int_{k_0>\lambda_s} \frac{d\vec{k}}{(2\pi)^3 2k_0} \frac{1}{(2kk_1)^2[D_1 + 2kp_1]} = \frac{1}{16\pi^2 m_{f_1}^2 D_1} \ln\left(\frac{D_1 E_3}{\lambda_s M_W^2}\right),$$

$$\int_{k_0>\lambda_s} \frac{d\vec{k}}{(2\pi)^3 2k_0} \frac{1}{(2kk_1)(2kp_1)[D_1 + 2kp_1]} = -\frac{1}{16\pi^2 M_W^2 D_1}\left[\ln\left(\frac{\lambda_s M_W^2}{D_1 E_3}\right)\ln\left(\frac{M_W^2}{m_{f_1}^2}\right)\right.$$
$$\left. + \mathrm{Li}_2\left(1 - \frac{1-\beta}{2}\frac{E}{E_3}\right) + \mathrm{Li}_2\left(1 - \frac{1+\beta}{2}\frac{E}{E_3}\right)\right],$$

$$\int_{k_0>\lambda_s} \frac{d\vec{k}}{(2\pi)^3 2k_0} \frac{1}{(2kp_1)^2[D_1 + 2kp_1]} =$$
$$= -\frac{1}{16\pi^2 M_W^2 D_1}\left[\ln\left(\frac{2\lambda_s M_W}{D_1}\right) + 1 + \frac{1}{2\beta}\ln\left(\frac{1-\beta}{1+\beta}\right)\right],$$

$$\int_{k_0>\lambda_s} \frac{d\vec{k}}{(2\pi)^3 2k_0} \frac{1}{(2kk_1)(2kk_1')[D_1 + 2kp_1]} =$$
$$= \int_{k_0>\lambda_s} \frac{d\vec{k}}{(2\pi)^3 2k_0} \frac{1}{(2kp_1)[D_1 + 2kp_1]}\left[\frac{1}{2kk_1} + \frac{1}{2kk_1'}\right]. \tag{C.6}$$

From these integrals one can determine the correction factor corresponding to the $|\mathcal{I}_+^2|$ term in Eq. (2.2.21):

$$-\int_{k_0>\lambda_s} \frac{d\vec{k}}{(2\pi)^3 2k_0} |\mathcal{I}_+^2| = -\frac{\alpha}{\pi}\,\mathrm{Re}\left\{\frac{iD_1^*}{M_W \Gamma_W}\left[-\ln\frac{2\lambda_s M_W}{D_1} - 1 - \frac{1}{2\beta}\ln\frac{1-\beta}{1+\beta}\right.\right.$$
$$+ Q_{f_1}^2\left\{\ln\frac{\lambda_s M_W^2}{D_1 E_3}\left[\ln\frac{M_W^2}{m_{f_1}^2} - 1\right] + \mathrm{Li}_2\left(1 - \frac{1-\beta}{2}\frac{E}{E_3}\right) + \mathrm{Li}_2\left(1 - \frac{1+\beta}{2}\frac{E}{E_3}\right)\right\}$$
$$+ Q_{f_1'}^2\left\{\ln\frac{\lambda_s M_W^2}{D_1 E_3'}\left[\ln\frac{M_W^2}{m_{f_1'}^2} - 1\right] + \mathrm{Li}_2\left(1 - \frac{1-\beta}{2}\frac{E}{E_3'}\right) + \mathrm{Li}_2\left(1 - \frac{1+\beta}{2}\frac{E}{E_3'}\right)\right\}\right]\right\}. \tag{C.7}$$

Here E_3' denotes the energy of f_1', i.e. $E_3' = E - E_3$. The correction factor corresponding to the $|\mathcal{I}_-^2|$ term in Eq. (2.2.21) is obtained by replacing $(D_1, f_1, f_1', E_3, E_3')$ by $(D_2, f_2, f_2', E_4, E_4')$.

Finally we study the hard-photon suppression for the non-factorizable corrections. To this end we consider the integrals

$$J_n = \mathrm{Re}\left\{\int_{\lambda_s<k_0<\Lambda} \frac{d\vec{k}}{(2\pi)^3 2k_0} \frac{M_W^{n-2}}{k_0^n} \frac{D_i}{D_i + 2kp_i}\right\} \tag{C.8}$$

for $n = 1$ and 2. From the results for $I_{1,2}$ one straightforwardly obtains

$$J_1 = \frac{1}{16\pi^2 E \beta M_W} \operatorname{Re} \left\{ D_i \left[\operatorname{Li}_2\left(\frac{-1 + \beta}{z}\right) - \operatorname{Li}_2\left(\frac{-1 - \beta}{z}\right) \right] \right\} \tag{C.9}$$

and

$$J_2 = \frac{1}{4\pi^2} \operatorname{Re} \left\{ 1 + \ln\left(\frac{D_i}{2E\lambda_s}\right) + \frac{z + 1 - \beta}{2\beta} \ln(z + 1 - \beta) - \frac{z + 1 + \beta}{2\beta} \ln(z + 1 + \beta) \right\}. \tag{C.10}$$

Again a suppression of $\mathcal{O}(\Gamma_W/E)$ is observed for $n = 1$, whereas for $n = 2$ the dependence on the cut-off Λ is suppressed by $\mathcal{O}(M_W \Gamma_W/[E\Lambda])$. So, again Λ can be replaced by infinity if it is sufficiently large. For explicit expressions for the non-factorizable corrections we refer to Chapter 4 and to the literature [6, 8].

References

[1] W. Beenakker, F.A. Berends and A.P. Chapovsky, *Nucl. Phys.* **B548** (1999) 3-59.

[2] W. Beenakker *et al.*, *Nucl. Phys.* **B500** (1997) 255.

[3] K. Melnikov and O. Yakovlev, *Phys. Lett.* **B324** (1994) 217;
    V.S. Fadin, V.A. Khoze and A.D. Martin, *Phys. Rev.* **D49** (1994) 2247.

[4] D. Bardin, *et al.*, in *Physics at LEP2*, eds. G. Altarelli, T. Sjöstrand and
    F. Zwirner, (CERN 96-01, Genève, 1996) Vol. 2, p. 3, *hep-ph/*9709270.

[5] W. Beenakker *et al.*, in *Physics at LEP2*, eds. G. Altarelli, T. Sjöstrand and
    F. Zwirner, (CERN 96-01, Genève, 1996) Vol. 1, p. 79, *hep-ph/*9602351.

[6] W. Beenakker, A.P. Chapovsky and F.A. Berends, *Phys. Lett.* **B411** (1997) 203
    and *Nucl. Phys.* **B508** (1997) 17.

[7] F.A. Berends and R. Kleiss, *Z. Phys.* **C27** (1985) 155.

[8] A. Denner, S. Dittmaier and M. Roth, *Nucl. Phys.* **B519** (1998) 39 and *Phys.
    Lett.* **B429** (1998) 145.

[9] M. Böhm *et al.*, *Nucl. Phys.* **B304** (1988) 463;
    W. Beenakker, K. Kołodziej and T. Sack, *Phys. Lett.* **B258** (1991) 469.

[10] J. Fleischer, F. Jegerlehner and M. Zrałek, *Z. Phys.* **C42** (1989) 409;
     K. Kołodziej and M. Zrałek, *Phys. Rev.* **D43** (1991) 3619;
     J. Fleischer, F. Jegerlehner and K. Kołodziej, *Phys. Rev.* **D47** (1993) 830.

[11] W. Beenakker, F.A. Berends and T. Sack, *Nucl. Phys.* **B367** (1991) 287.

[12] A. Denner and T. Sack, *Z. Phys.* **C46** (1990) 653 and papers quoted therein.

[13] V.S. Fadin and V.A. Khoze, *Yad. Fiz.* **48** (1988) 487; *Sov. J. Nucl. Phys.* **48**
     (1988) 309;
     V.S. Fadin and V.A. Khoze, *Sov. J. Nucl. Phys.* **48** (1988) 309;
     V.S. Fadin, V.A. Khoze and A.D. Martin, *Phys. Lett.* **B311** (1993) 311;
     D. Bardin, W. Beenakker and A. Denner, *Phys. Lett.* **B317** (1993) 213;
     V.S. Fadin et al., *Phys. Rev.* **D52** (1995) 1377.

[14] W. Beenakker, F.A. Berends and A.P. Chapovsky, *Phys. Lett.* **B435** (1998) 233.

[15] W. Beenakker and A. Denner, Proceedings of the Zeuthen Workshop on Elementary Particle Theory: Loops and Legs in Gauge Theories, Rheinsberg, Germany, April 19-24, 1998, *Acta Phys. Pol.* **B29** (1998) 2821.

[16] W. Beenakker and A. Denner, *Int. J. Mod. Phys.* **A9** (1994) 4837.

3 Final-state radiation

In this chapter we will explain the mechanism of the large distortion of the W line-shape, as found in the previous chapter. For this purpose we discuss a toy model involving Z-pair production, which can be analysed both exactly in α and by means of the DPA technique. Moreover, estimates of the effect for W bosons are made. The material of this chapter has been published in the literature, [1].

3.1 Introduction

As is well known [2], the Z line shape as measured in $e^+e^- \to Z \to \bar{f}f$ is distorted due to initial-state radiation (ISR). Without ISR the total cross-section $\sigma(s)$ as a function of the square of the centre-of-mass energy s gives the line shape. With ISR the centre-of-mass energy available to produce a Z boson changes and, as a consequence, so does the shape of the total cross-section $\sigma(s)$. Experimentally the latter is measured. If one would measure the square of the modified centre-of-mass energy s', one would determine $\sigma(s')$ and thereby the pure line-shape. It should be noted that final-state radiation (FSR) only marginally corrects the overall size of $\sigma(s)$, but not its shape. Therefore FSR is less relevant for the usual Z line-shape measurement.

When one produces two resonances, or one resonance and a stable particle, the line shape of such a resonance will be measured from the invariant-mass distribution of its decay products. Examples are pair production of W bosons, Z bosons, $t\bar{t}$ or HZ. Depending on how one measures the invariant-mass distribution of the decay products of the particular resonance, one finds the pure line shape or a distorted one. This time also FSR can cause the distortion.

It is the main purpose of this chapter to point out that such a FSR-induced distortion can arise. For exhibiting the effect we take an example for which we can perform both exact and approximate calculations. An ideal example is the double-resonance process

$$\nu_\mu \bar{\nu}_\mu \to ZZ \to e^+e^- \nu_\tau \bar{\nu}_\tau. \tag{3.1.1}$$

The diagrams corresponding to this process are shown in Fig. 3-1 (A)–(D). Here QED corrections apply only to the decay $Z \to e^+e^-$ and not to the other Z decay or the initial state. When the Z line shape is obtained from measuring the invariant-mass distribution of the e^+e^- pair, FSR will distort it in a way reminiscent of the usual ISR distortion in single Z production. The virtue of the example is threefold. In the first place, process (3.1.1) is free of the gauge-invariance problems that are inherent in the production of unstable particles. This holds in spite of the fact that we have left out all non-double-resonant mechanisms for producing the $e^+e^- \nu_\tau \bar{\nu}_\tau$ final state. Secondly, the QED radiative corrections only lead to FSR. So, the effect of FSR on the line shape can be studied without the additional presence of ISR phenomena.
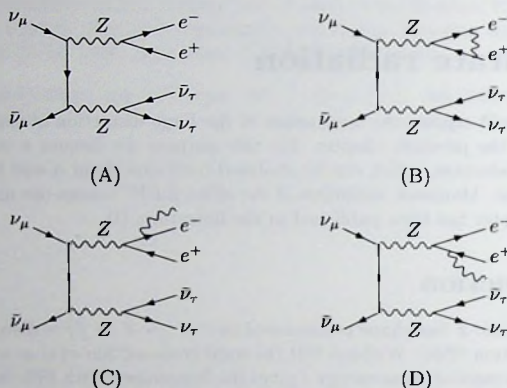
Figure 3-1. The diagrams corresponding to the lowest-order process (3.1.1) (A) and the associated QED radiative corrections (B,C,D). In order to obtain the complete set of diagrams one has to add the diagrams with interchanged Z bosons.

Thirdly, the effect can be calculated exactly. In more realistic examples, involving for instance e^+e^- initial states, Z-pair production with both Z bosons decaying into charged particles, or W-pair production, additional classes of QED radiative corrections emerge, like ISR [3, 4, 5] or non-factorizable interference corrections ([6] and Chapter 4). Moreover, in order to avoid gauge-invariance problems, the QED corrections often have to be calculated in an approximation, which for instance restricts the calculation to the leading logarithmic corrections and/or the leading terms in a pole-scheme expansion around the resonances [3, 7], as has been done in Chapter 2. Nevertheless the FSR distortion of the line shape will still be one of the main features. In these more complicated cases Monte Carlo studies including radiative corrections would be needed. Here we focus exclusively on the line-shape deformation and its impact on the determination of the resonance mass.

Although we start with reaction (3.1.1), we shall also comment on the more realistic case of the W line shape at LEP2, for which numerical results were presented in Chapter 2.

3.2   The Z-pair example: exact calculation

For process (3.1.1) we first consider the Born approximation, to which two double-resonant diagrams contribute. After integration over the Z production angle and the

fermion decay angles, one obtains

$$\frac{d\sigma_0(M_1^2, M_2^2)}{dM_1^2 \, dM_2^2} = \Pi(M_1^2, M_2^2) \frac{\Delta_1(M_1^2)}{|D_1(M_1^2)|^2} \frac{\Delta_2(M_2^2)}{|D_2(M_2^2)|^2} = F(M_1^2, M_2^2), \quad (3.2.1)$$

where M_1^2 and M_2^2 denote the invariant masses of the e^+e^- and $\nu_\tau \bar{\nu}_\tau$ pairs, respectively. The spin-averaged production cross-section takes the form

$$\Pi(M_1^2, M_2^2) = \frac{G_\mu^2 M_Z^4}{4\pi s} (2g_\nu)^4 \frac{\sqrt{\lambda}}{s} \left[-2 + \frac{s^2 + (M_1^2 + M_2^2)^2}{(s - M_1^2 - M_2^2)\sqrt{\lambda}} \ln\left(\frac{s - M_1^2 - M_2^2 + \sqrt{\lambda}}{s - M_1^2 - M_2^2 - \sqrt{\lambda}}\right) \right], \quad (3.2.2)$$

with λ the Kallen function

$$\lambda = s^2 + M_1^4 + M_2^4 - 2(sM_1^2 + sM_2^2 + M_1^2 M_2^2), \quad (3.2.3)$$

which is in agreement with the literature [8]. The decay parts are given by

$$\Delta_1(M_1^2) = \frac{G_\mu M_Z^2}{6\pi\sqrt{2}} (g_{V\ell}^2 + g_{A\ell}^2) \frac{1}{\pi} M_1^2 = \frac{1}{\pi} M_1^2 \frac{\Gamma_{Z \to e^+e^-}}{M_Z},$$

$$\Delta_2(M_2^2) = \frac{G_\mu M_Z^2}{6\pi\sqrt{2}} 2g_\nu^2 \frac{1}{\pi} M_2^2 = \frac{1}{\pi} M_2^2 \frac{\Gamma_{Z \to \nu_\tau \bar{\nu}_\tau}}{M_Z}, \quad (3.2.4)$$

whereas the resonance shapes are dominated by

$$D_{1,2}(M_{1,2}^2) = M_{1,2}^2 - M_Z^2 + i M_{1,2}^2 \frac{\Gamma_Z}{M_Z}. \quad (3.2.5)$$

Note that we have used the standard LEP1 representation in the above formulae, involving G_μ and the effective couplings of the Z boson to leptons ($g_{V\ell}$, $g_{A\ell}$) and neutrinos (g_ν).

Applying virtual and soft photonic corrections to (3.2.1) yields

$$\frac{d\sigma_{vs}(M_1^2, M_2^2)}{dM_1^2 \, dM_2^2} = \frac{d\sigma_0(M_1^2, M_2^2)}{dM_1^2 \, dM_2^2} \left[1 + \frac{2\alpha}{\pi} (L - 1) \ln \epsilon + \frac{\alpha}{\pi} \left(\frac{3}{2} L + \frac{\pi^2}{3} - 2 \right) \right], \quad (3.2.6)$$

with

$$L = \ln\left(\frac{M_1^2}{m_e^2}\right). \quad (3.2.7)$$

Here we have defined the soft photons in the rest frame of the Z: $E_\gamma < \epsilon M_1/2 \ll \Gamma_Z$. Photon bremsstrahlung involving more energetic photons introduces an explicit dependence on the photon energy E_γ, resulting in a distribution in the invariant masses of both the e^+e^- pair ($\bar{M}_1^2$) and the $e^+e^-\gamma$ system (M_1^2 = virtuality of the Z boson):

$$\frac{d\sigma_{\text{brem}}(M_1^2, \bar{M}_1^2, M_2^2)}{dM_1^2 \, d\bar{M}_1^2 \, dM_2^2} = \frac{d\sigma_0(M_1^2, M_2^2)}{dM_1^2 \, dM_2^2} \frac{\alpha}{\pi} (L' - 1) \frac{1 + z^2}{1 - z} \frac{1}{M_1^2}, \quad (3.2.8)$$

where

$$z = \frac{\bar{M}_1^2}{M_1^2} = \frac{1}{\zeta}, \quad L' = \ln\left(\frac{\bar{M}_1^2}{m_e^2}\right) = L + \ln z. \tag{3.2.9}$$

When correction (3.2.6) is combined with (3.2.8) and an integration over $\bar{M}_1^2$ is performed, the correction to $d\sigma_0/(dM_1^2\,dM_2^2)$ takes on the form of the usual FSR factor $1+3\alpha/(4\pi)$. This is in agreement with the KLN theorem, which implies that the large logarithmic contributions ($\propto L$, L') vanish upon summation (integration) over all degenerate final states. So, the resonance shape is not deformed when one measures the M_1^2 distribution, i.e. the invariant-mass distribution of the $e^+e^-\gamma$ system.

In our special example this choice of distribution is, of course, the natural one. However, in more realistic processes it is in general unclear whether the photon is radiated from the initial state, the unstable particles, or the final state. This introduces the freedom to either choose M_1^2 or $\bar{M}_1^2$ for the definition of the invariant-mass distribution of the unstable particle.

If one measures the $\bar{M}_1^2$ distribution one will find a distorted line shape. The reason is that (3.2.8) now has to be integrated over M_1^2 values ranging from $\bar{M}_1^2$ to $(\sqrt{s} - M_2)^2$. This causes the $\bar{M}_1^2$ line shape to receive contributions from effectively *higher* Z-boson virtualities. This is to be compared with the single-Z-production case where the ISR-corrected line shape receives contributions from effectively *lower* Z-boson virtualities. Due to the fact that roughly speaking the resonance shape is symmetric around the resonance mass, one expects now a distortion of the resonance shape that is approximately the LEP1 distortion reflected with respect to the resonance mass.

The bremsstrahlung contribution to the line shape $d\sigma/(d\bar{M}_1^2\,dM_2^2)$ arising from Eq. (3.2.8) reads

$$\frac{d\sigma_{\text{brem}}(\bar{M}_1^2, M_2^2)}{d\bar{M}_1^2\,dM_2^2} = \frac{\alpha}{\pi}\,(L'-1)\int_{1+\epsilon}^{\zeta_{\max}} d\zeta\,F(\zeta\bar{M}_1^2, M_2^2)\left[\frac{2}{\zeta-1} - \frac{1+\zeta}{\zeta^2}\right], \tag{3.2.10}$$

where the function F is defined in (3.2.1) and $\zeta_{\max} = (\sqrt{s} - M_2)^2/\bar{M}^2$. Combining (3.2.6) and (3.2.10) gives the $\mathcal{O}(\alpha)$ correction to the line shape. Just like at LEP1 it will be necessary to resum the soft corrections, as will become clear from the discussion in the following section. Based on LEP1 experience [2] a suitable expression for this resummation is given by

$$\frac{d\sigma_{\text{res}}(\bar{M}_1^2, M_2^2)}{d\bar{M}_1^2\,dM_2^2} = \int_1^{\zeta_{\max}} d\zeta\,G(\zeta)\,F(\zeta\bar{M}_1^2, M_2^2), \tag{3.2.11}$$

with

$$\begin{aligned}
G(\zeta) &= \beta\,(\zeta-1)^{\beta-1}(1+\delta_{\text{res}}^{\text{vs}}) - \frac{\beta}{2}\frac{1+\zeta}{\zeta^2} \\
\beta &= \frac{2\alpha}{\pi}\,(L'-1) \\
\delta_{\text{res}}^{\text{vs}} &= \frac{\alpha}{\pi}\left(\frac{3}{2}L' + \frac{\pi^2}{3} - 2\right).
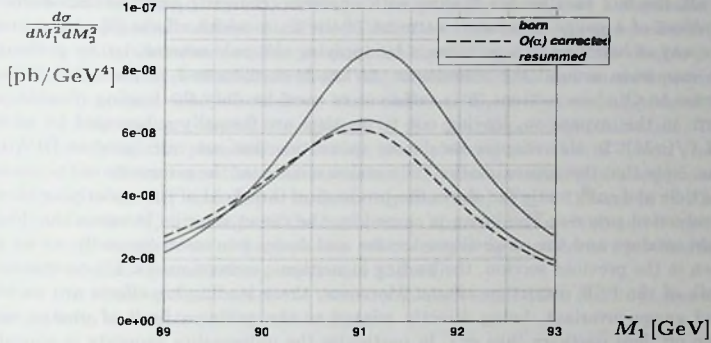\end{aligned} \tag{3.2.12}$$

Figure 3-2. The FSR-induced distortion of the line shape $d\sigma/(d\tilde{M}_1^2\, dM_2^2)$ corresponding to process (3.1.1) for $M_2 = M_Z$. Centre-of-mass energy: $\sqrt{s} = 200\,\text{GeV}$.

In Fig. 3-2 we display the FSR-induced distortion effects on the Z-boson line shape $d\sigma/(d\tilde{M}_1^2\, dM_2^2)$ for a centre-of-mass energy of $\sqrt{s} = 200\,\text{GeV}$ and a fixed invariant mass $M_2 = M_Z$. However, the actual distortion phenomena do not depend on the precise value of M_2. The parameter input used in the numerical evaluation is:

$$M_Z = 91.1867\,\text{GeV},\ \Gamma_Z = 2.4948\,\text{GeV},$$
$$G_\mu = 1.16639 \times 10^{-5}\,\text{GeV}^{-2},\ m_e = 0.51099906\,\text{MeV},$$
$$\alpha^{-1} = 137.0359895,\ g_\nu = 0.50125,\ g_{V\ell} = -0.03681,\ g_{A\ell} = -0.50112.$$

The sizeable distortion effects are clearly visible, just as the importance of the soft-photon resummation. Compared with the Born line shape, the $\mathcal{O}(\alpha)$ (resummed) QED corrections induce a shift in the peak position of $-199\,\text{MeV}$ ($-112\,\text{MeV}$) and a reduction of the peak height by 29% (26%). The size of these effects is a direct result of the non-cancellation of the leading logarithmic corrections, which can be understood from the observation that a fixed value for $\tilde{M}_1$ makes it impossible to sum over all degenerate final states. Another noteworthy observation is the close similarity of the curves in Fig. 3-2 to the ones for the Z line shape at LEP1 [2]. As predicted, the two sets of curves are approximately related by reflection with respect to the Born peak position.

3.3   The Z-pair example: approximations

As mentioned before, in order to calculate QED corrections to more realistic processes like W-pair production one in general has to resort to approximations. First

of all, the fact that we are dealing with unstable (charged) particles introduces the problem of a gauge-invariant treatment of the finite-width effects [3]. An appropriate way of handling this problem is by applying the pole scheme, i.e. by performing an expansion around the resonances, as has been discussed in Sect. 2.1. When it comes to $\mathcal{O}(\alpha)$ corrections, it is sufficient to consider only the leading (double-pole) term in this expansion, leaving out terms that are formally suppressed by at least $\alpha L \Gamma/(\pi M)$. In this chapter we denote quantities that are calculated in DPA by a bar. Note that the approximation only makes sense near the resonance of the unstable particle and sufficiently far above the production threshold of the underlying on-shell production process. The latter is caused by the direct relation between the double-pole residues and the on-shell production and decay processes. Secondly, as we have seen in the previous section, the leading logarithmic corrections ($\propto L'$) constitute the bulk of the FSR distortion effects. Moreover, these leading-log effects are universal and gauge invariant, being directly related to the collinear limit of photon radiation off light particles (like $e^{\pm}$). In particular the universality property is appealing, since it implies that the description of the leading-log corrections does not depend on the specific features of the unstable particles and their photonic interactions. Therefore, it is worthwhile to further restrict the double-pole calculations to the leading logarithms. This additional approximation is referred to as the leading-log approximation (LLA). Before making any comments on processes like W-pair production, we first concentrate on our Z-pair example and check the validity of the indicated approximations.

We start off with the definition of the double-pole approximation. At Born level it amounts to

$$\frac{d\bar{\sigma}_0(M_1^2, M_2^2)}{dM_1^2\, dM_2^2} = \Pi(M_Z^2, M_Z^2)\, \frac{\Delta_1(M_Z^2)}{|\bar{D}_1(M_1^2)|^2}\, \frac{\Delta_2(M_Z^2)}{|D_2(M_2^2)|^2}, \tag{3.3.1}$$

with

$$\bar{D}_{1,2}(M_{1,2}^2) = M_{1,2}^2 - M_Z^2 + iM_Z\Gamma_Z. \tag{3.3.2}$$

As mentioned before, the QED radiative corrections introduce an ambiguity in defining the invariant-mass distributions of the unstable particles. The most transparent way of illustrating this is by considering the case that the photon is radiated from such an unstable particle. For the description of the resonance before (after) radiation the natural choice of invariant mass involves the fermion pair with (without) the photon. The pole expansion can now in principle be performed around either resonance. In practice one has to choose one particular invariant mass for the distributions. For the purpose of studying FSR-induced distortion effects, we shall choose the e^+e^- invariant mass $\bar{M}_1$ in the following, although the $e^+e^-\gamma$ invariant mass M_1 would have been more natural for our special example (3.1.1). The corresponding double-pole approximation forces us to replace $M_1^2 = \zeta\bar{M}_1^2$ by ζM_Z^2, introducing an explicit dependence on the photon energy in the double-pole residues. This would even affect the (neutral) resonance-pair-production stage of the process. However, as can be verified explicitly, only semi-soft photons with energy $E_\gamma = \mathcal{O}(\Gamma_Z) \ll M_Z$

contribute to the $\mathcal{O}(\alpha)$ corrected double-pole residues (for details see a discussion in Sect. 2.2, in particular columns 3 and 4 of Table 2-1). As a result, ζ can be effectively replaced by unity whenever possible, re-establishing the usual form of the double-pole approximation in terms of off-shell Breit–Wigner distributions and on-shell production/decay processes. The effects from hard photons $(E_\gamma \gg \Gamma_Z)$ are suppressed by at least Γ_Z/M_Z and are therefore neglected in the double-pole approximation. The picture underlying this phenomenon is that hard photons move the Z-boson virtuality (M_1^2) far off resonance for near-resonance $\bar{M}_1^2$ values, resulting in a suppressed contribution to the $\bar{M}_1^2$ line shape. In fact, only the (soft) $1/(\zeta - 1)$ term in (3.2.10) contributes to the $\bar{M}_1^2$ line shape in the double-pole approximation. It should be noted that this very suppression of hard-photon effects serves as *a posteriori* justification of the soft-photon resummation proposed in (3.2.11).

With this observation in mind, the bremsstrahlung contribution (3.2.10) takes the following form in double-pole approximation:

$$\frac{d\bar{\sigma}_{\text{brem}}(\bar{M}_1^2, M_2^2)}{d\bar{M}_1^2\, dM_2^2} = \frac{d\bar{\sigma}_0(\bar{M}_1^2, M_2^2)}{d\bar{M}_1^2\, dM_2^2} \int\limits_{1+\epsilon}^{\infty} d\zeta\, \frac{\bar{\beta}}{\zeta - 1}\, \frac{|\bar{D}_1(\bar{M}_1^2)|^2}{|\bar{D}_1(\zeta\bar{M}_1^2)|^2}. \tag{3.3.3}$$

Here $\bar{\beta}$ can be derived from β by setting $\bar{M}_1^2 = M_2^2$. Note that the upper integration boundary $\zeta_{\max}$ has been extended to infinity, which is motivated by the fact that hard-photon effects are sufficiently suppressed (again, see a discussion in Sect. 2.2). The remaining integral can be performed analytically. Combining with the virtual and soft corrections, which can be readily derived from (3.2.6), we obtain in the double-pole LLA

$$\frac{d\bar{\sigma}(\bar{M}_1^2, M_2^2)}{d\bar{M}_1^2\, dM_2^2} = \frac{d\bar{\sigma}_0(\bar{M}_1^2, M_2^2)}{d\bar{M}_1^2\, dM_2^2}\left\{ 1 + \frac{3}{4}\,\bar{\beta} + \bar{\beta}\operatorname{Re}\left[\frac{i\bar{D}_1^*(\bar{M}_1^2)}{M_Z\Gamma_Z}\ln\left(\frac{\bar{D}_1(\bar{M}_1^2)}{M_Z^2}\right)\right]\right\}. \tag{3.3.4}$$

In a way similar to the previous section the soft-photon corrections can be resummed, but this time the integral can be carried out explicitly in the double-pole LLA:

$$\begin{aligned}
\frac{d\bar{\sigma}_{\text{res}}(\bar{M}_1^2, M_2^2)}{d\bar{M}_1^2\, dM_2^2} &= \frac{d\bar{\sigma}_0(\bar{M}_1^2, M_2^2)}{d\bar{M}_1^2\, dM_2^2}\left(1 + \frac{3}{4}\,\bar{\beta}\right)\int\limits_1^{\infty} d\zeta\, \bar{\beta}\,(\zeta - 1)^{\beta - 1}\,\frac{|\bar{D}_1(\bar{M}_1^2)|^2}{|\bar{D}_1(\zeta\bar{M}_1^2)|^2} \\
&= \frac{d\bar{\sigma}_0(\bar{M}_1^2, M_2^2)}{d\bar{M}_1^2\, dM_2^2}\left(1 + \frac{3}{4}\,\bar{\beta}\right)\frac{\pi\bar{\beta}}{\sin(\pi\bar{\beta})}\operatorname{Re}\left[\frac{i\bar{D}_1^*(\bar{M}_1^2)}{M_Z\Gamma_Z}\left(\frac{\bar{D}_1(\bar{M}_1^2)}{M_Z^2}\right)^{\bar{\beta}}\right].
\end{aligned} \tag{3.3.5}$$

Having calculated the same quantities as in the previous section, we are now in the position to check the validity of the double-pole LLA. It turns out that the approximated results exhibit the same FSR distortions as the exact ones. Upon closer investigation, we observe for the $\mathcal{O}(\alpha)$ (resummed) QED corrections a shift in the peak position of $-193\,\text{MeV}$ $(-113\,\text{MeV})$ and a reduction of the peak height by 29%

(26%). This is in excellent agreement with the distortion parameters of the exact calculation, proving the viability of the adopted approximations.[1]

Based on the results in the double-pole LLA, it is possible to derive simple and sufficiently accurate rules of thumb for the distortion parameters:

- $\mathcal{O}(\alpha)$ corrections: the shift in the peak position $\Delta \bar{M}_1^{\mathrm{peak}}$ and the corresponding peak reduction factor κ^{peak} with respect to the Born line shape can be approximated by

$$
\begin{aligned}
\Delta \bar{M}_1^{\mathrm{peak}} &\approx -\frac{\pi \bar{\beta} \, \Gamma_Z/8}{\kappa^{\mathrm{peak}} - 3\bar{\beta}/2} = -196 \, \mathrm{MeV}, \\
\kappa^{\mathrm{peak}} &\approx 1 + \bar{\beta} \ln\left(\frac{\Gamma_Z}{M_Z}\right) + \frac{3}{4}\bar{\beta} + \frac{\pi^2}{16}\bar{\beta}^2 = 0.70; \qquad (3.3.6)
\end{aligned}
$$

- resummed corrections: now the distortion parameters read

$$
\begin{aligned}
\Delta \bar{M}_1^{\mathrm{peak}} &\approx -\frac{\pi}{8} \bar{\beta} \Gamma_Z (1 + \frac{\bar{\beta}}{2}) = -111 \, \mathrm{MeV}, \\
\kappa^{\mathrm{peak}} &\approx \left(\frac{\Gamma_Z}{M_Z}\right)^{\bar{\beta}} (1 + \frac{3}{4}\bar{\beta})(1 + \frac{5\pi^2}{48}\bar{\beta}^2 - \frac{\pi^2}{32}\bar{\beta}^3) = 0.74. \quad (3.3.7)
\end{aligned}
$$

This is in perfect agreement with the observed exact and double-pole distortion parameters. The analogy with the rules of thumb derived for the Z line shape at LEP1 [9] confirms the relation between the FSR-induced distortion effects in double Z-resonance production and the ISR-induced distortion effects in single Z-resonance production at LEP1.

3.4   Some comments on the W line shape at LEP2

As has been shown in the previous section, the double-pole LLA constitutes a reliable framework for a gauge-invariant and universal description of FSR-induced distortion phenomena in double-resonance production. The essence of these phenomena is fully contained in the correction factor presented in (3.3.5), which applies to each individual distorted Breit–Wigner distribution. For two distorted distributions the effect is hence multiplicative. Consequently, the reduction factor for a double-invariant-mass distribution is given by the product of the reduction factors for the individual single-invariant-mass distributions. However, the shift in the peak position does not change in the presence of more than one resonance; it only depends on the decay products of the unstable particle that is investigated. The only differences between process (3.1.1) and the more realistic process of W-pair production at LEP2 are the resonance parameters ($M_W = 80.22 \, \mathrm{GeV}$ and $\Gamma_W = 2.08 \, \mathrm{GeV}$) and the fact that $\bar{\beta}$ depends on

---

[1]For completeness we note that all curves in the double-pole LLA are displaced by a small amount with respect to the exact ones. This is caused by the fact that the Born results differ by subleading terms in the pole expansion.

the decay products of the decaying particle. For instance, the leptonic W decays involve only *one* charged lepton instead of two. As a result, we should use (3.3.5) with $\bar{\beta} \to \frac{\alpha}{\pi} [\ln(M_W^2/m_\ell^2) - 1]$ for $\ell = e, \mu, \tau$, which is scaled down by at least a factor of two compared with the Z-pair example. For W bosons decaying into an electron or positron, the resummed FSR distortion effects amount to a shift in the peak position of -45 MeV and a peak reduction factor of 0.86 per distorted resonance (i.e. 0.74 for a double-invariant-mass distribution), as can also be read off from (3.3.7).[2]

From the previous discussions it should be clear that FSR-induced distortion effects can be sizeable and should be taken into account properly in the Monte Carlo programs that are used for the W-mass determination at LEP2.

---

[2] In more realistic event-selection procedures also a minimum opening angle (θ_0) between the lepton and photon might be required for a proper identification of both particles. The effect of this can be represented by using $\ln(4/\theta_0^2)$ instead of $[\ln(M_W^2/m_\ell^2) - 1]$ in the definition of β.

References

[1] W. Beenakker, F.A. Berends and A.P. Chapovsky, *Phys. Lett.* **B435** (1998) 233.

[2] D. Bardin et al., in *Z Physics at LEP1*, eds. G. Altarelli et al. (CERN 89-08, Geneva, 1989), Vol. 1, p. 89.

[3] W. Beenakker and A. Denner, *Int. J. Mod. Phys.* **A9** (1994) 4837;
W. Beenakker et al., *hep–ph/9602351*, in *Physics at LEP2*, eds. G. Altarelli, T. Sjöstrand and F. Zwirner (CERN 96-01, Geneva, 1996), Vol. 1, p. 79.

[4] D. Bardin, D. Lehner and T. Riemann, *Nucl. Phys.* **B477** (1996) 27.

[5] A. Ballestrero and R. Chierici, *Phys. Lett.* **B422** (1998) 305.

[6] W. Beenakker, A.P. Chapovsky and F.A. Berends, *Nucl. Phys.* **B508** (1997) 17;
Phys. Lett. **B411** (1997) 203;
A. Denner, S. Dittmaier and M. Roth, *Nucl. Phys.* **B519** (1998) 39; *Phys. Lett.* **B429** (1998) 145.

[7] M. Veltman, *Physica* **29** (1963) 186;
R.G. Stuart, *Phys. Lett.* **B262** (1991) 113;
A. Aeppli, G.J. van Oldenborgh and D. Wyler, *Nucl. Phys.* **B428** (1994) 126.

[8] D. Bardin, A. Leike and T. Riemann, *Phys. Lett.* **B344** (1995) 383.

[9] W. Beenakker, F.A. Berends and S.C. van der Marck, *Z. Phys.* **C46** (1990) 687.

4 Non-factorizable corrections

In this chapter we will discuss the non-factorizable corrections and their implications on W-pair production. We develop a calculational technique aimed specifically at the evaluation of this kind of corrections. We then perform an alternative calculation, which serves as a check. The material of this chapter has been published in the literature, [1].

4.1 Introduction

As was pointed out in Chapter 2, only soft and semi-soft photons give large enough contributions to the non-factorizable corrections. In order to give a gauge-invariant definition of the non-factorizable QED corrections in the semi-soft limit, we introduced in Sects. 2.2.1 and 2.2.2 semi-soft currents of which certain interference terms give rise to the non-factorizable corrections. For each virtual correction term there is a corresponding real bremsstrahlung term. Upon integration over the photon momentum, k^μ, many of these terms cancel pairwise. This is a consequence of two facts: the virtual correction cancels against the corresponding real one if

- all the "particle" poles are situated in the same half-plane of the complex k_0-plane (see e.g. the so-called initial–final state interferences).

  or

- the on-shell integral is taken in the soft-photon limit (equivalent to the usual cancellation of infrared divergences).

These theorems will be discussed later in this chapter. By using these theorems one can rewrite the result based on the current interferences in an equivalent, but simplified form, which can be described as follows. One starts with the *manifestly* non-factorizable corrections, i.e. those not having two resonant W-propagators as explicit overall factors. To this set a part of the Coulomb-like diagram will then be added, such that the total expression is gauge invariant. Thus one uses parts of Feynman diagrams as starting point, leading to the same results as the currents of Chapter 2. This is not surprising, since these currents were introduced by considering parts of Feynman diagrams. In order to show the explicit equivalence one has to invoke the above mentioned cancellation theorems.

In addition we will restrict ourselves in first instance to the simplest class of charged-current four-fermion processes, involving a purely leptonic final state:

$$e^+(q_1)e^-(q_2) \to W^+(p_1) + W^-(p_2) \to \nu_\ell(k_1')\ell^+(k_1) + \ell'^-(k_2)\bar\nu_{\ell'}(k_2'). \qquad (4.1.1)$$
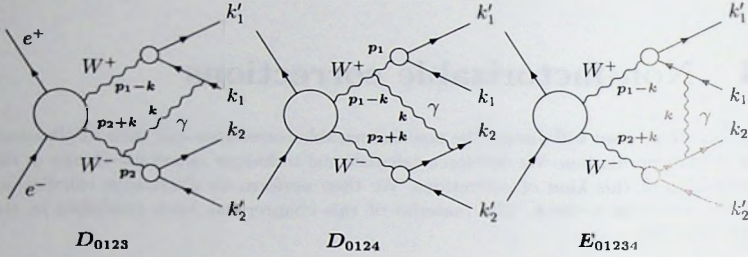
Figure 4-1. Virtual diagrams contributing to the manifestly non-factorizable W-pair corrections in the purely leptonic case. The scalar functions corresponding to these diagrams are denoted by D_{0123}, D_{0124}, and E_{01234}.

Whenever possible, all external fermions are taken to be massless. The relevant manifestly non-factorizable contributions consist of the final–final and intermediate–final state photonic interactions displayed in Fig. 4-1. In principle also manifestly non-factorizable vertex corrections exist, which arise when the photon in Fig. 4-1 does not originate from a W-boson line but from the $\gamma WW / ZWW$ vertex (hidden in the central blob). Those contributions can be shown to vanish in the double-pole approximation, using power-counting arguments [2]. As was already mentioned the manifestly non-factorizable initial–final state interference effects disappear in our approach. This happens upon adding virtual and real corrections, as will be briefly explained later.

The double-pole contribution of these virtual corrections to the differential cross-section can be written in the form

$$d\sigma_{\text{virt}} = 32\pi\alpha \, \text{Re} \left[i(p_2 \cdot k_1) D_1 D_{0123} + i(p_1 \cdot k_2) D_2 D_{0124} + i(k_1 \cdot k_2) D_1 D_2 E_{01234} \right] d\sigma^0_{\text{DPA}},$$

$$(4.1.2)$$

where $D_{1,2} = p_{1,2}^2 - M_W^2 + i M_W \Gamma_W$ are the inverse (Breit–Wigner) W-boson propagators. The functions D_{0123}, D_{0124}, and E_{01234} are the scalar integrals corresponding to the diagrams shown in Fig. 4-1, with the integration measure defined as $d^4k/(2\pi)^4$. The propagators occurring in these integrals are labelled according to: $0 = $ photon, $1 = W^+$, $2 = W^-$, $3 = \ell^+$, and $4 = \ell'^-$. Note that the factorization property exhibited in Eq. (4.1.2) is a direct consequence of the semi-soft photon approximation, which is inherent in our approach. As a result, the propagators hidden inside the central blobs of Fig. 4-1 are Born-like, i.e. unaffected by the presence of the non-factorizable photonic interactions.

In a similar way, only interferences of the real-photon diagrams can give contributions to the manifestly non-factorizable corrections. The relevant interferences can be read off from Fig. 4-1 by taking the exchanged photon to be on-shell. The infrared divergences contained in the virtual corrections will cancel against those present in the corresponding bremsstrahlung interferences.
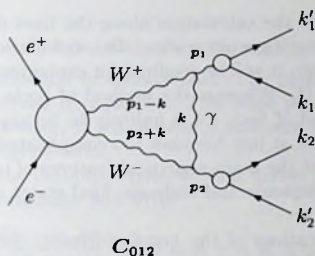
C_{012}

Figure 4-2.   The gauge-restoring "Coulomb" contribution. The corresponding scalar function is denoted by C_{012}. In Sect. 4.3.3 we shall briefly indicate the distinction between the non-factorizable "Coulomb" contribution, valid outside the threshold region, and the usual one, which is also valid inside that region.

The expression (4.1.2) contains some of the current interference terms of Chapter 2, all others vanish except the contribution from the Coulomb-like diagram in Fig. 4-2, which gives

$$d\sigma_{\mathrm{virt}}^{\mathrm{C}}(p_1|p_2) = 32\pi\alpha \operatorname{Re}\left[i(p_1 \cdot p_2)C_{012}\right] d\sigma_{\mathrm{DPA}}^0. \qquad (4.1.3)$$

The scalar three-point function C_{012} is defined according to the above-defined notation. The terminology "Coulomb" interaction should not lead to confusion. It is a contribution that is a part of the diagram in Fig. 4-2. In Sect. 4.3.3 we shall briefly indicate the distinction between the non-factorizable "Coulomb" contribution, valid outside the threshold region, and the usual one, which is primarily valid inside that region.

From the diagrams in Fig. 4-1 it is clear that we have to calculate four- and five-point scalar functions and related bremsstrahlung interference expressions, all in the semi-soft photon approximation. In the next two sections we focus on the analytical results as obtained with the modified standard technique (MST), consisting of various elements. In particular the decomposition of the virtual and real five-point functions into a sum of four-point functions is given some special attention in Sect. 4.2.[1] As such, the basic building blocks of the MST are the four-point functions D and the related bremsstrahlung interference terms D^{R}. A general relation between the two entities is discussed in Sect. 4.2.4. As a final step we derive in Sect. 4.3 the relevant scalar four-point functions D in the semi-soft photon approximation by applying the Feynman-parameter technique. The related D^{R} functions are obtained by using a "particle-pole" expression and performing certain substitutions.

---

[1] For higher n-point functions ($n > 5$) this decomposition can be carried out in an analogous way. Thus in principle the methods outlined in Sects. 4.2.1 and 4.2.2 provide the basic tools for considering more involved non-factorizable corrections, e.g. for six-fermion final states.

In Sect. 4.4 we present the calculation along the lines of Ref. [3], which involves the method of direct momentum integration. This calculation will serve as a check of the MST results. Moreover, it will be required for explaining the observed differences with the results of Ref. [3]. Whereas the method of Sects. 4.2 and 4.3 seems to be quite general, the method of Sect. 4.4 is unlikely to be applied to n-point functions with $n > 5$. As we will see, it just becomes too complicated.

In Sect. 4.5 we present the main analytical features of our study and we indicate how the results for semileptonic and hadronic final states can be obtained from the purely leptonic case.

The numerical implications of the non-factorizable corrections are discussed in Sect. 4.6. Since the non-factorizable corrections vanish in the special case of initial-final state interference, they are independent from the W production angle. Our calculations confirm that the non-factorizable corrections vanish in all cases when the integrations over both invariant masses of the virtual W bosons are performed [4]. The practical consequence of the latter is that pure angular distributions are unaffected by non-factorizable $\mathcal{O}(\alpha)$ corrections. So, the studies of non-Abelian triple gauge-boson couplings at LEP2 [5] are not affected by these corrections. The non-factorizable $\mathcal{O}(\alpha)$ corrections, however, do affect the invariant-mass distributions (W line-shapes). These distributions play a crucial role in extracting the W-boson mass from the data through direct reconstruction of the Breit–Wigner resonances. The non-factorizable corrections to the line-shapes turn out to be similar for quark and lepton final states, provided the integrations over the decay angles have been performed. Finally, in Sect. 4.7 we draw some conclusions.

4.2   Modified standard technique: basic ingredients

In this section the basic ingredients are presented for the evaluation of non-factorizable corrections in the MST. As a first step we discuss the decomposition of virtual and real five-point functions into a sum of four-point functions. Subsequently we demonstrate how virtual and real contributions can be related in the semi-soft photon approximation. Having established the five-point decompositions and the relation between virtual and real contributions, the actual calculation in the MST boils down to the evaluation of scalar four-point integrals.

4.2.1   Decomposition of the virtual five-point function

In this subsection we derive the decomposition of the virtual scalar five-point function into a sum of scalar four-point functions. The derivation follows Ref. [6]. The reason for repeating this calculation lies in the fact that it will serve as guideline for the decomposition of the real five-point function, which has not been considered before.

Let us consider the following general five-point function:

$$E_{01234} = \int \frac{d^4k}{(2\pi)^4} \frac{1}{N_0 N_1 N_2 N_3 N_4}, \tag{4.2.1}$$

where

$$N_0 = k^2 - \lambda^2 + io \quad \text{and} \quad N_i = (k + p_i)^2 - m_i^2 + io. \tag{4.2.2}$$

Here io denotes an infinitesimal imaginary part. The plus sign accompanying this imaginary part is determined by causality. The mass parameter λ is in principle arbitrary. In our case, however, it will denote a non-zero photon mass, needed for regularizing the infrared divergences.

Before starting with the decomposition, we first derive a useful identity. To this end we exploit Lorentz covariance and write

$$\int \frac{d^4k}{(2\pi)^4} \frac{k^\mu}{N_0 N_1 N_2 N_3} = c_1 p_1^\mu + c_2 p_2^\mu + c_3 p_3^\mu. \tag{4.2.3}$$

The integral on the left-hand side is ultraviolet-finite and, when properly regularized, also infrared-finite. The quantities c_i on the right-hand side are therefore finite coefficients, dependent on masses and the invariants $p_i \cdot p_j$ $(i, j = 1, 2, 3)$. Contracting this expression with the antisymmetric Levi–Civita tensor, one obtains the identity

$$\int \frac{d^4k}{(2\pi)^4} \frac{\varepsilon_{p_1 p_2 p_3 k}}{N_0 N_1 N_2 N_3} = 0, \tag{4.2.4}$$

which will prove extremely useful in the following. Here we introduced the widely-used notation

$$\varepsilon_{\mu\nu\rho p} = \varepsilon_{\mu\nu\rho\sigma} p^\sigma, \quad \varepsilon_{\mu\nu pq} = \varepsilon_{\mu\nu\rho\sigma} p^\rho q^\sigma, \quad \cdots \tag{4.2.5}$$

The Levi–Civita tensor is defined here according to $\varepsilon^{0123} = -\varepsilon_{0123} = 1$. Note that this convention is different from the one used in Chapter 2, but it is in accordance with Ref. [6].

The actual derivation of the decomposition formula starts with the Schouten identity

$$a\, k^\mu = \sum_{i=1}^4 v_i^\mu\, (p_i \cdot k), \tag{4.2.6}$$

where the following notation was used:

$$v_1^\mu = \varepsilon^{\mu p_2 p_3 p_4}, \quad v_2^\mu = \varepsilon^{p_1 \mu p_3 p_4}, \quad v_3^\mu = \varepsilon^{p_1 p_2 \mu p_4}, \quad v_4^\mu = \varepsilon^{p_1 p_2 p_3 \mu},$$

$$a = \varepsilon_{p_1 p_2 p_3 p_4} = \varepsilon^{p_1 p_2 p_3 p_4}. \tag{4.2.7}$$

Note that from the quantity a one can construct the Gram-determinant of the system, $\Delta_4 = a^2$. The next step in the derivation is to contract the Schouten identity with k_μ, yielding

$$a\, k^2 = \sum_{i=1}^4 (k \cdot v_i)(k \cdot p_i). \tag{4.2.8}$$

Now we can substitute

$$k^2 = N_0 + \lambda^2 - io,$$

$$(k \cdot p_i) = \frac{1}{2}[N_i - N_0 - r_i], \quad \text{with } r_i = p_i^2 - m_i^2 + \lambda^2 \tag{4.2.9}$$

to arrive at

$$2a\left(N_0 + \lambda^2\right) = \sum_{i=1}^{4}(k \cdot v_i)(N_i - N_0 - r_i). \qquad (4.2.10)$$

In order to make the link to the scalar five-point function, one should divide this expression by $N_0 N_1 N_2 N_3 N_4$ and perform the integration over d^4k. As a result of Eq. (4.2.4) the N_i terms vanish. The terms $\sum (k \cdot v_i) N_0$ can be transformed according to

$$\sum_{i=1}^{4}(k \cdot v_i) = \varepsilon^{(k+p_1)(p_2-p_1)(p_3-p_1)(p_4-p_1)} - a, \qquad (4.2.11)$$

which can be verified by a direct check. After integration the first term will vanish. This can be most easily seen by making a change of integration variable, $k'^\mu = k^\mu + p_1^\mu$, and subsequently applying Eq. (4.2.4). The complete expression now reads

$$\int \frac{d^4k}{(2\pi)^4} \frac{aN_0 + 2a\lambda^2 + \sum r_i(k \cdot v_i)}{N_0 N_1 N_2 N_3 N_4} = 0. \qquad (4.2.12)$$

The final step is to multiply this expression by a and to apply the Schouten identity and Eq. (4.2.9) to the last term in the numerator. This allows us to express the complete numerator in terms of the propagators appearing in the denominator:

$$\int \frac{d^4k}{(2\pi)^4} \frac{2\lambda^2\Delta_4 - \frac{1}{2}w^2 + N_0\Delta_4 - \frac{1}{2}N_0\sum(v_i \cdot w) + \frac{1}{2}\sum N_i(v_i \cdot w)}{N_0 N_1 N_2 N_3 N_4} = 0, \qquad (4.2.13)$$

with

$$w^\mu = \sum_{j=1}^{4} r_j v_j^\mu. \qquad (4.2.14)$$

The final formula for the decomposition reads

$$\begin{aligned}
\left(w^2 - 4\lambda^2\Delta_4\right) E_{01234} &= (w \cdot v_1)\, D_{0234} + (w \cdot v_2)\, D_{0134} + (w \cdot v_3)\, D_{0124} + (w \cdot v_4)\, D_{0123} \\
&+ \left[2\Delta_4 - \sum_{i=1}^{4}(w \cdot v_i)\right] D_{1234},
\end{aligned} \qquad (4.2.15)$$

where D_{0234}, D_{0134}, etc., denote four-point scalar functions containing the propagators with labels $(0, 2, 3, 4)$, $(0, 1, 3, 4)$, etc.

The generalization of this decomposition to higher multipoint functions can be performed in a similar way [6]. In general, a scalar N-point function can be expressed in terms of the N underlying $(N - 1)$-point functions.

4.2.2   Decomposition of the real five-point function

Using the derivation presented above as guideline, we can now try to derive a similar decomposition for the real five-point function. As can be read off from Fig. 4-1, by

taking the exchanged photon to be on-shell, the real five-point function takes the form

$$E_{01234}^{R} = \int \frac{d^3k}{(2\pi)^3 \, 2\omega} \, \frac{1}{N_1' N_2' N_3' N_4'}, \tag{4.2.16}$$

where

$$\omega = \sqrt{\vec{k}^2 + \lambda^2}, \quad N_{1,2}' = N_{1,2}, \quad \text{and} \quad N_{3,4}' = N_{3,4}^*. \tag{4.2.17}$$

The photon is now on-shell, so $k^2 = \lambda^2$ and $N_0 = 0$. Note that the momenta p_i, hidden inside N_i, are time-like and have positive energy components. The area of the integration can be extended up to infinity, because the contribution of the hard photons is suppressed, and thus the cutoff dependence is beyond the DPA.

One can proceed in the same way as in the case of the decomposition of the virtual five-point function. The Schouten identity is still valid, but Eq. (4.2.4) in its old form does not work in the case of real-photon radiation, and should be modified. In the derivation of the virtual decomposition, Eq. (4.2.4) was used twice, leading to the nullification of

$$\int \frac{d^4k}{(2\pi)^4} \, \frac{\sum(k \cdot v_i)N_i}{N_0 N_1 N_2 N_3 N_4} \quad \text{and} \quad \int \frac{d^4k}{(2\pi)^4} \, \frac{N_0 \left[\sum(k \cdot v_i) + a\right]}{N_0 N_1 N_2 N_3 N_4}. \tag{4.2.18}$$

In the case of real-photon radiation, this will correspond to

$$\int \frac{d^3k}{(2\pi)^3 \, 2\omega} \, \frac{\sum(k \cdot v_i)N_i'}{N_1' N_2' N_3' N_4'} \quad \text{and} \quad \int \frac{d^3k}{(2\pi)^3 \, 2\omega} \, \frac{N_0 \left[\sum(k \cdot v_i) + a\right]}{N_1' N_2' N_3' N_4'}. \tag{4.2.19}$$

For the nullification of the second integral the validity of Eq. (4.2.4) is immaterial, since for the on-shell photon $N_0 = 0$ anyway. The first integral, however, is no longer necessarily zero. The fact that the photon is on-shell implies that $k^2 = \lambda^2$ and that the propagators N_i are linear in k. By simple power counting, one can conclude that this integral is formally ultraviolet-divergent. For this reason, the Lorentz-covariance argument used in Eq. (4.2.3) is not correct any more and Eq. (4.2.4) is invalidated.

Apart from the modification of Eq. (4.2.4) and the fact that $N_0 = 0$, the derivation of the decomposition for the real five-point function is not changed, resulting in

$$
\begin{aligned}
(w^2 - 4\lambda^2 \Delta_4) \, E_{01234}^{R} = & \; (w \cdot v_1) \, D_{0234}^{R} + (w \cdot v_2) \, D_{0134}^{R} + (w \cdot v_3) \, D_{0124}^{R} + (w \cdot v_4) \, D_{0123}^{R} \\
& - 2 \int \frac{d^3k}{(2\pi)^3 \, 2\omega} \, \frac{\sum a \, (k \cdot v_i) \, N_i'}{N_1' N_2' N_3' N_4'}.
\end{aligned}
\tag{4.2.20}
$$

The main difference with the virtual decomposition is the occurrence of the last term in Eq. (4.2.20). It turns out that the poles in this particular integral can be moved in such a way that $N_i' \to N_i$ for all i. Indeed, the integral can be rewritten in the following way:

$$\int \frac{d^3k}{(2\pi)^3 \, 2\omega} \, \frac{\sum(k \cdot v_i) \, N_i'}{N_1' N_2' N_3' N_4'} = \int \frac{d^3k}{(2\pi)^3 \, 2\omega} \, \frac{\sum(k \cdot v_i) \, N_i}{N_1 N_2 N_3 N_4} + \Delta^{(1)} + \Delta^{(2)}, \tag{4.2.21}$$

with

$$\Delta^{(1)} = \int \frac{d^3k}{(2\pi)^3\,2\omega} \frac{(k\cdot v_1)\,N_1 + (k\cdot v_2)\,N_2}{N_1 N_2} \Big[\frac{1}{N_3' N_4'} - \frac{1}{N_3 N_4}\Big],$$

$$\Delta^{(2)} = \int \frac{d^3k}{(2\pi)^3\,2\omega} \left\{ \frac{(k\cdot v_3)}{N_1 N_2}\Big[\frac{1}{N_4'} - \frac{1}{N_4}\Big] + \frac{(k\cdot v_4)}{N_1 N_2}\Big[\frac{1}{N_3'} - \frac{1}{N_3}\Big] \right\} \qquad (4.2.22)$$

Both $\Delta^{(1)}$ and $\Delta^{(2)}$ are in fact zero. Let us consider, for example, one of the terms contributing to $\Delta^{(2)} = \Delta_3^{(2)} + \Delta_4^{(2)}$, e.g.

$$\Delta_4^{(2)} = \int \frac{d^3k}{(2\pi)^3\,2\omega} \frac{(k\cdot v_4)}{N_1 N_2} \frac{2i\,\mathrm{Im}\,N_3}{N_3 N_3'}. \qquad (4.2.23)$$

This integral is ultraviolet-finite, even for an on-shell photon, and therefore no regularization is needed. Consequently, the Lorentz-covariance argument is valid:

$$\int \frac{d^3k}{2\omega} \frac{k^\mu}{N_1 N_2 N_3 N_3'} = c_1\, p_1^\mu + c_2\, p_2^\mu + c_3\, p_3^\mu, \qquad (4.2.24)$$

where the quantities c_i are finite coefficients. Contracting the last expression with $v_{4\,\mu} = \varepsilon_{p_1 p_2 p_3 \mu}$, one arrives at $\Delta_4^{(2)} = 0$. Using similar arguments one can prove that $\Delta^{(1)} = \Delta^{(2)} = 0$.

An important point in this line of reasoning was the use of Lorentz-invariance of the integration d^3k/ω. Such an integration is indeed Lorentz-invariant, provided that the area of integration is Lorentz-invariant. In the context of the double-pole approximation, the photon is treated inclusively, with the integration performed over all possible values of k up to infinity. If one would, however, consider an exclusive process, involving the introduction of a cutoff Ω_{max}, then the area of integration might fail to be Lorentz-invariant, and the decomposition stops at Eq.(4.2.20). In order to successfully proceed beyond that point for exclusive processes, one should make sure that the cut-off prescription, which defines the area of integration, does not introduce new independent four-vectors in the integral. If this condition is satisfied, a generalization of the decomposition to exclusive bremsstrahlung processes should be feasible.

So, in our approach, the following identity has been established:

$$\int \frac{d^3k}{(2\pi)^3\,2\omega} \frac{\sum(k\cdot v_i)\,N_i'}{N_1' N_2' N_3' N_4'} = \int \frac{d^3k}{(2\pi)^3\,2\omega} \frac{\sum(k\cdot v_i)\,N_i}{N_1 N_2 N_3 N_4}. \qquad (4.2.25)$$

As was already noted, the integral on the right-hand side is formally divergent. Its virtual analogue, being formally finite, vanishes:

$$\int \frac{d^4k}{(2\pi)^4} \frac{\sum(k\cdot v_i)\,N_i}{N_0 N_1 N_2 N_3 N_4} = 0. \qquad (4.2.26)$$

Performing a contour integration in the lower half of the complex k_0-plane, indicated by the integration contour C_O in Fig. 4-3, one can use this identity to relate the photon-pole contribution to the particle-pole contributions:
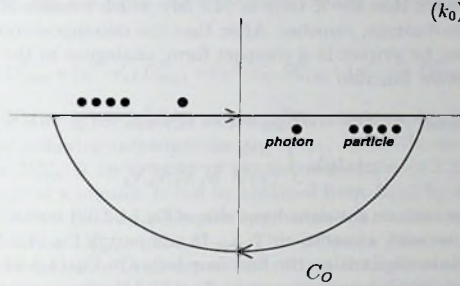
Figure 4-3. Integration contour in the lower half of the complex k_0-plane leading to Eq. (4.2.27).

$$-2\pi i \int \frac{d^3k}{(2\pi)^4 \, 2\omega} \frac{\sum(k \cdot v_i) N_i}{N_1 N_2 N_3 N_4} = -\int \frac{d^4k}{(2\pi)^4 N_0} \mathcal{P}ole \frac{\sum(k \cdot v_i) N_i}{N_1 N_2 N_3 N_4}. \qquad (4.2.27)$$

Here "$\mathcal{P}ole$" denotes the complex particle poles that should be taken into account. Note that the left-hand side of Eq. (4.2.27) corresponds to the real-photon radiation integral that we are pursuing to evaluate. The integral on the right-hand side does not correspond to on-shell photons any more, since $N_0 \neq 0$. Now we can use the Schouten identity to substitute

$$\sum_{i=1}^{4}(k \cdot v_i) N_i = \sum_{i=1}^{4}(k \cdot v_i) N_0 + 2ak^2 + \sum_{i=1}^{4} r_i (k \cdot v_i) \qquad (4.2.28)$$

on the right-hand side. After some rearrangements one obtains

$$2\pi i \int \frac{d^3k}{(2\pi)^4 \, 2\omega} \frac{\sum(k \cdot v_i) N_i}{N_1 N_2 N_3 N_4} = \int \frac{d^4k}{(2\pi)^4} \frac{\sum(k \cdot v_i) + 2a}{N_1 N_2 N_3 N_4} +$$
$$+ \int \frac{d^4k}{(2\pi)^4 N_0} \mathcal{P}ole \frac{\sum r_i (k \cdot v_i) + 2a\lambda^2}{N_1 N_2 N_3 N_4}. \qquad (4.2.29)$$

The first integral on the right-hand side can be simplified with the help of Eqs. (4.2.11) and (4.2.4), yielding

$$2\pi i \int \frac{d^3k}{(2\pi)^4 \, 2\omega} \frac{\sum(k \cdot v_i) N_i}{N_1 N_2 N_3 N_4} = a \int \frac{d^4k}{(2\pi)^4} \frac{1}{N_1 N_2 N_3 N_4} + \mathcal{R}, \qquad (4.2.30)$$

with

$$\mathcal{R} = \int \frac{d^4k}{(2\pi)^4 N_0} \mathcal{P}ole \frac{\sum r_i (k \cdot v_i) + 2a\lambda^2}{N_1 N_2 N_3 N_4}. \qquad (4.2.31)$$

In App. B it is shown that the $\mathcal{R}$ term in (4.2.30), which consists of a combination of particle-pole contributions, vanishes. After that the decomposition for the real five-point function can be written in a compact form, analogous to the decomposition of the virtual five-point function

$$(w^2 - 4\lambda^2\Delta_4)\,E_{01234}^{\mathrm{R}} = (w \cdot v_1)D_{0234}^{\mathrm{R}} + (w \cdot v_2)D_{0134}^{\mathrm{R}} + (w \cdot v_3)D_{0124}^{\mathrm{R}} + (w \cdot v_4)D_{0123}^{\mathrm{R}}$$
$$+ 2i\Delta_4 \int \frac{d^4k}{(2\pi)^4}\, \frac{1}{N_1 N_2 N_3 N_4}. \qquad (4.2.32)$$

Note that the last term on the right-hand side of Eq. (4.2.32) is exactly a virtual scalar four-point function with a coefficient $2i\Delta_4$. In comparing Eq. (4.2.15) to Eq. (4.2.32) one observes certain similarities: the first four terms in Eq. (4.2.32) are the radiative analogues of their virtual counterparts in Eq. (4.2.15). One may naively think that the last term in (4.2.32) should not be there, since it does not correspond to photon radiation. In fact, it is a direct consequence of having ultraviolet-divergent integrals during the intermediate steps of the derivation.

This concludes the derivation of the decomposition of the five-point function corresponding to inclusive bremsstrahlung. As was noted before, generalization to the case of exclusive bremsstrahlung is possible, provided that the cut-off is introduced in such a way that no new independent four-vectors appear in the integrals. In analogy to what was remarked for the virtual decomposition, also the generalization to higher multipoint radiation functions is possible and rather straightforward. One should simply follow the approach of Ref. [6] for multipoint scalar functions.

4.2.3   Application of the five-point decompositions

We can now apply the five-point decompositions to the non-factorizable W-pair corrections. The virtual scalar five-point function, corresponding to the third diagram in Fig. 4-1, reads in the double-pole approximation

$$w^2 E_{01234} = 2\Delta_4 D_{1234} + (w \cdot v_1)D_{0234} + (w \cdot v_2)D_{0134} + (w \cdot v_3)D_{0124} + (w \cdot v_4)D_{0123}, \qquad (4.2.33)$$

with

$$v_{1\mu} = -\varepsilon_{\mu p_2 k_1 k_2}, \qquad v_{2\mu} = +\varepsilon_{p_1 \mu k_1 k_2}, \qquad v_{3\mu} = -\varepsilon_{p_1 p_2 \mu k_2},$$
$$v_{4\mu} = +\varepsilon_{p_1 p_2 k_1 \mu}, \qquad w^\mu = D_1 v_1^\mu + D_2 v_2^\mu, \qquad \Delta_4 = [\varepsilon_{p_1 p_2 k_1 k_2}]^2. \quad (4.2.34)$$

Comparison with Eq. (4.2.15) reveals that the terms $-\sum(w \cdot v_i)\,D_{1234}$ have been neglected, since they are formally of higher order in the expansion in powers of Γ_W/M_W. Note that the scalar four-point function D_{1234} is purely a consequence of the decomposition (4.2.33). It does not involve the exchange of a photon and is therefore not affected by the semi-soft photon approximation. Since the factor $2\Delta_4/w^2$ is already doubly resonant, D_{1234} should be calculated for on-shell W bosons. The scalar four-point functions D_{0134} and D_{0234} are infrared-divergent and should be calculated in the semi-soft photon approximation.

In the same way, the five-point function corresponding to real-photon radiation is given by

$$w'^2 E_{01234}^R = 2i \left[D_{1234}^R + (w' \cdot v_1') D_{0234}^R + (w' \cdot v_2') D_{0134}^R + (w' \cdot v_3') D_{0124}^R + (w' \cdot v_4') D_{0123}^R \right].$$
(4.2.35)

The four vectors w' and v_i' are defined as before, but for real-photon emission. This is equivalent to the following substitutions: $p_1 \to -p_1$, $k_1 \to -k_1$ and $D_2 \to D_2^*$. The radiation function D_{1234}^R is an artefact of the decomposition (4.2.35) and does not involve the exchange of a photon. It can be obtained from D_{1234} by the substitutions $p_1 \to -p_1$ and $k_1 \to -k_1$. In the double-pole approximation, i.e. for on-shell W bosons, this implies the relation $D_{1234}^R = i\,\mathrm{Im}\, D_{1234}$. This property ensures the cancellation of the virtual non-factorizable D_{1234}-dependent corrections against the corresponding real-photon corrections, provided that the integration over the W-boson virtualities (i.e. $D_{1,2}$) is performed. This phenomenon is a general consequence of the semi-soft photon approximation [4].

4.2.4   Connection between virtual and real contributions

At this point we have reduced the calculation of the non-factorizable corrections to the evaluation of virtual and real four-point functions. We can, however, go one step further and establish a connection between the contribution from the photon-pole part of the virtual scalar functions, D^γ, and the corresponding radiative interferences. To this end, we consider for example the contributions related to D_{0123}^γ and D_{0123}^R. The contribution of the radiative interference to the cross-section (see Fig. 4-1) is given by

$$d\sigma_{\mathrm{nf}}^{\mathrm{real}}(D_{0123}^R) = d\sigma_{\mathrm{DPA}}^0\, \mathrm{Re} \int \frac{d^3k}{(2\pi)^3\, 2\omega} \frac{32\pi\alpha\,(p_2 \cdot k_1)\, D_1}{[D_1 + 2(p_1 \cdot k)][D_2^* + 2(p_2 \cdot k)][2(k_1 \cdot k) + io]},$$
(4.2.36)

where $k_0 = \omega = |\vec{k}|$.

This has to be compared with the corresponding photon-pole part of the virtual correction. This contribution is evaluated in the lower half of the complex k_0-plane, where the photon pole is situated at $k_0 = \omega = |\vec{k}| - io$:

$$d\sigma_{\mathrm{nf}}^{\mathrm{virt}}(D_{0123}^\gamma) = d\sigma_{\mathrm{DPA}}^0\, \mathrm{Re} \int \frac{d^3k}{(2\pi)^3\, 2\omega} \frac{32\pi\alpha\,(p_2 \cdot k_1)\, D_1}{[D_1 - 2(p_1 \cdot k)][D_2 + 2(p_2 \cdot k)][-2(k_1 \cdot k) + io]}.$$
(4.2.37)

This can be rewritten in the form

$$d\sigma_{\mathrm{nf}}^{\mathrm{virt}}(D_{0123}^\gamma) = d\sigma_{\mathrm{DPA}}^0\, \mathrm{Re} \int \frac{d^3k}{(2\pi)^3\, 2\omega} \frac{32\pi\alpha\,(p_2 \cdot k_1)\, D_1^*}{[D_1^* - 2(p_1 \cdot k)][D_2^* + 2(p_2 \cdot k)][-2(k_1 \cdot k) - io]}.$$
(4.2.38)

Comparing Eqs. (4.2.36) and (4.2.38), one can readily see that $d\sigma_{\mathrm{nf}}^{\mathrm{real}}(D_{0123}^R)$ can be obtained from the photon-pole contribution to the virtual correction $d\sigma_{\mathrm{nf}}^{\mathrm{virt}}(D_{0123}^\gamma)$,

by adding an overall minus sign and substituting[2] $D_1 \rightarrow -D_1^*$. In a similar way $d\sigma_{nf}^{real}(D_{0124}^R)$ can be obtained from the photon-pole contribution to the virtual correction $d\sigma_{nf}^{virt}(D_{0124}^\gamma)$, by adding an overall minus sign and substituting $D_2 \rightarrow -D_2^*$. The different substitution rule reflects the fact that we will determine D_{0124} and D_{0124}^γ from D_{0123} and D_{0123}^γ by substituting $(p_1, k_1) \leftrightarrow (p_2, k_2)$. Note that this is equivalent to evaluating D_{0124}^γ in the upper half of the complex k_0-plane.

Also the "Coulomb" and five-point contributions can be treated in this way, bearing in mind that the coefficients of the five-point decomposition also depend on $D_{1,2}$. In conclusion, the following relation emerges. The radiative interference is obtained from Eqs. (4.1.2) and (4.1.3) by adding a minus sign, by inserting the decomposition given in Eq. (4.2.33), and by substituting

- in the D_{0123}, D_{0134} terms: $D_{0123}, D_{0134} \rightarrow D_{0123}^\gamma, D_{0134}^\gamma$ followed by $D_1 \rightarrow -D_1^*$,
- in the D_{0124}, D_{0234} terms: $D_{0124}, D_{0234} \rightarrow D_{0124}^\gamma, D_{0234}^\gamma$ followed by $D_2 \rightarrow -D_2^*$,
- in the D_{1234} terms: $D_{1234} \rightarrow D_{1234}^R$ followed by $D_2 \rightarrow -D_2^*$,
- in the C_{012} terms: $C_{012} \rightarrow C_{012}^\gamma$ followed by $D_1 \rightarrow -D_1^*$.

Here both D_{0124}^γ and D_{0234}^γ are determined by substituting $(p_1, k_1) \leftrightarrow (p_2, k_2)$ in the expressions for D_{0123}^γ and D_{0134}^γ, respectively. As such, the above connection between real and virtual corrections implies that D_{0124}^γ and D_{0234}^γ are evaluated in the upper half-plane.

Note that the above-presented connection between the virtual and real non-factorizable corrections hinges on two things. First of all, the inclusive treatment of the bremsstrahlung photon, with the phase-space integration extending to infinity. Second, the fact that both virtual and real corrections are calculated in the semi-soft photon approximation, inherent in the double-pole approach.

As mentioned before, manifestly non-factorizable initial–final state interference effects are also possible in our approach. As stated in the beginning of this chapter, we will now briefly indicate why these effects vanish. In Sect. 4.1 this fact was used as the first of two theorems for establishing a link to the construction of the non-factorizable corrections in terms of currents in Chapter 2. Let us consider, for example, the initial–final state interference contribution corresponding to the photonic interaction between the positron $[e^+(q_1)]$ and the positively charged final-state lepton $[\ell^+(k_1)]$. In the semi-soft photon approximation, the contribution of the virtual interference to the cross-section is

$$d\sigma_{nf}^{virt}(D_{if}) = -d\sigma_{DPA}^0 \times \hspace{5cm} (4.2.39)$$

$$\times \mathrm{Re} \int \frac{d^4k}{(2\pi)^4} \frac{32i\pi\alpha\,(q_1 \cdot k_1)\,D_1}{[k^2 - \lambda^2 + io][D_1 - 2(p_1 \cdot k)][-2(k_1 \cdot k) + io][-2(q_1 \cdot k) + io]}.$$

Note that all particle poles are situated in the upper half of the complex k_0-plane. By closing the integration contour in the lower half-plane, one finds that the complete

---

[2]Note that $d\sigma_{DPA}^0$ is not affected by substitutions of the form $D_i \rightarrow -D_i^*$ $(i = 1, 2)$, since it only depends on $|D_1 D_2|^2$.

virtual correction is equal to the photon-pole contribution

$$d\sigma_{\text{nf}}^{\text{virt}}(D_{if}) = -d\sigma_{\text{DPA}}^0 \, \text{Re} \int \frac{d^3k}{(2\pi)^3 \, 2\omega} \frac{32\pi\alpha \, (q_1 \cdot k_1) \, D_i}{[D_1 - 2(p_1 \cdot k)][-2(k_1 \cdot k) + io][-2(q_1 \cdot k) + io]},$$
(4.2.40)

with $k_0 = \omega = \sqrt{\vec{k}^2 + \lambda^2 - io}$. On the other hand, the corresponding bremsstrahlung interference can be written as

$$d\sigma_{\text{nf}}^{\text{real}} = d\sigma_{\text{DPA}}^0 \, \text{Re} \int \frac{d^3k}{(2\pi)^3 \, 2\omega} \frac{32\pi\alpha \, (q_1 \cdot k_1) \, D_1^*}{[D_1^* + 2(p_1 \cdot k)][2(k_1 \cdot k) - io][-2(q_1 \cdot k) + io]}.$$
(4.2.41)

By comparing the last two expressions, one can readily derive that the virtual and real interferences differ by an overall minus sign and the substitution $D_1 \to -D_1^*$. In the next section we derive an explicit expression for infrared-divergent virtual scalar four-point functions [see Eq. (4.3.28)].[3] From this expression one can see that the substitution $D_1 \to -D_1^*$ does not change the real part of the interference (4.2.39), i.e. the sum of virtual and real interferences gives rise to a vanishing non-factorizable correction. Analogously, no other non-factorizable initial–final and initial–intermediate state photonic interferences contribute to the double resonant cross-section, if both virtual and real corrections are included. Similar arguments can be used to prove that initial-state up–down QED interferences vanish in our approach.

4.3   Modified standard technique: calculation

In this section we present the calculation of the relevant virtual scalar functions, using Feynman-parameter integrals. In addition the photon-pole parts of these functions are given, from which the real-photon corrections can be extracted. The striking difference with the usual calculations of scalar integrals lies in the systematic application of the semi-soft photon approximation.

4.3.1   Scalar four-point functions
in the semi-soft photon approximation

In this subsection we illustrate how to calculate a virtual scalar four-point function in the semi-soft photon approximation and how to extract the photon-pole part. Consider to this end

$$D_{\text{virt}} = \int \frac{d^4k}{(2\pi)^4} \frac{1}{[k^2 + io][2(p_1 \cdot k) + D_1 + io][2(p_2 \cdot k) + D_2 + io][2(p_3 \cdot k) + D_3 + io]},$$
(4.3.1)

where $D_i = p_i^2 - M_i^2$. In general, the energy components p_i^0 of the arbitrary momenta p_i are not necessarily positive. In contrast to the usual Feynman-parameter technique,

---

[3]In our example we need Eq. (4.3.28) with k_2 replaced by $-q_1$. Note that, as a result of this substitution, the invariant s_{12} becomes negative.

where the Feynman-parameter transformation is applied to all propagators, we apply it only to propagators that are linear in k:

$$D_{\text{virt}} = 2 \int\limits_0^1 d^3\xi \, \delta\Big(1 - \sum_{i=1}^3 \xi_i \Big) \, I_{\text{virt}}(\xi), \tag{4.3.2}$$

with

$$I_{\text{virt}}(\xi) = \int \frac{d^4k}{(2\pi)^4} \frac{1}{[k_0^2 - \vec{k}^2 + io][k_0 E(\xi) - \vec{k}\cdot\vec{p}(\xi) + A(\xi) + io]} \tag{4.3.3}$$

The quantities $A(\xi)$ and $p^\mu(\xi)$ are given by

$$A(\xi) = \sum_{i=1}^3 \xi_i \, D_i \quad \text{and} \quad p^\mu(\xi) = 2 \sum_{i=1}^3 \xi_i \, p_i^\mu. \tag{4.3.4}$$

The energy component $E(\xi)$ of $p^\mu(\xi)$ can be positive or negative. However, there is a freedom to choose $E(\xi) \leq 0$, because one can always perform a transformation of variables $k_0 \to -k_0$. Then

$$I_{\text{virt}}(\xi) = \int \frac{d^4k}{(2\pi)^4} \frac{1}{[k_0^2 - \vec{k}^2 + io][-k_0|E(\xi)| - \vec{k}\cdot\vec{p}(\xi) + A(\xi) + io]^3}. \tag{4.3.5}$$

In the complex k_0-plane the denominators give rise to poles. There are two photon poles, one in the upper and one in the lower half-plane. The second denominator gives rise to a "particle" pole in the upper half-plane, for any value of ξ_i. It should be noted that this combines the three particle poles present in (4.3.1), which could lie in the upper or lower half-plane. Closing the integration contour in the lower half-plane we get

$$I_{\text{virt}}(\xi) = -i \int \frac{d^3k}{(2\pi)^3} \frac{1}{2|\vec{k}| \, (-|\vec{k}| \, |E(\xi)| - x|\vec{k}| \, |\vec{p}(\xi)| + A(\xi) + io)^3}, \tag{4.3.6}$$

where $x = \cos\theta$, with θ being the angle between $\vec{p}(\xi)$ and $\vec{k}$. It is not very difficult to perform the rest of the integrations in momentum space. The final result is

$$I_{\text{virt}}(\xi) = -\frac{i}{8\pi^2} \frac{1}{A(\xi) \, (p^2(\xi) - io|E(\xi)|)}. \tag{4.3.7}$$

As we have seen in the previous section, the real-photon radiative interferences can be obtained from the photon-pole parts of the virtual corrections. Let us therefore consider the photon-pole part of (4.3.1) in the lower half of the complex k_0-plane:

$$D_{\text{virt}}^\gamma = -i \int \frac{d^3k}{(2\pi)^3} \frac{1}{2|\vec{k}| \, [2(p_1\cdot k) + D_1 + io][2(p_2\cdot k) + D_2 + io][2(p_3\cdot k) + D_3 + io]}, \tag{4.3.8}$$

with $k_0 = \sqrt{\vec{k}^2 - io}$. One can again proceed by introducing the Feynman parameters to obtain

$$I_{\text{virt}}^{\gamma}(\xi) = -i \int \frac{d^3k}{(2\pi)^3} \frac{1}{2|\vec{k}| \left[E(\xi) \sqrt{\vec{k}^2 - io} - x |\vec{k}| |\vec{p}(\xi)| + A(\xi) + io \right]^3}. \tag{4.3.9}$$

Equations (4.3.6) and (4.3.9) are the same up to small modifications. In the case of the full virtual scalar function, Eq. (4.3.6) was obtained after contour integration in the complex plane. In that case we had the freedom to choose the contour in such a way that $\text{Re}(k_0) \leq 0$. Now we have no such freedom. So, $E(\xi)$ cannot be considered as a regular quantity any more. It is clear that the final answer will be

$$I_{\text{virt}}^{\gamma}(\xi) = -\frac{i}{8\pi^2} \frac{1}{A(\xi) \left[p^2(\xi) + io E(\xi) \right]}. \tag{4.3.10}$$

This expression is very similar to the one derived for the full virtual scalar function. It can in fact be rewritten as

$$I_{\text{virt}}^{\gamma}(\xi) = -\frac{i}{8\pi^2} \frac{1}{A(\xi)} \left\{ \frac{1}{p^2(\xi) - io|E(\xi)|} - 2i\pi \, \theta[E(\xi)] \, \delta[p^2(\xi)] \right\}, \tag{4.3.11}$$

where the first term in the curly brackets corresponds to the full virtual scalar function and the second term is the necessary modification. The second term in Eq. (4.3.11) is the analogue of the "particle"-pole contribution in the approach of [3]. Note that this term has an extra factor i. If all quantities were to be real (stable-particle case), then this term would not contribute to the non-factorizable correction to the cross-section, for which only the real part is important. In Sect. 4.1 this fact was used as the second of two theorems for establishing a link to the construction of the non-factorizable corrections in terms of currents in Chapter 2. In the case of unstable particles, this "particle"-pole contribution is felt by the imaginary parts of the W-boson propagators, resulting in a potentially non-zero contribution to the cross-section. If one were to evaluate the photon-pole part of (4.3.1) in the upper half of the complex k_0-plane, one merely would have to replace $E(\xi)$ by $-E(\xi)$ in Eqs. (4.3.10) and (4.3.11).

In practice, we calculate the relevant four-point functions D_{virt} as well as the corresponding particle-pole contributions $D_{\text{virt}}^{\text{part}}$. The photon-pole part D_{virt}^{γ} is obtained as $D_{\text{virt}}^{\gamma} = D_{\text{virt}} - D_{\text{virt}}^{\text{part}}$, which can then be used to evaluate the real-photon radiative interferences. The complex half-plane where the particle-pole (photon-pole) contributions should be evaluated is fixed according to the rules given in Sect. 4.2.4.

4.3.2 Calculation of the scalar four-point functions

In this subsection we present the calculation of the virtual scalar four-point functions and the associated photon-pole parts. Everything is considered in the semi-soft photon approximation. Since the four-point function D_{1234} does not involve this approximation, we defer the corresponding results to App. A.1 and merely refer to the literature [7, 8] for its derivation.

Before listing the various results, we define our notation. To write down the analytical results we need to introduce some kinematic invariants:

$$m_{1,2}^2 = k_{1,2}^2, \quad s = (p_1 + p_2)^2, \quad s_{12} = (k_1 + k_2)^2,$$
$$s_{211'} = (k_2 + k_1 + k_1')^2, \quad s_{122'} = (k_1 + k_2 + k_2')^2, \qquad (4.3.12)$$

and some short-hand notations:

$$y_0 = \frac{D_1}{D_2}, \quad x_s = \frac{\beta - 1}{\beta + 1} + io, \quad \beta = \sqrt{1 - 4M_W^2/s},$$
$$\zeta = 1 - \frac{s_{122'}}{M_W^2} - io, \quad \zeta' = 1 - \frac{s_{211'}}{M_W^2} - io. \qquad (4.3.13)$$

The virtual infrared-finite four-point function

We start off with the calculation of the infrared-finite scalar four-point function D_{0123}, which corresponds to the first diagram shown in Fig. 4-1. This function is infrared-finite owing to the presence of finite decay widths in the propagators of the unstable W bosons. In the semi-soft photon limit we find

$$D_{0123} = \int \frac{d^4k}{(2\pi)^4} \frac{1}{[k^2 + io][D_1 - 2(p_1 \cdot k)][D_2 + 2(p_2 \cdot k)][-2(k_1 \cdot k) + io]}, \qquad (4.3.14)$$

where $D_{1,2} = p_{1,2}^2 - M_W^2 + io$. Originally the quantities $D_{1,2}$ are real, with the usual infinitesimal imaginary part. At the end of the calculation the analytical continuation to finite imaginary parts can be performed. Then $D_{1,2} = p_{1,2}^2 - M_W^2 + iM_W\Gamma_W$.

Applying the Feynman-parameter technique as explained in Sect. 4.3.1, we obtain the following representation

$$D_{0123} = \frac{-i}{4\pi^2} \int_0^1 d^3\xi\, \delta\left(1 - \sum_{i=1}^3 \xi_i\right) \frac{1}{A(\xi)\,[p^2(\xi) - io]} \qquad (4.3.15)$$

with

$$A(\xi) = \xi_1 D_1 + \xi_2 D_2, \quad p^\mu(\xi) = -2\xi_1 p_1^\mu + 2\xi_2 p_2^\mu - 2\xi_3 k_1^\mu. \qquad (4.3.16)$$

As was indicated before, the integral will be calculated for small final-state fermion masses and in the double-pole approximation. This implies

$$2(p_1 \cdot k_1) \approx p_1^2 \approx M_W^2 \quad \text{and} \quad 2(p_2 \cdot k_2) \approx p_2^2 \approx M_W^2. \qquad (4.3.17)$$

What is left is the integral over the space of Feynman parameters. The details of the integration are presented in App. A.2. The final answer reads

$$
\begin{aligned}
D_{0123} = {} & \frac{i}{16\pi^2 M_W^2} \frac{1}{[D_2 - \zeta D_1]} \left\{ 2\,\mathcal{L}\mathrm{i}_2\left(\frac{1}{y_0}; \frac{1}{\zeta}\right) - \mathcal{L}\mathrm{i}_2\left(x_s; \frac{1}{y_0}\right) - \mathcal{L}\mathrm{i}_2\left(\frac{1}{x_s}; \frac{1}{y_0}\right) \right. \\
& + \left. \mathcal{L}\mathrm{i}_2\left(x_s; \zeta\right) + \mathcal{L}\mathrm{i}_2\left(\frac{1}{x_s}; \zeta\right) + \left[\ln\frac{M_W^2}{m_1^2} + 2\ln(\zeta)\right]\left[\ln(y_0) + \ln(\zeta)\right] \right\}. \qquad (4.3.18)
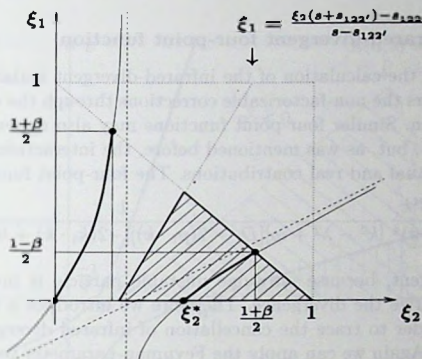\end{aligned}
$$

Figure 4-4. The integration area (shaded region) in the (ξ_1, ξ_2) Feynman-parameter space for the calculation of the particle-pole part D_{0123}^{part} of the infrared-finite scalar four-point function D_{0123}. The thicker curves indicate the solutions of $p^2(\xi) = 0$, with $\xi_2^* = 1 - M_W^2/s_{122'}$.

The function $\mathcal{L}i_2(x; y)$ is the continued dilogarithm

$$\mathcal{L}i_2(x; y) = \text{Li}_2(1 - xy) + \ln(1 - xy)\left[\ln(xy) - \ln(x) - \ln(y)\right], \qquad (4.3.19)$$

with $\text{Li}_2(x)$ the usual dilogarithm and x, y lying on the first Riemann sheet. The answer for the second infrared-finite scalar four-point function, D_{0124}, can be obtained from Eq. (4.3.18) by substituting $(p_1, k_1) \leftrightarrow (p_2, k_2)$.

Photon-pole part of the infrared-finite four-point function

As was explained in Sect. 4.3.1, the photon-pole part of a scalar function can be obtained from the full scalar function by subtracting the "particle"-pole contributions. According to Eq. (4.3.11), the "particle"-pole contributions in the lower half of the complex k_0-plane are given by

$$D_{0123}^{\text{part}} = \frac{1}{2\pi} \int\limits_{0}^{\xi_1 + \xi_2 < 1} \frac{d\xi_1 \, d\xi_2}{A(\xi)} \, \theta[E(\xi)] \, \delta[p^2(\xi)]. \qquad (4.3.20)$$

The integration area is defined by the θ-function for the energy and by the condition $\xi_1 + \xi_2 < 1$. The allowed area of integration and the curve where the δ-function has a non-zero value are schematically shown in Fig. 4-4. The depicted situation represents the most general case for the kinematics we are interested in.

After the integration over the δ-function has been performed, one is left with a simple one-dimensional integration of logarithmic type. The final result is

$$D_{0123}^{\text{part}} = \frac{1}{8\pi M_W^2} \frac{1}{D_2 - \zeta D_1} \left[\ln(1 - y_0 x_s) - \ln(1 - x_s/\zeta)\right]. \qquad (4.3.21)$$

The virtual infrared-divergent four-point function

Here we describe the calculation of the infrared-divergent scalar four-point function D_{0134}, which enters the non-factorizable corrections through the decomposition of the five-point function. Similar four-point functions may also appear in the initial–final state interactions, but, as was mentioned before, the interactions of this type vanish in the sum of virtual and real contributions. The four-point function

$$D_{0134} = \int \frac{d^4k}{(2\pi)^4} \frac{1}{[k^2 - \lambda^2 + io][D_1 - 2(p_1 \cdot k)][-2(k_1 \cdot k) + io][2(k_2 \cdots]}$$

(4.22)

is infrared-divergent, because only one unstable particle is involved, not enough to regularize the divergence. Therefore we introduce a regulator λ for the photon in order to trace the cancellation of infrared divergences and real corrections. Again we can apply the Feynman-parameter technique obtained in Sect. 4.3.1. However, special care has to be taken with the photon mass. As usual we can introduce Feynman parameters according to

$$D_{0134} = 2 \int_0^1 d^3\xi \, \delta\left(1 - \sum_{i=1}^3 \xi_i\right) I_{0134}(\xi),$$

(4.3.23)

with

$$I_{0134}(\xi) = \int \frac{d^4k}{(2\pi)^4} \frac{1}{[k^2 - \lambda^2 + io][-k_0 \, |E(\xi)| - \vec{k} \cdot \vec{p}(\xi) + A(\xi) + io]^3}$$

(4.3.24)

and

$$A(\xi) = \xi_2 \, D_1, \quad p^\mu(\xi) = -2\xi_1 \, k_1^\mu - 2\xi_2 \, p_1^\mu + 2\xi_3 \, k_2^\mu.$$

(4.3.25)

Again we can exploit the freedom to perform the variable transformation $k_0 \to -k_0$ in order to fix the sign of the energy component $E(\xi)$. After the integration over momentum space, the details of which can be found in App. A.3, we obtain

$$I_{0134}(\xi) = -\frac{i}{8\pi^2} \frac{\partial}{\partial p^2} \left\{ \frac{1}{\sqrt{A^2 - \lambda^2 p^2}} \ln\left(\frac{A - \sqrt{A^2 - \lambda^2 p^2}}{A + \sqrt{A^2 - \lambda^2 p^2}}\right) \right\}$$

(4.3.26)

with

$$\frac{p^2(\xi)}{4} = \xi_2^2 M_W^2 + \xi_1^2 m_1^2 + \xi_3^2 m_2^2 + \xi_1 \xi_2 M_W^2 - \xi_1 \xi_3 s_{12} + \xi_2 \xi_3 (M_W^2 - s_{211'}).$$

(4.3.27)

The masses of the final-state fermions, m_1 and m_2, are taken to be small in our approximation.

One is left with a twofold Feynman-parameter integration (see App. A.3), which results in

$$\begin{aligned} D_{0134} &= -\frac{i}{16\pi^2 s_{12}} \frac{1}{D_1} \left[\text{Li}_2\left(1 + \frac{\zeta' M_W^2}{s_{12}}\right) - 2\ln\left(\frac{M_W \lambda}{-D_1}\right) \ln\left(\frac{m_1 m_2}{-s_{12} - io}\right) \right. \\ &\quad \left. + \frac{\pi^2}{3} + \ln^2\left(\frac{M_W}{m_1}\right) + \ln^2\left(\frac{m_2}{\zeta' M_W}\right) \right]. \end{aligned}$$
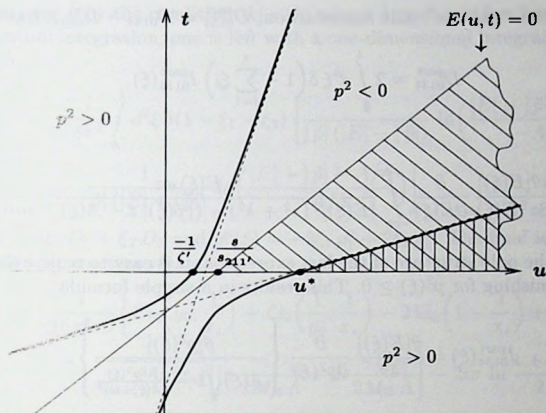
(4.3.28)

Figure 4-5. The area of integration in the (u, t)-plane for the calculation of the particle pole D_{0134}^{part}. The shaded region is the area of integration where $E(u, t) > 0$. The doubly-shaded region is the area of integration where $E(u, t) > 0$ and $p^2(u, t) > 0$. The thicker curves indicate the solutions of $p^2(u, t) = 0$, with $u^* \approx -\zeta' M_W^2/m_2^2$.

The answer for the second infrared-divergent scalar four-point function, D_{0234}, can be obtained from Eq. (4.3.28) by substituting $(p_1, k_1) \leftrightarrow (p_2, k_2)$.

Photon-pole part of the infrared-divergent four-point function

The procedure for calculating the photon-pole part D_{0134}^γ follows our general strategy, i.e. we calculate the corresponding "particle"-pole contributions and subtract them from the full virtual scalar function. The difference between this case and the one discussed in Sect. 4.3.2 lies in the fact that here both photon-pole and "particle"-pole contributions are infrared-divergent. So as to keep track of the cancellation of the infrared divergences, we again introduce a regulator mass λ for the photon.

In App. A.3 the following convenient representation for $I_{0134}(\xi)$ was derived in Eq. (A.14):

$$I_{0134}(\xi) = \frac{i}{16\pi^2 |E(\xi)|} \int_{-\infty}^{\infty} \frac{dz}{\left[-|E(\xi)| \sqrt{z^2 + \lambda^2} - |\vec{p}(\xi)| z + A(\xi) + io \right]^2}. \qquad (4.3.29)$$

From the general discussion in Sect. 4.3.1 we know that the photon-pole contribution to the four-point functions in the Feynman-parameter representation, $I_{\text{virt}}^\gamma(\xi)$, can be obtained from the complete virtual function, $I_{\text{virt}}(\xi)$, by a substitution $|E(\xi)| \rightarrow$

$-E(\xi)$. Then the "particle"-pole contribution, $D_{0134}^{\text{part}} = D_{0134} - D_{0134}^{\gamma}$, has the form

$$D_{0134}^{\text{part}} = 2 \int\limits_0^1 d^3\xi \, \delta\left(1 - \sum_{i=1}^3 \xi_i\right) I_{0134}^{\text{part}}(\xi), \tag{4.3.30}$$

where

$$I_{0134}^{\text{part}}(\xi) = -\frac{i\theta[E(\xi)]}{8\pi^2 E(\xi)} \frac{\partial}{\partial E(\xi)} \int\limits_{-\infty}^{+\infty} \frac{E(\xi) \, dz}{[E(\xi)]^2 (z^2 + \lambda^2) - (|\vec{p}(\xi)| \, z - A(\xi) -} \tag{4.3.31}$$

By analysing the pole structure of the last expression, it is easy to real⟨⟩⟨⟩⟨⟩ $_{0134}^{\text{part}}(\xi)$ is only non-vanishing for $p^2(\xi) \geq 0$. This results in a simple formula

$$I_{0134}^{\text{part}}(\xi) = \frac{\theta[E(\xi)]}{4\pi} \frac{\partial}{\partial p^2(\xi)} \left\{ \frac{\theta[p^2(\xi)]}{A(\xi)\sqrt{1 - \frac{\lambda^2 p^2(\xi)}{[A(\xi)+io]^2}}} \right\}. \tag{4.3.32}$$

What is left is the integration over the space of Feynman parameters. In order to simplify the calculation it is advisable to make the change of variables $\xi_1 = t/(1 + t + u)$ and $\xi_2 = 1/(1 + t + u)$. The area of integration in the (u, t)-plane is shown schematically in Fig. 4-5. The final result is

$$D_{0134}^{\text{part}} = \frac{1}{8\pi s_{12} D_1} \left[-\ln(-\zeta') + \ln\left(\frac{D_1}{iM_W^2}\right) - \ln\left(\frac{\lambda}{m_2}\right) \right]. \tag{4.3.33}$$

This is the same result as obtained in Sect. 4.4, where we will approach the various calculations in a significantly different way.

4.3.3   The Coulomb–like scalar three-point function

As was pointed out in the beginning of this chapter, a gauge-invariant definition of the non-factorizable corrections requires the proper inclusion of a Coulomb-like contribution. In this subsection we calculate the associated scalar three-point function in the semi-soft photon approximation. This three-point function is infrared-finite, but ultraviolet-divergent. This divergence occurs as a result of the fact that we neglect the k^2 dependence of the propagators, following our general semi-soft photon strategy. Although the virtual and real Coulomb-like contributions to the cross-section are separately ultraviolet-divergent, the sum is finite.

The virtual Coulomb-like scalar three-point function C_{012} is defined as (see Fig. 4-2):

$$C_{012} = \int \frac{d^4k}{(2\pi)^4} \frac{1}{[k^2 + io][D_1 - 2(p_1 \cdot k)][D_2 + 2(p_2 \cdot k)]}. \tag{4.3.34}$$

Similar to the calculation of the scalar four-point functions, we introduce the Feynman parameters only for the propagators that are linear in k. We limit the area of

integration over $\vec{k}$ by the condition $|\vec{k}| < \Lambda$, where $\Lambda \gg \Gamma_W$. After having performed the momentum integration, one is left with a one-dimensional integral over Feynman parameters:

$$
C_{012} = -\frac{i}{8\pi^2} \int_0^1 d^2\xi \, \delta(1 - \xi_1 - \xi_2) \left[\frac{1}{|\vec{p}| \, (|E| - |\vec{p}|)} \ln\left(\frac{|E| - |\vec{p}| - A/\Lambda}{-A/\Lambda} \right) \right.
$$
$$
\left. \frac{1}{|\vec{p}| \, (|E| + |\vec{p}|)} \ln\left(\frac{|E| + |\vec{p}| - A/\Lambda}{-A/\Lambda} \right) \right], \tag{4.3.35}
$$

where $A = \cdots + \xi_2 \, D_2$ and $p^\mu(\xi) = -2\xi_1 \, p_1^\mu + 2\xi_2 \, p_2^\mu$. The final integration over the Feynman parameters yields

$$
C_{012} = \frac{1}{8\pi^2 s\beta} \left\{ \mathcal{L}\mathrm{i}_2\left(y_0; \frac{1}{x_s} \right) + \mathcal{L}\mathrm{i}_2\left(\frac{1}{y_0}; \frac{1}{x_s} \right) - 2\,\mathrm{Li}_2\left(1 - \frac{1}{x_s} \right) + \frac{1}{2} \ln^2(y_0) \right.
$$
$$
\left. + \ln(x_s) \left[\ln \frac{-iD_1}{2M_W\Lambda} + \ln \frac{-iD_2}{2M_W\Lambda} \right] - 2i\pi \, \ln \frac{1 + x_s}{2} \right\}. \tag{4.3.36}
$$

In a similar way one can calculate the particle-pole contribution C_{012}^{part}, which can be used to extract the photon-pole part $C_{012}^\gamma = C_{012} - C_{012}^{\mathrm{part}}$. The final answer for the particle-pole contribution reads

$$
C_{012}^{\mathrm{part}} = \frac{1}{8\pi s\beta} \left\{ \ln(1 - x_s) + \ln(1 + x_s) - \ln(1 - y_0 x_s) - \ln\left(\frac{-iD_2}{M_W\Lambda} \right) \right\}. \tag{4.3.37}
$$

Note that the real part of C_{012}^{part} does not contribute to the non-factorizable corrections. Therefore, the Λ dependence effectively drops out from the particle-pole contribution.

One may wonder how the non-factorizable contributions (4.1.2) and (4.1.3) to the cross-section compare with the Coulomb contribution as calculated in the literature. Our calculation is based on the assumption of being at least a few widths away from the threshold [the accuracy of this approximation is of $\mathcal{O}(\Gamma_W/\Delta E)$], whereas the Coulomb effect in the literature is valid in the non-relativistic region, where it approximates the cross-section with accuracy $\mathcal{O}(\beta)$. Therefore one could try to compare them in an overlapping region, where $\Gamma_W \ll \Delta E \ll M_W$. The Coulomb effect calculated in Ref. [9] consists of two parts. One contribution that is also present for on-shell W-bosons, and one that comes from the off-shellness. The former is related to factorizable corrections and the latter is related to non-factorizable corrections and vanishes upon integration over the virtualities[4]. In the overlap region ($\Gamma_W \ll \Delta E \ll M_W$) this off-shell term equals the $1/\beta$ part of our full expression.

---

[4]Only soft and semi-soft virtual photons contribute to both parts. For the on-shell (factorizable) part of the Coulomb effect photons with momenta $\omega \approx \beta^2 M_W$ and $|\vec{k}| \approx \beta M_W$ are important (hence k^2 can not be neglected in the propagators of the unstable particles). On the other hand, only photons with momenta $\omega \approx \Gamma_W$ and $|\vec{k}| \approx \Gamma_W/\beta$ give the leading contribution to the off-shell part of the Coulomb effect. Far from the threshold, where $\Gamma_W \ll \Delta E \ll M_W$, the two regions in the photon-momentum space are well separated. Because of this the effects are additive. Near threshold, where $\Gamma_W \approx \Delta E$, the two regions start to intersect.

4.4   Direct momentum-integration method

In this section we present an alternative method of calculating the non-factorizable corrections, i.e. the so-called direct momentum-integration (DMI) method. As in Sects. 4.2 and 4.3, we use the semi-soft photon approximation and assume the charged final-state fermions to be massless, which is a good approximation for the process under consideration. In contrast to Sects. 4.2 and 4.3 we do not make any assumptions about the mass of the final-state neutrinos, because it does not simplify the calculation significantly. This gives us the opportunity to apply the results of this section to top-quark pair production. Following the approach of [3], we write the amplitudes corresponding to the diagrams shown in Fig. 4-1 in terms of virtual and real scalar four-/five-point functions. In contrast to the Feynman-parameter approach of Sect. 4.3, we do not introduce Feynman parameters, but perform instead a direct integration over momentum space [3]. The calculation can be considerably simplified by an appropriate choice of the frame.

First we calculate the infrared-finite virtual and real four-point functions. The calculation is close to the one presented in [3], but in contrast to [3] we make a clear separation between the virtual and real contributions. Our final result agrees with the one of [3], as well as with the one obtained in the MST in Sect. 4.3.2. Next we calculate the infrared-divergent virtual and real four-point functions. Again we perform a separation of the real and virtual contributions, and provide a careful treatment of the divergences. All this is needed in order to trace the cancellations of infrared and collinear divergences. We find complete agreement with our results obtained in Sect. 4.3.2. At the same time the structure of the divergences in our results appears to be significantly different from the one obtained by using the method of [3], even in the complete answer when virtual and real corrections are summed up. Although the infrared-divergent scalar four-point functions do not appear directly in the answer for the non-factorizable corrections, the observed difference with the method of [3] turns out to be indicative, because similar problems arise in the evaluation of the (infrared-divergent) five-point functions. Finally we calculate in the same way the virtual and real five-point functions. After summing up the virtual and real five-point functions, we find, in contrast to the result in [3], that all collinear divergences cancel exactly, even for cross-sections that are exclusive with respect to the virtualities of the W bosons.

In conclusion, the calculation presented in this section is an extension of the method of [3]. We provide a proper treatment of the infrared and collinear divergences, and make a clear separation of the virtual and real corrections. Because of this, the calculation becomes much more involved. We use the results obtained in this section as an independent check of the results of Sects. 4.2 and 4.3. Although the methods are completely different and the answer of this section is very complicated, a perfect numerical agreement between our two calculations is observed.

Before listing the various results, we first define the notation. For the calculations in the DMI method we need to specify the momenta in the centre-of-mass frame of

the initial state. Because of the semi-soft photon, double-pole approximation (DPA), which has been defined in Chapter 2, the four-momenta of the two intermediate W bosons are related in a simple way:

$$p_1^\mu = (E, \vec{p}) = E(1, \vec{v}) \quad \text{and} \quad p_2^\mu = (E, -\vec{p}) = E(1, -\vec{v}), \tag{4.4.1}$$

with $|\vec{v}| = \beta$ the (on-shell) velocity of the W bosons [see also Eq. (4.3.13)]. The other relevant momenta are

$$k_1^\mu = (E_1, \vec{k}_1) = E_1(1, \vec{v}_1) \quad \text{and} \quad k_2^\mu = (E_2, \vec{k}_2) = E_2(1, \vec{v}_2), \tag{4.4.2}$$

with $|\vec{v}_i| = \sqrt{1 - m_i^2/E_i^2}$ for ($i = 1, 2$). In addition we need the definition of some (polar) angles with respect to the direction of the W^+ boson: $\theta_i = \angle(\vec{v}, \vec{v}_i)$ and $x_i = \cos\theta_i$ (for $i = 1, 2$).[5] The difference of the azimuthal angles of $\vec{k}_1$ and $\vec{k}_2$ is given by ϕ_{12}. So, for $\phi_{12} = 0$ the final-state three-momenta $\vec{k}_i$ and $\vec{k}_i'$ lie in one plane. In the plane spanned by $\vec{k}_1$ and $\vec{k}_2$ we define $\theta_{12} = \angle(\vec{v}_1, \vec{v}_2)$ and $x_{12} = \cos\theta_{12}$.

4.4.1   Non-factorizable infrared-finite corrections

In this subsection we briefly describe the calculation of the infrared-finite four-point functions in the DMI scheme, following Ref. [3]. The result agrees with the one presented in [3], so this subsection is merely presented for completeness. The contribution of the infrared-finite virtual four-point function D_{0124} to the non-factorizable matrix element is given by

$$M_{0124} = \bar{M}_{\text{DPA}}^0 \frac{i}{D_1} \int \frac{d^4k}{(2\pi)^4} \frac{16\pi\alpha(p_1 \cdot k_2)}{[k^2 + io][2(k \cdot k_2) + io][D_1 - 2(p_1 \cdot k)][D_2 + 2(p_2 \cdot k)]}, \tag{4.4.3}$$

where $M_{\text{DPA}}^0 = \bar{M}_{\text{DPA}}^0/(D_1 D_2)$ is the Born matrix element of the process, involving the production of an intermediate W-boson pair and its subsequent decay. We start the calculation by decomposing the unstable W-boson propagators according to

$$\frac{1}{[D_1 - 2(p_1 \cdot k)][D_2 + 2(p_2 \cdot k)]} = \left[\frac{1}{D_1 - 2(p_1 \cdot k)} + \frac{1}{D_2 + 2(p_2 \cdot k)}\right]\frac{1}{D + 4\vec{p} \cdot \vec{k}}, \tag{4.4.4}$$

where $D = D_1 + D_2$. The first term has two particle poles: one in the lower and one in the upper half of the complex k_0-plane. We close the contour in the lower half-plane, resulting in one particle-pole and one photon-pole contribution. The second term has all its particle poles in the lower half-plane. By closing the integration contour in the upper half-plane, only one of the photon poles will contribute. Note that the

---

[5]Note that this definition of θ_2 is different from the definition of θ_4 in Chapter 2. In one case the W^- decay angle is defined with respect to the W^+-direction, and in the other with respect to the W^--direction. The definition of this chapter was adopted in order to keep in line with notations used in [3]. Once one keeps in mind this difference it should not lead to any confusion, as the transformation from one notation to the other is simply $\theta_4 = \pi - \theta_2$.

above decomposition mixes photon- and particle-pole contributions. In order to avoid possible confusion with the pure photon- and particle-pole contributions, we will write $M_{0124}^{'\gamma'}$ and $M_{0124}^{'\text{part}'}$ if the decomposition is used.

Particle-pole residue

We first concentrate on the particle-pole residue contributing to the first term in Eq. (4.4.4). This particle pole is situated at $k_0 = \vec{v}_2 \cdot \vec{k}$. The corresponding residue reads

$$M_{0124}^{'\text{part}'} = \bar{M}_{\text{DPA}}^0 \frac{4\pi\alpha}{D_1} \frac{1-\beta x_2}{2E} \int \frac{d^3k}{(2\pi)^3[(\vec{v}_2\cdot\vec{k})^2 - \vec{k}^2]} \frac{1}{[\frac{D}{2E} + 2\vec{v}\cdot\vec{k}][\frac{D_1}{2E} \qquad \vec{k}]}. \tag{4.4.5}$$

The propagators can be exponentiated by introducing an integration "time":

$$\bar{M}_{0124}^{'\text{part}'} = -\bar{M}_{\text{DPA}}^0 \frac{4\pi\alpha}{D_1} \frac{1-\beta x_2}{2E} \int_0^\infty d\tau \, d\tau_1 \, e^{i[\frac{D}{2E}\tau + \frac{D_1}{2E}\tau_1]} \int \frac{d^3k}{(2\pi)^3} \frac{e^{i\vec{k}\cdot\vec{r}}}{(\vec{v}_2\cdot\vec{k})^2 - \vec{k}^2}. \tag{4.4.6}$$

where

$$\vec{r} = 2\tau \, \vec{v} - \tau_1 \, (\vec{v}_2 - \vec{v}). \tag{4.4.7}$$

The integral is infrared-finite, so there is no need to introduce a non-zero photon mass as infrared regulator. The spatial integration can be recognized as a relativistic Coulomb potential of a moving particle:

$$\phi(r) = -4\pi \int \frac{d^3k}{(2\pi)^3} \frac{e^{i\vec{k}\cdot\vec{r}}}{(\vec{v}_2\cdot\vec{k})^2 - \vec{k}^2} = \frac{1}{\sqrt{r_\parallel^2 + r_\perp^2(1 - v_2^2)}}. \tag{4.4.8}$$

Here $r_\parallel$ and $r_\perp$ are the absolute values of the components of $\vec{r}$ parallel and perpendicular to $\vec{v}_2$:

$$r_\parallel = 2\beta x_2\tau - (1 - \beta x_2)\tau_1, \quad r_\perp = \beta(2\tau + \tau_1)\sin\theta_2. \tag{4.4.9}$$

Note that $1 - v_2^2 = m_2^2/E_2^2$ is small, but finite.

To do the remaining integrations over τ and τ_1, we can make a change of variables according to $(\tau, \tau_1) \to (\xi, y)$, with $\tau = \xi y$, $\tau_1 = \xi(1-y)$, and the Jacobian $|\frac{\partial(\tau, \tau_1)}{\partial(\xi, y)}| = \xi$. The area of integration changes from $\tau > 0$ and $\tau_1 > 0$ to $\xi > 0$ and $0 < y < 1$. After this change of variables, the quantities $r_\parallel$ and $r_\perp$ will be proportional to ξ, rendering the integration over ξ trivial. The last integral over y can be calculated in a straightforward way, yielding after some manipulations

$$\underline{x_2 < 0} \; : \; M_{0124}^{'\text{part}'} = \bar{M}_{\text{DPA}}^0 \, i\alpha \, \frac{1-\beta x_2}{D_1\eta(x_2)} \left[\ln\left(\frac{D}{D_1}\right) + \ln\left(\frac{1-\beta x_2}{-2\beta x_2}\right) \right], \tag{4.4.10}$$

$$\underline{x_2 > 0} \; : \; M_{0124}^{'\text{part}'} = \bar{M}_{\text{DPA}}^0 \, i\alpha \, \frac{1-\beta x_2}{D_1\eta(x_2)} \left[\ln\frac{\eta(x_2)}{D} + \ln\frac{\eta(x_2)}{D_1} + \ln\frac{2x_2(1-\beta x_2)}{\beta(1-x_2^2)} + \ln\frac{E_2^2}{m_2^2} \right], \tag{4.4.11}$$

where

$$\eta(x) = (1 + x\beta) D_1 + (1 - x\beta) D_2. \tag{4.4.12}$$

The result for $M_{0124}^{'part'}$ is not the same for $x_2 < 0$ and $x_2 > 0$. This is caused by the propagator decomposition (4.4.4). However, the complete result, with the photon-pole residue included, will be independent of the sign of x_2.

Photon-pole residues

Now we consider the photon-pole residues. There are two such contributions, one in each of the terms in the decomposition (4.4.4). We will indicate these two contributions by $M_{0124}^{\gamma,1}$ and $M_{0124}^{\gamma,2}$, respectively. For $M_{0124}^{\gamma,1}$ the contour is closed in the lower half of the complex k_0-plane. In that case the photon pole is situated at $k_0 = |\vec{k}| - io$, yielding

$$M_{0124}^{\gamma,1} = \bar{M}_{DPA}^0 \frac{\alpha}{2\pi} \frac{1 - \beta x_2}{D_1} \int \frac{d^2\Omega_k}{2\pi} \frac{1}{\eta(x)(1 - \vec{v}_2 \cdot \vec{n}_k)} \left[\ln\left(\frac{2\beta x + io}{1 - \beta x}\right) - \ln(D) + \ln(-D_1) \right]. \tag{4.4.13}$$

Here $\vec{n}_k$ stands for the unit vector in the $\vec{k}$ direction and Ω_k indicates the angular variables in spherical coordinates (with the polar axis defined along $\vec{p}$). For $M_{0124}^{\gamma,2}$ the contour is closed in the upper half of the complex k_0-plane. The corresponding residue can be obtained from Eq. (4.4.13) by adding an overall minus sign and by substituting $\beta \to -\beta$ and $D_1 \leftrightarrow D_2$ inside the square brackets:

$$M_{0124}^{\gamma,2} = -\bar{M}_{DPA}^0 \frac{\alpha}{2\pi} \frac{1 - \beta x_2}{D_1} \int \frac{d^2\Omega_k}{2\pi} \frac{1}{\eta(x)(1 - \vec{v}_2 \cdot \vec{n}_k)} \left[\ln\frac{-2\beta x + io}{1 + \beta x} - \ln(D) + \ln(-D_2) \right] \tag{4.4.14}$$

Next one can perform the integration over the azimuthal angle, with the help of the formula

$$\int_0^{2\pi} \frac{d\phi}{2\pi} \frac{1}{1 - \vec{v}_i \cdot \vec{n}_k} = \frac{1}{|x - x_i|}. \tag{4.4.15}$$

This expression is a possible source of collinear divergences, which are regularized by introducing the small non-zero fermion masses. In terms of this regularization, $|x - x_i|$ is replaced by $\sqrt{(x - x_i)^2 + m_i^2(1 - x_i^2)/E_i^2}$. The sum of the two photon-pole residues amounts to

$$M_{0124}^{\gamma} = \bar{M}_{DPA}^0 \frac{\alpha}{2\pi} \frac{1 - \beta x_2}{D_1} \int_{-1}^{1} \frac{dx}{\eta(x)|x - x_2|} \left\{ \ln\left(\frac{1 + \beta x}{1 - \beta x}\right) + \ln\left(\frac{D_1}{D_2}\right) + i\pi[\theta(-x) - \theta(x)] \right\}. \tag{4.4.16}$$

The last integration gives rise to integrals of logarithmic and dilogarithmic type. Let us single out the answer for the θ-function-dependent terms:

$$M_{0124}^{\gamma,\theta} = \bar{M}_{DPA}^0 \frac{\alpha}{2\pi} \frac{1 - \beta x_2}{D_1 \eta(x_2)} i\pi \left\{ C_1[\theta(-x_2) - \theta(x_2)] + 2C_2\,\theta(x_2) + 2C_3\,\theta(-x_2) \right\}, \tag{4.4.17}$$

where

$$C_1 = \ln\left(\frac{\eta(x_2)}{\eta(1)}\right) + \ln\left(\frac{\eta(x_2)}{\eta(-1)}\right) + \ln\left(\frac{4E_2^2}{m_2^2}\right), \quad C_2 = \ln\left(\frac{D}{\eta(-1)}\right) + \ln\left(\frac{1+x_2}{x_2}\right),$$

$$C_3 = \ln\left(\frac{\eta(1)}{D}\right) + \ln\left(\frac{x_2}{x_2-1}\right). \tag{4.4.18}$$

Separately, the particle-pole residue and the photon-pole residues depe⋯ on ⋯ sign of x_2. However, the sum of these terms does not. This dependence ⋯ ⋯ the intermediate stage of the calculation is a consequence of the decom⋯ ⋯ the unstable W-boson propagators.

The final answer for the contribution of the infrared-finite virtual ⋯ unction D_{0124} to the non-factorizable matrix element is given by

$$
\begin{aligned}
M_{0124} &= \bar{M}_{\rm DPA}^0 \frac{\alpha}{2\pi} \frac{1-\beta x_2}{D_1 \eta(x_2)} \left\{ \left[F_2(x_2|x_2) - F_2(-D_0|x_2) \right] \ln\left(\frac{D_1}{D_2}\right) \right. \\
&\quad - F_1\left(-D_0; \beta|x_2\right) + F_1\left(-D_0; -\beta|x_2\right) + F_1\left(x_2; \beta|x_2\right) - F_1\left(x_2; -\beta|x_2\right) \\
&\quad \left. + i\pi \left[2\ln\frac{\eta(x_2)}{D_1} + \ln\frac{\eta(1)}{\eta(-1)} + 2\ln\frac{1-\beta x_2}{\beta(1-x_2)} + \ln\frac{E_2^2}{m_2^2} \right] \right\},
\end{aligned}
\tag{4.4.19}
$$

where

$$D_0 = \frac{1}{\beta}\frac{D_1 + D_2}{D_1 - D_2}. \tag{4.4.20}$$

The logarithmic and dilogarithmic functions $F_{1,2}$ can be found in App. C.1. The final answer for M_{0124} agrees with the answer presented in [3]. It is also in complete numerical and analytical agreement with the corresponding expression in Sect. 4.3, which was calculated with the help of the MST.

The contribution from the other infrared-finite virtual four-point function, D_{0123}, can be obtained from Eq. (4.4.19) by substituting $(p_1, k_1) \leftrightarrow (p_2, k_2)$.

The pure photon-pole part

As was already explained in Sect. 4.2.4, the photon-pole parts of the virtual scalar functions can be related to the corresponding bremsstrahlung interferences. To this end, one needs to calculate the pure photon-pole contribution to the matrix element, without performing the decomposition of the unstable W-boson propagators, since this decomposition mixes photon- and particle-pole contributions.

This calculation is pretty much the same as the one discussed above. We present only the answer:

$$M_{0124}^\gamma = \bar{M}_{\rm DPA}^0 \frac{\alpha}{2\pi} \frac{1-\beta x_2}{D_1 \eta(x_2)} \left\{ \left[\ln\left(\frac{D_1}{D_2}\right) + i\pi \right] \left[F_2(x_2|x_2) - F_2(-D_0|x_2) \right] - \right.$$

$$-F_1\left(-D_0;\beta|x_2\right) + F_1\left(-D_0;-\beta|x_2\right) + F_1\left(x_2;\beta|x_2\right) - F_1\left(x_2;-\beta|x_2\right)\Big]. \quad (4.4.21)$$

Note that the photon pole has been evaluated in the upper half of the complex k_0-plane. The reason for this lies in the fact that we have opted to perform the calculations in the most economic way. In this approach D_{0124}^{τ} is obtained from D_{0123}^{τ} by substituting $(p_1, k_1) \leftrightarrow (p_2, k_2)$, which automatically shifts the photon-pole from the lower to the upper half-plane (see Sect. 4.2.4).

4.4.2   The infrared-divergent scalar four-point function

In this subsection we present the calculation of the infrared-divergent virtual scalar four-point function D_{0134}. In the DMI method such functions are not needed for the calculation of the non-factorizable corrections. They arise in the form of initial–final state interference. Such corrections vanish when the corresponding bremsstrahlung interferences are taken into account, as was explained in Sect. 4.2.4. We perform the calculation mainly to study how one can handle infrared and collinear divergences in the DMI scheme and to provide an independent check of the results obtained in Sect. 4.3.

The infrared-divergent virtual scalar four-point function D_{0134} is defined as

$$D_{0134} = \int \frac{d^4k}{(2\pi)^4} \frac{1}{[k^2 - \lambda^2 + io][D_1 - 2(p_1 \cdot k)][-2(k_1 \cdot k) + io][2(k_2 \cdot k) + io]}.$$
$$(4.4.22)$$

We regularize the infrared divergences by introducing a regulator mass λ for the photon. There are also collinear divergences, which are regularized by the small non-zero fermion masses.

The pole structure of this integral is such that no propagator decomposition is required. There is one photon pole in each of the half-planes of the complex variable k_0. There are two particle poles in the upper half-plane, and only one in the lower half-plane. Therefore, we opt to close the integration contour in the lower half-plane, resulting in only two contributions to the scalar function: one photon-pole residue and one particle-pole residue.

Particle-pole contribution

One can proceed in the same way as in Sect. 4.4.1. We take the residue at the particle pole $k_0 = \vec{v}_2 \cdot \vec{k}$ and exponentiate the propagators by introducing an integration over "time":

$$D_{0134}^{\text{part}} = \frac{i}{8EE_1E_2} \int\limits_0^\infty d\tau\, dt\, e^{i\tau\frac{D_1}{2E}} \int \frac{d^3k}{(2\pi)^3} \frac{e^{i\vec{r}\cdot\vec{k}}}{(\vec{k}\cdot\vec{v}_2)^2 - \vec{k}^2 - \lambda^2}, \quad (4.4.23)$$

where $\vec{r} = \tau\,(\vec{v} - \vec{v}_2) + t\,(\vec{v}_1 - \vec{v}_2)$. Again we can perform the integration over the momentum $\vec{k}$, which is similar to the λ-screened relativistic Coulomb potential of

a moving particle. As the scalar function is infrared-divergent, one should keep the photon mass λ. The result of the integration is

$$\phi_\lambda(r) = -4\pi \int \frac{d^3k}{(2\pi)^3} \frac{e^{i\vec{r}\cdot\vec{k}}}{(\vec{k}\cdot\vec{v}_2)^2 - \vec{k}^2 - \lambda^2} = \frac{e^{-\frac{\lambda}{\sqrt{1-v_2^2}}\sqrt{r_\parallel^2 + r_\perp^2(1-v_2^2)}}}{\sqrt{r_\parallel^2 + r_\perp^2(1-v_2^2)}}. \tag{4.4.24}$$

Here both λ and $1 - v_i^2$ are small. We will consider the limit $\lambda \to 0$ and $v \to 1$, such that $\lambda \ll \sqrt{1 - v_i^2}$.

The particle-pole contribution now takes the form

$$D_{0134}^{\text{part}} = -\frac{i}{32\pi E E_1 E_2} \int\limits_0^\infty d\tau \, dt \, e^{i\tau \frac{D_1}{2E}} \frac{e^{-\frac{\lambda}{\sqrt{1-v_2^2}}\sqrt{r_\parallel^2 + r_\perp^2(1-v_2^2)}}}{\sqrt{r_\parallel^2 + r_\perp^2(1-v_2^2)}}, \tag{4.4.25}$$

where $r_\parallel^2 + r_\perp^2(1 - v_2^2) = a + bt + ct^2$, with coefficients

$$\begin{aligned}
a &= \tau^2(1 - \beta x_2)^2 + \frac{m_2^2}{E_2^2}\tau^2\beta^2\sin^2\theta_2, \\
b &= 2\tau(1 - x_{12})(1 - \beta x_2) + 2\frac{m_2^2}{E_2^2}\tau\beta\sin\theta_2\sin\theta_{12}, \\
c &= (1 - x_{12})^2 + \frac{m_2^2}{E_2^2}\sin^2\theta_{12}.
\end{aligned} \tag{4.4.26}$$

The integral over t is logarithmically divergent in λ:

$$I_\lambda = \int\limits_0^\infty dt \frac{e^{-\frac{\lambda}{\sqrt{1-v_2^2}}\sqrt{a+bt+ct^2}}}{\sqrt{a + bt + ct^2}} \approx \frac{1}{\sqrt{c}}\left[-C + \ln\left(\frac{4\sqrt{c}\,m_2}{\lambda E_2(b + 2\sqrt{ac})}\right)\right], \tag{4.4.27}$$

where C is the Euler constant.

The last integration over τ is relatively simple, yielding

$$D_{0134}^{\text{part}} = \frac{1}{8\pi s_{12}}\frac{1}{D_1}\left[\ln\left(\frac{D_1}{iM_W^2}\right) - \ln\left(\frac{s_{211'}}{M_W^2} - 1\right) - \ln\left(\frac{\lambda}{m_2}\right)\right]. \tag{4.4.28}$$

The invariants s_{12} and $s_{211'}$ are defined in Eq. (4.3.12).

Photon-pole contribution

Next the photon-pole residue at $k_0 = \omega = \sqrt{\vec{k}^2 + \lambda^2} - io$ is determined:

$$D_{0134}^\gamma = -\frac{i}{16 E E_1 E_2}\int \frac{d^3k}{(2\pi)^3\omega} \frac{1}{(1 - \beta x)[\omega - \frac{D_1}{2E(1-\beta x)}][\omega - |\vec{k}|(\vec{n}_k\cdot\vec{v}_1)][\omega - |\vec{k}|(\vec{n}_k\cdot\vec{v}_2)]}. \tag{4.4.29}$$

We want to keep the propagators $[\omega - |\vec{k}|\,(\vec{n}_k\cdot\vec{v}_i)]$ as they are, instead of writing them as $|\vec{k}|\,[1 - \vec{n}_k\cdot\vec{v}_i]$, as was done in Ref. [3]. Keeping the exact form of the propagators leads to double-logarithmic collinear divergences. If, instead, the simplified version were to be used, then the double-logarithmic terms would be lost, and one cannot be sure whether the single-logarithmic divergence and the finite part would be correct.

First we perform the integration over $|\vec{k}|$. The presence of λ in the light-fermion propagators complicates things considerably. The light-fermion propagators can be rewritten in the following way:

$$\frac{1}{|\vec{k}|\,(\vec{n}_k\cdot\vec{v}_1)][\omega - |\vec{k}|\,(\vec{n}_k\cdot\vec{v}_2)]} =$$
$$\frac{1}{|\vec{k}|\,(\vec{n}_k\cdot\vec{v}_1 - \vec{n}_k\cdot\vec{v}_2)}\left[\frac{1}{\omega - |\vec{k}|\,(\vec{n}_k\cdot\vec{v}_1)} - \frac{1}{\omega - |\vec{k}|\,(\vec{n}_k\cdot\vec{v}_2)}\right]. \quad (4.4.30)$$

After the integration over $|\vec{k}|$ the photon-pole contribution will be of the form

$$D_{0134}^7 = \frac{i}{16\pi^2 E_1 E_2 D_1}\,[I_0 + I_1 + I_2], \quad (4.4.31)$$

where

$$I_0 = \int \frac{d^2\Omega_k}{4\pi}\,\frac{1}{[1 - \vec{n}_k\cdot\vec{v}_1][1 - \vec{n}_k\cdot\vec{v}_2]}\,\ln\left(\frac{-D_1}{E\lambda(1 - \beta x)}\right),$$

$$I_1 = \mathcal{P}\left\{\int \frac{d^2\Omega_k}{4\pi}\,\frac{1}{[\vec{n}_k\cdot\vec{v}_1 - \vec{n}_k\cdot\vec{v}_2][1 - (\vec{n}_k\cdot\vec{v}_1)^2]}\,\ln\left(\frac{1 - \vec{n}_k\cdot\vec{v}_1}{2}\right)\right\}. \quad (4.4.32)$$

The expression for I_2 can be obtained from I_1 by the substitution $\vec{v}_1 \leftrightarrow \vec{v}_2$. The integral I_0 is similar to the one that shows up in the approach of [3]. It contains only single-logarithmic collinear divergences. The integrals $I_{1,2}$ are new and give rise to double-logarithmic terms. They are evaluated as a principal-value integral, since the singularity present in $1/[\vec{n}_k\cdot\vec{v}_1 - \vec{n}_k\cdot\vec{v}_2]$ is an artefact of the split-up (4.4.30) and disappears in the sum $I_1 + I_2$.

As a next step we integrate over the azimuthal angle ϕ. We obtain for the first integral

$$I_0 = \frac{1}{2(1 - x_{12}^2)}\int_{-1}^{+1}\frac{dx}{(x - x_a)(x - x_b)}\left[\frac{J_1 - xK_1}{|x - x_1|} + \frac{J_2 - xK_2}{|x - x_2|}\right]\ln\left(\frac{-D_1}{E\lambda(1 - \beta x)}\right), \quad (4.4.33)$$

with

$$x_{a,b} = \frac{x_1 + x_2 \pm i\sin\theta_1\sin\theta_2\sin\phi_{12}}{1 + x_{12}},$$

$$J_1 = 1 - x_{12} - x_1(x_1 - x_2), \quad K_1 = x_2 - x_1 x_{12},$$

$$J_2 = 1 - x_{12} - x_2(x_2 - x_1), \quad K_2 = x_1 - x_2 x_{12}. \quad (4.4.34)$$

As indicated in Sect. 4.4.1, $|x - x_i|$ should be regularized by keeping the small non-zero fermion masses: $|x - x_i| \rightarrow \sqrt{(x - x_i)^2 + \mu_i^2}$, with $\mu_i^2 = m_i^2(1 - x_i^2)/E_i^2$. Using the result for the principal-value integral given in App. C.2, we find for the second integral

$$I_1 = \frac{1}{4|\vec{v}_1 - \vec{v}_2|} \int_{x_+}^{1} \frac{dx}{\sqrt{x^2 - x_+^2}} \left[\frac{1}{1 - v_1 x} + \frac{1}{1 + v_1 x} \right] \ln\left(\frac{1 - v_1 x}{1 + v_1 x} \right), \qquad (4.4.35)$$

where $x_{\pm} = \sqrt{(1 \pm x_{12})/2}$.

One is left with a one-dimensional integration over x. The integral can be expressed in terms of the dilogarithmic functions $\mathcal{F}_1$ and $\mathcal{F}_2$, defined in App. C.3:

$$I_{1,2} = \frac{1}{8x_-} [\mathcal{F}_1(x_+; v_{1,2}) + \mathcal{F}_2(x_+)]. \qquad (4.4.36)$$

The answer for the integral I_0 is

$$
\begin{aligned}
I_0 = {} & \frac{1}{1 - x_{12}} \ln\left(\frac{E\lambda\beta}{-D_1} \right) \ln\left(\frac{m_1 m_2}{s_{12}} \right) - \sum_{i=1}^{2} \frac{x_i - x_a}{4(1 - x_{12})} \mathcal{K}(-x_a; \frac{1}{\beta}|x_i; \mu_i^2) \\
& - \sum_{i=1}^{2} \frac{x_i - x_b}{4(1 - x_{12})} \mathcal{K}(-x_b; \frac{1}{\beta}|x_i; \mu_i^2),
\end{aligned}
\qquad (4.4.37)
$$

where the function $\mathcal{K}$ is introduced in App. C.3.

The complete expression for the infrared-divergent scalar four-point function is obtained as the sum of the particle-pole and photon-pole contributions. When comparing all the above results with the ones obtained in Sect. 4.3.2, complete numerical agreement is found for both virtual and real four-point functions, including collinear and infrared divergences.

4.4.3   Non-factorizable corrections from the five-point functions

In this subsection we describe the calculation of the scalar five-point functions using the DMI method. The contribution of the virtual five-point function to the non-factorizable matrix element is given by

$$M = i\bar{M}_{\text{DPA}}^0 \times$$
$$\qquad (4.4.38)$$
$$\int \frac{d^4k}{(2\pi)^4} \frac{16\pi\alpha(k_1 \cdot k_2)}{[k^2 - \lambda^2 + io][-2(k \cdot k_1) + io][2(k \cdot k_2) + io][D_1 - 2(k \cdot p_1)][D_2 + 2(k \cdot p_2)]}.$$

In analogy to Sect. 4.4.1, one can perform a decomposition of the unstable W-boson propagators

$$\frac{1}{[D_1 - 2(p_1 \cdot k)][D_2 + 2(p_2 \cdot k)]} = \left[\frac{1}{D_1 - 2(p_1 \cdot k)} + \frac{1}{D_2 + 2(p_2 \cdot k)} \right] \frac{1}{D + 4\vec{p} \cdot \vec{k}}.$$
$$\qquad (4.4.39)$$

In this way the matrix element splits into two terms. If the integration contour in the complex k_0-plane is chosen properly, each term involves one photon-pole contribution and one particle-pole contribution.

Particle-pole residues

We first calculate the particle-pole residue that contributes to the first term in Eq. (4.4.3). We proceed in the usual way, by taking the residue at $k_0 = \vec{v}_2 \cdot \vec{k}$ and subsequently integrating the propagators. In this case this procedure requires three integrations

$$M_2^{\text{part}'} = \frac{\alpha}{2} \frac{1 - x_{12}}{E^2} \int\limits_0^\infty dt \, d\tau \, d\tau_1 \, e^{i\left[\frac{D}{4E}\tau + \frac{D_1}{2E}\tau_1\right]} \int \frac{d^3k}{(2\pi)^3} \frac{e^{i\vec{r}_2 \cdot \vec{k}}}{(\vec{k} \cdot \vec{v}_2)^2 - \vec{k}^2 - \lambda^2},$$
(4.4.40)

where $\vec{r}_2 = \tau \vec{v} + \tau_1 (\vec{v} - \vec{v}_2) + t(\vec{v}_1 - \vec{v}_2)$. The integral over d^3k is the same as the one evaluated for the calculation of the infrared-divergent four-point function [see Eq. (4.4.24)]. Again, a non-zero photon mass λ is needed for the regularization of the infrared divergences. The particle-pole residue now amounts to

$$M_2^{\text{part}'} = -\bar{M}_{\text{DPA}}^0 \frac{i\alpha}{8} \frac{1 - x_{12}}{E^2} \int\limits_0^\infty dt \, d\tau \, d\tau_1 \, e^{i\left[\frac{D}{4E}\tau + \frac{D_1}{2E}\tau_1\right]} \frac{e^{-\frac{\lambda}{\sqrt{1-v_2^2}}\sqrt{r_\parallel^2 + r_\perp^2(1-v_2^2)}}}{\sqrt{r_\parallel^2 + r_\perp^2(1-v_2^2)}}, \quad (4.4.41)$$

where $r_\parallel^2 + r_\perp^2(1 - v_2^2) = a + bt + ct^2$, with coefficients

$$a = [\tau\beta x_2 - \tau_1(1 - \beta x_2)]^2 + \frac{m_2^2}{E_2^2}(\tau + \tau_1)^2 \beta^2 \sin^2\theta_2,$$

$$b = -2(1 - x_{12})[\tau\beta x_2 - \tau_1(1 - \beta x_2)] + 2\frac{m_2^2}{E_2^2}\beta(\tau + \tau_1)\sin\theta_{12}\sin\theta_2,$$

$$c = (1 - x_{12})^2 + \frac{m_2^2}{E_2^2}\sin^2\theta_{12}. \quad (4.4.42)$$

Following Sect. 4.4.2, first the integration over t is performed, yielding the logarithmically-divergent result

$$M_2^{\text{part}'} = -\bar{M}_{\text{DPA}}^0 \frac{i\alpha}{8E^2} \int\limits_0^\infty d\tau \, d\tau_1 \, e^{i\left[\frac{D}{4E}\tau + \frac{D_1}{2E}\tau_1\right]} \left[-C + \ln\left(\frac{4\sqrt{c}\, m_2}{\lambda E_2 (b + 2\sqrt{ac})}\right)\right], \quad (4.4.43)$$

To linearize $b + 2\sqrt{ac}$ with respect to one of the integration variables, one should make a change of variables according to $(\tau, \tau_1) \rightarrow (\xi, y)$, with $\tau = \xi y$, $\tau_1 = \xi(1 - y)$. In this way, the integration over ξ can be trivially performed:

$$M_2^{'\text{part}'} = \bar{M}_{\text{DPA}}^0 \frac{i\alpha}{8E^2} \int\limits_0^1 \frac{dy}{\left[\frac{D}{4E}y + \frac{D_1}{2E}(1 - y)\right]^2} \left\{-1 + \right.$$

$$\left. + \ln\left(\frac{4m_2(1 - x_{12})}{\lambda E_2 (b' + 2\sqrt{a'c'})}\right) + \ln\left(\frac{Dy + 2D_1(1 - y)}{4iE}\right)\right\}, \quad (4.4.44)$$

where the coefficients a', b', and c' follow from the coefficients a, b, and c, by substituting $\tau \to y$ and $\tau_1 \to (1-y)$.

The last integration is technically quite involved, but only gives rise to logarithms. Note that one should carefully analyse the infrared and collinear divergences, present in this integral. The final answer is formally different for $x_2 < 0$ and $x_2 > 0$. This is the same phenomenon as observed in Sect. 4.4.1, which can be attributed to the decomposition of the W-boson propagators. The result for the photon-pole residue will compensate this dual behaviour, leading to a combined result that is analytically the same for both $x_2 < 0$ and $x_2 > 0$. In a similar way the second pole residue, corresponding to the second term in Eq. (4.4.39), will formally depend on the sign of x_1.

We will not bore the reader with all the different cases and merely present the answer for the case $x_1 > 0$, $x_2 < 0$. Taking into account both particle-pole residues, the final answer reads

$x_1 > 0$, $x_2 < 0$:

$$
\begin{aligned}
M'^{\text{part}} = & -\bar{M}^0_{\text{DPA}} \frac{i\alpha}{2} \left\{ \frac{2}{D_1 D} \ln \frac{2\lambda E}{M_W^2} + \frac{2}{D_1 D} \ln \frac{E_2}{m_2} + \frac{2}{D_2 D} \ln \frac{D}{iM_W^2} - \frac{2}{D_1 D_2} \ln \frac{D_1}{iM_W^2} \right. \\
& \left. + \frac{2(1-\beta x_2)}{D_1 \eta(x_2)} \ln(1-\beta x_2) - \frac{2(1+\beta x_2)}{D_2 \eta(x_2)} \ln\left(\frac{D}{D_1}\right) + \frac{4\beta x_2}{D\eta(x_2)} \ln(-2\beta x_2) \right\} \\
& - \bar{M}^0_{\text{DPA}} \frac{i\alpha}{2} \left\{ x_2 \to x_1,\ m_2 \to m_1,\ E_2 \to E_1,\ D_1 \leftrightarrow D_2,\ \beta \to -\beta \right\}.
\end{aligned}
$$

$$(4.4.45)$$

Note that the terms $\ln(\frac{E_2}{m_2})$ and $\ln(\frac{E_1}{m_1})$ cause the difference with the results presented in Ref. [3].

Photon-pole residues

Next we determine the photon-pole residues. Each of the terms in the propagator decomposition (4.4.39) gives rise to one photon-pole residue, situated at $k_0 = \omega = \pm\sqrt{\vec{k}^2 + \lambda^2} - io$. In the same way as in Sect. 4.4.2, the light-fermion propagators occurring in the photon-pole residues can be rewritten according to Eq. (4.4.30). Again we introduce spherical coordinates, with the polar axis defined along $\vec{p}$. For the integration over $|\vec{k}|$ we keep the λ dependence of ω in order to get the correct divergences. The combined result of all photon-pole residues is given by

$$
M'^{\gamma'} = -\bar{M}^0_{\text{DPA}} \frac{\alpha}{\pi} (1-x_{12}) \int \frac{d^2\Omega_k}{4\pi} \left\{ \frac{\Psi(D_1, D_2, x)}{(1-\alpha_1)(1-\alpha_2)} + \frac{1}{D_1 D_2} \left[\Phi(\alpha_1, \alpha_2) + \Phi(\alpha_2, \alpha_1) \right] \right\},
$$

$$(4.4.46)$$

with

$$
\Psi(D_1, D_2, x) = \Psi_0 + \Psi_{12} + \Psi_\theta,
$$

$$\Psi_0 = -\frac{1}{D_1 D_2}\left[\ln\left(\frac{\lambda E}{M_W^2}\right) + i\pi\right],$$

$$\Psi_{12} = \frac{1-\beta x}{D_1 \eta(x)}\ln\left(\frac{D_1}{M_W^2\,(1-\beta x)}\right) + \frac{1+\beta x}{D_2 \eta(x)}\ln\left(\frac{D_2}{M_W^2\,(1+\beta x)}\right),$$

$$\Psi_\theta = \frac{2\beta x}{D \eta(x)}\, i\pi\,[\theta(\beta x) - \theta(-\beta x)],$$

$$\Phi = \frac{1}{(\alpha_1 - \alpha_2)(1 - \alpha_1^2)}\ln\left(\frac{1-\alpha_1}{2}\right), \tag{4.4.47}$$

and $\alpha_i = \quad (i = 1, 2)$.

The term in Eq. (4.4.46) also emerges in the calculations presented in [3], up to the divergent term (λE). This Ψ-term contains infrared divergences and logarithmic collinear divergences. The other two terms in Eq. (4.4.46) are of a type that was already encountered in Sect. 4.4.2. They will give rise to double-logarithmic collinear divergences.

As in Sect. 4.4.2, we proceed by performing the azimuthal integration. The remaining integration over $x = \cos\theta$ gives logarithms and dilogarithms. Most of the ingredients of this final step in the calculation have already been discussed above. Therefore we only give the answer. First we do so for the Ψ_θ-terms. As was observed for the particle-pole residues, the results depend on the sign of $x_{1,2}$. Adopting the same sign choice as in Eq. (4.4.45), we obtain

$x_1 > 0, x_2 < 0$:

$$\begin{aligned}
M_\theta^{\gamma'} &= \bar{M}_{\text{DPA}}^0 \frac{\alpha}{2\pi} i\pi \frac{1}{D}\left\{ \mathcal{R}_{\eta,2}\left[\ln\frac{\eta(-1)}{\eta(1)} - 2\ln\frac{\eta(x_2)}{D}\right] + \mathcal{R}_2\left[\ln\frac{4E_2^2}{m_2^2} + 2\ln\frac{-x_2}{1-x_2}\right] \right. \\
&\quad \left. + \sum_{j=a,b}\mathcal{R}_j\left[\ln\left(\frac{-1-x_j}{1-x_j}\right) - 2\ln\left(\frac{x_2-x_j}{-x_j}\right)\right]\right\} \\
&\quad + \bar{M}_{\text{DPA}}^0 \frac{\alpha}{2\pi} i\pi \frac{1}{D}\left\{ \mathcal{R}_{\eta,1}\left[\ln\frac{\eta(-1)}{\eta(1)} + 2\ln\frac{\eta(x_1)}{D}\right] - \mathcal{R}_1\left[\ln\frac{4E_1^2}{m_1^2} + 2\ln\frac{x_1}{1+x_1}\right] \right. \\
&\quad \left. + \sum_{j=a,b}\mathcal{R}_j\left[\ln\left(\frac{-1-x_j}{1-x_j}\right) + 2\ln\left(\frac{x_1-x_j}{-x_j}\right)\right]\right\}. \tag{4.4.48}
\end{aligned}$$

The coefficients $\mathcal{R}$ are given by ($i = 1, 2$)

$$\mathcal{R}_{\eta,i} = 2\beta D\,\frac{K_i D + \beta J_i (D_1 - D_2)}{(1 + x_{12})\,\eta(x_a)\,\eta(x_b)\,\eta(x_i)}, \quad \mathcal{R}_i = \frac{2\beta x_i}{\eta(x_i)} \quad \text{and} \quad \mathcal{R}_{a,b} = -\frac{\beta x_{a,b}}{\eta(x_{a,b})}. \tag{4.4.49}$$

As in Sect. 4.4.1, only the sum of the particle-pole residues and $M_\theta^{\gamma'}$ is independent of the sign of $x_{1,2}$.

The evaluation of the remaining terms in Eq. (4.4.46) is straightforward. The answers for the Ψ_0- and Φ-terms are given by

$$M_0^{\gamma'} = -\bar{M}_{\text{DPA}}^0 \frac{\alpha}{\pi}\frac{1}{D_1 D_2}\ln\left(\frac{m_1 m_2}{s_{12}}\right)\left[\ln\left(\frac{\lambda E}{M_W^2}\right) + i\pi\right], \tag{4.4.50}$$

$$M_\phi^{'\gamma'} = -\bar{M}_{\text{DPA}}^0 \frac{\alpha}{2\pi} \frac{1 - x_{12}}{D_1 D_2} \frac{1}{4x_-} \left[\mathcal{F}_1(x_+; v_2) + \mathcal{F}_1(x_+; v_1) + 2\, \mathcal{F}_2(x_+) \right]. \quad (4.4.51)$$

The functions $\mathcal{F}_1$ and $\mathcal{F}_2$ can be found in App. C.3.

Finally, the answer for the Ψ_{12}-term reads

$$M_{12}^{'\gamma'} = M_1^{'\gamma'} + M_2^{'\gamma'}, \quad (4.4.52)$$

with

$$\begin{aligned}
M_2^{'\gamma'} = \; & -\bar{M}_{\text{DPA}}^0 \frac{\alpha}{2\pi} \left\{ \frac{1 - \beta x_2}{D_1 \eta(x_2)} \left[\ln\!\left(\frac{4E_2^2}{m_2^2}\right) \ln\!\left(\frac{D_1}{M_W^2}\right) - F_1(x_2; -\beta) \right. \right. \\
& \left. - \sum_{i=a,b} \frac{1 - \beta x_i}{2 D_1 \eta(x_i)} \left[\ln\!\left(\frac{D_1}{M_W^2}\right) F_2(x_i | x_2) - F_1(\cdots) \right] \right. \\
& \left. - \frac{R_{\eta,2}}{D} \left[\ln\!\left(\frac{D_1}{M_W^2}\right) F_2(-D_0 | x_2) - F_1(-D_0; \cdots) \right] \right\} \\
& -\bar{M}_{\text{DPA}}^0 \frac{\alpha}{2\pi} \left\{ D_1 \leftrightarrow D_2, \; \beta \to -\beta \right\}. \quad (4.4.53)
\end{aligned}$$

Here D_0 is defined in Eq. (4.4.20) and the functions F_1 and F_2 are given in App. C.1. Note that the coefficient $R_{\eta,2}$ depends on β. The contribution $M_1^{'\gamma'}$ can be obtained by substituting $(E_2, m_2, x_2) \leftrightarrow (E_1, m_1, x_1)$ in Eq. (4.4.53).

The final answer for the contribution of the virtual five-point function to the non-factorizable matrix element can be obtained as

$$M = M^{'\text{part}'} + M_\theta^{'\gamma'} + M_0^{'\gamma'} + M_{12}^{'\gamma'} + M_\phi^{'\gamma'}, \quad (4.4.54)$$

with the various contributions given by Eqs. (4.4.45) and (4.4.48)–(4.4.53). This answer was compared numerically with the corresponding MST-expression in Sect. 4.2, which was derived by means of a decomposition of the five-point function into a sum of four-point functions. A complete numerical agreement was observed.

Pure photon-pole part

In order to calculate the real-photon radiative interference corresponding to the five-point function, one has to determine the photon-pole residue in the lower half-plane, without performing the propagator decomposition. The calculation is more or less the same as the one discussed above.

The answer can be written as

$$M^\gamma = M_0^\gamma + M_1^\gamma + M_2^\gamma + M_\phi^{'\gamma'}. \quad (4.4.55)$$

Note that the $M_\phi^{'\gamma'}$ contribution is the same as before [see Eq. (4.4.51)]. The other contributions are changed slightly:

$$M_0^\gamma = -\bar{M}_{\text{DPA}}^0 \frac{\alpha}{\pi} \frac{1}{D_1 D_2} \ln\!\left(\frac{m_1 m_2}{s_{12}}\right) \ln\!\left(\frac{\lambda E}{M_W^2}\right), \quad (4.4.56)$$

and

$$M_2^\gamma = M_2'^\gamma + M_{DPA}^0 \frac{\alpha}{2\pi} i\pi \left\{ \frac{1-\beta x_2}{D_1 \eta(x_2)} \ln\left(\frac{4E_2^2}{m_2^2}\right) - \sum_{i=a,b} \frac{1-\beta x_i}{2D_1 \eta(x_i)} F_2(x_i|x_2) \right.$$

$$\left. - \frac{R_{\eta,2}}{D} F_2(-D_0|x_2) \right\}. \tag{4.4.57}$$

The cont   can be obtained by substituting $(E_2, m_2, x_2) \leftrightarrow (E_1, m_1, x_1)$.

4.5   Complete results

Up to now we have focused on the case of purely leptonic final states. For the purely hadronic ones there are many more diagrams, as the photon can interact with all four final-state fermions. In order to make efficient use of the results presented in the previous sections, we first introduce some short-hand notations based on the results for the purely leptonic (LL) final states. These short-hand notations involve the summation of virtual and real corrections to the differential cross-section. For instance, the virtual corrections originating from the first diagram of Fig. 4-1 can be combined with the corresponding real-photon correction into the contribution $d\sigma_{LL}^{(4)}(k_1; k_1'|p_2)$. In a similar way, virtual and real five-point corrections can be combined into $d\sigma_{LL}^{(5)}(k_1; k_1'|k_2; k_2')$. The gauge-restoring "Coulomb" contribution will be indicated by $d\sigma^C(p_1|p_2)$. In terms of this notation the non-factorizable differential cross-section for purely leptonic final states becomes

$$d\sigma_{LL}(k_1; k_1'|k_2; k_2') = d\sigma_{LL}^{(4)}(k_1; k_1'|p_2) + d\sigma_{LL}^{(4)}(k_2; k_2'|p_1) + d\sigma_{LL}^{(5)}(k_1; k_1'|k_2; k_2') + d\sigma^C(p_1|p_2). \tag{4.5.1}$$

Analogously the non-factorizable differential cross-section for a purely hadronic final state (HH) can be written in the following way

$$d\sigma_{HH}(k_1; k_1'|k_2; k_2') = 3 \times 3 \left[\frac{1}{3} d\sigma_{LL}^{(4)}(k_1; k_1'|p_2) + \frac{2}{3} d\sigma_{LL}^{(4)}(k_1'; k_1|p_2) + \frac{1}{3} d\sigma_{LL}^{(4)}(k_2; k_2'|p_1) \right.$$

$$+ \frac{2}{3} d\sigma_{LL}^{(4)}(k_2'; k_2|p_1) + \frac{1}{3} \cdot \frac{1}{3} d\sigma_{LL}^{(5)}(k_1; k_1'|k_2; k_2') + \frac{2}{3} \cdot \frac{1}{3} d\sigma_{LL}^{(5)}(k_1'; k_1|k_2; k_2')$$

$$\left. + \frac{1}{3} \cdot \frac{2}{3} d\sigma_{LL}^{(5)}(k_1; k_1'|k_2'; k_2) + \frac{2}{3} \cdot \frac{2}{3} d\sigma_{LL}^{(5)}(k_1'; k_1|k_2'; k_2) + d\sigma^C(p_1|p_2) \right]. \tag{4.5.2}$$

In order to keep the notation as uniform as possible, the momenta of the final-state quarks are defined along the lines of the purely leptonic case with k_i (k_i') corresponding to down- (up-) type quarks. If one would like to take into account quark-mixing effects, it suffices to add the appropriate squared quark-mixing matrix elements $(|V_{ij}|^2)$ to the overall factor. Note that top quarks do not contribute to the double-pole residues, since the on-shell decay $W \rightarrow tb$ is not allowed. Therefore the approximation of massless final-state fermions is still justified.

Δ_1	Δ_2						
	-1	$-1/2$	$-1/4$	0	$1/4$	$1/2$	1
-1	$+0.81$	$+0.64$	$+0.50$	$+0.36$	$+0.21$	$+0.06$	-0.16
$-1/2$	$+0.64$	$+0.51$	$+0.39$	$+0.23$	$+0.07$	-0.07	-0.25
$-1/4$	$+0.50$	$+0.39$	$+0.27$	$+0.13$	-0.02	-0.15	-0.30
0	$+0.36$	$+0.23$	$+0.13$	$+0.00$	-0.13	-0.24	-0.38
$1/4$	$+0.21$	$+0.07$	-0.02	-0.13	-0.24	-0.32	-0.4
$1/2$	$+0.06$	-0.07	-0.15	-0.24	-0.32	-0.38	-0.4
1	-0.16	-0.25	-0.30	-0.36	-0.42	-0.47	$-0.$

Table 4-1. The relative non-factorizable correction $\delta_{nf}(M_1, M_2)$ [in %] to the   ant-mass distribution $d\sigma/[dM_1 dM_2]$ for some particular values of $M_{1,2}$. The invari $M_{1,2}$ are specified in terms of their distance from M_W in units of Γ_W, i.e. $\Delta_{1,2} = [M \quad - M_W]/\Gamma_W$. Centre-of-mass energy: $\sqrt{s} = 184$ GeV.

For a semileptonic final state (say HL), when the W^+ decays hadronically and the W^- leptonically, one can write

$$d\sigma_{HL}(k_1; k_1'|k_2; k_2') = 3\left[\frac{1}{3}\, d\sigma_{LL}^{(4)}(k_1; k_1'|p_2) + \frac{2}{3}\, d\sigma_{LL}^{(4)}(k_1'; k_1|p_2) + d\sigma_{LL}^{(4)}(k_2; k_2'|p_1)\right.$$
$$\left. + \frac{1}{3}\, d\sigma_{LL}^{(5)}(k_1; k_1'|k_2; k_2') + \frac{2}{3}\, d\sigma_{LL}^{(5)}(k_1'; k_1|k_2; k_2') + d\sigma^{C}(p_1|p_2)\right]. \quad (4.5.3)$$

4.6   Numerical results

In this section some numerical results will be presented. The quantity of interest is the relative non-factorizable correction δ_{nf}, defined as

$$\frac{d\sigma}{d\xi} = \frac{d\sigma_{DPA}^0}{d\xi}\,[1 + \delta_{nf}(\xi)], \quad (4.6.1)$$

where ξ represents some set of variables. Here we consider consecutively the distributions $d\sigma/[dM_1 dM_2 d\cos\theta_1]$, $d\sigma/[dM_1 dM_2]$, $d\sigma/dM_1$ and $d\sigma/dM_{av}$, with $M_i = \sqrt{p_i^2}$, $M_{av} = \frac{1}{2}(M_1 + M_2)$ and θ_1 is the decay angle between the lepton momentum $\vec{k}_1$ and the W^+-momentum $\vec{p}_1$ in the LAB system. Note in particular that the relative non-factorizable correction δ_{nf} is the same for $d\sigma/dM_1$ and $d\sigma/dM_1^2$ distributions.

The results are shown in Fig. 4-6 for the angular distribution, and in Table 4-1 and Fig. 4-7 for the invariant-mass distributions. The pure invariant-mass distributions play an important role in the extraction of the W-boson mass from the data through direct reconstruction of the Breit–Wigner resonances. In this context especially the position of the maximum of these Breit–Wigner curves is of importance. All results
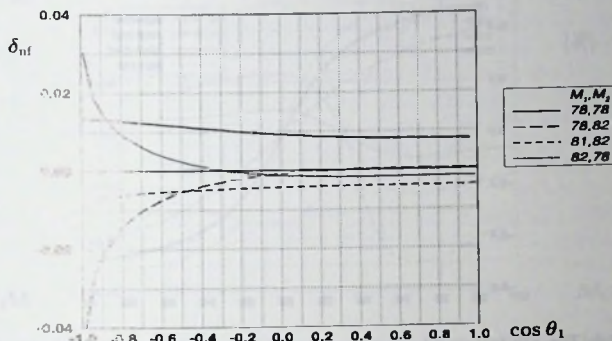
Figure 4-6. The relative non-factorizable correction $\delta_{nf}(M_1, M_2, \cos\theta_1)$ to the decay angular distribution $d\sigma/[dM_1 dM_2 d\cos\theta_1]$ for fixed values of the invariant masses $M_{1,2}$ [in GeV]. Centre-of-mass energy: $\sqrt{s} = 184$ GeV.
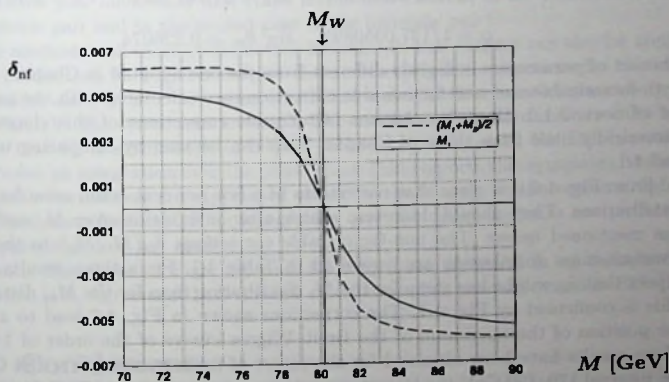

Figure 4-7. The relative non-factorizable correction $\delta_{nf}(M)$ to the single invariant-mass distributions $d\sigma/dM$. Shown are the corrections to the distributions with respect to M_1 and M_{av}. Centre-of-mass energy: $\sqrt{s} = 184$ GeV.
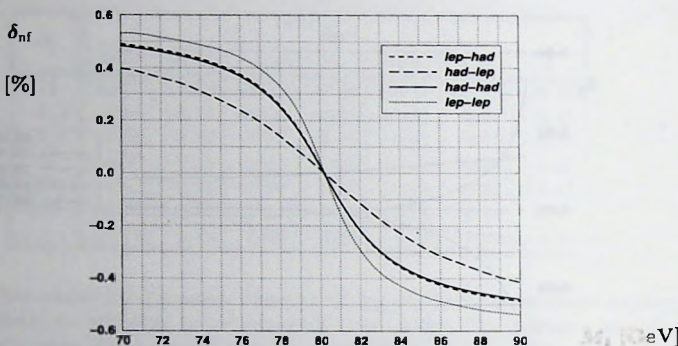
Figure 4-8. The non-factorizable corrections to $d\sigma/dM_1$ for $e^+e^- \rightarrow W^+W^- \rightarrow 4$ fermions with different final states. Final states: hadronic-hadronic, hadronic-leptonic, leptonic-hadronic, leptonic-leptonic. Centre-of-mass energy: $\sqrt{s} = 184$ GeV.

in this section are presented for the following set of input parameters:

$$M_W = 80.22 \text{ GeV}, \quad \Gamma_W = 2.08 \text{ GeV}, \quad M_Z = 91.187 \text{ GeV}, \quad \Gamma_Z = 2.49 \text{ GeV},$$

$$\alpha = 1/137.0359895, \quad \sin^2\theta_W = 0.226074.$$

This set of parameters is slightly different from the one adopted in Chapter 2, where both factorizable and non-factorizable corrections are calculated with the parameter set of Sect. 2.1.2. However, the non-factorizable corrections of this chapter differ numerically little from those of Chapter 2, as can be seen by comparing tables 2-3 and 4-1.

From Fig. 4-6 it is clear that corrections of a few per cent could arise for angular distributions. They should, however, vanish after integration over M_1 and M_2, as was mentioned before. The non-factorizable corrections $\delta_{\mathrm{nf}}(M_1, M_2)$ to the double invariant-mass distribution are presented in Table 4-1. From those results one can expect that δ_{nf} will be less steep for the M_1 distribution than for the M_{av} distribution. This is confirmed by Fig. 4-7. The corrections shown in Fig. 4-7 lead to a shift in the position of the maximum of the Breit–Wigner curves of the order of 1–2 MeV. These results have been obtained for the centre-of-mass energy $\sqrt{s} = 184$ GeV. On the interval 170–190 GeV the largest corrections are observed for 170 GeV, where the corrections are about a factor of two larger than those at 184 GeV. At 190 GeV the corrections are slightly smaller than those at 184 GeV.

In Fig. 4-8 the relative non-factorizable corrections to the invariant mass distribution $d\sigma/dM_1$ are shown for various final states (hadronic-hadronic, hadronic-leptonic, leptonic-hadronic, leptonic-leptonic). Qualitatively all corrections are similar. The
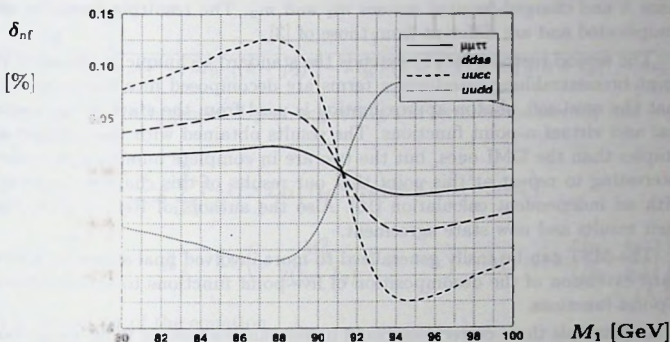
Figure 4-9. The non-factorizable corrections to $d\sigma/dM_1$ for $e^+e^- \to ZZ \to 4$ fermions with different final states. Final states: $d\bar{d}s\bar{s}$, $\mu^+\mu^-\tau^+\tau^-$, $u\bar{u}c\bar{c}$, $u\bar{u}d\bar{d}$. Centre-of-mass energy: $\sqrt{s} = 192$ GeV.

corrections are quantitatively different for the leptonic-hadronic and hadronic-leptonic cases because of the definition of M_1, which refers to the invariant mass of the fermion-anti-fermion pair mentioned first (thus in the first case M_1 is the invariant mass of the leptonic pair and in the second case of the hadronic pair).

The methods and most of the actual formulae in this chapter can also be applied to ZZ production. In Fig. 4-9 we plot the non-factorizable corrections for this case. We consider $d\bar{d}s\bar{s}$, $\mu^+\mu^-\tau^+\tau^-$, $u\bar{u}c\bar{c}$, $u\bar{u}d\bar{d}$ final states at the centre-of-mass energy of $\sqrt{s} = 192$GeV. The corrections are small. The smallness of the corrections results from the fact that δ_{nf} is asymmetric in respect to $k_1 \leftrightarrow k_1'$ or $k_2 \leftrightarrow k_2'$. For all observables that involve an integration over the phase space that respects this symmetry, the non-factorizable corrections are suppressed either by the charges or the vector couplings of the final-state fermions. If an integration over the decay angles is not performed this suppression does not apply.

Results like those of Figs. 4-8 and 4-9 have been obtained in an independent calculation [10]. Agreement between two calculations has been discussed in Ref. [11].

4.7   Conclusions

In this chapter we studied two methods to evaluate non-factorizable QED corrections in the double-pole, semi-soft photon approximation. We derived results for W-pair production, which are valid a few widths above threshold.

One technique (DMI) is an extension of that of Ref. [3] in the sense that the virtual and real photonic corrections are clearly separated and also regularized by a photon

mass λ and charged-fermion masses m_1 and m_2. The resulting formulae are rather complicated and are different from those of [3].

The second method (MST) extends the standard technique in the sense that five-point bremsstrahlung interference terms are decomposed into four-point terms and that the semi-soft photon approximation is used from the start in the evaluation of real and virtual n-point functions. The results obtained with this method are much simpler than the DMI ones, but the two are in complete numerical agreement. It is interesting to repeat at this point that our results of this chapter are in agreement with an independent calculation [10]. Also the authors of Ref. [3] have reanalyzed their results and now state agreement.

The MST can be easily generalized to more involved final states by a straightforward extension of the decomposition of five-point functions to the decomposition of n-point functions.

In principle these corrections could be relevant for tests of triple gauge boson couplings and for the determination of the W-boson mass. For the latter the corrections are of $\mathcal{O}(\alpha)$ and change the W line-shape by about 1%. For the former they vanish at the $\mathcal{O}(\alpha)$ level. In view of the present experimental accuracy, the common practice of neglecting non-factorizable corrections in the energy region at least a few widths above threshold is justified. When one gets into the threshold region, the Coulomb effect starts to dominate and should be given a separate treatment. Its numerical consequences in this non-relativistic region have been studied in the literature, see e.g. [12].

As was mentioned above, the methods and most of the actual formulae in this chapter can also be applied to ZZ, ZH production and to top-quark pair production with subsequent Wb decays. In the latter case the top-quark, W and b take the rôle of W, ν and ℓ, the gluon that of the photon. In that case the DMI formulae are directly applicable since no assumption on the neutrino mass was made. The MST formulae would need a small modification. This top-quark case will be discussed in the next chapter.

Appendix A: Feynman-parameter integrals

A.1   The on-shell four-point function

In this appendix we use Ref. [7] to present a compact expression for the on-shell four-point function D_{1234}, which appears in the decomposition of the virtual five-point function in Sect. 4.2.3. The result for D_{1234}^R can be obtained from D_{1234} by the substitutions $p_1 \rightarrow -p_1$ and $k_1 \rightarrow -k_1$. The results of [8] provide an independent check on the formula presented here.

As was mentioned before, the four-point function D_{1234} has to be calculated without semi-soft photon approximation and in the on-shell limit. The resulting function,

defined as

$$D_{1234} = \int \frac{d^4 k}{(2\pi)^4} \frac{1}{[(k-p_1)^2 - M_W^2][(k+p_2)^2 - M_W^2][(k-k_1)^2 - m_1^2][(k+k_2)^2 - m_2^2]} \tag{A.1}$$

does not contain any divergences. Upon neglecting the fermion masses m_1 and m_2, the answer reads

$$M_W^2 a(z_1 - z_2) \cdots = \sum_{k=1}^{2} (-1)^k \left\{ \mathcal{L}i_2\left(r_{14}; -z_k\right) + \mathcal{L}i_2\left(\frac{1}{r_{14}}; -z_k\right) \right.$$

$$\left. - \mathcal{L}i_2\left(-\frac{2(p_2 \cdot \ldots)}{M_W^2} \cdots\right) - \mathcal{L}i_2\left(-\frac{M_W^2}{2(p_1 \cdot k_2)} + io; -z_k\right) + \ln(-z_k) \ln\left[\frac{(p_1 \cdot k_2)}{(k_1 \cdot k_2)}\right] \right\} \tag{A.2}$$

where r_{14} is a solution of the equation

$$r_{14} + \frac{1}{r_{14}} = -\frac{s - 2M_W^2}{M_W^2} - io. \tag{A.3}$$

The quantities $z_{1,2}$ are the solutions of the equation

$$az^2 + bz + c + ido = 0, \tag{A.4}$$

with coefficients

$$a = 2(k_1 \cdot k_2) - 2(p_2 \cdot k_1), \quad c = 2(k_1 \cdot k_2) - 2(p_1 \cdot k_2).$$

$$b = M_W^2 + \frac{4(p_1 \cdot k_2)(p_2 \cdot k_1)}{M_W^2} - \frac{4(p_1 \cdot p_2)(k_1 \cdot k_2)}{M_W^2}, \quad d = -2(k_1 \cdot k_2). \tag{A.5}$$

A.2   The infrared-finite four-point function

In this appendix we briefly describe some of the details of the Feynman-parameter integral belonging to D_{0123} (see Sect. 4.3.2). The integral to be evaluated is given by Eq. (4.3.15). In the notation adopted in Sect. 4.3 this integral reads

$$D_{0123} = -\frac{i}{4\pi^2 D_2} \int_0^1 d\xi_1 \int_0^{1-\xi_1} \frac{d\xi_2}{[y_0 \xi_1 + \xi_2][p^2(\xi) - io]}, \tag{A.6}$$

with

$$\frac{p^2(\xi)}{4M_W^2} = \xi_2^2(1-\zeta) + \xi_1 \xi_2(-1 - \zeta + x_s + 1/x_s) + \xi_1 + \xi_2 \zeta + \frac{m_1^2}{M_W^2}(1 - \xi_1 - \xi_2)^2. \tag{A.7}$$

We perform the following change of variables:

$$\xi_1 = \frac{1}{1 + t + u} \quad \text{and} \quad \xi_2 = \frac{t}{1 + t + u}. \tag{A.8}$$

Accordingly, the area of integration changes from

$$\xi_1 > 0, \quad \xi_2 > 0, \quad \xi_1 + \xi_2 < 1, \tag{A.9}$$

to

$$0 < t < \infty, \quad 0 < u < \infty. \tag{A.10}$$

The Jacobian of the transformation is given by

$$\left| \frac{\partial(\xi_1\xi_2)}{\partial(tu)} \right| = \frac{1}{[1 + u + t]^3}. \tag{A.11}$$

The final integral to be evaluated looks like

$$M_W^2 D_{0123} = - \frac{i}{16\pi^2 D_2} \int\limits_0^\infty \frac{du\,dt}{[y_0 + t][t^2 + t(x_s + 1/x_s) + 1 + u(1 + t\zeta) + \frac{m_1^2}{M_W^2} u^2]}. \tag{A.12}$$

The second expression in the denominator of the integrand is linear in u up to the small term $u^2 m_1^2/M_W^2$, which is needed to regularize the collinear divergences of the integral. When performing partial fractioning of the integrand, this term should not be neglected; it has to be treated as a small parameter.

Performing first the integration over u and then the integration over t, we obtain the final result (4.3.18) for D_{0123}, expressed in terms of logarithms and dilogarithms.

A.3   The infrared-divergent four-point function

Next we present a few steps in the calculation of the Feynman-parameter integral belonging to D_{0134} (see Sect. 4.3.2). The first step involves the integration over momentum space, as represented by Eq. (4.3.24). The contour will be closed in the lower half of the complex k_0-plane, where only one pole is situated at $k_0 = \sqrt{\vec{k}^2 + \lambda^2} - io$. We introduce cylindric variables in the $\vec{p}(\xi)$ direction:

$$I_{0134}(\xi) = - \frac{i}{8\pi^2} \int \frac{\rho\,d\rho\,dz}{\sqrt{\rho^2 + z^2 + \lambda^2}\left[-|E(\xi)|\sqrt{\rho^2 + z^2 + \lambda^2} - |\vec{p}(\xi)|\,z + A(\xi) + io\right]^3}. \tag{A.13}$$

The integration over ρ becomes trivial:

$$I_{0134}(\xi) = \frac{i}{16\pi^2|E(\xi)|} \int\limits_{-\infty}^\infty \frac{dz}{\left[-|E(\xi)|\sqrt{z^2 + \lambda^2} - |\vec{p}(\xi)|\,z + A(\xi) + io\right]^2}. \tag{A.14}$$

The last integration simplifies if one uses the representation:

$$I_{0134}(\xi) = \frac{i}{16\pi^2\lambda\,|E(\xi)|} \frac{\partial}{\partial|E(\xi)|} \int\limits_{-\infty}^\infty \frac{dz/\sqrt{z^2 + 1}}{-|E(\xi)|\sqrt{z^2 + 1} - |\vec{p}(\xi)|\,z + A(\xi)/\lambda + io}. \tag{A.15}$$

Introducing the standard variable transformation $t = \sqrt{z^2 + 1} - z$, the final integration can be performed, leading to the result given in Eq. (4.3.26).

The second stage of the calculation involves the integration over the Feynman parameters. We start with Eq. (4.3.26). This time we combine a change of variables, analogous to the one utilized in the previous appendix, with a rescaling :

$$\xi_3 = \frac{t}{1 - u + t}, \quad \xi_2 = \frac{1}{1 + u + t} \quad \text{followed by} \quad t \to \frac{M_W}{m_2} t, \quad u \to \frac{M_W}{m_1} u. \quad (A.16)$$

In this w   es the form

$$D_{0134} = \qquad \int\limits_{0}^{\infty} du\, dt\, \frac{\partial}{\partial p'^2} \left\{ \frac{1}{\sqrt{A'^2 - \lambda^2 p'^2}} \ln\left(\frac{A' - \sqrt{A'^2 - \lambda^2 p'^2}}{A' + \sqrt{A'^2 - \lambda^2 p'^2}} \right) \right\}, \quad (A.17)$$

where the   of A' and p'^2 have now changed. Those quantities are rescaled versions of   an   . The rescaling is performed in such a way that p'^2 changes to

$$\frac{p'^2}{4M_W^2} = t^2 + u^2 - \frac{s_{12}}{m_1 m_2} tu + \frac{\zeta' M_W}{m_2} t + \frac{M_W}{m_1} u + 1. \quad (A.18)$$

In order to linearize this expression with respect to u, one has to introduce one more variable transformation

$$t = t' + cu, \quad \text{with} \quad c = \frac{m_1 m_2}{s_{12}}, \quad (A.19)$$

which leads to

$$\frac{p'^2}{4M_W^2} = t'^2 - \frac{s_{12}}{m_1 m_2} t'u + \frac{\zeta' M_W}{m_2} t' + \frac{M_W}{m_1} u + 1. \quad (A.20)$$

After changing the order of integration according to

$$\int\limits_{0}^{\infty} du \int\limits_{0}^{\infty} dt \to \int\limits_{0}^{\infty} du \int\limits_{-cu}^{\infty} dt' = \int\limits_{0}^{\infty} dt' \int\limits_{0}^{\infty} du + \int\limits_{-\infty}^{0} dt' \int\limits_{-t'/c}^{\infty} du, \quad (A.21)$$

one can perform the rest of the Feynman-parameter integrations to obtain the final result (4.3.28) for D_{0134}.

Appendix B: Why $\mathcal{R}$ vanishes

In this appendix it will be shown that the second term in Eq. (4.2.30), given by

$$\mathcal{R} = \int \frac{d^4 k}{(2\pi)^4 N_0} \mathcal{P}ole \frac{\sum r_i (k \cdot v_i) + 2a\lambda^2}{N_1 N_2 N_3 N_4}, \quad (B.1)$$
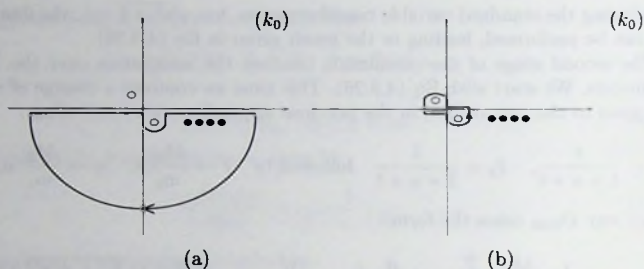
Figure 4-10. The pole structure of $\mathcal{R}$ in the semi-soft photon approximation (a) and the transformation of the integration contour in the complex k_0-plane (b). The solid circles denote the particle poles, the open circles the photon poles.

is actually zero. In this integral the photon is not necessarily on-shell, because the residue is not taken in the photon pole. However, by power counting we can conclude that only soft and semi-soft photons give a noticeable contribution to the integral. All other contributions are formally of higher order in the expansion in powers of Γ_W/M_W. Therefore we use the semi-soft photon approximation to evaluate this integral. As a result, all particle poles are situated in the same half-plane of the complex k_0 variable, as is shown in Fig. 4-10(a).

Next one can deform the integration contour in the way depicted in Fig. 4-10(b). Note that the orientation of the contour is reversed. Figure 4-10 shows that the sum of the particle-pole residues is equal to the sum of the photon-pole residues with the opposite sign. This is a consequence of the semi-soft photon approximation and of the fact that all particle poles turned out to be in the same half-plane of the complex k_0 variable. The latter is the result of the transformation (4.2.25) introduced in Sect. 4.2.2.

Let us consider the following general integral

$$\mathcal{R}(p) = \int \frac{d^4k}{(2\pi)^4 N_0} \mathcal{P}ole \frac{p \cdot k}{N_1 N_2 N_3 N_4}, \tag{B.2}$$

where p^μ is an arbitrary vector. In the semi-soft photon approximation the denominators can be written as $N_0 = k^2 - \lambda^2 + io$ and $N_i = 2(p_i \cdot k) + p_i^2 - m_i^2 + io$. As mentioned in Sect. 4.2.2, the momenta p_i are time-like and have positive energy components, i.e. $E_i \geq |\vec{p}_i|$. For simplicity we take the photon to be massless, i.e. $\lambda^2 = 0$, but the arguments that follow do not depend on this. Deforming the integration contour as described above, and subsequently taking the residues in the photon poles,

one can write

$$\mathcal{R}(p) = 2\pi i \int \frac{d^3k}{(2\pi)^4 \, 2\omega} \, \frac{(p \cdot k)}{N_1 N_2 N_3 N_4}\bigg|_{\omega = -|\vec{k}| + io} + 2\pi i \int \frac{d^3k}{(2\pi)^4 \, 2\omega} \, \frac{(p \cdot k)}{N_1 N_2 N_3 N_4}\bigg|_{\omega = |\vec{k}| - io}$$

(B.3)

In spherical coordinates this takes the form

$$\mathcal{R}(p) = \int \frac{d|\vec{k}| \, d^2\Omega_k}{(2\pi)^4} \, \frac{|\vec{k}|^2 \, (E + f(\Omega_k)|\vec{p}|)}{\prod_{i=1}^{4} \left[-2|\vec{k}| \, (E_i + f_i(\Omega_k)|\vec{p}_i|) + p_i^2 - m_i^2 + io \right]}$$

$$- \int \frac{d|\vec{k}| \, d^2\Omega_k}{(2\pi)^4} \, \frac{|\vec{k}|^2 \, (E - f(\Omega_k)|\vec{p}|)}{\prod_{i=1}^{4} \left[2|\vec{k}| \, (E_i - f_i(\Omega_k)|\vec{p}_i|) + p_i^2 - m_i^2 + io \right]}.$$

(B.4)

In the second term one can make a change of variables according to $|\vec{k}| \to -|\vec{k}|$ and $\vec{n}_k \to -\vec{n}_k$, to obtain

$$\mathcal{R}(p) = i\pi \int_{-\infty}^{\infty} \frac{d|\vec{k}| \, d^2\Omega_k}{(2\pi)^4} \, \frac{|\vec{k}|^2 \, (E + f(\Omega_k)|\vec{p}|)}{\prod_{i=1}^{4} \left[-2|\vec{k}| \, (E_i + f_i(\Omega_k)|\vec{p}_i|) + p_i^2 - m_i^2 + io \right]}.$$

(B.5)

This integral is ultraviolet-finite and all poles are situated in the same half-plane of the complex variable $|\vec{k}|$, since $E_i \geq |\vec{p}_i|$ and $|f_i(\Omega_k)| \leq 1$. By closing the contour in the opposite half-plane, one finds $\mathcal{R}(p) = 0$. From this it trivially follows that $\mathcal{R} = 0$.

Appendix C:
Special functions and integrals in the DMI method

C.1   The functions F_1 and F_2

In this appendix we present the functions F_1 and F_2, which are used in the calculations in Sect. 4.4. The function F_1 is defined as

$$F_1(a; \beta | x_i) = \int_{-1}^{1} \frac{dx}{x - a} \, \ln(1 + \beta x) \left[\theta(x - x_i) - \theta(x_i - x) \right].$$

(C.1)

Here a is a complex number with a non-zero imaginary part, and β and x_i are real numbers with absolute value smaller than 1. The analytical expression for this function is given by

$$F_1(a; \beta | x_i) = -2 \, \text{Li}_2 \left(\frac{1 + x_i \beta}{1 + a\beta} \right) + \text{Li}_2 \left(\frac{1 - \beta}{1 + a\beta} \right) + \text{Li}_2 \left(\frac{1 + \beta}{1 + a\beta} \right) +$$

(C.2)

$$+ \ln \frac{\beta(1 + a)}{1 + a\beta} \ln(1 - \beta) + \ln \frac{\beta(a - 1)}{1 + a\beta} \ln(1 + \beta) - 2 \ln \frac{\beta(a - x_i)}{1 + a\beta} \ln(1 + x_i \beta).$$

In addition we need this function in the special case $a = x_i$, without non-zero imaginary part. There, the integral $F_1(x_i; \beta | x_i)$ is logarithmically divergent. This is a collinear divergence and should be regularized by keeping the small non-zero fermion masses. The answer in this case is

$$F_1(x_i; \beta | x_i) = \ln(1 + x_i \beta) \ln\left(\frac{4E_i^3}{m_i^2}\right) - \text{Li}_2\left(\beta \frac{1 + x_i}{1 + x_i \beta}\right) - \text{Li}_2\left(\beta \frac{x_i - 1}{1 + x_i \beta}\right). \tag{C.3}$$

The other function, F_2, is defined as

$$F_2(a | x_i) = \int\limits_{-1}^{1} \frac{dx}{x - a} \left[\theta(x - x_i) - \theta(x_i - x)\right]. \tag{C.4}$$

For a and x_i the same restrictions as indicated for the function F_1 apply. The corresponding analytical expressions are

$$F_2(a | x_i) = -2\ln(x_i - a) + \ln(-1 - a) + \ln(1 - a), \tag{C.5}$$

and

$$F_2(x_i | x_i) = \ln\left(\frac{4E_i^2}{m_i^2}\right). \tag{C.6}$$

C.2   The azimuthal principal-value integral

In this appendix we present the result for the azimuthal principal-value integral, used in Sect. 4.4:

$$I_\phi = \mathcal{P}\left(\int\limits_0^{2\pi} \frac{d\phi}{2\pi} \frac{1}{A - B\cos\phi}\right), \tag{C.7}$$

with

$$A = (v_1 - v_2 \cos\theta_{12}) \cos\theta \quad \text{and} \quad B = v_2 \sin\theta_{12} \sin\theta. \tag{C.8}$$

The principal-value integration yields

$$I_\phi = \begin{cases} +\frac{1}{\sqrt{A^2 - B^2}} & \text{for} \quad A/B \in (+1, +\infty) \quad \text{or equivalently} \quad \cos\theta \in (+x_+, +1) \\ -\frac{1}{\sqrt{A^2 - B^2}} & \text{for} \quad A/B \in (-\infty, -1) \quad \text{or equivalently} \quad \cos\theta \in (-1, -x_+) \end{cases}, \tag{C.9}$$

where

$$x_+ = \sqrt{\frac{v_2^2(1 - x_{12}^2)}{v_1^2 + v_2^2 - 2v_1 v_2 x_{12}}} \quad \text{and} \quad \sqrt{A^2 - B^2} = |\vec{v}_1 - \vec{v}_2|\sqrt{x^2 - x_+^2}. \tag{C.10}$$

In non-collinear situations one can take $v_{1,2} \to 1$, resulting in $x_+ = \sqrt{(1 + x_{12})/2}$.

C.3   The functions $\mathcal{F}_1$, $\mathcal{F}_2$ and $\mathcal{K}$

In this appendix we present the functions $\mathcal{F}_1$, $\mathcal{F}_2$, and $\mathcal{K}$, used in Sect. 4.4 for the infrared-divergent four- and five-point functions.

The function $\mathcal{F}_1$ is defined as

$$\mathcal{F}_1(x_+; v) = \int_{x_+}^{1} \frac{dx}{\sqrt{x^2 - x_+^2}} \frac{1}{1 - vx} \ln\left(\frac{1 - vx}{1 + vx}\right). \tag{C.11}$$

Here x_+ is real with $0 \le x_+ < 1$, and the quantity v is real and close to unity. For $v \to 1$ the answer for this integral is given by

$$\mathcal{F}_1(x_+; v) = \frac{1}{\sqrt{1 - x_+^2}} \left[-\frac{1}{2} \ln^2\left(\frac{1 - v}{2}\right) - \frac{\pi^2}{6} + \frac{1}{2} \ln^2(1 - x_+^2) - \ln(x_+) \ln(1 - x_+^2) \right]. \tag{C.12}$$

The function $\mathcal{F}_2$ is defined as

$$\mathcal{F}_2(x_+) = \int_{x_+}^{1} \frac{dx}{\sqrt{x^2 - x_+^2}} \frac{1}{1 + x} \ln\left(\frac{1 - x}{1 + x}\right), \tag{C.13}$$

which amounts to

$$\mathcal{F}_2(x_+) = \frac{1}{\sqrt{1 - x_+^2}} \left[\mathrm{Li}_2(x_+^2) - \frac{\pi^2}{6} + \ln(x_+) \ln(1 - x_+^2) \right]. \tag{C.14}$$

In our explicit formulae, the functions $\mathcal{F}_1$ and $\mathcal{F}_2$ always enter as a sum. This sum can be represented in a compact form:

$$\mathcal{F}_1(x_+; v) + \mathcal{F}_2(x_+) = \frac{1}{\sqrt{1 - x_+^2}} \left[-\frac{1}{2} \ln^2\left(\frac{1 - v}{2}\right) - \mathrm{Li}_2\left(\frac{x_+^2}{x_+^2 - 1}\right) - \frac{\pi^2}{3} \right]. \tag{C.15}$$

The function $\mathcal{K}$ is defined as

$$\mathcal{K}(A; B|x_0; \mu^2) = \int_{-1}^{1} \frac{dx}{(x + A)\sqrt{(x - x_0)^2 + \mu^2}} \ln(B - x), \tag{C.16}$$

A being a complex number with a non-zero imaginary part, and B being real and larger than 1. The quantities x_0 and μ are real, with $|x_0| < 1$ and $\mu^2 \ll 1$. The resulting analytical expression is somewhat more complicated:

$$\mathcal{K}(A; B|x_0; \mu^2) = \frac{-1}{A + x_0} \left\{ \mathcal{L}i_2\left(1; \frac{A + 1}{A + x_0}\right) - \mathcal{L}i_2\left(1; \frac{A + x_0}{A - 1}\right) - \mathcal{L}i_2\left(\frac{B - x_0}{B - 1}; \frac{A + 1}{A + x_0}\right) \right.$$
$$+ \mathcal{L}i_2\left(\frac{B + 1}{B - x_0}; \frac{A + x_0}{A - 1}\right) - \frac{1}{2} \ln^2\left(\frac{B - x_0}{B - 1}\right) + \ln(B - 1) \ln\left(\frac{A + 1}{A + x_0}\right)$$
$$\left. + \ln(B - x_0) \ln\left(\frac{\mu^2}{4(1 - x_0^2)} \frac{A - 1}{A + x_0}\right) \right\}. \tag{C.17}$$

References

[1] W. Beenakker, A.P. Chapovsky and F.A. Berends, *Phys. Lett.* **B411** (1997) 203 and *Nucl. Phys.* **B508** (1997) 17.

[2] W. Beenakker and A. Denner, *Int. J. Mod. Phys.* **A9** (1994) 4837;
W. Beenakker et al., *hep-ph/9602351*, in *Physics at LEP2*, eds. G. Altarelli, T. Sjöstrand and F. Zwirner (CERN 96-01, Geneva, 1996), Vol. 1, p. 79.

[3] K. Melnikov and O. Yakovlev, *Nucl. Phys.* **B471** (1996) 90.

[4] V.S. Fadin, V.A. Khoze and A.D. Martin, *Phys. Lett.* **B320** (1994) 141; *Phys. Rev.* **D49** (1994) 2247;
K. Melnikov and O. Yakovlev, *Phys. Lett.* **B324** (1994) 217.

[5] G. Gounaris et al., *hep-ph/9601233*, in *Physics at LEP2*, eds. G. Altarelli, T. Sjöstrand and F. Zwirner (CERN 96-01, Geneva, 1996), Vol. 1, p. 525.

[6] W.L. van Neerven and J.A.M. Vermaseren, *Phys. Lett.* **B137** (1984) 241;
for earlier references see:
D.B. Melrose, *Nuovo Cimento* **40A** (1965) 181, *and references therein.*

[7] A. Denner, U. Nierste and R. Scharf, *Nucl. Phys.* **B367** (1991) 637.

[8] G.J. van Oldenborgh and J.A.M. Vermaseren, *Z. Phys.* **C46** (1990) 425;
G. 't Hooft and M. Veltman, *Nucl. Phys.* **B153** (1979) 365.

[9] V.S. Fadin et al., *Phys. Rev.* **D52** (1995) 1377.

[10] A. Denner, S. Dittmaier and M. Roth, *Nucl. Phys.* **B519** (1998) 39 and *Phys. Lett.* **B429** (1998) 145.

[11] W. Beenakker and A. Denner, Proceedings of the Zeuthen Workshop on Elementary Particle Theory: Loops and Legs in Gauge Theories, Rheinsberg, Germany, April 19-24, 1998, *Acta Phys. Pol.* **B29** (1998) 2821.

[12] V.A. Khoze and W.J. Stirling, *Phys. Lett.* **B356** (1995) 373.

References

5 Interconnection effects in top-quark pair production

In this chapter the treatment of QED interconnection effects in W-pair production, as explained in Chapter 4, will be carried over to QCD and $t\bar{t}$ production. The material of this chapter has been published in the literature, [1].

5.1 Introduction

At present and future collider experiments, a detailed investigation of the production of top-quark pairs will substantially contribute to our knowledge of the top-quark properties and thereby of the Standard Model. An improved measurement of the top-quark mass m_t, for instance, can serve to obtain improved indirect sensitivity to the mass of the Standard Model Higgs boson. This is achieved by combining the high-precision measurements of the electroweak parameters at LEP/SLC with the direct measurements of the top-quark and W-boson masses.

Pairs of top quarks can be produced in hadron collisions at the Tevatron ($p\bar{p}$) and LHC (pp), as well as in e^+e^- and $\gamma\gamma$ collisions at a future linear collider. Since the top quark has a large width as compared to the QCD hadronization scale, $\Gamma_t \approx 1.4\,\text{GeV} \gg \Lambda_{\text{QCD}} \approx 200 - 300\,\text{MeV}$, it predominantly decays before hadronization takes place. Therefore the perturbative approach can be used for describing top quarks. The main lowest-order (partonic) mechanisms for the pair production of top quarks are

$$e^+e^-, \gamma\gamma \to t\bar{t} \to bW^+\bar{b}W^- \to 6 \text{ fermions}, \qquad (5.1.1)$$

$$q\bar{q}, gg \to t\bar{t} \to bW^+\bar{b}W^- \to 6 \text{ fermions}. \qquad (5.1.2)$$

A lot of effort has been put into an adequate theoretical description of these reactions (see e.g. Ref. [2] for two review papers). Most of these studies treat the top quarks as stable particles, which is a reasonable first approximation since $\Gamma_t/m_t = \mathcal{O}(1\%)$. For the reactions $q\bar{q}, gg \to t\bar{t}$ these studies comprise QCD [3] and electroweak [4] one-loop corrections, as well as the resummation of soft-gluon effects [5]. Also for the reactions $e^+e^-, \gamma\gamma \to t\bar{t}$ both the QCD [6] and electroweak [7] one-loop corrections are known. Moreover, the $t\bar{t}$ threshold, with its sizeable QCD [8] and Yukawa interactions [9], has been analysed in detail.

One would, however, like to treat the top quark as an unstable particle, with a Breit–Wigner distribution describing its line shape. The most economic approach for treating processes that involve the production and subsequent decay of unstable particles is the so-called leading-pole approximation (LPA) [10]. This approximation is based on an expansion of the complete amplitude around the poles of the unstable

particles, which can be viewed as a prescription for performing an effective expansion in powers of Γ_i/M_i. Here M_i and Γ_i stand for the masses and widths of the various unstable particles. The residues in the pole expansion are physically observable and therefore gauge-invariant. The actual approximation consists in retaining only the terms with the highest degree of resonance. In the case of top-quark pair production only the double-pole residues are hence considered and the LPA becomes a double-pole approximation (DPA). This approximation will be valid sufficiently far above the $t\bar{t}$-threshold. If in reactions (5.1.1) and (5.1.2) also the W bosons are treated as unstable particles, then also for these particles the leading pole residues should be taken. In this approach the complete set of corrections to reactions (5.1.1) and (5.1.2) naturally splits into two groups: factorizable and non-factorizable corrections. The factorizable corrections are directly linked to the density matrices for on-shell production and decay of the unstable particles. The non-factorizable corrections can be viewed as describing interactions that interconnect different (production/decay) stages of the off-shell process. A detailed discussion of this method with all its subtleties can be found in Ref. [11] and in Chapter 2, where the method has been applied to the complete set of $\mathcal{O}(\alpha)$ radiative corrections to the process $e^+e^- \to W^+W^- \to 4$ fermions. For $t\bar{t}$ production partial results along this line exist [12], involving a subset of the factorizable corrections to the reaction $e^+e^- \to t\bar{t} \to bW^+\bar{b}W^- \to 6$ fermions. However, the non-factorizable corrections are needed for a complete $\mathcal{O}(\alpha_S)$ calculation.

In this chapter we apply our calculations presented in Chapter 4 to the non-factorizable $\mathcal{O}(\alpha_S)$ corrections to $t\bar{t}$ production at various colliders. We discuss the effect on the invariant-mass distribution of the off-shell top quark and the resulting shift in the maximum of the distorted Breit–Wigner distribution.

5.2   Definition of the non-factorizable corrections

In the LPA approach reactions like (5.1.1) and (5.1.2), which involve unstable particles during intermediate stages, can be viewed as consisting of separate subprocesses, i.e. the production and decay of the unstable particles. Having this picture in mind, the complete set of radiative corrections can be separated naturally into a sum of corrections to these subprocesses, called factorizable corrections, and those corrections that interconnect various subprocesses, called non-factorizable corrections. It should be noted, as was explained in Chapter 2, that it is often misleading to identify the non-factorizable contributions on the basis of diagrams. Such a definition is in general not gauge-invariant. Rather one should realize that only real/virtual semi-soft gluons[1] with $E_g = \mathcal{O}(\Gamma_i)$ will contribute, the contributions of the hard gluons being suppressed by Γ_i/E_g. This is a consequence of the fact that the various subprocesses are typically separated by a big space-time interval of $\mathcal{O}(1/\Gamma_i)$ due to the propagation of the unstable particles. The subprocesses can be interconnected only by the

---

[1]These gluons will still be perturbative in our case as their typical energy ($E_g \sim \Gamma_{t,W} \gtrsim 1.4\,\text{GeV}$) largely exceeds the QCD hadronization scale ($\Lambda_{\text{QCD}} \approx 200 - 300\,\text{MeV}$).
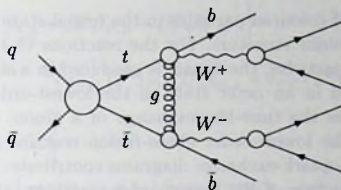
Figure 5-1. The generic structure of the complete $t\bar{t}$-production process $q\bar{q} \rightarrow t\bar{t} \rightarrow bW^+\bar{b}W^-$ → 6 fermions in the LPA. The open circles denote the various production and decay subprocesses. As an example also the non-factorizable semi-soft gluon interaction between the two top-quark decay subprocesses is shown.

radiation of semi-soft gluons with energy of $\mathcal{O}(\Gamma_t)$, which induce interactions that are sufficiently long range. Hard gluons ($E_g = \mathcal{O}(M_t) \gg \Gamma_t$) as well as massive particles induce short-range interactions and therefore contribute exclusively to the factorizable corrections, which are governed by the relatively short time interval $\sim 1/M_t$ on which the decay and production subprocesses occur. A more detailed discussion of these issues can be found in Refs. [11, 13, 14] and in Chapter 2.

In Fig. 5-1 we show schematically the partonic process $q\bar{q} \rightarrow t\bar{t} \rightarrow bW^+\bar{b}W^- \rightarrow$ 6 fermions. The process consists of five subprocesses, which we will denote by $t\bar{t}_{\text{prod}}$, t_{dec}, $\bar{t}_{\text{dec}}$, W^+_{dec}, and W^-_{dec}. In Fig. 5-1 these subprocesses are indicated by the open circles. The non-factorizable semi-soft gluon interactions interconnect any two different subprocesses, as is exemplified in Fig. 5-1 for the two top-quark decay subprocesses. The coupling of such a gluon to a certain subprocess can be written in terms of semi-soft currents. In contrast to soft-gluon currents, the effect of the gluon momentum on the unstable-particle propagators cannot be neglected in the semi-soft currents. The various non-factorizable corrections to the cross-section are just given by all possible interferences of the semi-soft currents. This will be made more explicit in the next section.

5.3   Colour dependence
of the non-factorizable corrections

We start off by considering the simpler case of stable W bosons. At the end of this section we will indicate what happens if the W bosons decay hadronically. For stable W bosons one can identify three subprocesses: $t\bar{t}_{\text{prod}}$, t_{dec}, $\bar{t}_{\text{dec}}$. The non-factorizable corrections are given by the semi-soft gluon interferences between these different subprocesses. As only semi-soft gluons contribute, the virtual and real matrix elements factorize in terms of lowest-order matrix elements and semi-soft currents. In view of

the possible presence of coloured particles in the initial state $(q\bar{q}, gg)$, this factorization depends on the colour structure. For the reactions (5.1.1), which involve only colourless initial-state particles, the $t\bar{t}$ pair is produced in a singlet state. In contrast, the $t\bar{t}$ pair is produced in an octet state in the lowest-order annihilation process $q\bar{q} \rightarrow t\bar{t}$, which involves the time-like exchange of a gluon. Both singlet and octet states are present in the lowest-order gluon-fusion reaction $gg \rightarrow t\bar{t}$, since in that case also space-like top-quark-exchange diagrams contribute. Because of these differences in the colour structure of the lowest-order reactions, also the non-factorizable corrections will come out differently, as we will see from the following discussion.

In order to keep the notation as general as possible, we write the lowest-order partonic reactions in the generic form

$$Q_1(q_1)Q_2(q_2) \rightarrow t(p_1)\bar{t}(p_2) \rightarrow b(k_1)W^+(k_1')\,\bar{b}(k_2)W^-(k_2') \tag{5.3.1}$$

where $Q_1 Q_2 = \{e^+e^-, \gamma\gamma, q\bar{q}, gg\}$. The corresponding lowest-order matrix element will be denoted by $(\mathcal{M}_0)_{ij}^{c_2 c_1}$, where i, j indicate the $t, \bar{t}$ colour indices in the fundamental representation. The colour indices c_1, c_2 belonging to Q_1, Q_2 depend on the specific initial state: they are absent for the colourless e^+e^- and $\gamma\gamma$ initial states, and they are in the fundamental/adjoint representation for the $q\bar{q}/gg$ initial states. The momentum, Lorentz index, and colour index of the semi-soft gluon will be denoted by k, μ, and a, respectively.

By using the relation

$$(T^a)_{ij}(T^a)_{kl} = \frac{1}{2}\left(\delta_{il}\,\delta_{kj} - \frac{1}{N}\,\delta_{ij}\,\delta_{kl}\right) \tag{5.3.2}$$

for the $SU(N)$ generators T^a in the fundamental representation (with $N = 3$ for QCD), the virtual and real non-factorizable corrections take the generic form:

$$d\sigma_{\mathrm{nf}}^{\mathrm{virt}} = \frac{1}{K_{\mathrm{in}}}\frac{d\Gamma_0}{2s}\,(\mathcal{M}_0^*)_{i''j''}^{c_2''c_1''}(\mathcal{M}_0)_{i'j'}^{c_2 c_1}\,\mathrm{Re}\left\{i\int\frac{d^4k}{(2\pi)^4 k^2}\left(\Delta_{\mathrm{nf}}^{\mathrm{virt}}\right)_{i''i'j'j''}^{c_2'c_2;c_1'c_1''}\right\}, \tag{5.3.3}$$

$$d\sigma_{\mathrm{nf}}^{\mathrm{real}} = \frac{-1}{K_{\mathrm{in}}}\frac{d\Gamma_0}{2s}\,(\mathcal{M}_0^*)_{i''j''}^{c_2''c_1''}(\mathcal{M}_0)_{i'j'}^{c_2 c_1}\,\mathrm{Re}\left\{\int\frac{d\vec{k}}{(2\pi)^3 2k_0}\left(\Delta_{\mathrm{nf}}^{\mathrm{real}}\right)_{i''i'j'j''}^{c_2'c_2;c_1'c_1''}\right\}. \tag{5.3.4}$$

Here the pre-factor consists of the lowest-order phase-space factor in the LPA $[d\Gamma_0]$, the partonic flux factor $[1/(2s)]$, and the initial-state spin and colour average $[1/K_{\mathrm{in}}]$. The non-factorizable kernels can be expressed in terms of semi-soft currents according to

$$\left(\Delta_{\mathrm{nf}}^{\mathrm{virt}}\right)_{i''i'j'j''}^{c_2'c_2;c_1'c_1''} = \frac{1}{2}\,\delta_{c_2'c_2}\,\delta_{c_1'c_1''}\Bigg\{ \tag{5.3.5}$$

$$\delta_{i''j''}\,\delta_{j'i'}\left[\mathcal{J}_t^\mu(\mathcal{J}_{t\bar{t}} - \bar{\mathcal{J}}_{tt} - \tilde{\mathcal{J}}_\oplus)_\mu + \mathcal{J}_{\bar{t}}^\mu(\mathcal{J}_{t\bar{t}} + \bar{\mathcal{J}}_{tt} + \tilde{\mathcal{J}}_\oplus)_\mu + 2\mathcal{J}_t^\mu\mathcal{J}_{\bar{t},\mu}\right]$$

$$+\quad \delta_{i''i'}\,\delta_{j'j''}\left[N\mathcal{J}_t^\mu(\mathcal{J}_{t\bar{t}} + \bar{\mathcal{J}}_{tt} + \tilde{\mathcal{J}}_\oplus)_\mu + N\mathcal{J}_{\bar{t}}^\mu(\mathcal{J}_{tt} - \bar{\mathcal{J}}_{tt} - \tilde{\mathcal{J}}_\ominus)_\mu\right.$$

$$- \frac{2}{N} \left(\mathcal{J}_t^\mu \mathcal{J}_{\bar{t},\mu} + \mathcal{J}_t^\mu \mathcal{J}_{t\bar{l},\mu} + \mathcal{J}_{\bar{t}}^\mu \mathcal{J}_{t\bar{l},\mu} \right) \Big] \Big\}$$

$$+ \ \left(Q_{\text{in}}^a \right)^{c_2' c_2; c_1' c_1'} \left\{ \delta_{j'j''} \left(T^a \right)_{i''i'} \mathcal{J}_t^\mu \mathcal{J}_{\oplus,\mu} + \delta_{i''i'} \left(T^a \right)_{j'j''} \mathcal{J}_{\bar{t}}^\mu \mathcal{J}_{\ominus,\mu} \right\},$$

$$\left(\right)^{c_2' c_2; c_1' c_1'}_{; j'' } = \frac{1}{2} \delta_{c_2' c_2} \delta_{c_1 c_1'} \Big\{ \tag{5.3.6}$$

$$\delta_{i''j''} \, \delta_{j'i'} \left[\mathcal{I}_t^{* \, \mu} (\mathcal{I}_{t\bar{l}} - \tilde{\bar{\mathcal{I}}}_{t\bar{l}} - \tilde{\mathcal{I}}_0)_\mu + \mathcal{I}_{\bar{t}}^{* \, \mu} (\mathcal{I}_{t\bar{l}} + \tilde{\bar{\mathcal{I}}}_{t\bar{l}} + \tilde{\mathcal{I}}_0)_\mu + 2 \mathcal{I}_t^{* \, \mu} \mathcal{I}_{\bar{t},\mu} \right]$$

$$+ \ \delta_{i''i'} \, \delta_{j'j''} \left[N \mathcal{I}_t^{* \, \mu} (\mathcal{I}_{t\bar{l}} + \tilde{\bar{\mathcal{I}}}_{t\bar{l}} + \tilde{\mathcal{I}}_0)_\mu + N \mathcal{I}_{\bar{t}}^{* \, \mu} (\mathcal{I}_{t\bar{l}} - \tilde{\bar{\mathcal{I}}}_{t\bar{l}} - \tilde{\mathcal{I}}_0)_\mu \right.$$

$$- \ \frac{2}{N} \left(\mathcal{I}_t^{* \, \mu} \mathcal{I}_{\bar{t},\mu} + \mathcal{I}_t^{* \, \mu} \mathcal{I}_{t\bar{l},\mu} + \mathcal{I}_{\bar{t}}^{* \, \mu} \mathcal{I}_{t\bar{l},\mu} \right) \Big] \Big\}$$

$$+ \ \left(Q_{\text{in}}^a \right)^{c_2' c_2; c_1' c_1'} \left\{ \delta_{j'j''} \left(T^a \right)_{i''i'} \mathcal{I}_t^{* \, \mu} \mathcal{I}_{0,\mu} + \delta_{i''i'} \left(T^a \right)_{j'j''} \mathcal{I}_{\bar{t}}^{* \, \mu} \mathcal{I}_{0,\mu} \right\}.$$

The terms proportional to $\delta_{i''j''} \delta_{j'i'}$ project on the lowest-order singlet $t\bar{t}$ states, whereas the terms proportional to $\delta_{i''i'} \, \delta_{j'j''}$ completely factorize the lowest-order cross-section. The colour structure

$$Q_{\text{in}}^a = \begin{cases} 0 & \text{for } e^+ e^-, \gamma\gamma \\ \delta_{c_1 c_1'} (T^a)_{c_2' c_2} + \delta_{c_2' c_2} (T^a)_{c_1 c_1'} & \text{for } q\bar{q} \\ \delta_{c_1 c_1'} (F^a)_{c_2' c_2} + \delta_{c_2' c_2} (F^a)_{c_1 c_1'} & \text{for } gg \end{cases} \tag{5.3.7}$$

depends on the specific initial state and in general does not project on explicit lowest-order $t\bar{t}$ colour states. Here F^a are the $SU(N)$ generators in the adjoint representation, which are defined in terms of the $SU(N)$ structure constant according to $(F^a)_{bc} = -if^{abc}$. Note that for $e^+ e^-$ and $\gamma\gamma$ initial states the currents $\tilde{\mathcal{J}}_{\ominus}^\mu$, $\tilde{\mathcal{J}}_{\oplus}^\mu$ and $\tilde{\mathcal{I}}_0^\mu$ completely drop out of Eqs. (5.3.3) and (5.3.4), as it should be for colourless particles in the initial state.

The semi-soft currents appearing in the virtual non-factorizable corrections are given by

$$\mathcal{J}_t^\mu = - g_s \left[\frac{p_1^\mu}{kp_1 + io} - \frac{k_1^\mu}{kk_1 + io} \right] \frac{D_1}{D_1 + 2kp_1},$$

$$\mathcal{J}_{\bar{t}}^\mu = - g_s \left[\frac{p_2^\mu}{-kp_2 + io} - \frac{k_2^\mu}{-kk_2 + io} \right] \frac{D_2}{D_2 - 2kp_2} \tag{5.3.8}$$

for gluon emission from the decay stages of the process, and

$$\mathcal{J}_{t\bar{l}}^\mu = g_s \left[\frac{p_1^\mu}{kp_1 + io} + \frac{p_2^\mu}{-kp_2 + io} \right], \qquad \tilde{\mathcal{J}}_{t\bar{l}}^\mu = g_s \left[\frac{p_1^\mu}{kp_1 + io} - \frac{p_2^\mu}{-kp_2 + io} \right],$$

$$\mathcal{J}_{\oplus}^\mu = - g_s \left[\frac{q_1^\mu}{kq_1 + io} - \frac{q_2^\mu}{kq_2 + io} \right], \qquad \tilde{\mathcal{J}}_{\oplus}^\mu = - g_s \left[\frac{q_1^\mu}{kq_1 + io} + \frac{q_2^\mu}{kq_2 + io} \right],$$

$$\mathcal{J}_{\ominus}^\mu = g_s \left[\frac{q_1^\mu}{-kq_1 + io} - \frac{q_2^\mu}{-kq_2 + io} \right], \qquad \tilde{\mathcal{J}}_{\ominus}^\mu = g_s \left[\frac{q_1^\mu}{-kq_1 + io} + \frac{q_2^\mu}{-kq_2 + io} \right] \tag{5.3.9}$$

for gluon emission from the production stage of the process. Here g_s is the QCD gauge coupling and $D_{1,2} = p_{1,2}^2 - m_t^2 + im_t\Gamma_t$ is a shorthand notation for the inverse top-quark propagators. Note the difference in the sign of the io parts appearing in the currents $\mathcal{J}_\ominus$, $\tilde{\mathcal{J}}_\ominus$ and $\mathcal{J}_\ominus$, $\tilde{\mathcal{J}}_\ominus$. These infinitesimal imaginary parts are needed to ensure a proper incorporation of causality.

The corresponding semi-soft real-gluon currents read

$$\mathcal{I}_t^\mu = -g_s \left[\frac{p_1^\mu}{kp_1} - \frac{k_1^\mu}{kk_1} \right] \frac{D_1}{D_1 + 2kp_1}, \qquad \mathcal{I}_{\bar{t}}^\mu = g_s \left[\frac{p_2^\mu}{kp_2} - \frac{k_2^\mu}{kk_2} \right] \frac{D_2}{D_2 + 2\cdots} \qquad \text{.3.10)}$$

and

$$\mathcal{I}_{t\bar{t}}^\mu = g_s \left[\frac{p_1^\mu}{kp_1} - \frac{p_2^\mu}{kp_2} \right], \qquad \tilde{\mathcal{I}}_{t\bar{t}}^\mu = g_s \left[\frac{p_1^\mu}{kp_1} + \frac{p_2^\mu}{kp_2} \right],$$

$$\mathcal{I}_0^\mu = -g_s \left[\frac{q_1^\mu}{kq_1} - \frac{q_2^\mu}{kq_2} \right], \qquad \tilde{\mathcal{I}}_0^\mu = -g_s \left[\frac{q_1^\mu}{kq_1} + \frac{q_2^\mu}{kq_2} \right]. \qquad \text{(5.3.11)}$$

By simple power counting one can explicitly see from the above specified currents that the contributions of hard gluons are suppressed and that effectively only semi-soft gluons with $E_g = k_0 = \mathcal{O}(\Gamma_t)$ contribute. In view of the pole structure of the virtual corrections, governed by the infinitesimal imaginary parts io, many of the non-factorizable corrections will vanish when virtual and real-gluon corrections are added up. For instance, as was explained in Chapter 4, all initial–final state interferences will vanish, leaving behind a very limited subset of 'final-state' interferences [11, 14]. The following holds for the remaining interferences:

$$\mathcal{I}_t^{*\mu}\tilde{\mathcal{I}}_{t\bar{t},\mu} \to -\mathcal{I}_t^{*\mu}\mathcal{I}_{t\bar{t},\mu}, \qquad \mathcal{I}_{\bar{t}}^{*\mu}\tilde{\mathcal{I}}_{t\bar{t},\mu} \to \mathcal{I}_{\bar{t}}^{*\mu}\mathcal{I}_{t\bar{t},\mu},$$

with similar effective replacements for $\tilde{\mathcal{J}}_{t\bar{t}}$. As a result of these properties of the non-factorizable corrections, a factorization per colour structure emerges:

$$d\sigma_{\mathrm{nf}} = \delta_{\mathrm{nf}} \left[\frac{N^2 - 1}{2N} d\sigma_{\mathrm{Born},1} - \frac{1}{2N} d\sigma_{\mathrm{Born},8} \right], \qquad (5.3.12)$$

$$\delta_{\mathrm{nf}} = 2\mathrm{Re} \left\{ i \int \frac{d^4 k}{(2\pi)^4 [k^2 + io]} \left[\mathcal{J}_t^\mu \mathcal{J}_{\bar{t},\mu} + \mathcal{J}_t^\mu \mathcal{J}_{t\bar{t},\mu} + \mathcal{J}_{\bar{t}}^\mu \mathcal{J}_{t\bar{t},\mu} \right] \right.$$
$$\left. - \int \frac{d\vec{k}}{(2\pi)^3 2k_0} \left[\mathcal{I}_t^{*\mu}\mathcal{I}_{\bar{t},\mu} + \mathcal{I}_t^{*\mu}\mathcal{I}_{t\bar{t},\mu} + \mathcal{I}_{\bar{t}}^{*\mu}\mathcal{I}_{t\bar{t},\mu} \right] \right\}. \qquad (5.3.13)$$

Here $d\sigma_{\mathrm{Born},1}$ and $d\sigma_{\mathrm{Born},8}$ are the lowest-order multi-differential cross-sections in DPA for producing the intermediate $t\bar{t}$ pair in a singlet and octet state, respectively. For completeness we note that

$$d\sigma_{\mathrm{Born}}^{e^+e^-,\gamma\gamma} = d\sigma_{\mathrm{Born},1}^{e^+e^-,\gamma\gamma}, \quad d\sigma_{\mathrm{Born}}^{q\bar{q}} = d\sigma_{\mathrm{Born},8}^{q\bar{q}}, \quad d\sigma_{\mathrm{Born}}^{gg} = d\sigma_{\mathrm{Born},1}^{gg} + d\sigma_{\mathrm{Born},8}^{gg}. \qquad (5.3.14)$$

The non-factorizable factor δ_{nf} can be obtained from the formulae of Chapter 4. The results of Sect. 4.4 (DMI method) should be used, since those allow for massive decay products from the unstable particles, which is the case for the top-quark decay.

We conclude by considering the case that also the W bosons are unstable. This adds two decay subprocesses, W_{dec}^{+} and W_{dec}^{-}, to the three we have considered so far. If the W bosons decay leptonically, nothing changes as the gluon cannot couple to the W decay subprocesses in that case. For a hadronically decaying W boson additional interferences have to be taken into account. However, such interferences transition vanish as a result of the singlet nature of the W-boson decays [i.e. $\mathrm{Tr}(T^a)=0$].

5.4   Numerical results

With the help of Eqs. (5.3.12)–(5.3.14) we can now in principle evaluate all kinds of multi-differential distributions, with and without non-factorizable corrections. Although the factorized structure of the non-factorizable corrections is very transparent in Eq. (5.3.12), integration of the multi-differential cross-sections will affect this structure. For instance, in Eq. (5.3.12) the correction to the singlet cross-section differs by a factor -8 with respect to the octet one. However, for the calculation of the relative non-factorizable corrections to a one-dimensional distribution, one has to evaluate the ratio of the integrated Eqs. (5.3.12) and (5.3.14). Since δ_{nf} depends on the integration variables, the thus-obtained singlet and octet correction factors will not necessarily differ by the factor -8.

At this point we stress that any observable that is inclusive in both top-quark invariant masses, such as the total cross-section, will not receive any non-factorizable corrections. This is a typical feature of these interconnection effects (see e.g. Chapter 4 of this thesis or [14]). As an example of a distribution that is subject to non-vanishing non-factorizable corrections we focus on the invariant-mass distribution of the top quark, which can be used for the mass determination. To this end we determine the non-factorizable correction $\delta_{nf}(M)$ for the distribution

$$\frac{d\sigma}{dM} = \frac{d\sigma_{\mathrm{Born}}}{dM}\left[1 + \delta_{nf}(M)\right], \tag{5.4.1}$$

where M is the invariant mass of the b-quark and the W^+ boson. The maximum of the Breit–Wigner distribution can be used to determine the top-quark mass. The linearized shift of this maximum as induced by the non-factorizable corrections is given by

$$\Delta M = \frac{1}{8}\,\Gamma_t^2\,\frac{d\delta_{nf}(M)}{dM}\bigg|_{M=m_t}. \tag{5.4.2}$$

The correction $\delta_{nf}(M)$ is calculated for the four different mechanisms of $t\bar{t}$ production, i.e. initiated by e^+e^-, $\gamma\gamma$, $q\bar{q}$ and gg. For the centre-of-mass energies of these (partonic) reactions we take $\sqrt{s} = 355\,\mathrm{GeV}$ and $500\,\mathrm{GeV}$. These values exemplify the non-factorizable corrections in the vicinity of the threshold and far above it. As mentioned before, the adopted approximation in our calculation (LPA) forces us to stay
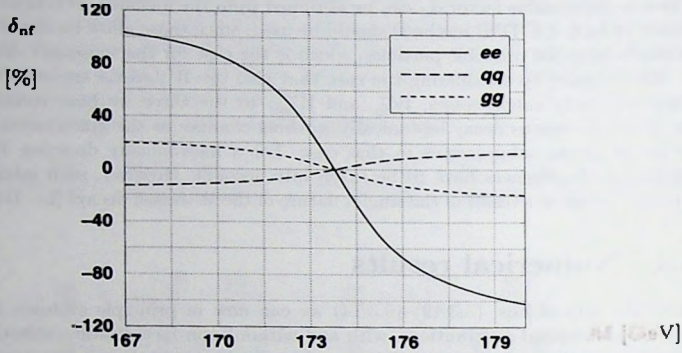
Figure 5-2. The relative non-factorizable correction $\delta_{nf}(M)$ to the single invariant mass distribution $d\sigma/dM$. Centre-of-mass energy: $\sqrt{s} = 355$ GeV.

sufficiently far above the $t\bar{t}$ threshold (read: a few times Γ_t). The numerical values for the input parameters are

$$m_t = 173.8 \, \text{GeV}, \quad M_W = 80.26 \, \text{GeV}, \quad M_Z = 91.187 \, \text{GeV}, \tag{5.4.3}$$

and

$$\Gamma_t = 1.3901 \, \text{GeV}, \tag{5.4.4}$$

the latter being the $\mathcal{O}(\alpha_S)$ corrected top-quark width. The correction δ_{nf} is proportional to α_S, for which we have to choose the relevant scale. For $\sqrt{s} = 355$ GeV the main contribution originates from the non-factorizable Coulomb effect present in δ_{nf}. Its typical momentum is determined by the top-quark width Γ_t and velocity β: $\Gamma_t/\beta \sim 6.8$ GeV. At 500 GeV softer gluons contribute and therefore the typical gluon momentum is $\Gamma_t \sim 1.4$ GeV. Therefore we choose

$$\alpha_S(1.4 \, \text{GeV}) \approx 0.3536 \quad \text{for} \quad \sqrt{s} = 500 \, \text{GeV}, \tag{5.4.5}$$

$$\alpha_S(6.8 \, \text{GeV}) \approx 0.1955 \quad \text{for} \quad \sqrt{s} = 355 \, \text{GeV}, \tag{5.4.6}$$

corresponding to $\alpha_S(M_Z) = 0.1180$ at the Z peak. It should be noted that choosing another scale in α_S will only affect the normalization of the correction.

In Fig. 5-2 the non-factorizable correction δ_{nf} is plotted as a function of the invariant mass M at the centre-of-mass energy of 355 GeV. The δ_{nf} values for the pure singlet e^+e^- initial state and the pure octet $q\bar{q}$ initial state differ approximately by the afore-mentioned factor of -8. For the gg initial state the Born octet part is larger than the singlet one, resulting in a non-factorizable correction that lies between the e^+e^- and the $q\bar{q}$ case. The correction for the $\gamma\gamma$ initial state is virtually
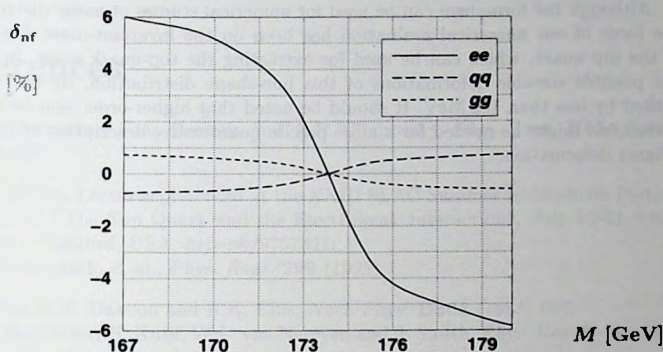
Figure 5-3. The relative non-factorizable correction $\delta_{nf}(M)$ to the single invariant-mass distribution $d\sigma/dM$. Centre-of-mass energy: $\sqrt{s} = 500$ GeV.

indistinguishable from the e^+e^- one and is therefore not displayed. Evidently the distortion effects from the singlet corrections are very large, which is due to a large non-factorizable Coulomb correction inside δ_{nf}. The maximum of the Breit–Wigner distribution is hardly affected by this large correction. One finds for the various initial states $e^+e^-(\gamma\gamma)$, gg and $q\bar{q}$ $\Delta M \approx -85$, -15 and $+10$ MeV respectively. The situation at 500 GeV is depicted in Fig. 5-3. The overall correction is small, which is typical for non-factorizable corrections further away from threshold. The shift in the maximum of the Breit–Wigner distribution is of the order of 5 MeV for the e^+e^- and $\gamma\gamma$ initial states, and even smaller for the $q\bar{q}$ and gg initial states.

In order to obtain hadronic distributions from the partonic ones, the results for the $q\bar{q}$ and gg initial states should of course be properly folded with the parton densities of the colliding hadrons ($p\bar{p}$ at the Tevatron, pp at the LHC). The bulk of the partonic contributions originates from the energy region not far above the $t\bar{t}$ threshold ($s \lesssim 8m_t^2$, i.e. $\sqrt{s} \lesssim 500$ GeV), which is exemplified by the partonic energies 355 and 500 GeV used in our analysis.

5.5   Conclusions

In this chapter we have summarized the gauge-invariant description for calculating the $\mathcal{O}(\alpha_S)$ non-factorizable QCD corrections to pair production of top quarks. The formalism is presented in a general way, making it applicable to all relevant initial states. The resulting final formula for the non-factorizable corrections involves the same quantity δ_{nf} for all reactions. This quantity can be numerically calculated using expressions available in the literature.

Although the formalism can be used for numerical studies of many distributions, the focus of our numerical evaluation has been on the invariant-mass distribution of the top quark, which can be used for extracting the top-quark mass. In spite of the possible sizeable deformations of this line-shape distribution, its maximum is shifted by less than 100 MeV. It should be noted that higher-order non-factorizable corrections might be needed for a more precise quantitative description of the Breit-Wigner deformation.

References

[1] W. Beenakker, F.A. Berends and A.P. Chapovsky, *Phys. Lett.* **B454** (1999) 129-138.

[2] A.B. Arbuzov, Lectures presented at the XXIII SLAC Summer Institute on Particle Physics "The Top Quark and the Electroweak Interaction", July 10-21, 1995, SLAC, Stanford, USA, *hep-ph*/9707321;
A. Quadt et al., *Phys. Rept.* **299** (1998) 1.

[3] P. Nason, S. Dawson and R.K. Ellis, *Nucl. Phys.* **B303** (1988) 607;
W. Beenakker, H. Kuijf, W.L. van Neerven and J. Smith, *Phys. Rev.* **D40** (1989) 54;
W. Beenakker, W.L. van Neerven, R. Meng, G.A. Schuler and J. Smith, *Nucl. Phys.* **B351** (1991) 507.

[4] W. Beenakker, A. Denner, W. Hollik, R. Mertig, T. Sack and D. Wackeroth, *Nucl. Phys.* **B411** (1994) 343.

[5] E. Laenen, J. Smith and W.L. van Neerven, *Nucl. Phys.* **B369** (1992) 543;
E. Berger and H. Contopanagos, *Phys. Lett.* **B361** (1995) 115 and *Phys. Rev.* **D54** (1996) 3085;
S. Catani, M. Mangano, P. Nason and L. Trentadue, *Phys. Lett.* **B378** (1996) 329 and *Nucl. Phys.* **B478** (1996) 273.

[6] J. Jersak, E. Laerman and P.M. Zerwas, *Phys. Rev.* **D25** (1982) 1218;
B. Kamal, Z. Merebashvili and A.P. Contogouris, *Phys. Rev.* **D51** (1995) 4808;
J.H. Kühn, E. Mirkes and J. Steegborn, *Z. Phys.* **C57** (1993) 615;
M. Drees, M. Krämer, J. Zunft and P.M. Zerwas, *Phys. Lett.* **B306** (1993) 371.

[7] W. Beenakker, S.C. van der Marck and W. Hollik, *Nucl. Phys.* **B365** (1991) 24;
A.A. Akhundov, D.Y. Bardin and A. Leike, *Phys. Lett.* **B261** (1991) 321;
A. Denner, S. Dittmaier and M. Strobel, *Phys. Rev.* **D53** (1996) 44.

[8] V.S. Fadin and V.A. Khoze, *JETP Lett.* **46** (1987) 525 and *Sov. J. Nucl. Phys.* **48** (1988) 309;
W. Kwong, *Phys. Rev.* **D43** (1991) 1488;
M. Jezabek, J.H. Kühn and T. Teubner, *Z. Phys.* **C56** (1992) 653;
Y. Sumino, K. Fujii, K. Hagiwara, M. Murayama and C.K. Ng, *Phys. Rev.* **D47** (1993) 56;
M. Peter and Y. Sumino, *Phys. Rev.* **D57** (1998) 6912;
A.H. Hoang, J.H. Kühn and T. Teubner, *Nucl. Phys.* **B452** (1995) 173;
A.H. Hoang, *Phys. Rev.* **D56** (1997) 5851;

A. Czarnecki and K. Melnikov, *Phys. Rev. Lett.* **80** (1998) 2531;
A.H. Hoang and T. Teubner, *Phys. Rev.* **D58** (1998) 114023;
K. Melnikov and A. Yelkhovsky, *Nucl. Phys.* **B528** (1998) 59;
O. Yakovlev, *hep–ph*/9808463.

[9] H. Inazawa and T. Morii, *Phys. Lett.* **B203** (1988) 279;
K. Hagiwara, K. Kato, A.D. Martin and C.K. Ng, *Nucl. Phys.* B344 (1990) 1;
J. Feigenbaum, *Phys. Rev.* **D43** (1991) 264;
M.J. Strassler and M.E. Peskin, *Phys. Rev.* **D43** (1991) 1500;
W. Beenakker and W. Hollik, *Phys. Lett.* **B269** (1991) 425;
V.S. Fadin and O. Yakovlev, *Sov. J. Nucl. Phys.* **53** (1991) 1053;
M. Jezabek and J.H. Kühn, *Phys. Lett.* **B316** (1993) 360.

[10] R.G. Stuart, *Phys. Lett.* **B262** (1991) 113;
A. Aeppli, G.J. van Oldenborgh and D. Wyler, *Nucl. Phys.* **B428** (1994) 126.

[11] W. Beenakker, F.A. Berends and A.P. Chapovsky, *Nucl. Phys.* B548 (1999) 3-59.

[12] C.R. Schmidt, *Phys. Rev.* **D54** (1996) 3250.

[13] Yu.L. Dokshitzer, V.A. Khoze, L.H. Orr and W.J. Stirling, *Nucl. Phys.* **B403** (1993) 65.

[14] K. Melnikov and O. Yakovlev, *Phys. Lett.* **B324** (1994) 217;
V.S. Fadin, V.A. Khoze and A.D. Martin, *Phys. Rev.* **D49** (1994) 2247.

Samenvatting

Instabiliteit en stralingseffecten in paarproductie van W-bosonen

Het Standaard Model van de wisselwerking tussen verschillende elementaire deeltjes wordt geacht een nauwkeurige beschrijving te geven van alle tegenwoordige versneller-experimenten. Tot nu toe komen alle experimentele resultaten overeen met de voorspelde resultaten van het Standaard Model. Hoewel dit op een succesverhaal lijkt, is verder onderzoek noodzakelijk. Er zijn namelijk effecten, voorspeld door het Standaard Model, die nog niet ontdekt zijn. Bijvoorbeeld het bestaan van een nieuw deeltje, het Higgs-boson. Bovendien zijn er aanwijzingen dat het Standaard Model tekortschiet bij extreem hoge energieën. Al met al genoeg motivatie om het Standaard Model nader te onderzoeken en verder te toetsen. Toekomstige versneller-experimenten zullen bij hogere energieën en met een grotere nauwkeurigheid uitgevoerd worden. De resultaten van deze experimenten zullen vergeleken moeten worden met de voorspelde uitkomsten van het Standaard Model. Deze voorspelde uitkomsten dienen van dezelfde kwaliteit te zijn en eenzelfde nauwkeurigheid te hebben als de experimentele gegevens. De complexiteit van de berekeningen met hoge nauwkeurigheid stelt een duidelijke uitdaging aan de theorie. In dit proefschrift wordt ingegaan op dit soort van berekeningen voor paarproductie van instabiele deeltjes. In het bijzonder wordt de paarproductie van W-bosonen gedetailleerd bestudeerd. De twee voornaamste fenomenologische doeleinden van de experimentele studie van dit proces zijn het verkrijgen van de massa van het W-boson en het bepalen van de drievoudige ijkboson-koppelingen. De massa van het W-boson kan, gecombineerd met precieze kennis van andere grootheden van het Standaard Model, zoals de massa van het Z-boson en het top-quark, de mogelijke waarden inperken van de massa van het nog-te-ontdekken Higgs-boson. Zelfs kan de precieze massa aanwijzingen geven voor mogelijke uitbreidingen van het Standaard Model. Aan de hand van de drievoudige ijkboson-koppelingen kan een zeer fundamentele eigenschap van de electrozwakke theorie getest worden: de niet-abelse ijkgroep structuur.

Het doel van dit proefschrift is tweeledig. Aan de ene kant worden de één-lus $\mathcal{O}(\alpha)$ stralingscorrecties voor het proces $e^+e^- \rightarrow 4$ fermionen bestudeerd. Immers elk W-deeltje vervalt in twee fermionen, zodat de eindtoestand voor paarproducie van W-bosonen vier fermionen bevat. De volledige $\mathcal{O}(\alpha)$ berekening is niet doenlijk wegens de grote complexiteit en ook niet zinvol omdat vele bijdragen klein zijn. De leidende termen worden verkregen door een expansie rond de polen van de W-bosonen uit te voeren. Een dergelijke berekening van stralingscorrecties is van fenomenolo-

gisch belang voor de huidige LEP2 experimenten. Aan de andere kant wordt in dit proefschrift het idee uitgewerkt, dat het genoemde pool-schema in het algemeen een geschikte en tamelijk krachtige methode is voor het werken met processen waarin instabiele deeltjes een rol spelen. Dit maakt het onderzoek relevant voor vele toekomstige experimenten waarin instabiele deeltjes geproduceerd zullen worden

In hoofdstuk II wordt de methode van pool-expansies en de verde....... .... de stralingscorrecties in een som van factoriseerbare en niet-factoriseerba.. .... .ties besproken. Deze opslitsing is van essentieel belang voor de methode. [........sen waarin instabiele deeltjes een rol spelen kunnen beschouwd worden als b......... uit verschillende goed gescheiden subprocessen, waar de instabiele deeltjes ....den geproduceerd en vervolgens vervallen. De factoriseerbare correcties zijn .... die correcties die slechts één van de subprocessen beinvloeden. De niet-fa........are correcties zijn die correcties, die verschillende subprocessen met elkaa. ....ien. Dit leidt tot correlaties tussen de verschillende subprocessen. De proble...... .... betrekking tot ijkinvariantie, samenhangend met deze werkwijze, worden i. ...... besproken. De $\mathcal{O}(\alpha)$ electrozwakke factoriseerbare correcties worden berekend en worden gecombineerd met de niet-factoriseerbare correcties, die worden uitgerekend in hoofdstuk IV. Aan het eind van hoofdstuk II worden numerieke resultaten gepresenteerd. Deze resultaten omspannen voor de eerste keer de werkzame doorsnedes met complete $\mathcal{O}(\alpha)$ stralingscorrecties voor de paarproductie van niet op hun massa-schil liggende W-bosonen.

In hoofdstuk III wordt de kwestie van de eindtoestandsstraling besproken, welke aanleiding geeft tot een opmerkelijk resultaat in hoofdstuk II. Dit resultaat houdt in dat eindtoestandsstraling een aanzienlijke correctie kan geven voor de invariante-massadistributie van een instabiel deeltje, iets dat a priori tamelijk onverwacht is. Gewoonlijk resulteert de begintoestandsstraling in sterke effecten (versterkt door de zogenaamde colineaire logaritmen). Soortgelijke versterkte effecten zijn in principe ook in zowel virtuele als reële eindtoestandsstraling aanwezig. Deze uitdrukkingen zijn afkomstig uit een speciale kinematische configuratie, waarbij een foton wordt afgestraald door een bijna massaloos fermion in een bijna colineaire richting. In deze situatie is het moeilijk deze twee deeltjes van elkaar te onderscheiden, hetgeen het mogelijk maakt ze te beschouwen als ontaarde toestanden. Het Kinoshita-Lee-Nauenberg theorema stelt echter dat deze colineaire logaritmen wegvallen wanneer men over alle ontaarde toestanden middelt. In het geval van begintoestandsstraling blijven deze termen wel bestaan, omdat het niet mogelijk is een dergelijke middeling uit te voeren. Experimenteel is er slechts één (e^+e^-) begintoestand. In het geval van eindstraling vallen deze logaritmen gewoonlijk weg. In de aanwezigheid van instabiele deeltjes, die bijvoorbeeld in een fermionpaar vervallen, kan de invariante massa van het fermionpaar beschouwd worden als een extra quantumgetal, die de verschillende ontaarde toestanden van elkaar onderscheidt. Zodra dit quantum-getal "vastligt" (bijvoorbeeld als men de invariante-massadistributie beschouwt), treden de KLN cancellaties niet meer op en zodoende geeft de eindstraling grote correcties, net als de beginstraling. Teneinde de lezer ervan te overtuigen dat dit niet door onze methode van pool-expansie

veroorzaakt wordt, wordt een eenvoudig model geanalyseerd waarin de berekening analytisch uitgevoerd kan worden, zonder gebruik te maken van de pool-expansie. Hetzelfde effect komt ook hier naar voren.

In hoofdstuk IV wordt een berekening van de niet-factoriseerbare correcties en hun implicaties voor W-paarproductie gepresenteerd. Een rekenmethode die speciaal gericht is op de evaluatie van deze correcties wordt ontwikkeld. Deze rekenmethode gebruikt de decompositie van de "veel-punts" scalaire functies (zowel reëel als virtueel) in een van "lagere-punts" functies en is zo ontwikkeld dat ze ook toepasbaar is voor complexere processen waarin meer instabiele deeltjes een rol spelen.

Als een andere toepassing van de methodes die in hoofdstuk IV ontwikkeld zijn worden in hoofdstuk V één-lus QCD "interconnectie" effecten in paarproductie van top-quarks berekend. Sinds de ontdekking van het top-quark in 1994 heeft dit proces centraal gestaan in het bestuderen van de eigenschappen van het top-quark. Een nauwkeurige theoretische voorspelling voor dit proces is daarom gewenst. De perturbatieve QCD "interconnectie" effecten kunnen op een natuurlijke en eenvoudige wijze berekend worden. Derhalve kan dit hoofdstuk beschouwd worden als een illustratie van de kracht en de universaliteit van de technieken die in dit proefschrift besproken zijn.

List of publications

- *Non-factorizable corrections to W-pair production*,
  W. Beenakker, A.P. Chapovsky and F.A. Berends,
  Phys. Lett. **B411** (1997) 203-210.

- *Non-factorizable corrections to W-pair production: methods and analytic results*,
  W. Beenakker, A.P. Chapovsky and F.A. Berends,
  Nucl. Phys. **B508** (1997) 17-63.

- *Final-state radiation and line-shape distortion in resonance pair production*,
  W. Beenakker, F.A. Berends and A.P. Chapovsky,
  Phys. Lett. **B435** (1998) 233-239.

- *Radiative corrections to pair production of unstable particles: results for $e^+e^- \rightarrow$ 4 fermions*,
  W. Beenakker, F.A. Berends and A.P. Chapovsky,
  Nucl. Phys. **B548** (1999) 3-59.

- *Radiative corrections to W-pair mediated four-fermion production at LEP2*,
  W. Beenakker, F.A. Berends and A.P. Chapovsky,
  Proceedings of the IVth International Symposium on Radiative Corrections,
  Barcelona, September 8-12, 1998, ed. J. Sola.

- *One-loop QCD interconnection effects in pair production of top quarks*,
  W. Beenakker, F.A. Berends and A.P. Chapovsky,
  Phys. Lett. **B454** (1999) 129-136.

- *An effective-Lagrangian approach to unstable particles*,
  W. Beenakker, F.A. Berends and A.P. Chapovsky,
  in preparation.

- *Coulomb effects in W^+W^- production*,
  V.S. Fadin, V.A. Khoze, A.D. Martin and A. Chapovsky,
  Phys. Rev. **D52** (1995) 1377-1385.

- *Screened-Coulomb ansatz for the non-factorizable radiative corrections*,
  A.P. Chapovsky and V.A. Khoze,
  accepted for publication in *Eur. Phys. J.*

List of publications

Curriculum Vitae

Op 25 augustus 1974 ben ik geboren te Novosibirsk in Rusland. In 1991 behaalde ik het diploma aan School №130 te Akademgorodok (Novosibirsk). Datzelfde jaar g   ik   natuurkunde studeren aan de Novosibirsk Staatsuniversiteit. In januari 1994 b   praktisch werk aan de Theoretische Divisie van het Budker Instituut v   ca (Novosibirsk) onder leiding van prof. dr. V.S. Fadin. In 1995 slaagde i   dediging van het diploma werk op het onderwerp "Coulomb effects in   action"en verkreeg ik het natuurkunde diploma (cum laude).

Per   ri 1996 trad ik als onderzoeker in opleiding in dienst van de Stichting voor   damenteel Onderzoek der Materie (FOM). Ik werkte op het Instituut-Lorentz van de Universiteit Leiden onder leiding van prof. dr. F.A. Berends en dr. W.J.P. Beenakker. De resultaten van dit onderzoek zijn beschreven in dit proefschrift. Tijdens deze periode gaf ik werkcolleges bij het college Quantumtheorie 2. Tevens bezocht ik diverse zomer- en winterscholen.

Stellingen

behorende bij het proefschrift
"Instability and radiative effects in pair production of W-bosons"

1. The non-factorizable corrections to the pair production of unstable particles vanish at high energies, $\delta_{\text{nf}} \sim E^{-4}$. If unstable particles are charged, the Coulomb effect dominates radiative corrections close to threshold. The following ansatz describes the non-factorizable corrections to the double invariant mass distribution reasonably well for all energies

$$\delta_{\text{Ans}} = -\alpha \frac{(1-\beta)^2}{\beta} \arctan\left(\frac{M_1^2 + M_2^2 - 2M^2}{2M\Gamma}\right),$$

   where β, M and Γ are respectively the velocity, mass and width of the unstable particle.

<div align="right">

This thesis,
A.P. Chapovsky and V.A. Khoze,
Eur. Phys. J. **C9** (1999) 449-457.

</div>

2. N-loop non-factorizable corrections can be written in terms of semi-soft currents similar to the ones discussed in this thesis. For example, the virtual non-factorizable correction has the form

$$\delta_{\text{nf}} \sim \frac{1}{N!} \left[\int \frac{d^4 k}{k^2} [\mathcal{J}_0 \mathcal{J}_+ + \mathcal{J}_0 \mathcal{J}_- + \mathcal{J}_+ \mathcal{J}_-]\right]^N,$$

   where the product of semi-soft currents, $\mathcal{J}_+$ and $\mathcal{J}_-$, is defined by the rule $\mathcal{J}_\pm^\mu(k, D_\pm) * \mathcal{J}_\pm^\nu(l, D_\pm) \equiv \mathcal{J}_\pm^\mu(k, D_\pm) \mathcal{J}_\pm^\nu(l, D_\pm \pm 2p_\pm \cdot k)$.

<div align="right">

This thesis.

</div>

3. It is common to use either a fixed or a running width in (radiative) W-pair mediated 4 fermion $(+\gamma)$ production. A fixed width guarantees $U(1)$ gauge invariance only. $SU(2)$ gauge invariance can be achieved by using in addition a complex mixing angle. The accuracy of this procedure is $\mathcal{O}(\Gamma_W/M_W)$, the same as of the double-pole approximation discussed in this thesis.

<div align="right">

This thesis,
A. Denner *et al.*, hep–ph/9904472.

</div>

4. The Dyson resummation of the self-energies for unstable particles rearranges the perturbative expansion in α and thus in general breaks gauge invariance. In order to restore the gauge invariance of the amplitudes one has to perform an additional expansion in some parameter. In case of the pole-scheme expansion the parameter is Γ/M, whereas in the fermion-loop scheme it is αN_f.

<div align="right">

This thesis,
E.N. Argyres *et al.*, *Phys. Lett.* **B358** (1995) 339;
W. Beenakker *et al.*, *Nucl. Phys.* **B500** (1997) 255.

</div>

5. The Dyson resummation can be done in a gauge invariant way by using nonlocal effective lagrangians.

<div align="right">

W. Beenakker, F.A. Berends and A.P. Chapovsky,
in preparation.

</div>

6. The gauge breaking terms due to a wrong treatment of the width can spoil the results significantly not only in the case of W production, but also in processes involving other unstable particles, like a top quark.

7. The exponential decay law has to be violated at small times because the energy spectrum of the states is bounded from below. This is called the quantum Zeno effect; it is neglected in the double-pole approximation.

<div align="right">

B. Misra and E.C.G. Sudarshan,
J. Math. Phys. **18** (1977) 756.

</div>

8. Consider a soldered Π-like tube with liquid in both knees of the tube with some level difference. Both effects of friction of the vapour over the walls of the tube and over the buffer gas have to be taken into account in order to understand correctly the velocity with which the liquid levels become even.

9. The following two curious observations might have some deep explanation. The number of leptonic fermionic modes in the Standard Model is the same as the number of bosonic modes with which they interact. If the chiral symmetry breaking in QCD would occur via the fundamental scalar fields, then the number of quark fermionic modes would be the same as the number of bosonic modes with which they interact.

<div align="right">

A.P. Chapovsky
Leiden, 23 September 1999

</div>